Arene ruthenium iminophosphonamide complexes : synthesis, reactivity and application in transfer hydrogenation of ketones

Iana Sinopalnikova

Université Fédérale
Toulouse Midi-Pyrénées

THÈSE

En vue de l'obtention du

DOCTORAT DE L'UNIVERSITÉ DE TOULOUSE

Délivré par l'Université Toulouse 3 - Paul Sabatier

Cotutelle internationale : Institut de composés d'organoéléments A.N. Nesmeyanov de l'Académie des sciences de la Russie, INEOS RAS

Présentée et soutenue par

Iana SINOPALNIKOVA

Le 21 juin 2019

Complexes iminophosphonamides de ruthénium(II): synthèse, réactivité et applications pour l'hydrogénation par transfert de cétones

Ecole doctorale : **SDM - SCIENCES DE LA MATIERE - Toulouse**

Spécialité : **Chimie Organométallique et de Coordination**

Unité de recherche :
LCC - Laboratoire de Chimie de Coordination

Thèse dirigée par
RINALDO POLI et Alexander KALSIN

Jury

Mme Olivia REINAUD, Rapporteure
Mme Alexandra SKATOVA, Rapporteure
Mme Elena MILAEVA, Examinatrice
M. Dmitry VALYAEV, Examinateur
M. Rinaldo POLI, Directeur de thèse
M. Alexander M. KALSIN, Co-directeur de thèse

Acknowledgements

First and foremost I want to thank my co-supervisors Dr. Alexander M. Kalsin and Prof. Rinaldo Poli. It has been an honor to be their Ph. D. student. I appreciate all their contributions of time, ideas, and funding to make my Ph.D experience productive and stimulating. I would like to thank Dr. Elena S. Shubina, Dr. Natalia V. Belkova, Dr. Oleg A. Filippov for their advices in scientific discussions. I gratefully acknowledge Tat'yana A. Peganova for her help in synthetic work.

Many thanks to Agnès Labande, Sandrine Vincendeau and Florence Gayet for their friendship and help in the laboratory. I gratefully acknowledge Dr. Jean-Claude Daran for his patience with crystals. I want to thank Eric Deydier for his help with DFT-calculation.

I would like to thank the postdocs Ekaterina Bellan, Ph. D. Kateryna Bretosh, Ph. D. Alina Grineva, Ph. D. Lucas Thevenin and Ph. D. Rabdan Tikhov for all their friendly support.

I gratefully acknowledge the funding sources that made my Ph.D work possible. I would like to thank the French government for financial support through Mechnikov's scholarship.

Résumé de thèse

Titre: Complexes Iminophosphonamides Arènes de Ruthénium : synthèse, réactivité et applications en hydrogénation par transfert de cétones.

Les nouveaux complexes iminophosphonamide (NPN) arènes de ruthénium à 18ē et 16ē, [(η^6-arène)RuCl{$R_2P(NR')_2$}] (**3a-c,e,f**), [(η^6-C_6Me_6)RuCl{Ph_2P(N-Me)(N-*p*-Tol)}] (**3d**) and [(η^6-arène)Ru{$R_2P(NR')_2$}]$^+$(X^-) (**4a-c,f**) (**a**, R = Ph, R' = *p*-Tol; **b**, R = Et, R' = *p*-Tol; **c**, R = Ph, R' = Me; **e**, R = Ph, R' = *p*-C_6H_4COOEt; **f**, R = Ph, R' = *p*-Tol. X = BF_4, PF_6; arène = C_6Me_6, *p*-cymène) ont été synthétisés et complètement caractérisés. Les paramètres thermodynamiques de la dissociation du chlorure des complexes NPN à 18ē ont été dérivés dans des solvants polaires et non-polaires par les méthodes spectroscopiques UV-visible, RMN 1D ^{1}H et 2D EXSY ^{1}H à température variable, mettant en lumière l'influence du ligand NPN sur les paramètres d'équilibre. L'enthalpie de dissociation ΔH_d diminue avec l'augmentation du pouvoir donneur des substituants des atomes de N et P (**3e** > **3a**,**f** > **3b** > **3d** > **3c**) et de la polarité du solvant, donnant lieu à la dissociation spontanée et exothermique de **3c** dans les solvants polaires. La coordination de ligands neutres (MeCN, pyridine, CO) aux complexes **4a,c,f** correspondants à 16ē est réversible ; la stabilité des adduits dépend du pouvoir π-accepteur du ligand. La carbonylation de **4a** et **4f** produit des exemples rares de complexes carbonyles arènes de ruthénium cationiques (**5a**, **5f**), alors que l'adduit monocarbonyle dérivé de **4c** réagit ultérieurement avec une seconde molécule de CO, produisant rapidement le complexe carbonyle-carbamoyle **5c'**, où une molécule de CO s'est insérée dans la liaison Ru–N. Les nouveaux complexes carbonyles **5a,f** et **5c'** ont été isolés et leur structure a été déterminée.

Pour la première fois, il a été montré que des complexes NPN de ruthénium sont catalytiquement actifs en hydrogénation par transfert des cétones. L'activité catalytique augmente avec l'introduction du ligand *p*-cymène et des substituants élecro-donneurs sur les atomes de N. Les complexes contenant les ligands NPN avec substitution N-aryle sont activés par une base forte. Des réactions modèles et des études cinétiques, couplées à des calculs par DFT, ont établi que l'intermédiaire clé est un complexe hydrure. Les complexes avec substitution N-Me sont actifs en absence de base et leur forme active est probablement le complexe cationique à 16ē.

Mots clés: complexes de ruthénium, ligands zwitterioniques, dissociation de chlorure, carbonylation, hydrogénation par transfert, mécanisme d'activation.

Summary

Subject: Arene Ruthenium iminophosphonamide complexes: synthesis, reactivity and application in transfer hydrogenation of ketones.

Novel half-sandwich 18ē and 16ē arene ruthenium iminophosphonamide (NPN) complexes [(η^6-Arene)RuCl{$R_2P(NR')_2$}] (**3a-c,e,f**), [(η^6-C_6Me_6)RuCl{Ph_2P(N-Me)(N-*p*-Tol)}] (**3d**) and [(η^6-arene)Ru{$R_2P(NR')_2$}]$^+$(X^-) (**4a-c,f**) (**a**, R = Ph, R' = *p*-Tol; **b**, R = Et, R' = *p*-Tol; **c**, R = Ph, R' = Me; **e**, R = Ph, R' = *p*-C_6H_4COOEt; **f**, R = Ph, R' = *p*-Tol. X = BF_4, PF_6. Arene = C_6Me_6, *p*-Cymene) were synthesized and fully characterized. The thermodynamics of chloride dissociation from the 18ē NPN complexes has been assessed in both polar and apolar solvents, using variable-temperature UV-visible, NMR and 2D EXSY ^{1}H NMR methods, highlighting the NPN ligand influence on the equilibrium parameters. The dissociation enthalpy ΔH_d decreases upon increasing the electron-donating ability of the N-,P- substituents (**3e** > **3a**,**f** > **3b** > **3d** > **3c**) and the solvent polarity, resulting in the exothermic spontaneous dissociation of **3c** in polar solvents. The coordination of neutral ligands (MeCN, pyridine, CO) to the corresponding 16ē complexes **4a,c,f** is reversible; the stability of the adducts depends on the π-accepting ability of ligand. Carbonylation of **4a** and **4f** results rare examples of cationic arene ruthenium carbonyl complexes (**5a**, **5f**), while the monocarbonyl adduct derived from **4c** reacts further with a second CO molecule, rapidly converting to the carbonyl-carbamoyl complex **5c'**, where one CO molecule is inserted into the Ru–N bond. The new carbonyl complexes **5a,f** and **5c'** were isolated and structurally characterized.

For the first time, it has been shown that ruthenium NPN complexes are active catalysts for the transfer hydrogenation of ketones. The catalytic activity increases with the introduction of the *p*-cymene arene ligand and more electron-donating N substituents. The complexes containing NPN ligands with N-Aryl substitution are activated by a strong base. Model reactions and kinetic studies, backed up by DFT calculations, have established that the key intermediate is a hydride complex. The complexes with N-Me substituted are activated without base, for them we propose cationic complex to be an active intermediate.

Keywords: ruthenium complexes, zwitterionic ligand, chloride dissociation, carbonylation, transfer hydrogenation, activation mechanism.

Contents.

Introduction

The diverse reactivity of transition metal complexes and the considerable economic efficiency of the preparation of previously hard-to-get chemicals led to the rapid development of metal complex catalysis. At the same time, there remains a need to improve the efficiency and rational design of chemical processes, which is almost impossible without creating new catalysts and studying in detail the sequence of interconversions with the participation of the catalyst. The transition metal complexes with κ^2-N,N heteroallylic – amidinates $RC(NR')_2^-$ (NCN) and iminophosphonamides $R_2P(NR')_2^-$ (NPN) – ligands have been used as catalysts for various organic reactions, for example, olefin oligomerization and polymerization, addition of amines to unsaturated substrates, and olefin cyclopropanation. However, NPN complexes have been studied fragmentarily, mainly for early transition metals and lanthanides. A few platinum metal group iminophosphonamides have been reported for palladium and ruthenium before 2009, when the Kalsin group started a systematic studies of these complexes. The studies of the catalytic activity of NPN complexes are also scarce; for late transition metals, they are limited to cross-coupling reactions of the Tsuji-Trost and Suzuki-Miyaura types and to the polymerization and cyclopropanation of alkenes.

For the past few years, our group has carried out systematic studies of the iminophosphonamide (NPN) complexes of the platinum group metals. It was demonstrated experimentally, from the deformational electron density obtained from precision X-ray data for the palladium complex $[Pd\{(p\text{-}^iPrC_6H_4N)_2PPh_2\}_2]$, that the iminophosphonamide ligand is zwitterionic (N^-–P^+–N^-) having single P–N bonds and bearing full negative charges at the nitrogen atoms. This fact is due to ability of the NPN ligand to donate either 4 or 6 electrons, and therefore to be able to compensate electron deficiency at the metal center. In addition, ruthenium complexes with such ligands are isoelectronic analogues of the well-known Noyori–Ikaria catalysts and, therefore, are potential catalysts for the reduction of carbonyl substrates under transfer hydrogenation reaction conditions. The peculiarities of the electronic effect of iminophosphonamide ligands should be clearly manifested in the reactivity of the half-sandwich arene ruthenium NPN complexes. However, prior to the present work, only one example of a [(NPN)Ru] complex was

described in the literature. Thus, the synthesis of arene ruthenium iminophosphonamide complexes and the study of their catalytic properties is of strong interest.

The goal of this thesis work is a comprehensive study of arene ruthenium iminophosphonamide complexes, including the study of their physicochemical properties and application in the catalytic reduction of ketones by transfer hydrogenation. To achieve this goal, the following tasks were set:

1. Synthesis of a series of new 18ē and 16ē arene ruthenium NPN complexes with differing arene ligand and N-,P-substituents in the NPN ligand.

2. Study of the interconversion processes between the 18ē and 16ē complexes by NMR and UV-visible spectroscopy; identification of the factors affecting the reactivity of these complexes.

3. Study of the catalytic activity of ruthenium NPN complexes in the reduction of a model ketone by transfer hydrogenation with isopropanol: kinetic studies, determination of the structure of intermediates, transition states and the reaction mechanism.

I. Literature review.

The catalytic homogeneous hydrogenation of unsaturated compounds is one of the most important processes in modern organic chemistry. It is a key reaction for industrial applications from fine organic chemicals to the synthesis of pharmaceuticals. Ruthenium homogeneous hydrogenation catalysts, which have been known for almost 50 years,[1,2] prove to be some of the most useful catalysts for these reactions. Ruthenium complexes display favorable reactivity and selectivity, especially in the catalytic reduction of polar bonds, that often surpass those of the usual stars of alkene hydrogenation, namely the complexes of rhodium and iridium.[3-7] For example, Ru complexes can be used to catalyze the H_2-hydrogenation of a wider range of Z-α-(acylamino)acrylic acids and esters than cationic Rh-complexes.[3] Certain ruthenium complexes with amine ligands are much more active than other metal complexes for the catalytic reduction of ketones, especially those devoid of heteroatom functionality.[5,6] This high activity often comes with high enantioselectivity in the hydrogenation of prochiral ketones and high selectivity for the hydrogenation of carbonyl over olefin functional groups.[8] Ruthenium complexes also have promising catalytic activity in imine hydrogenation.[4,7]

There are two ways to accomplish a homogeneous hydrogenation: a ‘‘direct hydrogenation’’ using pure hydrogen under pressure and “transfer hydrogenation”, with the transfer of two hydrogen atoms from a source of hydrogen to the substrate. Transfer hydrogenations are mild methodologies for the reduction of ketones or imines to the corresponding secondary alcohols or amines without the direct use of molecular hydrogen (Scheme 1). Isopropanol, which is used as a solvent, or formic acid and its salts, are the most commonly used hydrogen donors. The role of the catalyst is to transfer hydrogen atoms from the hydrogen donor (DH_2) to a hydrogen acceptor (e.g. a ketone)

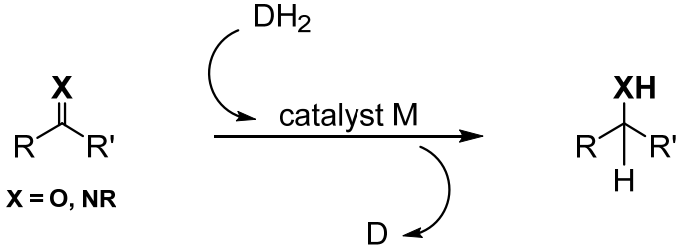

Scheme 1. Concept of transfer hydrogenation (DH_2 = ^{i}PrOH, HCOOH).

The first example of transfer hydrogenation of aldehyde by ethanol using aluminum ethylate was discovered in 1925 by Meerwein.[9] In the same year, Werley reported the reduction of butyraldehyde using the same aluminum ethylate in the presence of geraniol as a hydrogen donor.[10] A year later, in 1926, Ponndorf expanded its scope to the reduction of ketones with aluminum isopropoxide in isopropanol.[11] The mechanism of reduction was the transfer of hydrogen atoms from alcohol to the carbonyl substrate (Scheme 2), giving primary (from aldehydes) or secondary (from ketones) alcohols.

Later, Oppenauer[12] discovered that the reaction could be run in the opposite direction, i.e. secondary alcohols could be oxidized to the corresponding ketones in the presence of acetone (Scheme 2). In these reversible hydrogen transfer reactions, employing an excess of either isopropanol as alcohol or acetone as ketone leads to either MPV reduction or Oppenauer oxidation, respectively.

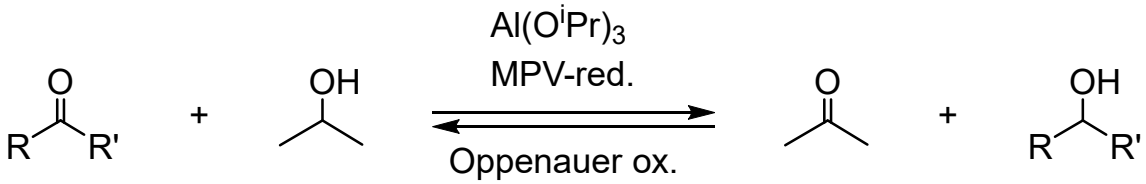

Scheme 2. Meerwein-Ponndorf-Verley reduction and Oppenauer oxidation.

The major problem of the MPV-Oppenauer reactions is that the aluminum alkoxide is often required in stochiometric amounts, which is a drawback for industrial applications where scaling up is often necessary.[13]

The next milestone of TH was the discovery of late transition-metal catalysts involving first-, second-, and third-row transition metals of groups 8, 9, 10, and 11. The pioneering work reported by Henbest, Mitchell, and co-workers in the 1960s showed that an iridium hydride complex could catalyze the hydrogenation of cyclohexanones and α,β-unsaturated ketones to alcohols with isopropanol.[14,15] In the 1970s, Sasson and Blum also provided seminal contributions to the development of transition metal-catalyzed TH. They demonstrated that complex $[RuCl_2(PPh_3)_3]$ is active in the biphasic TH of acetophenone with isopropanol at high temperature.[16,17] Low conversions and high temperatures were the main disadvantages of the first catalysts. Since then, many efficient catalytic systems

have been developed that operate under milder conditions, mainly using ruthenium, iridium and rhodium complexes.[18]

Examples of catalytic systems based on ruthenium complexes.

In 1985, thanks to innovative research group Prof. Shvo, a new type of ruthenium catalysts has appeared.[19-22] These catalysts are dimeric ruthenium(II) hydridocarbonyl complexes with the general formula $[(\eta^5\text{-}R_4C_4COH)(\mu\text{-}H)(CO)_4Ru_2]$ (**L1** in Scheme 3), containing an intramolecular O···H···O hydrogen bond. There are various aryl and alkyl substituents on the cyclopentadienyl ring. These compounds effectively catalyze the TH of aldehydes, ketones and imines.

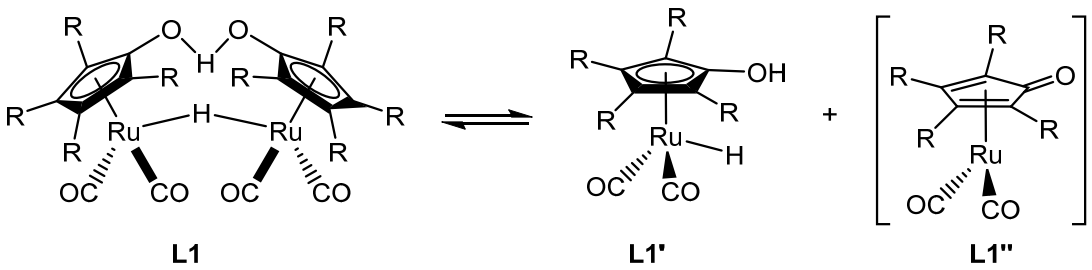

Scheme 3. Shvo's Catalyst dimeric type (**L1**) and its equilibrium monomers.

The **L1** complex is in equilibrium with the monomers **L1'** and **L1''**. Monomer **L1'** is able to hydrogenate a hydrogen-acceptor (ketone, aldehyde, imine), while **L1''** monomer can dehydrate a hydrogen-donor (isopropanol, formic acid). The processes of hydrogenation-dehydrogenation translate **L1'** and **L1''** into each other.[20, 21]

The TH-reaction involving Shvo's catalysts and formic acid as hydrogen donor was studied using various ketones and aldehydes.[22] The reactivity of various carbonyl substrates is given in Table 1.

Table 1. Reduction of aldehydes and ketones with formic acid (1: 1), catalyzed by complex **L1** (R = Ph), at T = 100°C.

№	Substrate	Product		TOF, h^{-1}
		Formula	Conversion, %	
1	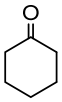	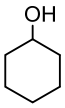	100	3800
2	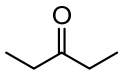	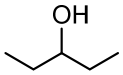	92	2760
3	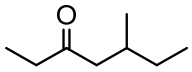	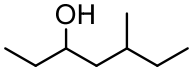	92	2160
4	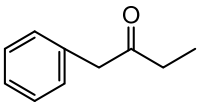	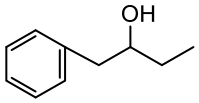	93	2700
5	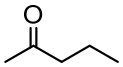	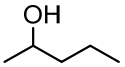	98	2340
6	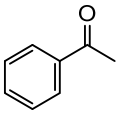	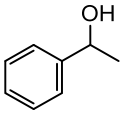	93	2700
7	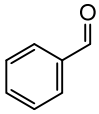	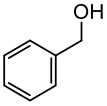	99	20563
8	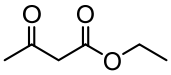	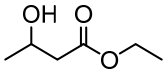	97	1754
9	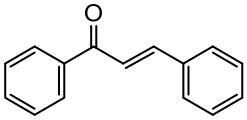	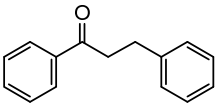	90	2250
		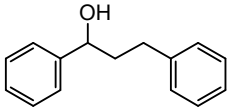	10	
10			96	760

TOF – turnover frequency

Simple cyclic and acyclic ketones react with practically the same activity, with the exception of cyclohexanone, which is slightly more active (Table 1, lines 1-6). With aliphatic aldehydes, the reaction is not selective, since aldol condensation adducts are formed. All yields are greater than 90%. Simple alkenes are not reactive under these conditions. However, double bonds that are conjugated with a carbonyl group are

selectively reduced under the conditions of this reaction (in the presence of a large excess of formic acid, the carbonyl group can also be reduced) (Table 1, lines 9-10). The authors note that when formic acid is used as a hydrogen donor, a partial esterification of the resulting alcohol occurs. To obtain esters, it is necessary to use a fivefold excess of formic acid relative to the carbonyl substrate, and the corresponding pure alcohol is formed by adding small amounts of sodium formate and water.[22]

Samek and Backwall reported that Shvo's **L1** catalysts promote the efficient TH-hydrogenation (TOF > 800 h^{-1}) of many imines of the type $PhN=CR^1R^2$ (where R^1, R^2 = aryl and alkyl substituents) to the corresponding amines in high yields (Table 2) by transferring hydrogen from isopropanol.[20] The authors found that ketimine reacts faster than aldimines, and the presence of electron-donating substitutes on the imine increases the rate of the catalytic TH- reaction. It was also noted that the rate of hydrogenation of imines directly depends on the polarity of the solvent. The use of benzene as a co-solvent significantly accelerates the reduction process.

Table 2. TH of imine with isopropanol, catalyzed by complex **L1** (R = Ph), 70°C.

№	Imine	Product		t, min	TOF, h^{-1}
		Formula	Conversion, %		
1	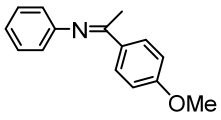	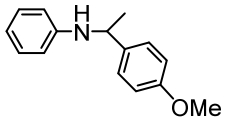	97	45	840
2	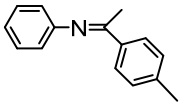	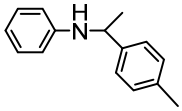	96	45	800
3	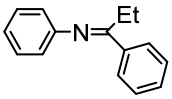	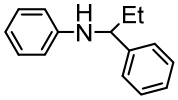	95	60	730
4	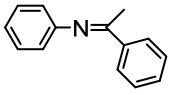	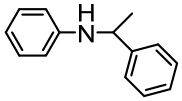	97	90	700
5	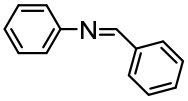	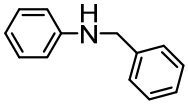	98	300	300
6	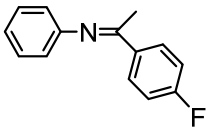	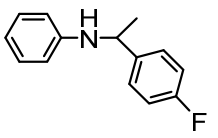	95	480	120

A special place in coordination chemistry and organometallic catalysis is occupied by a family of catalysts with N-heterocyclic carbene (NHC) ligands (Figure 1) due to their high coordinating ability and almost unlimited possibilities of structural modifications that allow precise control of steric and electronic properties at the metal center. Various chelate or pincer ligands, including chiral catalysts with NHC-ligands based on iridium, rhodium and ruthenium complexes, were obtained. The first results on transfer hydrogenation using Ru-NHC catalysts were reported by Peris and Danopoulos.[24-25] These authors used 2,6-bis(1-alkylimidazolium-3-yl)pyridine salts as a new source of tridentate bis(carbenes) to coordinate with ruthenium precursors, obtaining the **L2** and **L3** complexes with the pincer NHC-ligand (Figure 1). Both of these complexes exhibited high catalytic activities in the TH reduction of carbonyl compounds from ^{i}PrOH. In particular, **L3** gave TOF = 15200 h^{-1} when cyclohexanone was chosen as the reaction substrate. Later, Yu's group prepared the new ruthenium complex **L4** containing a pincer-type pyridyl based (pyrazol-3-yl)-N-heterocyclic carbene ligand and revealed its excellent activity in the TH of ketones.[26] In 2006, Gade et al. described the synthesis and catalytic applications of the first Ru complex bearing an oxazolinyl-carbene ligand with a half-sandwich structure (**L5**). The obtained catalyst **L5** showed a moderate activity in the reduction of ketones by ^{i}PrOH.[27]

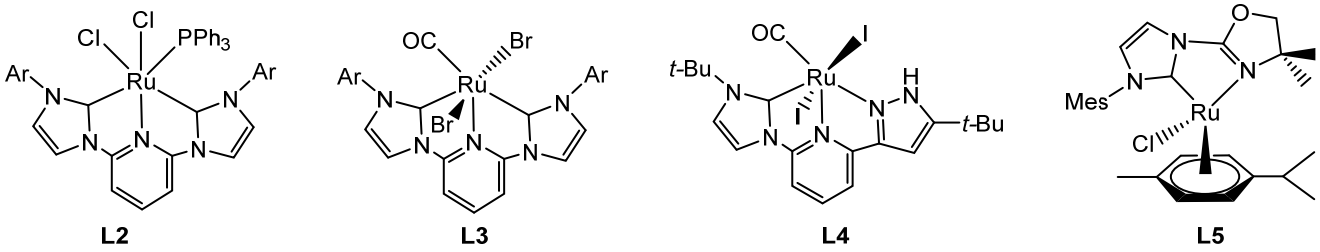

Figure 1. Ruthenium catalysts containing NHC-ligands for TH.

A significant contribution to the study of the TH-reaction of carbonyl substrates was made by the group Prof. Baratta.[28-30] They developed new highly active catalysts for this reaction based on ruthenium complexes with aminomethylpyridine ligands, some examples of which are presented in Figure 2.

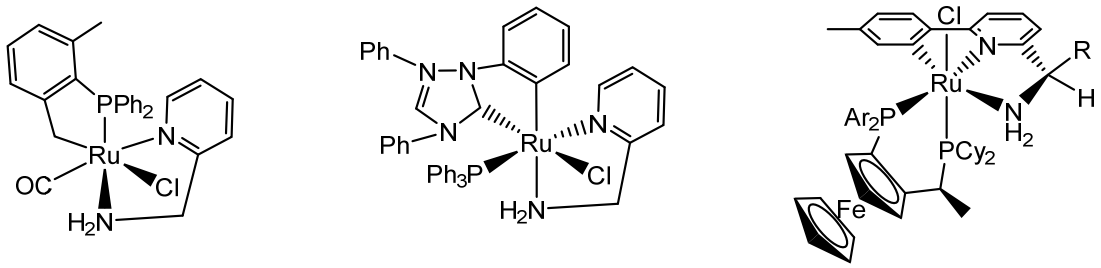

L6 **L7** **L8**

Figure 2. Examples of ruthenium catalysts developed by the Baratta's group.

Using **L6** containing 2-(aminomethyl)pyridine ligand, a large number of alkylaryl, dialkyl (linear and cyclic) and diarylketones could be quantitatively reduced by isopropanol to the corresponding alcohols within a few minutes at 82°C using a very small amount of catalyst (substrate/**L6** = 2000:1). The activity (TOF) is in the range of $19*10^3$ – $63*10^3$ h^{-1}(Table 3), depending on the stereo-electronic characteristics of the substrate.[28] However, by combining a 2-(aminomethyl)pyridine ligand and an N-heterocyclic carbene ligand, the authors obtained an even more active catalyst **L7** (TOF = $50*10^3$ – $140*10^3$ h^{-1}.[29]

Table 3. Reduction of ketones with isopropanol in the presence of NaOH, catalyzed by Baratta's complexes **L6-L8**, at T = 82°C.

№	Substrate	Catalyst L6		Catalyst L7		Catalyst L8*		
		TOF, h^{-1}	Convers., % (min)	TOF, h^{-1}	Convers., % (min)	TOF, h^{-1}	Convers., % (min)	*ee*, %
1	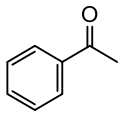	$60*10^3$	98 (5)	$110*10^3$	99 (5)	$180*10^3$	98 (10)	95 S
2	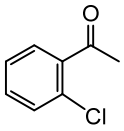	$29*10^3$	99 (10)	$50*10^3$	90 (10)	$70*10^3$	92 (60)	91 S
3	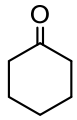	$19*10^3$	99 (15)	$100*10^3$	99 (5)	-	-	-
4	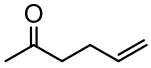	$30*10^3$	95 (10)	$50*10^3$	96 (15)	-	-	-
5	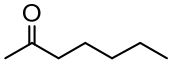	$63*10^3$	99 (10)	$70*10^3$	96 (10)	-	-	-
6	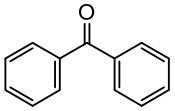	$36*10^3$	95 (5)	-	-	-	-	-
7	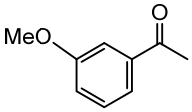	-	-	$70*10^3$	98 (10)	$140*10^3$	97 (30)	97 S

* T = 60°C

It should be noted that the further development of Prof. Baratta's group[30] led to the preparation of new chiral pincer complexes **L8** with the general formula [RuCl(CNN)-(Josiphos)] (Josiphos = 1-[1-(dicyclohexylphosphano)ethyl]-2-(diarylphosphano)-ferrocene), which are not only effective catalysts for the TH-reaction, but also highly enantioselective with respect to the carbonyl group (to 99%). At very low catalyst concentrations (0.005 – 0.002 mol%), it was possible to achieve extremely high activity (TOF = 10^5 – 10^6 h^{-1}) for a wide range of ketones.

In 1995, Noyori and Ikaria reported the synthesis of a series of [RuCl(η^6-Arene)(N-arylsulfonyl-DPEN)] complexes (**L9**, DPEN = 1,2-diphenylethylene-1,2- diamine). It was shown that these complexes are highly enantioselective catalysts for the TH of various aromatic ketones[8,31-33] and imines[33-34] (Scheme 4).

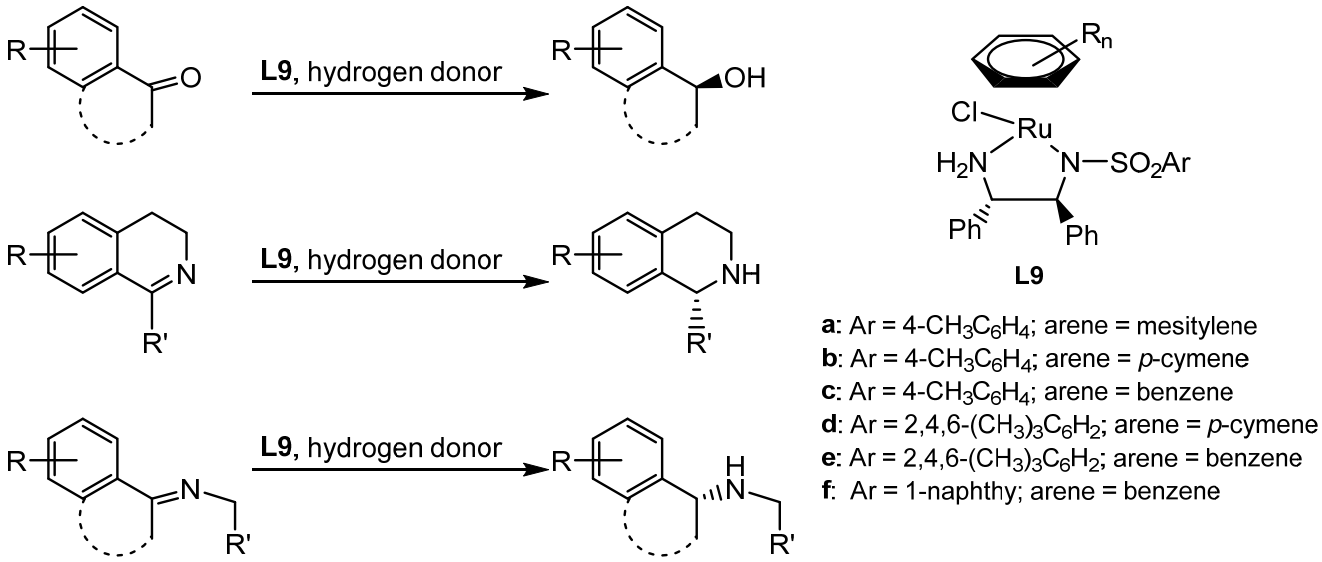

Scheme 4. Asymmetric TH reduction of ketones and imines catalyzed by Noyori's complex **L9** (Hydrogen source: ^{i}PrOH or HCOOH-Et$_3$N).

Prior to the Noyori-Ikaria catalysts, when using chiral phosphine ligands, the preparation of enantiomerically enriched secondary alcohols was difficult due to their facile racemization. The use of chiral nitrogen κ^2-N,N and κ^2-N,O has solved this problem. A catalytic system based on such chiral chelate ligands with NH groups (for example, 2-aminoethanol or mono-N-tosylated diamine (*S,S*)-TsNHCHPhCHPhNH$_2$) with ruthenium complex [RuCl$_2$(Arene)]$_2$ in the presence of a base in isopropanol dehydrates and racemises the resulting alcohols very slowly.[35] This allowed the development of efficient catalysts for the asymmetric hydrogenation of ketones and imines. It is noteworthy that the use of N,N-dimethylated ligands gives ruthenium complexes that are inactive in the reaction, which indicates the participation of the NH-group in the catalytic cycle.[33] Active catalysts can be obtained from the chloride precursors [(η^6-Arene)RuCl((S,S)-H$_2$NCHRCHRNTs)] (*S,S*-**L9**) $_2$ in the presence of a base in isopropanol.

In 1999, Prof. Ikaria[36] reported that *S,S*-**L9** catalyzes the asymmetric reduction of 1,2-diarylethane-1,2-dione (benzyl) in a mixture of formic acid/triethylamine, giving

(*R,R*)-hydrobenzoins quantitatively with high diastereomeric (97%) and enantiomeric (> 99% *ee*) purity (Scheme 5). Like chiral 1,2-diols, (*R,R*) -hydrobenzoins are important building blocks in stereoselective organic synthesis.

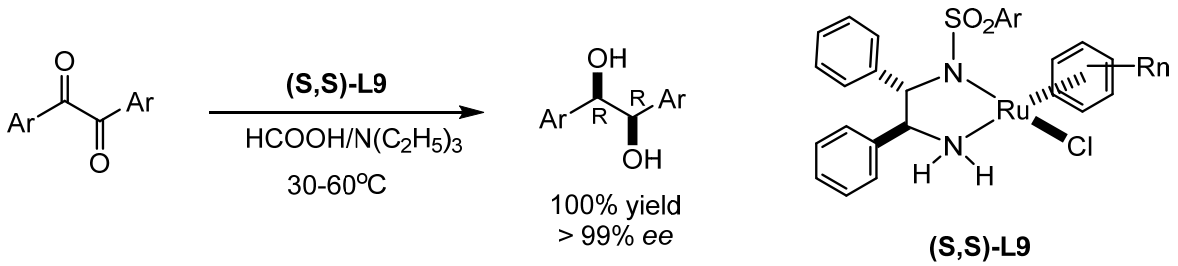

Scheme 5. Synthesis of hydrobenzoins using asymmetric TH-reactions using a Noyori's catalyst **L9**.

The same group also reported on the synthesis of optically active alcohols through the asymmetric TH of the corresponding ketones with the *S,S*-**L9** catalyst under the same reaction conditions.[37] The resulting functionalized alcohols were further converted to optically active aminoalcohols with high enantioselectivity (Scheme 6).

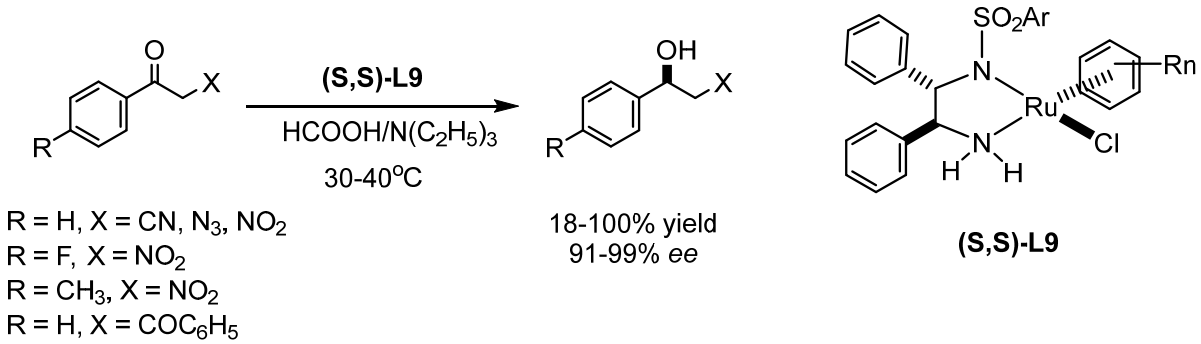

Scheme 6. Synthesis of optically active aminoalcohols with catalyst *S,S*-**L9**.

Thus, using the Noyori-Ikaria catalysts, it was possible to enantioselectively reduce a large range of aromatic ketones using isopropanol or formic acid as a hydrogen donor.[33] The corresponding chiral alcohols were formed with very high yields and *ee* (Table 4).

Table 4. Asymmetric reduction of aromatic ketones, catalyzed by the complexes of Noyori **L9**, at T = 40°C.

Ketone		^{i}PrOH		HCO_2H	
		yield, %	***ee*, %**	**yield, %**	***ee*, %**
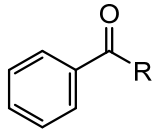	R = H	95	97 S	> 99	98 S
	R = C_2H_5	94	97 S	96	97 S
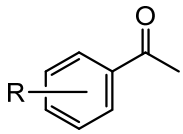	R = *m*-Cl	98	98 S	> 99	97 S
	R = *p*-Cl	95	93 S	> 99	95 S
	R = *m*-OCH_3	96	96 S	> 99	98 S
	R = *p*-OCH_3	53	72 S	> 99	97 S
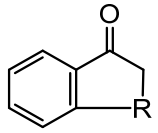	R = CH_2	45	91 S	> 99	99 S
	R = $(CH_2)_2$	65	97 S	> 99	99 S
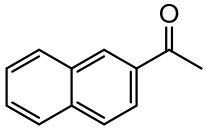		93	98 S	> 99	96 S
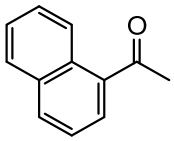		92	93 S	93	83 S

It should be noted that the TH-reaction of ketones with formic acid, catalyzed by complexes of type *S,S*-**L9**, proceeds with high chemoselectivity, without affecting the olefinic bond, ester groups, sulfides, nitro groups, arylchlorides and cyanides, furan, thiophene and quinoline rings (Scheme 7).[33]

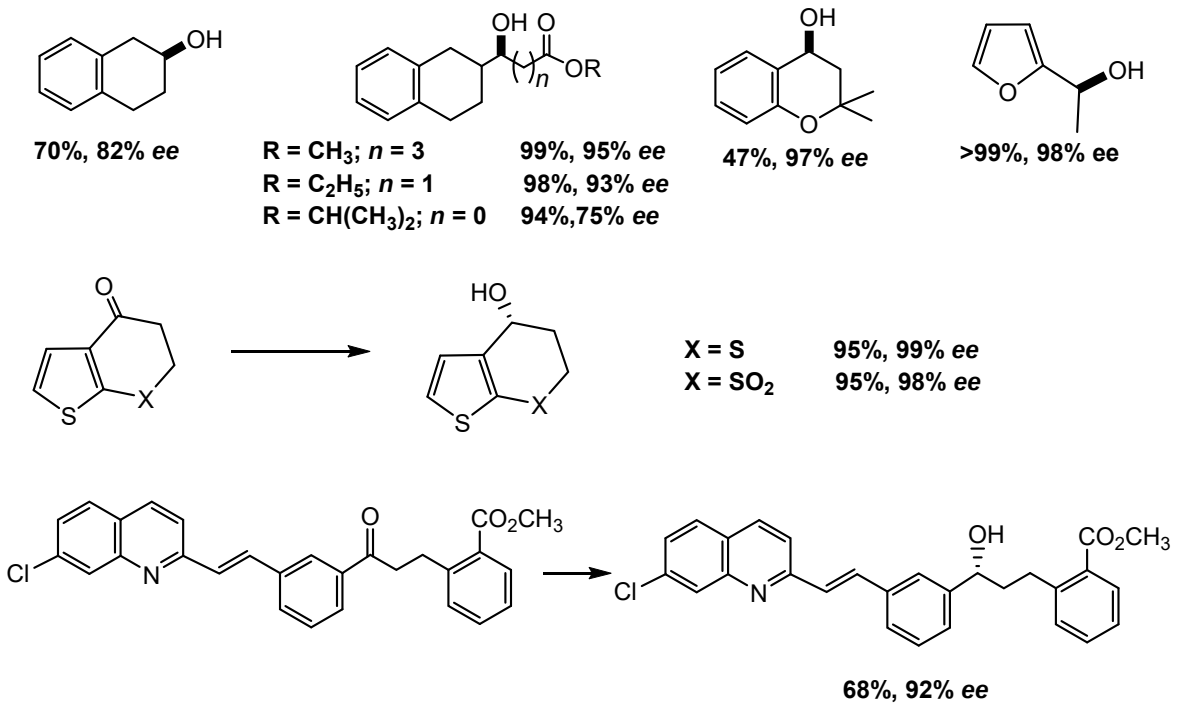

Scheme 7. Examples of chemoselective reduction of ketones by the *S,S*-**L9** complex.

The asymmetric TH of imines remains poorly studied. Currently, the ruthenium arene complexes type of **L9** effectively catalyze the reduction of imines with an azeotropic mixture of formic acid and triethylamine in a 5:2 ratio in various polar solvents, such as acetonitrile, DMF, DMSO, acetone and dichloromethane at 28°C.[34] A variety of chiral amines were formed with very high *ee* yields (Figure 3).

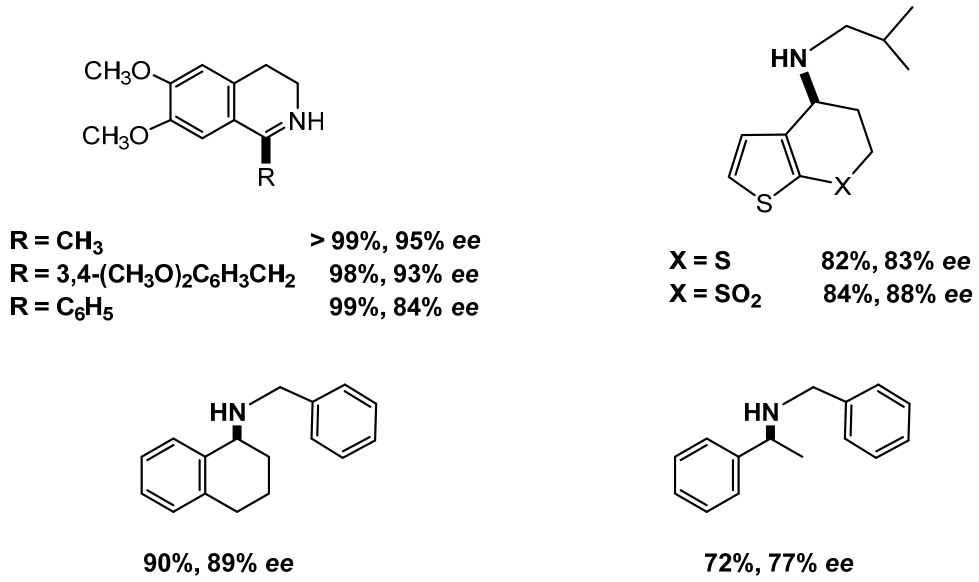

Figure 3. Asymmetric TH- reduction of the imines with an azeotropic mixture of formic acid and triethylamine (5: 2), catalyzed by the *S,S*-**L9** complex.

The search of new catalysts similar in enantioselectivity to the Noyori-Ikaria catalysts is actively underway. For example, Süss-Fink and colleagues synthesized a new family of cationic organometallic complexes **L10**, **L11** containing the chiral 1,2-diaminocyclohexane ligand (Figure 4). The water-soluble and water-stable compounds provided good conversion and enantioselectivity for catalyzing the TH of prochiral aromatic ketones and imines in aqueous solution. [38-39]

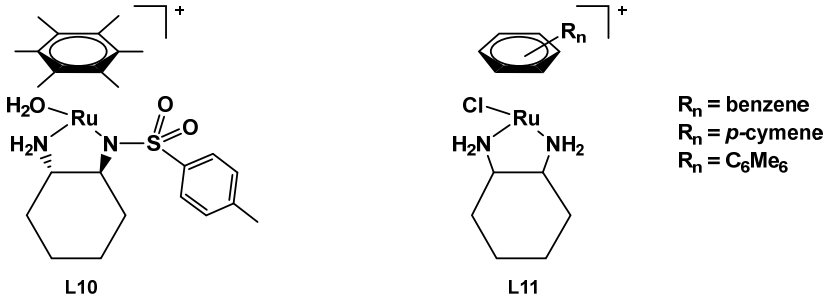

Figure 4. Cationic catalysts **L10**-**L11** of the Süss-Fink group.

In the early 2000s, Wills and co-authors reported on the development of a series of new **L12** – **L15** complexes, a structural variation of Noyori's catalysts (Figure 5).[40-46] These complexes contain a linking group (a "tether") between the arene and the κ^2-N,N-ligand. This tether prevents the arene ligand rotation and increases the stereochemical rigidity of the system. Furthermore, it allows the introduction of additional substituents that will affect the enantioselective properties of the complexes. For example, changing substituents at the 3,5 positions of arene ring in the complex **L12** can switch the selectivity from electronic to steric control.[42,46] Complex **L13**, in which an SO_2 group is part of the tether, is an effective catalyst for the TH of ketones with comparable activity to the Noyori-Ikaria catalysts.[40,41] The **L14** complex, in which the binding of an arene to a diamine occurs directly through the main N-group, manifests itself as a highly active catalyst for the reduction of ketones, in many ways surpassing the catalysts of Noyori-Ikaria.[43] For example, the complete conversion of acetophenone with a mixture of HCOOH/Et_3N solvents using 0.5 mol% **L14** at 40°C occurs in 3 hours, whereas the same reaction with the usual Noyori catalyst is completed in 24 hours.[43]

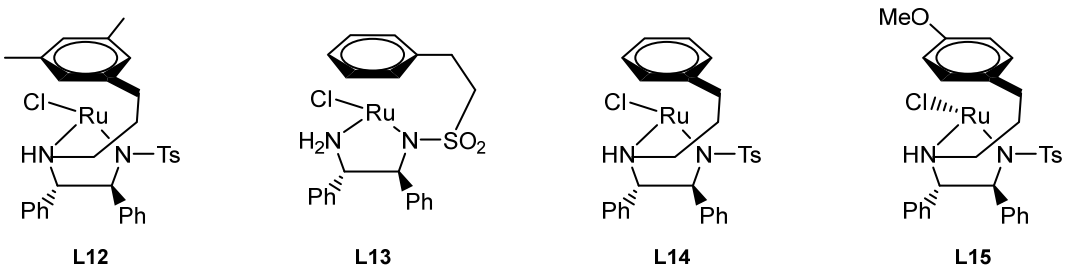

Figure 5. Examples of Wills's catalysts.

It should be noted that the catalysts of the type **L12** – **L15** were also effective in aqueous solution with sodium formate. Scheme 8 summarizes a series of aryl ketone reductions using the **L15** catalyst.[47]

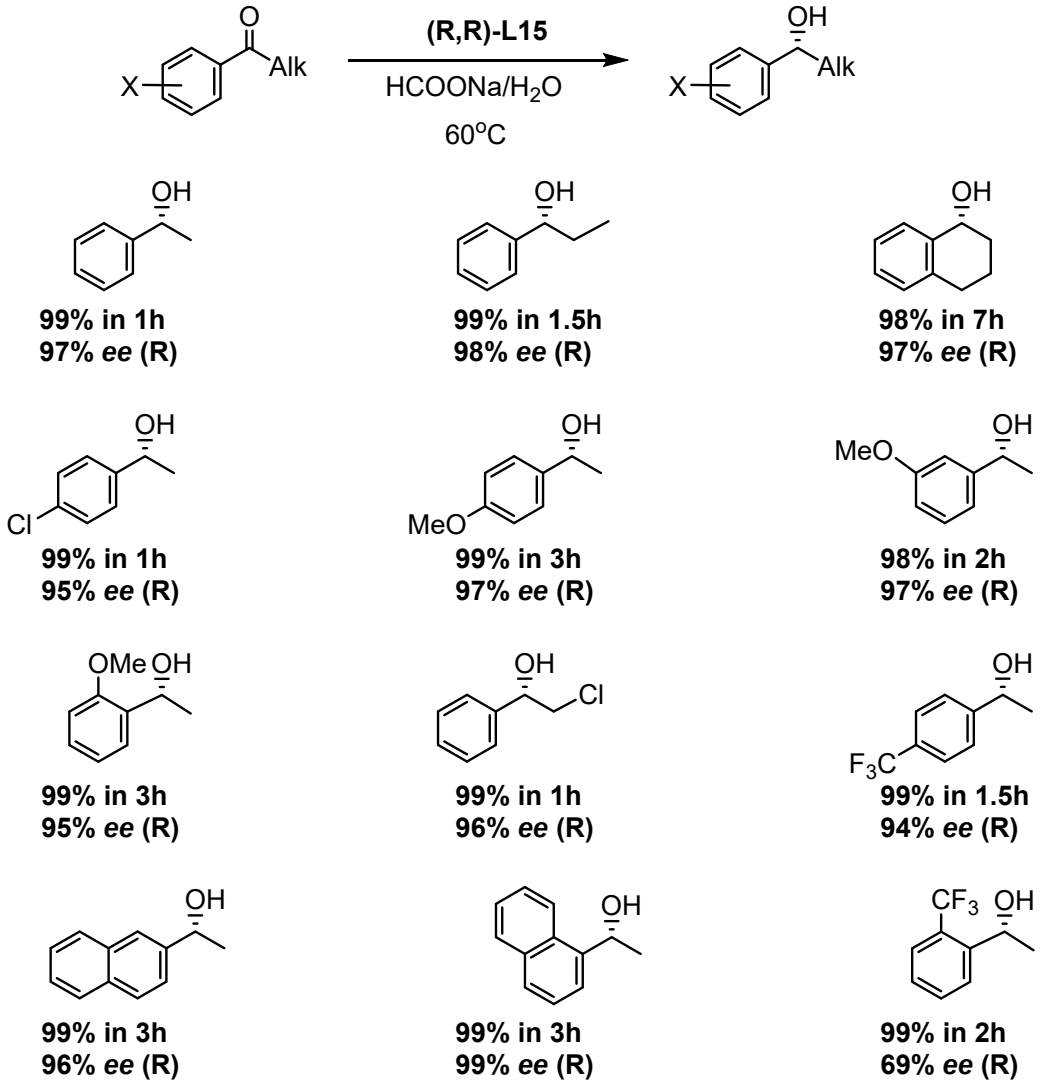

Scheme 8. Reduction of ketones in water using catalyst **L15**.

Williams, studying the possibility of using an alternative source of hydrogen in TH, noted the excellent activity of the **L14** catalyst in the reduction of acetophenone derivatives in the presence of *cis*-1,4-butandiol (Figure 9).[48] Diol provides an effective source of hydrogen by isomerization, first to 4-hydroxybutanal, then the formation of lactol and its subsequent irreversible oxidation to lactone. The higher activity of the associated catalyst **L14**, in comparison with the complexes of Noyori-Ikaria, allows the reaction to be carried out at a lower temperature.

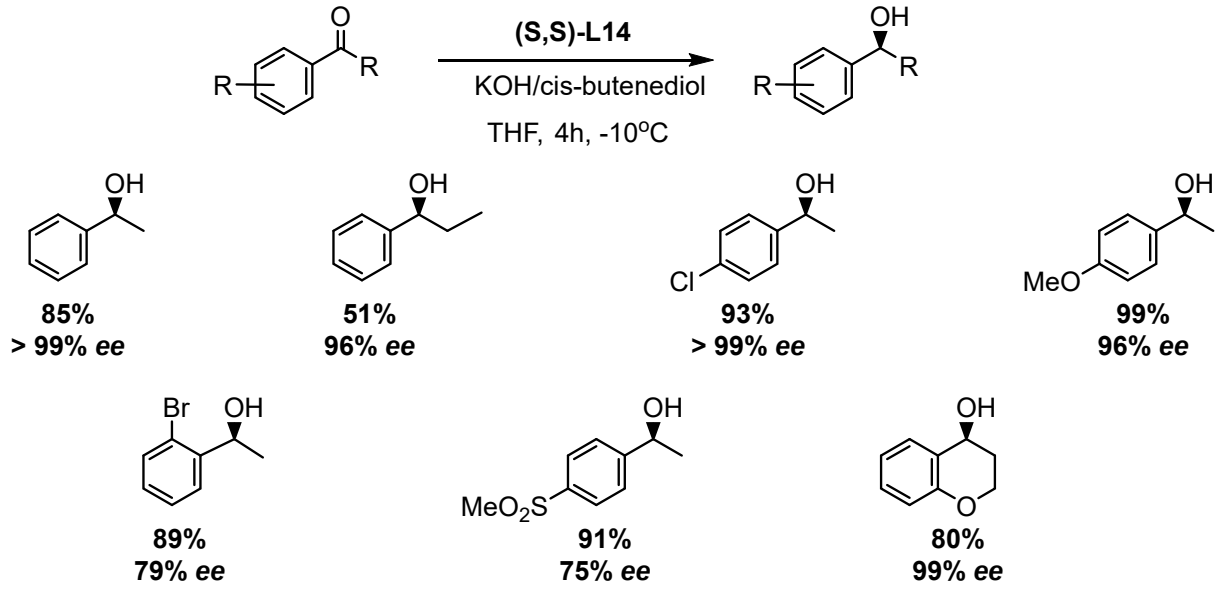

Scheme 9. Ketone reduction catalyzed by the **L14** complex with *cis*-1,4-butandiol as a hydrogen source.

Chiral diamines are rather difficult to synthesize, so the discovery of the possibility of using N,O- and N,P-ligands instead of diamines has greatly improved the practical use of the Noyori-Ikaria catalysts. Thus, readily available chiral β-amino alcohols, for example ephedrine,[49] make it possible to produce the cheaper but equally enantioselective ruthenium arene complex **L16** (Figure 6). Mixed N,P-chelate ligands have attracted considerable attention in both coordination chemistry and catalysis, due to their unusual electronic properties and pronounced hemilabile character resulting from the presence of two very different binding sites.[50] In 2003, a half-sandwich chelate catalyst **L17** bearing the 1-(2-methylpyridine) phosphole ligand was prepared and gave extremely high TOF ($1.2*10^6\ h^{-1}$) for the TH of ketones.[51]

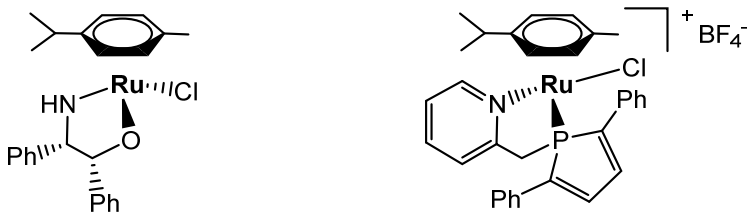

Figure 6. A half-sandwich chelate catalyst containing N,O-ligand (**L16**) and N,P-ligand (**L17**).

Prof. Stradiotto's group has developed another type of highly efficient half-sandwich ruthenium catalysts with N, P-ligand [(η^6-Arene)Ru(κ^2-P,N)(Cl)] (**L18**, **L18^H**, **L19**) (Figure 7).

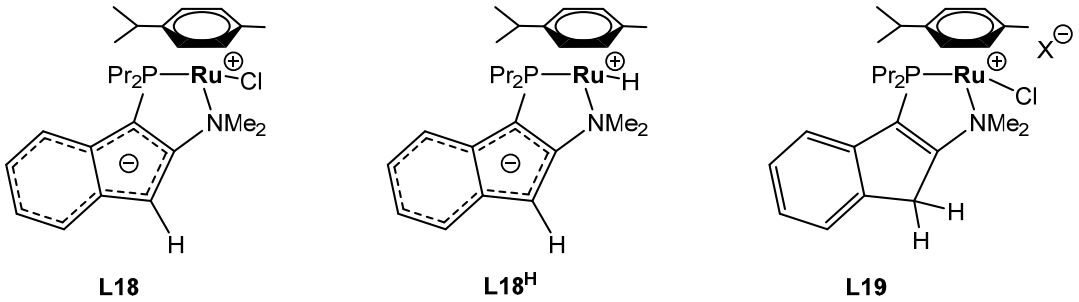

Figure 7. Catalysts developed by the Stradiotto group.

Despite the absence of an NH functional group, complex **L18** catalyzed the TH of a wide range of ketones with almost quantitative yields within a few minutes with 0.05 mol % of catalyst, with TOF values reaching 220 000 h^{-1} (Table 5).[52] The cationic complex **L19** is less active than the complex **L18**, the acetophenone conversion to 1-phenylethanol reaching 23% in 15 minutes. It is noteworthy that the zwitter-ionic hydride complex **L18^H** (Figure 7), which is formed quantitatively when complex **L18** was treated with KO^{t}Bu base in ^{i}PrOH, is not active in the TH-reaction of ketones.[52]

Table 5. TH of ketones in the presence of complex **L18** (0.05 mol%) and KO^{t}Bu (1 mol%) in ^{i}PrOH.

Ketone	Time, min	Conversion, %	TOF, h^{-1}
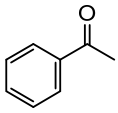	5	99	180 000
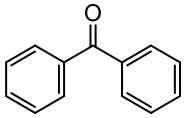	5	98	220 000
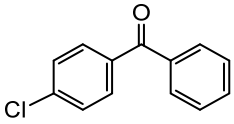	15	94	180 000
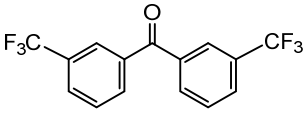	5	97	180 000
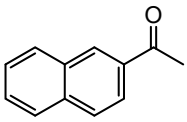	15	95	125 000
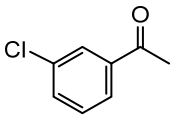	15	99	57 000
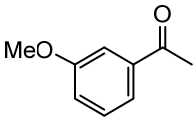	5	97	120 000
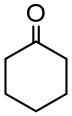	5	99	54 000
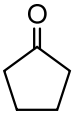	5	99	91 000
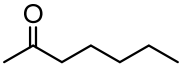	15	99	150 000

Mechanisms for the transfer hydrogenation reaction.

Recently, many mechanistic studies of the TH reaction have been conducted and two main pathways have been proposed: direct hydrogen transfer and the hydridic route, depending on the type of metal used as the catalyst. As a rule, direct hydrogen transfer is realized for main group metals, while the hydridic route is operating for transition metals.

1. Direct hydrogen transfer.

The pathway through a ‘‘direct hydrogen transfer’’ was proposed for the Meerwein-Ponndorf-Verley (MPV) reduction (Scheme 10). It proceeds *via* a concerted process, which involves the coordination of a ketone on a metal atom with the formation of a six-membered transition state. The hydrogen donor (isopropanol) and the hydrogen acceptor (ketone) are in close proximity to the metal center. The hydrogen is transferred directly to the hydrogen acceptor without the involvement of free metal hydride intermediates.[23,53,54] Such a mechanism requires that the metal atom has a free coordination site for substrate coordination and is characteristic of the main group metals, lanthanides and early transition metals.

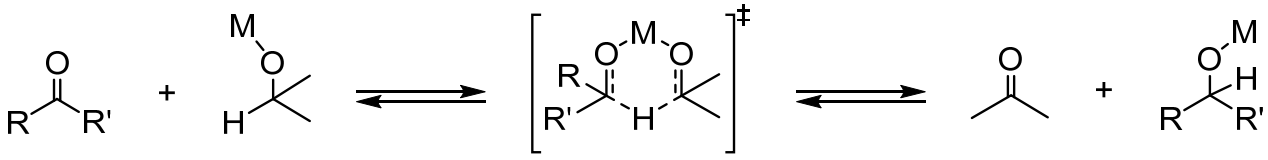

Scheme 10. The direct hydrogen transfer mechanism in the MPV reduction.

2. The hydridic route.

A common feature of the hydridic route is the involvement of a metal hydride as a key intermediate in the hydrogen transfer. The hydridic route proceeds in a stepwise manner. Initially, a hydrogen donor (formic acid, triethylamine, isopropanol) reacts with the catalyst to form a metal hydride complex. Hydrogen is then transferred from the hydride complex to the acceptor (carbonyl substrate) (Scheme 11).[23,53,54]

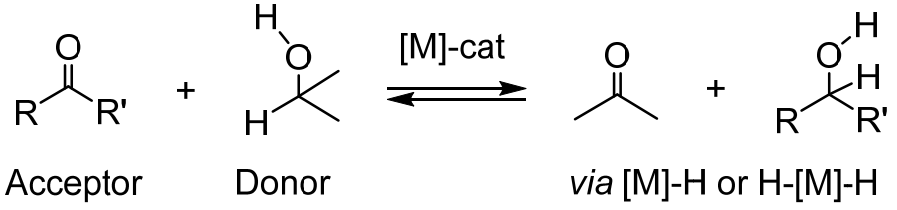

Scheme 11. The stepwise hydridic mechanism proposed for transition metals.

This mechanism is typical of late transition metals such as Ru(II), Rh(I), Ir(I). Depending on the metal, the hydridic route can be divided further into the monohydridic and the dihydridic route.[53]

In the monohydridic route only one of the hydrogen atoms is transferred from the substrate to the metal (Scheme 12A), whereas in the dihydridic route both hydrogen atoms are transferred to the metal (Scheme 12B). The two mechanisms can be distinguished from each other by means of deuterium labeling, since the hydrogen atoms will keep their identity throughout the reaction in the monohydridic route (Scheme 12A). In the dihydridic route the hydrogen atoms will be scrambled between carbon and oxygen and therefore lose their identity (Scheme 12B).[53]

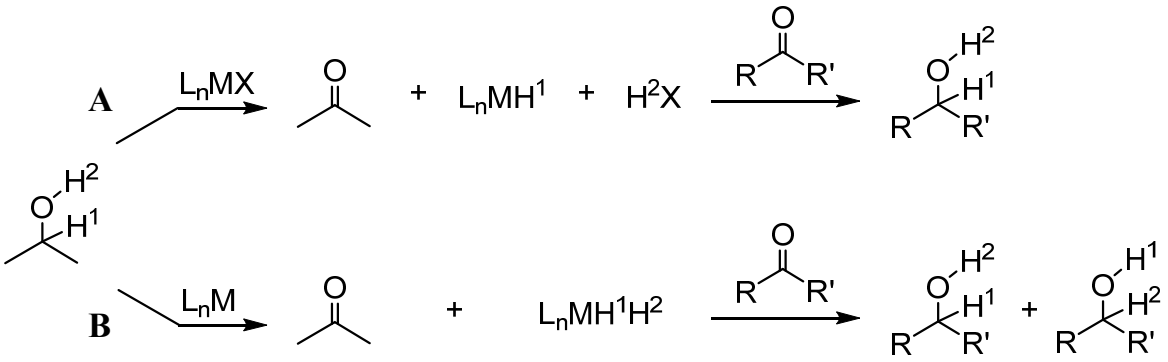

Scheme 12. Monohydridic (path A) versus dihydridic (path B) mechanism.

The monohydride mechanism can be further divided into two principally different pathways: *inner sphere* mechanism and *outer sphere* mechanism.

2.1 TH of the substrate by the *inner sphere* mechanism.

The mechanism for transition metal catalysts operating by the *inner sphere* mechanism is shown in Scheme 13.[55] The catalytically active ruthenium hydride complex with a free coordination site coordinates the unsaturated substrate in step I. Then, in step II, the hydride ligand migrates to the *β*-position of the substrate. The hydrogen donor in step III protonates the formed alkoxide or amide with the release of the corresponding product, and the isopropoxide anion is coordinated with the ruthenium atom. Then, in step IV, the hydride complex returns as a result of *β*-elimination. Removal of the oxidation product (ketone) ends the cycle in step V.

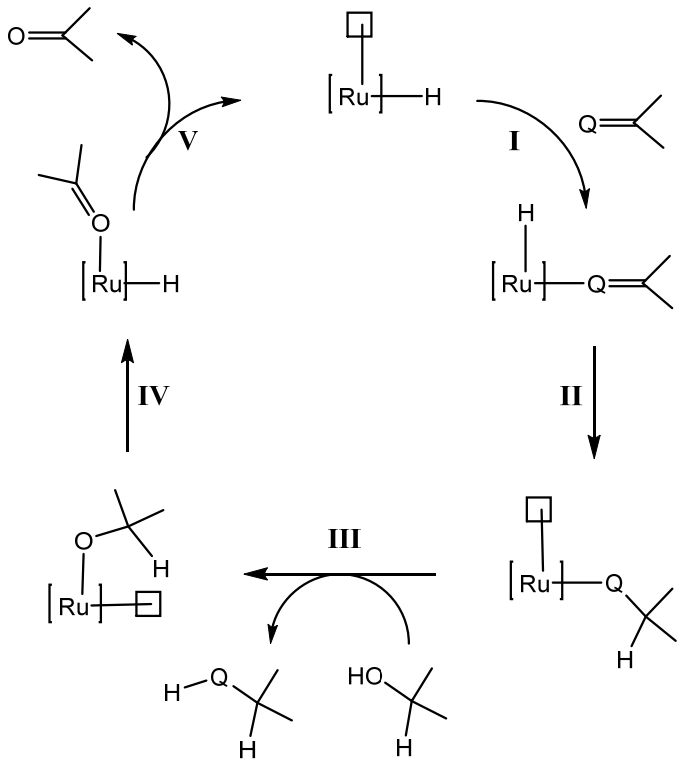

Scheme 13. The *inner sphere* mechanism of TH (Q = O, NH).

The work of Mizushima et al.[56] will be used to illustrate this cycle for ruthenium (Scheme 14). These authors showed that complex *cis*-$Ru(H)_2(PPh_3)_4$ is an active precatalyst for the transfer hydrogenation from isopropanol to ketones and imines.[56,57] They noted that the same activity for the reduction of the imine $PhCH_2N{=}CMePh$ by 2-propanol catalyzed by the dihydride was observed whether KOH was present or not. The well-known transfer hydrogenation catalyst $RuCl_2(PPh_3)_3$ is inactive in the absence of a base. The authors suggested that the PPh_3 ligand is labile and dissociates from the dihydride complex with the opening of a coordination site. The dihydride complex then coordinates the imine to give an amide intermidate. Mizushima et al. provided evidence for this step by running the reaction with deuterium labels on the solvent and catalyst. When the solvent is CD_3OD and the precatalyst is $RuH_2(PPh_3)_4$, hydride is added to the imine $MePhC{=}NCH_2Ph$ and, after protonation, the corresponding amine was formed.[56] When the precatalyst is $Ru(H)(D)(PPh_3)_4$ in CD_3OD both hydride and deuteride are added to the imine. The last steps in Scheme 14 have not been detected but are reasonable based on precedents in the literature. The amido complex is thought to react with 2-propanol to produce an alkoxide complex and the product amine. A stoichiometric reaction of this type has been observed by Bryndza et al. where the ruthenium amido complex

$Ru(C_5Me_5)(NHPh)(PMe_3)_2$ reacts with MeOH to produce the alkoxide $Ru(C_5Me_5)(OMe)(PMe_3)_2$.[58]

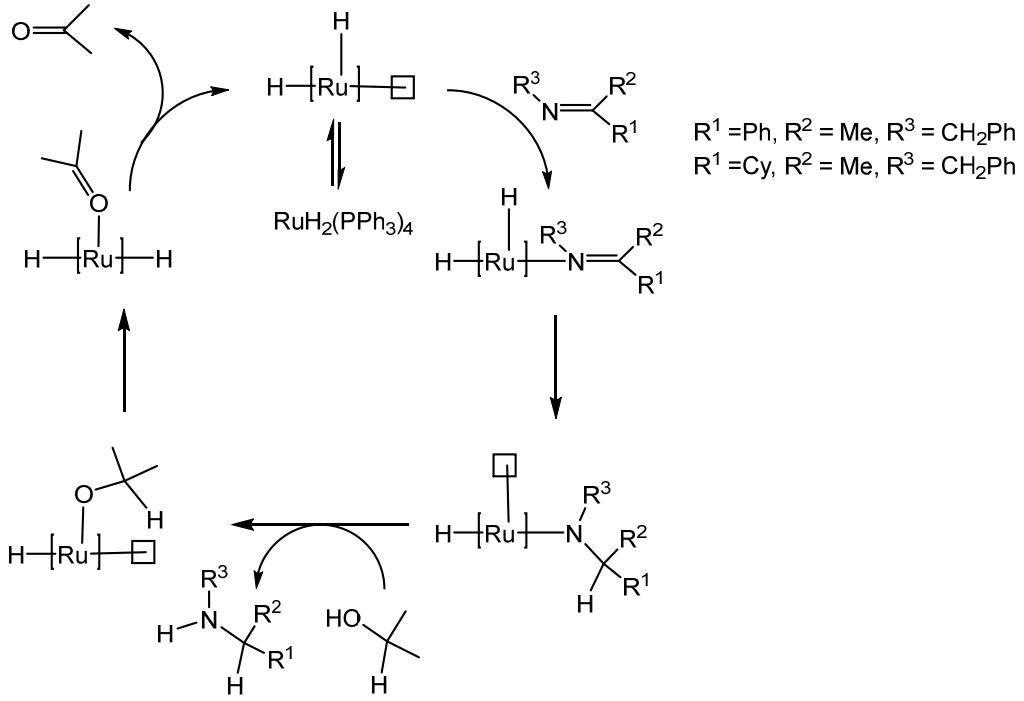

Scheme 14. The TH *inner sphere* mechanism of imines, catalyzed by the complex $RuH_2(PPh_3)_4$.

2.2 TH of the substrate by the *outer sphere* mechanism with ancillary ligand assistance

The mechanism of the catalytic reduction of ketones with the Noyori-Ikaria catalysts **L9** showed the importance of the presence of a NH group for a highly selective reaction. A thorough study of the mechanism showed that the NH-group of the ligand participates in the catalytic cycle, contributing to the realization of a highly organized six-membered pericyclic transition state (Scheme 15). For such catalysts, Prof. Noyori introduced the term «metal-ligand bifunctional catalysis».[32,35]

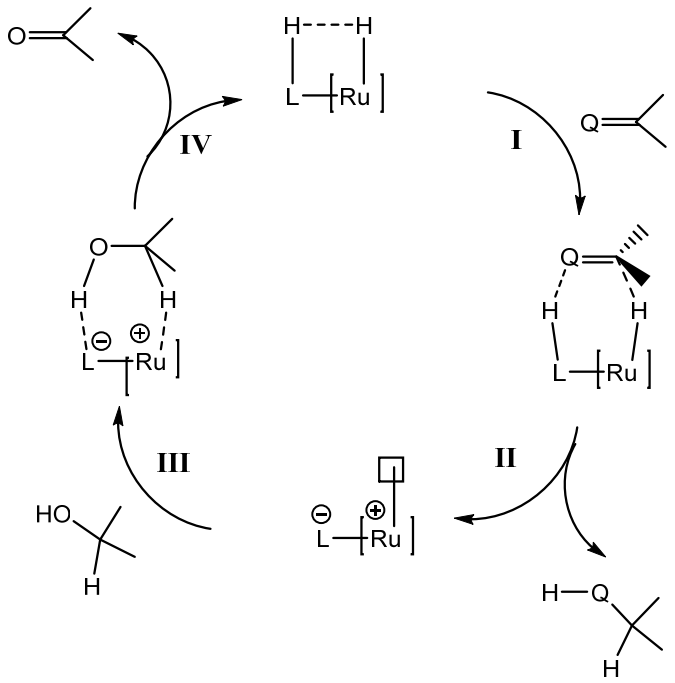

Scheme 15. TH of unsaturated substrates by *outer sphere* mechanism with the assistance of the ligand (Q = O, NR).

Scheme 15 refers to the general case of hydrogen transfer from a hydrogen source YCHOH to the metal, where Y can be R_2, as in isopropanol, or O, as in formic acid. In steps I and II there is concerted or stepwise transfer of H^+ from the ligand and H^- from the ruthenium complex to the substrate $R^1R^2C = Q$, where Q = O, NR^3. This results in the hydrogenated product $R^1R^2CH\text{-}QH$ and the creation of, formally, a 16-electron Ru center. The ruthenium hydride is then thought to be regenerated by a pericyclic transition state structure involving the hydrogen donor RCH_2OH. Thus, the ligand is actively involved in the catalytic cycle, since it a) ensures the precoordination of the substrate to reduce the entropy barrier, b) activates the carbon atom of the substrate through the formation of a hydrogen bond with the heteroatom and serves as a proton source and c) provides enantioselective recognition of the prochiral substrate. Usually, the substrate is located in the outer coordination sphere of the catalytic complex and is not coordinated directly with the metal.

In particular, the catalytic mechanism for the TH of ketones (Scheme 16) with such complexes consists in the concerted transfer of a proton and hydride from **L9a** to the substrate through a cyclic six-membered transition state, leading to alcohol and a 16-electron complex of **L9b**. The regeneration of **L9a** occurs as a result of the reverse reaction

of the transfer of a proton and a methine hydrogen atom from isopropanol to the nitrogen atom of the ligand and the metal, respectively.

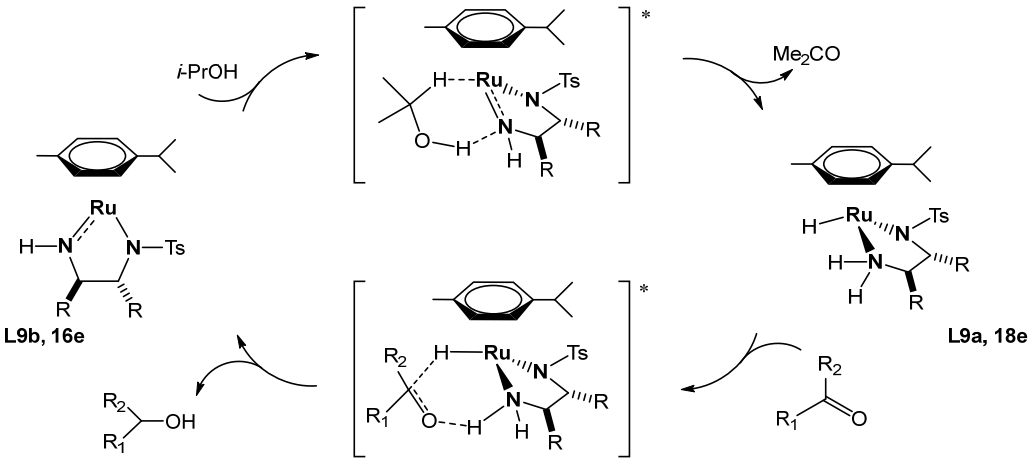

Scheme 16. Catalytic cycle of **L9** through a consistent six-membered transition state.

To confirm this mechanism, DFT calculations were performed, which showed that the isolated complexes **L9a** and **L9b** are active intermediates of TH.[55,59,60]

Thus, over the past two decades, significant progress has been made in the creation of new active reaction catalysts. Thanks to the development of experimental research methods and to the contribution of theoretical calculations, an improved understanding of the reaction mechanisms of TH, determining the activity and enantioselectivity of catalysts, has been achieved.

II. Discussion of the results.

II.1. Synthesis, structure and reactivity of arene ruthenium iminophosphonamides complexes.

The new 18ē arene chloride ruthenium NPN complexes (**3**) were synthesized from the arene dichloride complexes $[(\eta^6\text{-Arene})RuCl_2]_2$ by metathesis exchange with iminophosphonamide anions, which formed in situ by the deprotonation of aminoiminophosphoranes (**1**). In turn, **1** was obtained by the monodeprotonation of the diaminophosphonium salts (**2**), which was synthesized by Kirsanov' condensation from the *in situ* generated bromophosphonium salts with primary amines.[61] The general synthesis is summarized in Scheme 18.

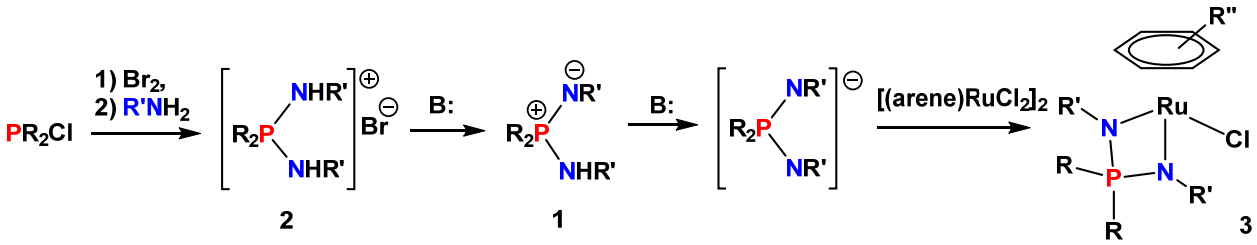

Scheme 18. Synthesis of the arene ruthenium NPN complexes **3**.

II.1.1. Synthesis of aminoiminophosphoranes 1.

Aminoiminophosphoranes **1a-e** with differing substituents at the nitrogen and phosphorus atoms were used as precursors of NPN ligands (Figure 8).

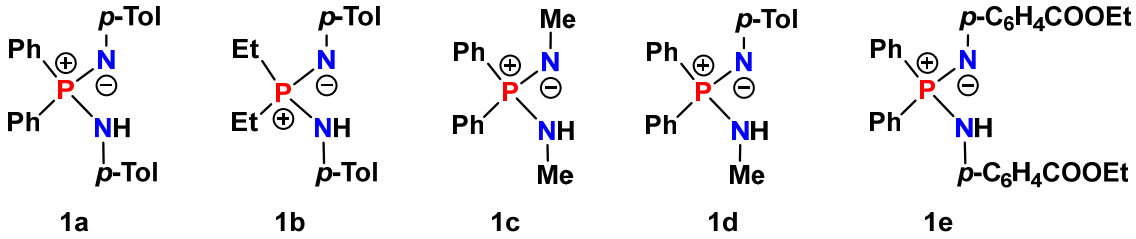

Figure 8. Aminoiminophosphoranes 1a-e.

The diaminophosphonium salts $[R_2P(NHR')_2]Br$ (**2**) were prepared in high yields, according to the earlier developed procedure.[61] They were synthesized by the interaction

of the primary amines with *in situ* generated trihalophosphoranes (Scheme 19). The obtained diaminophosphonium salts $[R_2P(NHR')_2]Br$ (**2a-c,e**) are listed in Table 6.

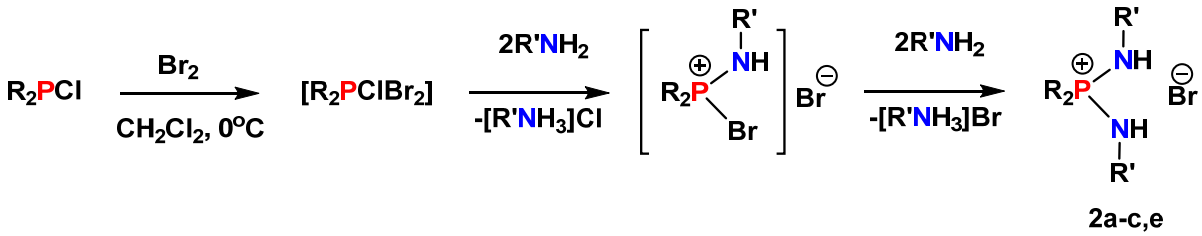

Scheme 19. Synthesis of diaminophosphonium salts **2a-c,e**.

Table 6. Yields in synthesis of diaminophosphonium salts $[R_2P(NHR')_2]Br$ (**2a-c,e**).

№	R	R'	Yield
2a	Ph	*p*-Tol	75%
2b	Et	*p*-Tol	82%
2c	Ph	Me	80%
2e	Ph	*p*-C_6H_4-CO_2Et	35%

It should be noted that the second step of the amination of bromophosphonium salt $[R_2P(NR')Br]Br$ intermediate is relatively slow. In light of this it is necessary to use an excess of amine (0.2 – 1 equiv.) to increase the product yield. Otherwise, the residual monoamine bromophosphonium salt intermediate was hydrolyzed during the final work up to the aminophosphine oxide $[R_2P(NHR')O]$,[61], which is difficult to separate.

In addition, the improvement of the purification procedure for **2a-c** relative to the reported literature procedure allows reaching higher yields. The final recrystallization was performed from ethanol for **2a** and from a CH_2Cl_2/ethyl acetate mixture for **2b**, whereas **2c** was purified by rinsing with benzene and acetone. The diaminophosphonium salts **2a-c,e** were characterized by NMR spectroscopy (^1H, $^{31}P\{^1H\}$, $^{13}C\{^1H\}$) and by elemental analysis. In the ^1H NMR spectrum, the NH hydrogen of **2a** (δ 9.26) is more acidic than the NH groups of **2b** (δ 8.77) and **2c** (δ 6.61) thus reflecting the electron-releasing effect of the N- and P-substituents on the electron density at the nitrogen atoms.

The diaminophosphonium salts can then be deprotonated to give the aminoiminophosphoranes (**1**) (Scheme 20) and the iminophosphonamide anions. The

monodeprotonation of the salts **2a-c,e** formed the corresponding aminoiminophosphoranes (**1a-c,e**) in quantitative yields (Table 7).

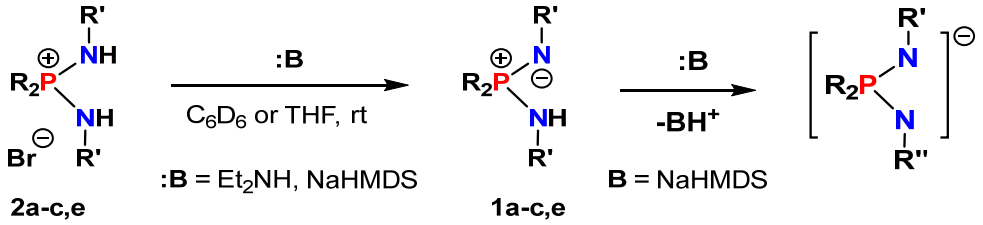

Scheme 20. Synthesis of aminoiminophosphoranes **1a-c,e**.

Table 7. Yields in synthesis of aminoiminophosphoranes $R_2P(NHR')(NR')$ (**1a-c,e**).

№	R	R'	:B	Yield
1a	Ph	Tol	Et_2NH	97%
1b	Et	Tol	NaHMDS	92%
1c	Ph	Me	NaHMDS	96%
1e	Ph	*p*-C_6H_4-CO_2Et	Et_2NH	98%

Earlier in our laboratory, *n*-BuLi was employed to obtain aminoiminophosphoranes **1a-c,** and only **1a** was synthesized in high yield. The results of the reaction of **1b,c** with *n*-BuLi were poorly reproduced and the yields were relatively low,[63] because the isolation of these aminoiminophosphoranes is very laborious due to their complexation with lithium salts. In this work, we showed that the compounds **2b,c** can be monodeprotonated by 1 equiv. of strong bases like sodium bis(trimethylsilyl)amide (NaHMDS) to give the corresponding aminoiminophosphoranes **1b,c** with quantitative yields and these products are easily isolated. The more acidic **2a** and **2e** are deprotonated easily with equimolar amount of diethylamine (Et_2NH) and triethylamine (Et_3N). The most convenient base was Et_2NH, since the byproduct $[Et_2NH_2]Br$ is more fully precipitated from the reaction solution in benzene than $[Et_3NH]Br$.

The synthesis of a new aminoiminophosphorane **1d** with asymmetrically substituted nitrogen atoms (R'= Me/*p*-Tol) was accomplished by stepwise amination of trihalophosphoranes with *p*-toluidine (2 equiv.) and methylamine (Scheme 21). In this reaction, the second step of amination is carried out with a significant excess of

methylamine and the diaminophosphonium salt **2d** is immediately deprotonated by a strong base to **1d**.

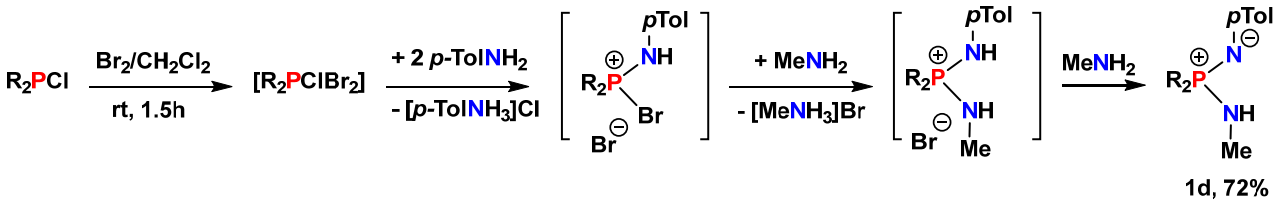

Scheme 21. Synthesis of aminoiminophosphorane **1d**.

The synthesized aminoiminophosphoranes **1a, 1b, 1d, 1e** were characterized by NMR spectroscopy (^{1}H, ^{31}P{^{1}H}, ^{13}C{^{1}H}) and by elemental analysis. We were not able to obtain a satisfactory elemental analysis and ^{13}C{^{1}H} NMR for **1c** due to its high moisture sensitivity. Therefore, compound **1c** was characterized only by ^{1}H and ^{31}P{^{1}H} NMR spectroscopy.

In the ^{31}P{^{1}H} NMR spectrum the phosphorus signals of **1a-e** (δ -3.5 – +23.3) are shifted by 27-32 ppm to less positive values compared to those of **2a-c, 2e** (δ +27.7 – +50.4) due to the appearance of a negative charge on the nitrogen atom. In the ^{1}H NMR spectrum, the NH resonances are significantly shifted to higher fields: **1a** (δ 5.55), **1b** (δ 3.85), **1d** (δ 2.16), **1e** (δ 6.29). The signals from the chemically inequivalent substituents at the nitrogen atoms in aminoiminophosphoranes **1** are averaged, tentatively due to rapid intramolecular N-H…N proton exchange.[64] The same exchange mechanism is presumably responsible for not observing the NH signal for **1c**.

It should be noted that, in contrast to the diaminophosphonium salts **2**, which are resistant to moisture, the aminoiminophosphoranes **1** are easily susceptible to hydrolysis, and their moisture sensitivity rises with the basicity of nitrogen atoms (donor N-substituents). Apparently, the hydrolytic instability of **1** is due to the presence of a highly basic anionic center on the nitrogen atom, which can serve as a hydroxide ion source in an equilibrium acid-base reaction with water molecules (Scheme 22). The final hydrolysis products are stable aminophosphine oxides, which do not have basic nitrogen atoms.

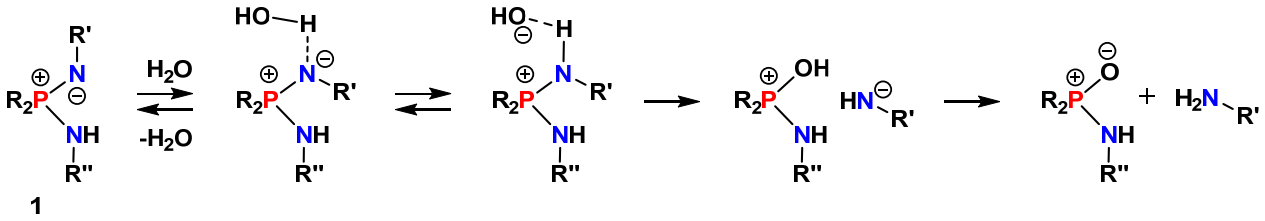

Scheme 22. Possible mechanism of hydrolysis **1**.

Further deprotonation of **1a-e** with 1 equiv. of a strong base results in the formation of salts of iminophosphonamide anions $[R_2P(NR')(NR'')]^-M^+$ (**[1a-e]**$^-$) (Scheme 23). These salts are usually not isolated due to extremely high moisture sensitivity. They are generated *in situ* and are directly used in ligand exchange reactions.[65-67]

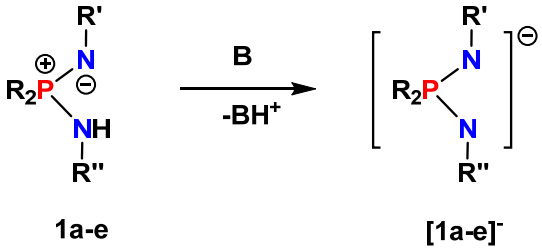

Scheme 23. Generation *in situ* of iminophosphonamide anions **[1a-e]**$^-$.

II.1.2. Synthesis of arene ruthenium iminophosphonamides complexes.

The sodium iminophosphonamides $[R_2P(NR')(NR'')]^-Na^+$, generated *in situ* by reaction of **1a-d** with NaHMDS, react with the dimeric ruthenium complex $[(\eta^6\text{-}C_6Me_6)Ru(\mu\text{-}Cl)Cl]_2$ to give the corresponding 18 electronic (18ē) arene ruthenium hexamethylbenzene complexes (**3a-d**) with the chelating bidentate NPN ligand (Scheme 24). Similar complexes with the *p*-cymene arene (**3e,f**) are easily obtained by interaction between the relatively acidic **1a,e** with $[(\eta^6\text{-}p\text{-cymene})Ru(\mu\text{-}Cl)Cl]_2$ in the presence of 1.2 equiv. of Et_2NH. Complexes **3a-f** are formed in high yields; noticeable loss of the product only occurs during isolation in the case of the most moisture-sensitive complexes **3b-d** (Table 8).

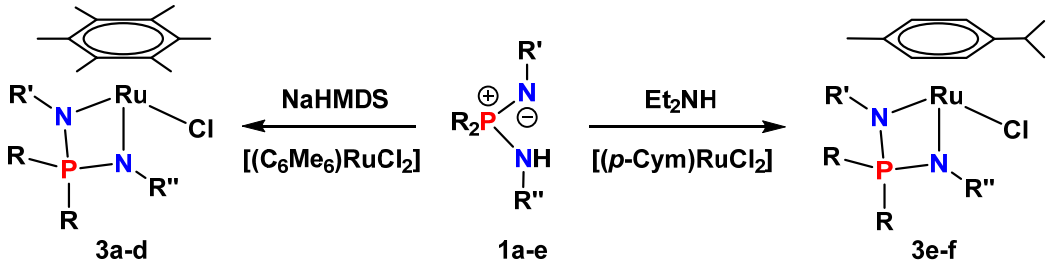

Scheme 24. Synthesis of 18ē ruthenium chloride NPN complexes **3a-f**.

Table 8. Yields in synthesis of ruthenium complexes [(η^6-Arene)RuCl{$R_2P(NR')(NR'')$}] (**3a-f**).

№	R	R', R"	Arene	Yields
3a	Ph	*p*-Tol	C_6Me_6	86%
3b	Et	*p*-Tol	C_6Me_6	73%
3c	Ph	Me	C_6Me_6	62%
3d	Ph	*p*-Tol, Me	C_6Me_6	77%
3e	Ph	*p*-$C_6H_4CO_2Et$	*p*-cymene	93%
3f	Ph	*p*-Tol	*p*-cymene	88%

In the $^{31}P\{^1H\}$ NMR spectra of **3a-f** in C_6D_6 the phosphorus resonance is shifted to more positive values (δ 42.9 – 71.1) compared to the corresponding aminoiminophosphorane precursors. In the ^1H and $^{13}C\{^1H\}$ NMR spectra in C_6D_6 the two chemically inequivalent substituents at the phosphorus atom give two set of signals, whereas the substituents at the nitrogen atoms are equivalent and are represented by one set of signals. The ^1H, $^{31}P\{^1H\}$ and $^{13}C\{^1H\}$NMR spectra of complexes **3a-f** strongly depend on the solvent and temperature, which is caused by the exchange processes occurring in solutions of these complexes. A detailed description of these processes and their study by NMR spectroscopy will be described in Section II.1.4.1.A.

The chloride ligand in **3a-c** was easily exchanged with the non-coordinating anions (PF_6^-, BF_4^-) by treating with the corresponding sodium salts in dichloromethane to afford the new 16ē cationic complexes **4a-c** (Scheme 25) in nearly quantitative yields (Table 9). As it turns out, the replacement of C_6Me_6 in **3a** with *p*-cymene leads to the strengthening of the Ru-Cl bond, thus removal of the chloride anion in complex **3f** occurs only under the action of a soluble silver salt with the formation of the cationic complex **4f**.

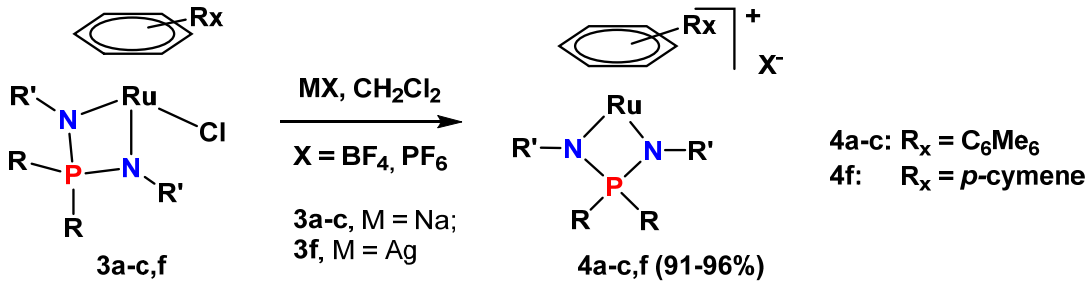

Scheme 25. Synthesis of 16ē ruthenium cationic NPN complexes **4a-c,f**.

The complexes **4a-c,f** were fully characterized by NMR spectroscopy (^{1}H, ^{31}P{^{1}H}, ^{13}C{^{1}H}) and elemental analysis. Their molecular structures were confirmed by single crystal X-ray diffraction studies and it is discussed in Section II.1.3.

Table 9. Yields in synthesis of ruthenium complexes [(η^{6}-Arene)Ru{$R_2P(NR')_2$}]$^{+}X^{-}$ (**4a-c,f**).

№	R	R’	Arene	$M^{+}X^{-}$	Yields
4a	Ph	*p*-Tol	C_6Me_6	$NaPF_6$	96%
4b	Et	*p*-Tol	C_6Me_6	$NaBF_4$	93%
4c	Ph	Me	C_6Me_6	$NaPF_6$	96%
4f	Ph	*p*-Tol	*p*-cymene	$AgPF_6$	91%

Due to the appearance of a positive charge, the phosphorus resonance of the 16ē cationic complexes **4a-c,f** in the ^{31}P{^{1}H} NMR spectra is strongly shifted by ~30 ppm to more positive values compared to the neutral complexes **3a-c,f**. In the ^{1}H and ^{13}C{^{1}H} NMR spectra of **4a-c,f** the N-and P-substituents are chemically equivalent, which indicates the presence of symmetry planes passing through the NPN and RPR planes (C_{2v}-symmetric complexes in solution). X-ray diffraction studies also confirm this symmetry in the crystal (Section II.1.3).

It is important to note that all 16ē complexes **4a-c,f**, in spite of their formal electronic unsaturation, are remarkably stable in solution to air and moisture in sharp contrast to the 18ē complexes **3a-c,f**, which hydrolyze to produce the corresponding phosphine oxides $R_2P(O)(NHR')$.

Thus, as a result of the synthetic work, a series of 10 new neutral 18ē and cationic 16ē arene ruthenium iminophosphonamides complexes with various N- and P-substituents in the NPN ligand and with different arenes, was obtained.

II.1.3. Structures of the arene ruthenium iminophosphonamide complexes.

Molecular structure.

The molecular structures of the arene ruthenium chloride NPN complexes **3a-f** (Figure 9-14) and of the cationic NPN complexes **4a-c,f** (Figure 15-18) were confirmed by single crystal X-ray diffraction studies. The selected structural parameters are given in Table 10 and 11.

The 18ē complexes **3a-f** exhibit a three-legged piano stool geometry with a pseudo octahedral configuration of the ligands around the ruthenium atom: three coordination sites occupied by the η^6-arene, two by the chelate κ^2- NPN ligand and one by the chloride ligand.

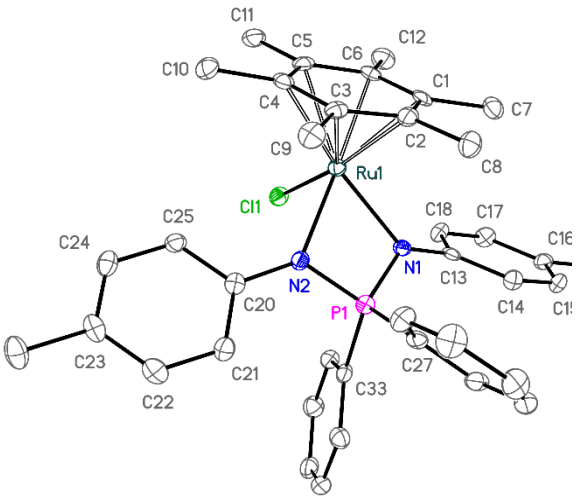

Figure 9. ORTEP diagram of the complex **3a**.

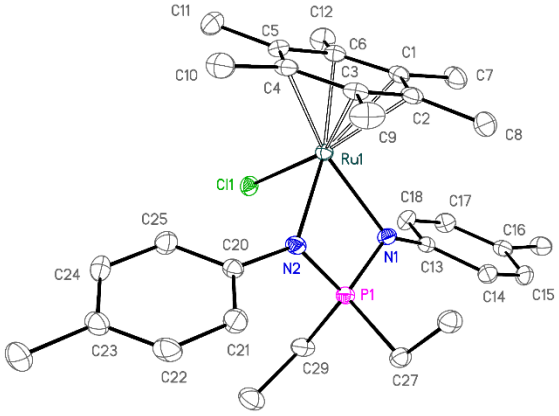

Figure 10. ORTEP diagram of the complex **3b**.

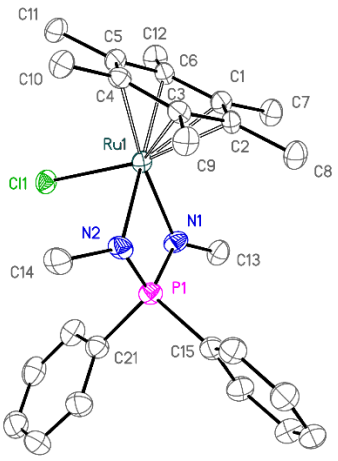

Figure 11. ORTEP diagram of the complex **3c**.

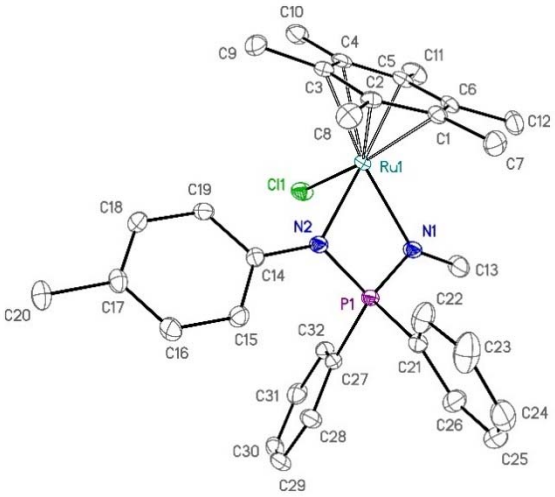

Figure 12. ORTEP diagram of the complex **3d**

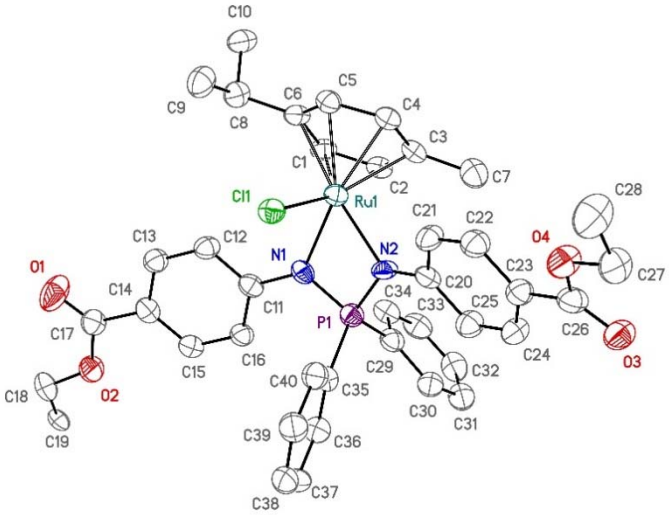

Figure 13. ORTEP diagram of the complex **3e.**

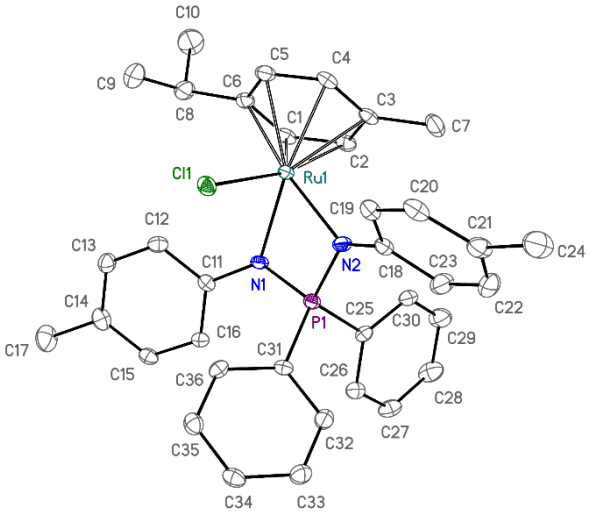

Figure 14. ORTEP diagram of the complex **3f**

Table 10. Selected geometrical parameters of complexes **3a-f**.

Parameters	3a	3b	3c	3d	3e	3f
			Distances (Å):			
Ru…Arene(centroid)	1.675(3)	1.666(2)	1.662(4)	1.673(2)	1.660(8)	1.667(2)
Ru–C(arene)	2.175 – 2.233(3)	2.171 – 2.217(2)	2.159 – 2.218(4)	2.167 – 2.242(2)	2.17 – 2.25 (2)	2.153 – 2.216(2)
Ru–N_1	2.137(2)	2.151(2)	2.137(4)	2.137(2)	2.147(8)	2.145(2)
Ru–N_2	2.171(2)	2.161(2)	2.159(4)	2.174(1)	2.145(5)	2.126(2)
P–N_1	1.600(2)	1.603(2)	1.605(4)	1.589(2)	1.625(6)	1.606(3)
P–N_2	1.613(3)	1.615(2)	1.602(4)	1.617(2)	1.591(8)	1.600(2)
Ru–Cl	2.438(3)	2.437(2)	2.445(4)	2.428(4)	2.411(2)	2.415(1)
			Angles (°):			
N_1–Ru–N_2	68.08(9)	68.08(7)	69.39(14)	68.27(6)	67.9(2)	68.24(9)
N_1–P–N_2	97.30(12)	97.22(10)	99.36(19)	97.96(8)	96.3(4)	96.73(13)
Ru–N_1–P	97.98(11)	96.81(9)	95.94(18)	98.04(8)	96.3(4)	96.88(12)
Ru–N_2–P	96.25(11)	96.07(9)	95.15(17)	95.73(7)	98.2(3)	97.84(12)
Ru–N_1–N_2–P	173.7(15)	166.3(12)	175.9(3)	179.5	171.8(5)	174.27(15)
Arene(centroid)-Ru-P	142.2	148.7	148.2	145.7	140.6	142.2
Σ(N_1)	359.2(5)	354.5(4)	357.6(8)	358.9	357.7	357.2(6)
Σ(N_2)	358.6(5)	354.6(4)	344.4(8)	356.9	359.5	358.2(6)

In the chloride complexes **3a-f**, the main structural parameters are similar: the Ru-arene(centroid) distance is in the 1.660 – 1.675 Å range, the average Ru-N bonds are in the 2.135 – 2.156 Å interval, the P-N bonds are in the 1.603 – 1.609 Å interval, the Ru-Cl bonds are 2.411 – 2.445 Å, and the N_1-Ru-N_2 chelate angles (68.0 – 69.4°) are almost the same.

The effect that the substituents on the nitrogen and phosphorus atoms have on geometric parameters was analysed for the series of complexes **3a-c**. Complexes **3a,b**, differing by the phosphorus substituents (Ph in **3a**, Et in **3b**) have similar average Ru-N (2.154 Å and 2.156 Å, respectively) and Ru-Cl (2.438 Å and 2.437 Å, respectively) bonds lengths. This suggests that the nature of the P substituents do not have a significant effect on the strength of the NPN ligand binding. The introduction of more donor substituents at the nitrogen atom in complex **3c**, as compared with **3a**, shortens the Ru-N bond (2.148 Å)

and lengthens the Ru-Cl bond (2.445 Å). It should be noted that complex **3a** has a significant difference in the two Ru-N bond lengths (Ru-N_1, 2.137 Å; Ru-N_2, 2.171 Å), which is probably due to the weak intramolecular CH···Cl bonding interaction with one *ortho*-hydrogen (H_{18A}) of the N_2-tolyl substituents. In **3b**, there are two symmetric C-H···Cl contacts with *ortho*-H (H_{18A}, H_{25A}) of both N-tolyl substituents. The H_{18A}···Cl distances in **3a** (2.762 Å) and in **3b** (2.813 Å) fall below the sum of the van der Waals radii of 2.95 Å[68,69] and the corresponding Cl···H-C angles (140.4° in **3a** and 140.8° in **3b**) are typical for such type of non-directed interactions. In both structures, the chlorine atom is almost coplanar with the plane of the tolyl ring involved in the H···Cl contact and the corresponding Cl-H_{18A}-C_{18}-C_{13} torsion angle is 7.6° and 8.4° for **3a** and **3b**, respectively. A few other H···Cl intra- and intermolecular close contacts are observed in **3a,b** with the hydrogen atoms of the C_6Me_6 ligand (the Cl···H_{11C}, Cl···H_{11B} distances in **3a** are 2.772, 2.749 Å and the Cl···H_{11C}, Cl···H_{8A} distances in **3b** are 2.899, 2.871 Å) and of the P-substituent (in **3a**, Cl···H_{34A} = 2.868 Å; in **3b**, Cl···H_{29A} = 2.812 Å). Similar intra- and intermolecular close contacts can be seen in **3c** between the chlorine atom and the hydrogen atoms of the N_2-bonded methyl group (Cl···H_{14B} = 2.872 Å) and of C_6Me_6 (Cl···H_{10C} = 2.840 Å).

Similarly to a previously published β-diketiminate arene ruthenium complex,[70] the η^6-coordinated arene in both **3a,b** has a staggered conformation with respect to the N,N,Cl atoms. The C-C bonds length in the arene noticeably alternate: the C_2-C_3, C_4-C_5 and C_1-C_6 bonds, which are *trans* to N_1, N_2 and Cl_1, are significantly shorter (1.412 – 1.421 Å for **3a** and 1.417 – 1.423 Å for **3b**) than the C_1-C_2, C_3-C_4 and C_5-C_6 bonds (1.436 – 1.442 Å for **3a** and 1.442 – 1.447 Å for **3b**). In contrast to that, the coordinated arene in **3c** shows a nearly eclipsed conformation with the chloride and the NPN ligand, only N_1 significantly deviating from the Ru-C_6Me_6(centroid)-C_1 plane with a N_1-Ru-C_6Me_6(centroid)-C_1 torsion angle of 18.5°. This results in a shortening of the C_4-C_5 bond *trans* to N_1 (1.417 Å), while the other C-C bonds are slightly longer (1.428 – 1.441 Å).

It was expected that the Ru-Cl bond length in**3d** with asymmetric N-substituents would be intermediate between those in **3a** (2.438 Å) and **3c** (2.445 Å). On the other hand, this distance (2.428 Å) is even slightly shorter than in **3a**. It is likely that the small variability of the Ru-Cl bond length (± 0.01 Å) is mainly associated with intra- and

intermolecular contacts in the crystal packing, and therefore cannot be used to compare the Ru-Cl bond strength in the series of complexes **3a-d**.

The effect of the arene ligand is most observed on the Ru-N and Ru-Cl distances. When going from hexamethylbenzene (**3a**) to the *p*-cymene ligand (**3f**), these distances shorten by ~ 0.02 Å (the average Ru-N and Ru-Cl bond lengths are 2.154 Å and 2.438 Å in **3a** and 2.135 Å and 2.415 Å in **3f**, respectively). Analogously, a shortened Ru-Cl bond (2.411 Å) is also observed for the *p*-cymene complex **3e**. Such a simultaneous Ru-N and Ru-Cl bond shortening suggests that the poorer donating and lower steric requirements of the *p*-cymene ligand relative to C_6Me_6 lead to a strengthening of the Ru-N and Ru-Cl bonds.

An important structural characteristic of these iminophosphonamide complexes is the geometry of the four-member RuNPN metallacycle. The Ru-N_1-N_2-P torsion angle α in **3a-f** is close to 180° showing small puckering of the RuNPN metallacycle from planarity (180–α angle is 6.3° for **3a**, 13.7° for **3b**, 4.1° for **3c,** 0.5° for **3d**, 8.2° for **3e**, 5.7° for **3f**). It is worth noting that the pyramidalization of the nitrogen atoms is rather small in all **3a-f** complexes (Σ(N) is in the 354.5 – 359.2° range), while it is strong for one of the nitrogen atoms (N_2) in **3c**, for which the sum of the bond angles is 344.4°. The N_2 pyramidalization in **3c** indicates that a high unpaired electron density is localized on this atom and notably cannot be delocalized on any other electron system, such as the aromatic N-tolyl groups in **3a,b,d,f**. In fact, as shown by a recent computational study, the puckering of the MNPN metallacycle and the pyramidilization of nitrogen atoms in the iminophosphonamide complexes are low-energy processes and can vary over a wide range only due to the effects of crystal packing.[71]

In the literature, there are structural data on related arene ruthenium complexes with amidinate ligands (NCN) and triazenide ligands (NNN). In iminophosphonamide complexes **3a-f** the Ru-N bonds (2.135 – 2.156 Å) and the Ru-Cl bonds (2.411 – 2.445 Å) are slightly longer than those in analogous 18ē arene ruthenium amidinate (2.078 – 2.139 Å and 2.400-2.434 Å, respectively)[72-76] or triazenide (2.104 – 2.133 Å and 2.386-2.397 Å, respectively)[77] complexes, perhaps due to high negative charge located at the nitrogen atoms of the zwitterionic NPN ligand. The Ru–Cl bond is elongated in arene ruthenium complexes with highly efficient σ,π-donating β-diketiminate (2.461 – 2.521 Å)[70,78,79] or dianionic bis(imidazolin-2-iminate) (2.485 Å)[80] ligands. The Ru-C_6Me_6(centroid)

distances in the NPN complexes are close (within 0.01 Å) to those reported in the literature for NCN complexes.[72] It is important to note that the N_1-Ru-N_2 chelate angle in **3a-f** (68.1 – 69.4°) is significantly larger than that in the analogous 18ē ruthenium amidinate complexes 61.6 – 62.7°),[72-75,81] since the P-N bonds are longer than the corresponding C-N bonds in the amidinates. In the 18ē NCN complexes the pyramidalization of the nitrogen atoms is insignificant (Σ(N) are 359.8 – 355.5°), and the puckering of the metallacycle from the planarity is in the 10-15° range.[71] A more significant puckering (18.3°)[75] is possible only for sterically loaded structures.

Moving from the neutral 18ē chloride complexes (**3a-f**) to the cationic 16ē ruthenium complexes (**4a-c,f**), significant changes are observed in the structural parameters (Figure 15-18, Table. 11). The 16ē cationic complexes **4a-c,f** expectedly exhibit a two-legged piano-stool geometry with the chelating NPN ligand positioned nearly perpendicular to the arene ring; the C_6Me_6(centroid)-Ru-P angle is 174.1 – 176.8°. The Ru-Arene(centroid) distance is 1.652 – 1.675 Å, similar to that in **3a-c,f** (1.662 – 1.675 Å). The Ru-N bonds lengths in **4a-c,f** (2.016 – 2.043 Å) are significantly shorter than in **3a-c,f** (2.136 – 2.156 Å) due to stronger binding with the positively charged ruthenium atom and its electronic unsaturation. It is known that the NPN ligand can act not only as a strong σ-donor but also as a π-donor and is therefore able to compensate the electron deficiency at the metal center. Obviously, in the complexes **4a-c, f**, the NPN ligands are 6ē σ,π-donors, which leads to the strengthening of Ru-N bonds.

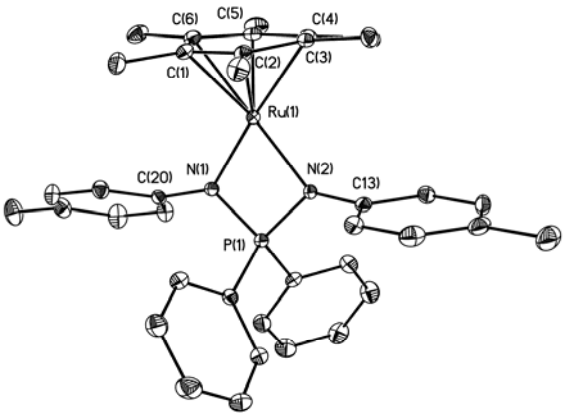

Figure 15. ORTEP diagram of the complex **4a**

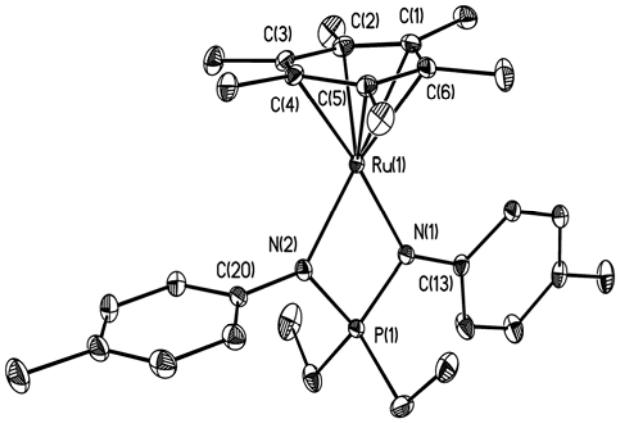

Figure 16. ORTEP diagram of the complex **4b**

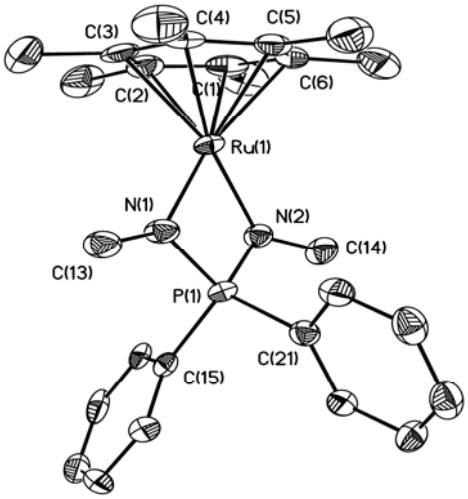

Figure 17. ORTEP diagram of the complex **4c**.

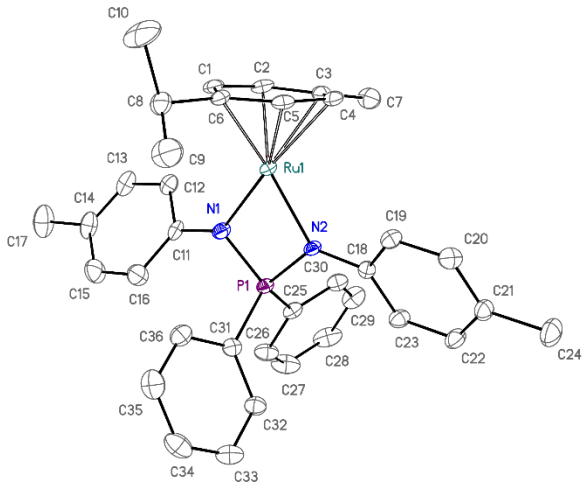

Figure 18. ORTEP diagram of the complex **4f.**

Table 11. Selected geometrical parameters of 16ē complexes **4a-c,f**.

Parameters	4a	4b	4c	4f
		Distances (Å):		
Ru…Arene(centroid)	1.662(2)	1.675(1)	1.652(4)	1.659(3)
Ru–C(arene)	2.149 – 2.252(2)	2.143 – 2.275(1)	2.142 – 2.208(4)	2.159 – 2.204(3)
Ru–N_1	2.017(2)	2.0119(11)	2.011(4)	2.031(2)
Ru–N_2	2.036(2)	2.0733(10)	2.020(3)	2.017(3)
P–N_1	1.623(2)	1.6352(10)	1.615(4)	1.626(3)
P–N_2	1.624(2)	1.6233(10)	1.619(4)	1.627(3)
		Angles (°):		
N_1–Ru–N_2	72.33(9)	72.17(4)	72.93(14)	72.42(10)
N_1–P–N_2	94.87(12)	95.22(5)	95.57(18)	94.59(13)
Ru–N_1–P	96.54(11)	94.82(5)	95.50(17)	96.24(12)
Ru–N_2–P	95.81(11)	97.56(5)	95.01(17)	96.73(12)
Ru–N_1–N_2–P	173.23(15)	175.02(6)	169.7(2)	178.43(16)
Arene(centroid)–Ru–P	176.0	174.1	175.6	176.8
Ru–C_1–C_4/Ru–N_1–N_2	6.3	5.7	26.1	10.0
Σ(N_1)	360.0(5)	359.8(2)	359.0(8)	360.0(6)
Σ(N_2)	354.9(5)	360.0(2)	356.9(8)	358.9(5)

Among the **4a-c,f** complexes studied, there is a weak substituent effect at the Ru-Arene(centroid) and Ru-N bond lengths, which slightly shorten with the introduction of donor N-methyl substituents in **4c** to 1.652 Å and 2.016 Å, respectively, compared to the N-tolyl-substituted complexes **4a,b,f** (the Ru-Arene(centroid) distance is 1.659 – 1.675 Å and the Ru-N bond lengths are 2.027 – 2.043 Å. However, such small differences do not allow making significant conclusions, since in all the complexes there are multiple weak contacts with the counterion, which can also slightly affect their structural parameters.

In general, it should be noted that the metallacycle geometry in **4a-c,f** is almost the same: the N_1-Ru-N_2 chelate angle in **4a-c,f** is 72.2 – 72.9°, the nitrogen atoms pyramidalization is minimal (Σ(N) = 354.9 – 360.0°), and the Ru-N_1-P-N_2 metallacycle puckering from planarity is in the 1.6 - 10.3° range.

An essential structural feature of the **4a-c** complexes is that the C_6Me_6 ring is not planar but significantly distorted towards a boat conformation. In compounds **4a** and **4b,** four Ru–C(arene) bonds are shorter (2.149 – 2.178 Å in **4a** and 2.143 – 2.199 Å in **4b**) than the other two bonds, namely Ru-C_1 and Ru-C_4 (2.238, 2.252 Å for **4a** and 2.228, 2.275 Å for **4b**). Unlike in the 18ē complexes **3a,b**, the C-C bonds in C_6Me_6 in **4a,b** do not alternate, instead the bonds C_2-C_3 and C_5-C_6 (1.440 – 1.444 Å) are slightly longer than the other four C-C bonds (1.418–1.428 Å) as a result of stronger bonding of these carbon atoms with the ruthenium atom. Importantly, in **4a,b** the longer Ru-C_1 and Ru-C_4 bonds are always *trans* to the Ru-N bonds (the dihedral angle between the planes Ru-C_1-C_4 and Ru-N_1-N_2 is 5.7 – 6.3°) with the longest Ru-C_4 bond *trans* to the shortest Ru-N_2 bond. A similar arene ring distortion and the Ru-C(arene) bond distribution was previously observed for the only described arene ruthenium iminophosphonamide complex [(η^6-*p*-cymene)Ru{(^{i}PrN)$_2$PPh(NH^{i}Pr)}](BPh$_4$)[82] (**L20**) and for a dicationic arene ruthenium complexes with a bis(imidazolin-2-imine) ligand.[80] This ring distortion appears to be the result of effective back-bonding from the ruthenium atom to the arene ligand π-system.

Conversely, in **4c** the arene and the NPN ligand are in a staggered conformation (the dihedral angle between cymenen the planes Ru-C_2-C_5 and Ru-N_1-N_2 is 86.1°), which leads to slight shortening of the Ru-C_2 and Ru-C_5 distances (2.142, 2.163 Å) compared to the other four Ru-C(arene) bonds (2.177 – 2.208 Å) resulting in a flipped boat conformation of the arene. Similar to **4c**, the *p*-cymene ligand in **4f** is almost planar: the Ru-C_1 and Ru-C_4 (2.202 – 2.204 Å) are slightly longer than the other Ru-C(arene) bonds (2.159 – 2.180

Å). The orientation of the arene ligand in **4f** relative to the NPN ligand is close to that observed in compound **4a** (the angle between the Ru-C_1-C_4 and Ru-N_1-N_2 planes is 10.0°). This structural peculiarity may result from weaker back-bonding from the ruthenium atom to the arene ligand in **4f** and may be related to the lower donor ability of the *p*-cymene ligand and to the orientation of the ring substituents relative to the NPN ligand.

In the literature there is only one X-ray diffraction study of a cationic arene ruthenium complex with an amidinate ligand [(η^6-C_6Me_6)Ru(^{i}PrN-C(Me)-N^{i}Pr}](PF$_6$)[83] (**L21**) and one with an iminophosphonamide ligand (**L20**).[82] As for the NPN complexes, the Ru-N bonds lengths in the NCN complex are shorter and the chelate angle N-Ru-N is slightly larger than in corresponding 18ē chloride NCN complexes. However, the average of the Ru-N bond lengths for the NCN complex **L21** is notably bigger (2.062 Å)[83] than for the NPN complexes **4a-c,f** (2.016 – 2.043 Å) and for complex **L20** (2.014 Å).[82] Slightly shorter Ru–N distances were reported for 16ē cationic β-diketiminates (1.994 – 1.997 Å)[70] and bis(imidazolin-2-iminates) (1.977 – 2.003 Å)[80] due to the effective σ,π-donation from the nitrogen atoms of the κ^2-N,N-ligand to the metal. In contrast to 16ē ruthenium NPN complexes **4a-c,f** and **L20**, the chelate metallacycle Ru–N–C–N is strongly puckered in the analogous amidinate 16ē arene ruthenium complex **L21** (31.4°)[83] and [(C_5Me_5)Ru(^{t}BuN-C(Mes)-N^{t}Bu}] (**L22**) (39.8°).[84] This is required for additional stabilization of the coordinatively unsaturated species by a π-heteroallyl system.

Thus, the X-ray diffraction studies have shown that there are significant structural differences between the arene ruthenium iminophosphonamide complexes and related complexes with monoanionic amidinate or triazenide ligands. In chloride NPN complexes **3a-f** the Ru-Cl bonds are longer (by 0.02 – 0.04 Å), and in the cationic NPN complexes **4a-c,f** the Ru-N bonds are shorter (by 0.02 – 0.05Å) and the distortion of the metallacycle planarity is minimal MNPN (1.6 – 10.3°), relative to analogous arene ruthenium complexes with heteroallyl ligands. These structural parameters indicate the proximity of the electronic properties of monoanionic NPN, β-diketiminate and dianionic bis(imidazolin-2-iminate) ligands capable of effective σ,π-donation from the κ^2-N,N-ligand to a metal atom. Within the **3a-f** series, *p*-cymene strengthens the Ru-Cl bond, and more donor substituents at nitrogen atoms weaken it.

Electronic structure.

The metallacycle planarity and the shortened Ru-N bonds in the 16ē arene ruthenium iminophosphonamide complexes **4a-c,f**, as well as their greater stability, indicate stabilization of the electronically unsaturated ruthenium atom due to additional π-donation from the nitrogen atoms of the ligand. The highest occupied molecular orbital (HOMO) of zwitterionic NPN ligand may have either C_{2v} or C_s symmetry. The latter can efficiently donate the π-electron density from the nitrogen atoms to the d_{xz}-orbital of the metal located in the plane of ligand (Figure 19A). In contrast, the C_{2v} symmetry of the HOMO orbital in the amidinate ligand allows π-donation only by lateral coordination of the amidinate ligand resulting in a strong folding of the four-membered metallacycle (Figure 19B). Indeed, the electron deficient ruthenium NCN complexes can be stabilized by intramolecular π-coordination of the amidinate ligand, which leads to strong puckering of the Ru–N–C–N metallacycle,[83-84] The lateral coordination of the amidinate ligand stabilizes these 16ē complexes inefficiently since it weakens the M–N σ-bonds; such species are very reactive.

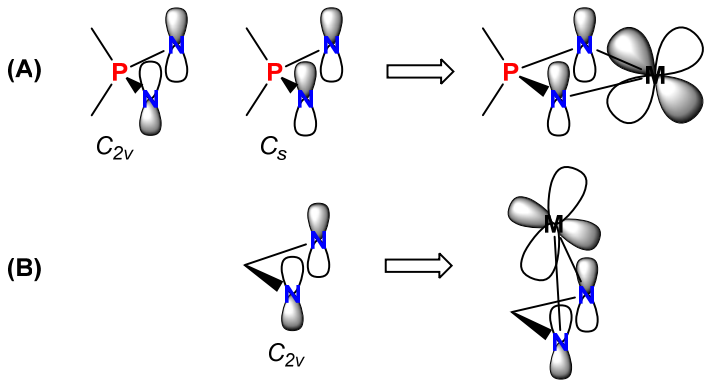

Figure 19. Schematic drawing of the HOMO orbitals of (A) NPN and (B) NCN ligands (on the left); possible π-bonding with the d-orbital of the metal (on the right).

Arene ruthenium NPN complexes were studied by UV-vis spectroscopy. In the UV-vis spectra the 16ē complexes **4a-c,f** have a broad medium intensity band at λ_{max} = 540 – 590 nm shifted to lower energies compared to the corresponding 18ē complexes **3a-c,f** having a band at λ_{max} = 430 – 450 nm (Figure 20). Similar bands have also been observed for 16ē pentamethylcyclopentadienyl amidinate [(C_5Me_5)Ru(^{t}BuN-C(Mes)-N^{t}Bu}] (**L22**)

(λ_{max} = 520–530 nm)[84] and dithiolate [(η^6-Arene)Ru(SXyl)$_2$] (λ_{max} = 660 – 700 nm) complexes.[85]

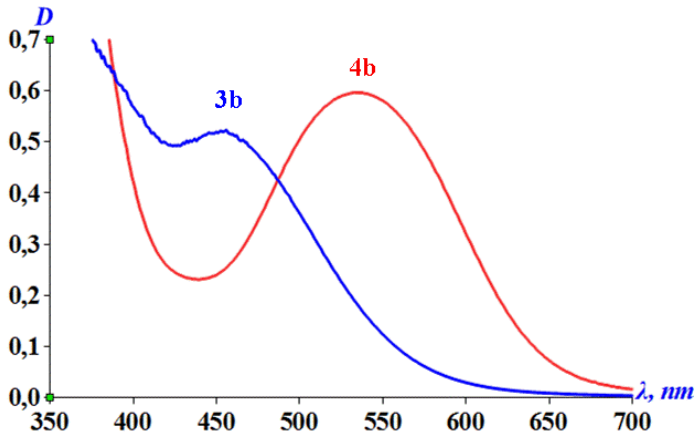

Figure 20. UV-vis spectra of complexes **3b** (18ē) and **4b** (16ē) in CH_2Cl_2 at room temperature.

In 18ē complexes **3a-b,f** the arene and phosphorus atom substituents do not affect the position of the absorption band in the UV-vis spectra (450 nm). Only the strongly donating Me groups on the N atoms in **3c** slightly shift λ_{max} to higher energies (430 nm) (Table 12). At the same time, in 16ē NPN complexes **4a-c,f** only the nature of the arene ligand is of primary importance for the position of the absorption band. Replacing the arene fragment C_6Me_6 (complexes **4a-c**) by *p*-cymene (complex **4f**) leads to a significant shift of the absorption band to lower energies (λ_{max} = 540-550 nm for **4a-c** and 590 nm for **4f**).

Table 12. λ_{max} the absorption bands for NPN complexes (CH_2Cl_2) in UV-vis spectra.

№	Complexes	λ_{max}, nm
3a	(η^6-C_6Me_6)RuCl{Ph_2P(N-*p*-Tol)$_2$}	450
3b	(η^6-C_6Me_6)RuCl{Et_2P(N-*p*-Tol)$_2$}	450
3c*	(η^6-C_6Me_6)RuCl{Ph_2P(N-Me)$_2$}	430
3f	(η^6-*p*-cymene)RuCl{Ph_2P(N-*p*-Tol)$_2$}	450
4a	[(η^6-C_6Me_6)Ru{Ph_2P(N-*p*-Tol)$_2$}]PF_6	540
4b	[(η^6-C_6Me_6)Ru{Et_2P(N-*p*-Tol)$_2$}]BF_4	540
4c	[(η^6-C_6Me_6)Ru{Ph_2P(N-Me)$_2$}]PF_6	550
4f	[(η^6-*p*-cymene)Ru{Ph_2P(N-*p*-Tol)$_2$}]PF_6	590

**toluene*

According to quantum chemical calculations by the density functional theory (DFT)[1] calculation performed for **3a**, **3f**, **4a** and **4f** in the gas phase with PBE functional and def2-TZVP basis set, the longer wavelength absorption band in the 16ē arene ruthenium NPN complexes is attributed to a *d-d** transition. The HOMO of complexes **4a** and **4f** is the antibonding combination of the ruthenium d_{xy} orbital with the A_2-symmetric group orbital of the NPN ligand (linear combination of the nitrogen atoms p_y orbitals, C_s symmetry of Figure 19A) and is located at a very similar energy for the two compounds (-7.4 eV in the gas phase and -5.1 eV in CH_2Cl_2 solution, Table 13). In both **4a** and **4f**, the lowest unoccupied molecular orbital (LUMO) is a combination of the ruthenium unoccupied d_{yz} orbital and occupied B_2 π-orbital of the arene ligand (Figure 21). The greater electron-donating ability of C_6Me_6 leads to a higher energy LUMO by 0.4 eV in **4a** compared to **4f** (Table 13). Hence, the bands observed at 540 nm (**4a**) and 590 nm (**4f**) in the UV-vis spectra appear consistent with a ligand-to-metal charge-transfer transition. The HOMO-LUMO gap for **4a** and **4f** are calculated in CH_2Cl_2 as 2.05 and 1.65 eV (Table 13), respectively, thus reflecting a significant red shift for the absorption of **4f** compared to **4a**.

It should be noted that the LUMO in complexes **4** is the orbital available to accept the electron pair donated by the external ligand (L or Cl) upon formation of the 18ē adduct.

[1] The calculation was carried out by Dr. Oleg A. Filippov (INEOS RAS, Moscow).

Hence, the lower energy of the LUMO in **4f** is responsible for the stronger bonding of chloride in the *p*-cymene complex vs those containing C_6Me_6, as reflected by the computed and measured Ru–Cl bond lengths.

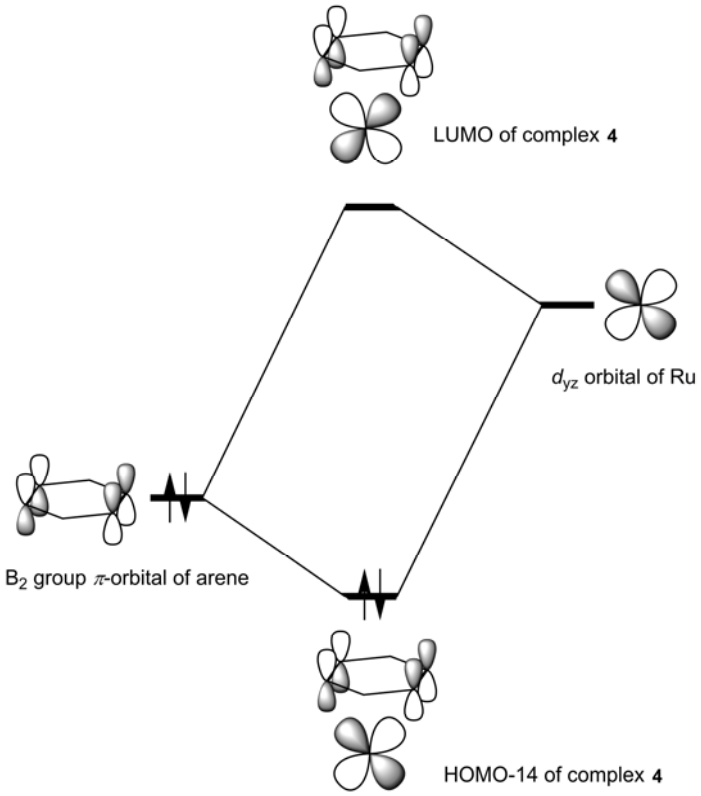

Figure 21. The schematic MO diagram of overlapping of d_{yz} orbital of Ru and B_2 π-orbital of arene in complexes **4**.

Table 13. The HOMO, LUMO energies and the HOMO-LUMO gap for **4a** and **4f** calculated in the gas phase and CH_2Cl_2 solution in comparison to the energy of the experimentally observed band (all in eV).

	4a		**4f**	
	Gas phase	**CH_2Cl_2**	**Gas phase**	**CH_2Cl_2**
HOMO	-7.45	-5.06	-7.37	-5.05
LUMO	-5.50	-3.01	-5.92	-3.40
Gap	1.95	2.05	1.45	1.65
Expt		2.32		2.10

II.1.4. Ligand exchange in the coordination sphere of the ruthenium atom in arene ruthenium iminophosphonamide complexes.

II.1.4.1. Dissociation of 18ē complexes 3.

From the X-ray diffraction study (Section II.1.3.), it was concluded that the Ru-Cl bond in the 18ē complexes **3** is relatively weak in comparison with related amidinate complexes. It was also shown that the corresponding cationic complexes **4** are stable, despite their formally unsaturated 16ē configuration. In this section, we report our studies, by NMR and UV-vis spectroscopy, probing the possibility of chloride dissociation from complexes **3a-d,f** in solutions with the formation of cationic complexes **[4]$^+$Cl$^-$** (Scheme 26).

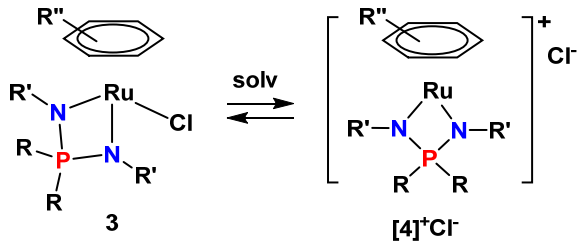

Scheme 26. Chloride dissociation from complexes **3**.

A) NMR spectroscopic studies.

Initial studies dealt with the chemical shift dependence of the phosphorus atom signal in the $^{31}P\{^1H\}$ NMR spectra of complexes **3a-c** as a function of on the solvent polarity (Table 14) at room temperature, relative to the position of the corresponding cationic **4a-c** complex resonance.

Table 14. Data of $^{31}P\{^1H\}$ NMR (δ, ppm) for **3a-c** in different solvents.

№	C_6D_6	Low polar solvents		Polar solvents		^{31}P for 4a-c in $CDCl_3$
		CD_2Cl_2	$CDCl_3$	$MeNO_2$	MeOD	
3a	43.3	–	43.9	–	69.9	71.9
3b	71.1	–	72.4	80.2	–	102.3
3c	59.8	68.4		–		80.8

The $^{31}P\{^{1}H\}$ NMR resonances of **3a-c** are highly dependent on the polarity of the solvent used. The resonance of **3a** in apolar C_6D_6 and in the more polar $CDCl_3$ are observed in the typical range for neutral chloride complexes at δ 43.3 and 43.9, respectively. In the highly polar solvent MeOD, however, the resonance is strongly shifted to more positive values (δ 69.9), close to the signal of the cationic complex **4a** (δ 71.9, $CDCl_3$) (Figure 22a). Analogously, the phosphorus resonance of **3b** in C_6D_6 and $CDCl_3$ are observed at δ 71.1 and 72.4, respectively, while in nitromethane the signal significantly shifts to δ 80.2, close to the signal of the cationic complex **4b** (δ 102.3, $CDCl_3$) (Figure 22b). For complex **3c** with the better donor N-methyl-substituted NPN ligand, the phosphorus resonance in more polar CD_2Cl_2 (δ 68.4) is strongly downfield shifted relative to C_6D_6 (δ 59.8) and becomes close to the signal of the cationic complex **4c** (δ 80.8) (Figure 22c).

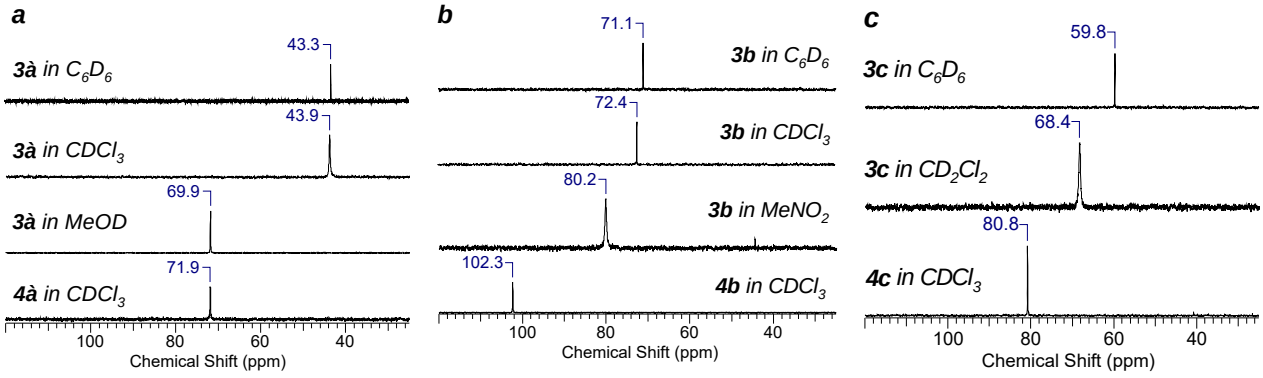

Figure 22. $^{31}P\{^{1}H\}$ NMR spectra of complex **3a** (**a**), **3b** (**b**), **3c** (**c**) in different solvents.

In the ^{1}H and $^{13}C\{^{1}H\}$ NMR spectra in $CDCl_3$ and CD_2Cl_2, compounds **3a-d,f** give only one set of signals for the two chemically inequivalent substituents at the phosphorus atom. Apparently, fast exchange between the two P-substituents takes place in polar solvents. Only for complex **3e** with the most electron-accepting N-substituents, two sets of signals were observed for the phenyl rings in $CDCl_3$. However, these signals are broad due to the exchange.

These NMR data indicate that complexes **3** are able to establish dissociation equilibria in polar solvents with formation of the symmetric cationic complexes $\mathbf{[4]^{+}Cl^{-}}$ (Scheme 27). The spectral pattern depends only on the polarity of the solvent. The tendency of the Ru-Cl bond to dissociate is mainly caused by the electron donating ability of the

nitrogen atom substituents: more electron donating groups facilitate the dissociation process.

The arene ruthenium complexes having monoanionic β-diketiminate[70] and dianionic bis(imidazolin-2-iminate)[80] ligands have also been reported earlier to undergo facile chloride dissociation, whereas in the amidinate ruthenium complexes the counter-ion dissociation has been observed only for the weakly coordinating triflate ligand but not for the chloride.[81] Hence, the capability of the iminophosphonamide ligand to donate electrons and to stabilize the electron-deficient states is much higher than that of the amidinate ligand and comparable to the β-diketiminate and zwitterionic bis(imidazolin-2-iminate) ligands.

A series of experiments to determine the thermodynamic parameters ΔG_d, ΔH_d, ΔS_d for the chloride-ion dissociation process in complexes **3a-f** was performed by NMR and UV-vis spectroscopy.

It can be assumed that the exchange process (Scheme 27), in which the chlorine atom changes the direction of coordination, and the substituents R_a and R_b exchange their positions relative to the arene ligand, being dissociative, has a pseudo first order kinetics in low-polar solvents.

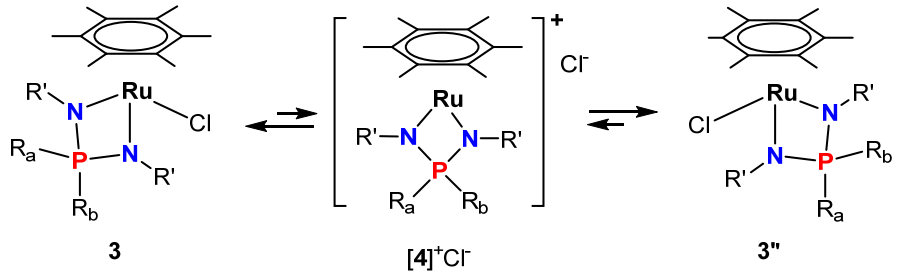

Scheme 27. The exchange between P-substituents via putative dissociation-association of the chloride anion.

The free dissociation energy $\Delta G^{\ddagger}_{d}$ should be close to the free activation energy of this exchange process $\Delta G^{\ddagger}_{ex}$ (Figure 23), which can be calculated from the measured exchange rate. The rate of the exchange process can be obtained by ^{1}H NMR spectroscopy, either from the determination of the coalescence temperature of the signals involved in the reversible process or from a 2D EXSY experiment.[86] These two methods are complementary: the first allows studying relatively fast exchange processes, whereas

EXSY is more suitable for slower ones. The mathematical apparatus necessary for calculating the dissociation rate constants and activation energies is given in the experimental part (Section III).

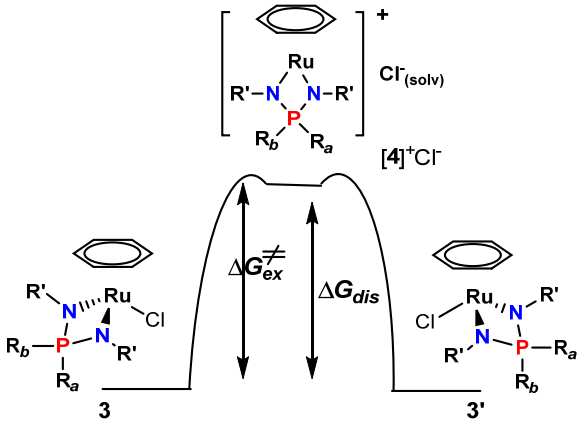

Figure 23. The exchange of the positions of R_a and R_b as a result of the dissociation of the Ru-Cl bond**.**

As mentioned in Section II.1.4.1.A., the R_a and R_b substituents in **3a-f** were found to be different in the ^{1}H NMR spectra in C_6D_6 at room temperature. For instance, the distinct signals of the *ortho*-H nuclei of two different phenyl rings in compound **3c** are observed at δ 7.98 and 7.70 ($\Delta\nu_{ab}$ = 170 Hz) at 298 K (Figure 24), but all the phenyl ring signals are broadened.

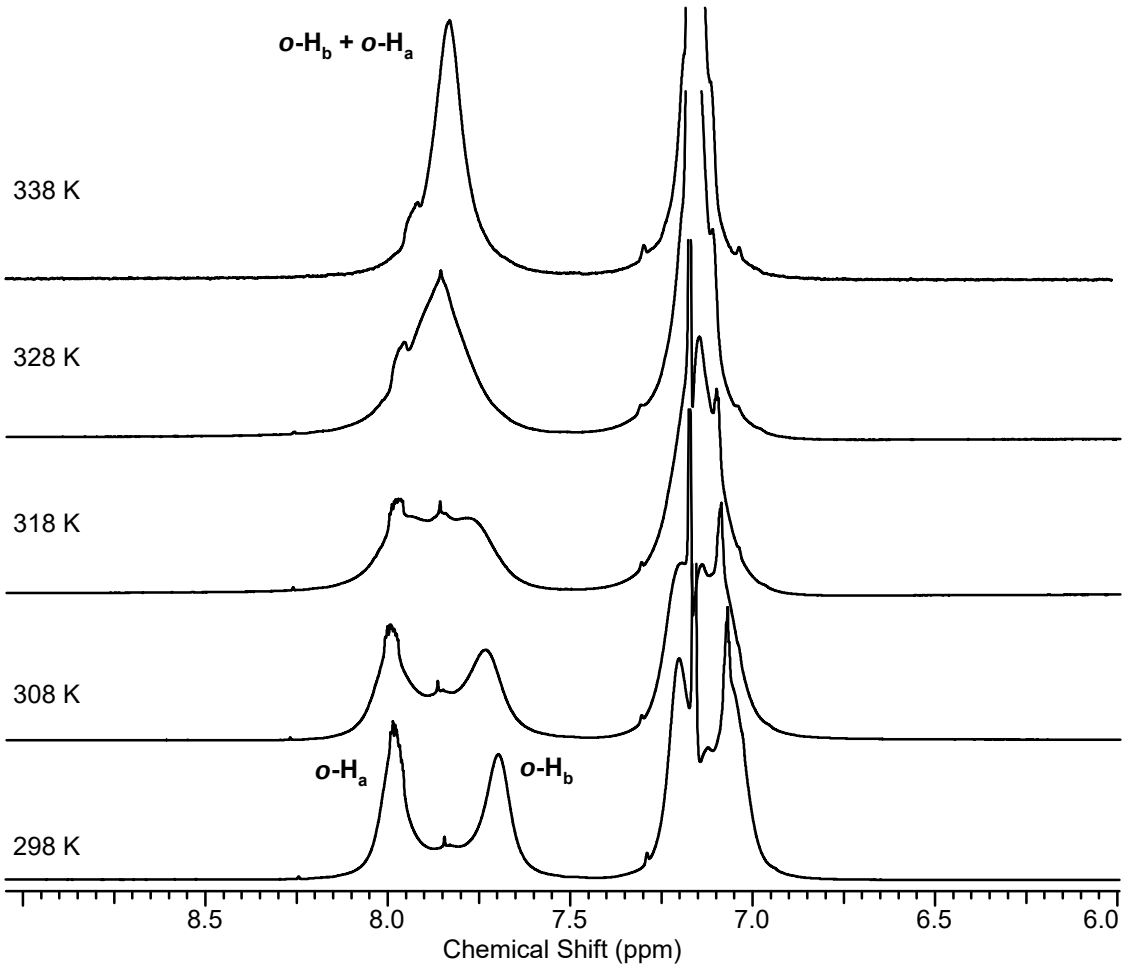

Figure 24. VT ^{1}H NMR spectra of complex **3c** recorded in C_6D_6 at T = 298 – 338 K.

Heating the solution led to coalescence of the *ortho*-H signals at T_c = 323±5 K and finally to only one signalat δ 7.83 at 338 K. From the coalescence temperature and from the chemical shift difference, the rate constant (k_{ex} = 380 s^{-1}) and activation free energy ($\Delta G^{\ddagger}_{ex}$ = 15.2±0.2 kcal/mol) for the degenerative exchange process **3c** in **[4c]$^{+}$Cl^{-}** were calculated.

Similarly, we attempted to study the dissociation process of complex **3b** with the less donor NPN ligand in toluene-d_8 in the range of 273 – 353 K. However, the coalescence for the P-Et methyl resonances at δ 0.40 and 1.39 could not be reached below the boiling point of toluene-d_8 (Figure 25).

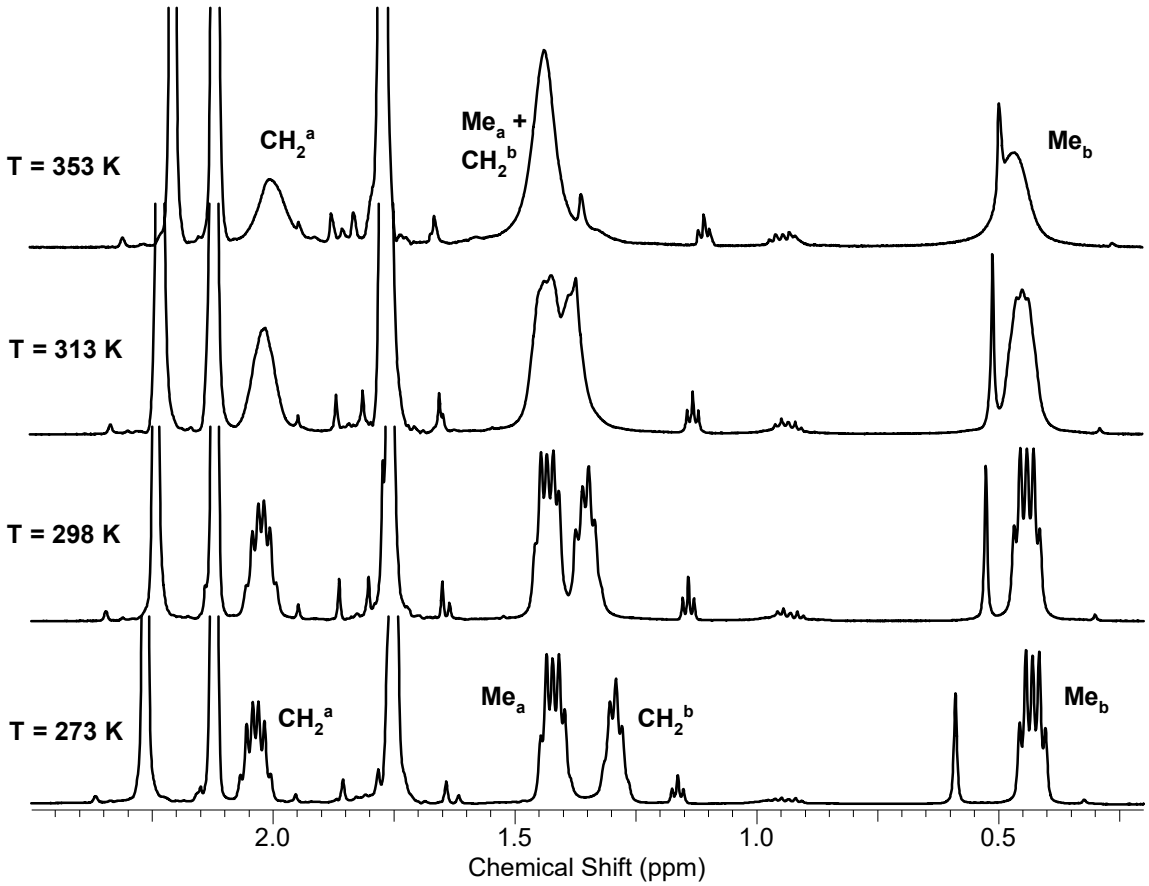

Figure 25. VT ^{1}H NMR spectra of complex **3b** recorded in toluene-d_8 at T = 273 – 353 K.

On the other hand, coalescence could be observed in the more polar dichloromethane (Figure 26). Only one averaged broad signal for the PEt CH_3 groups was observed at δ 1.05 in the ^{1}H NMR spectrum at 298 K, which indicates their chemical equivalence on the NMR timescale. As the temperature decreases, this signal broadens and is then divided into two signals for the inequivalent CH_3 groups. At 193 K, two separate resonances are observed at δ 0.46 and δ 1.49 ($\Delta\nu$ = 618 Hz) for Me_a and Me_b. At the coalescence temperature of T_c = 238 ±5 K, the estimated exchange rate constant is 1370 s^{-1} and the free energy of activation $\Delta G^{\neq}_{ex}$ calculated from the Eyring equation is 10.4±0.2 kcal/mol.

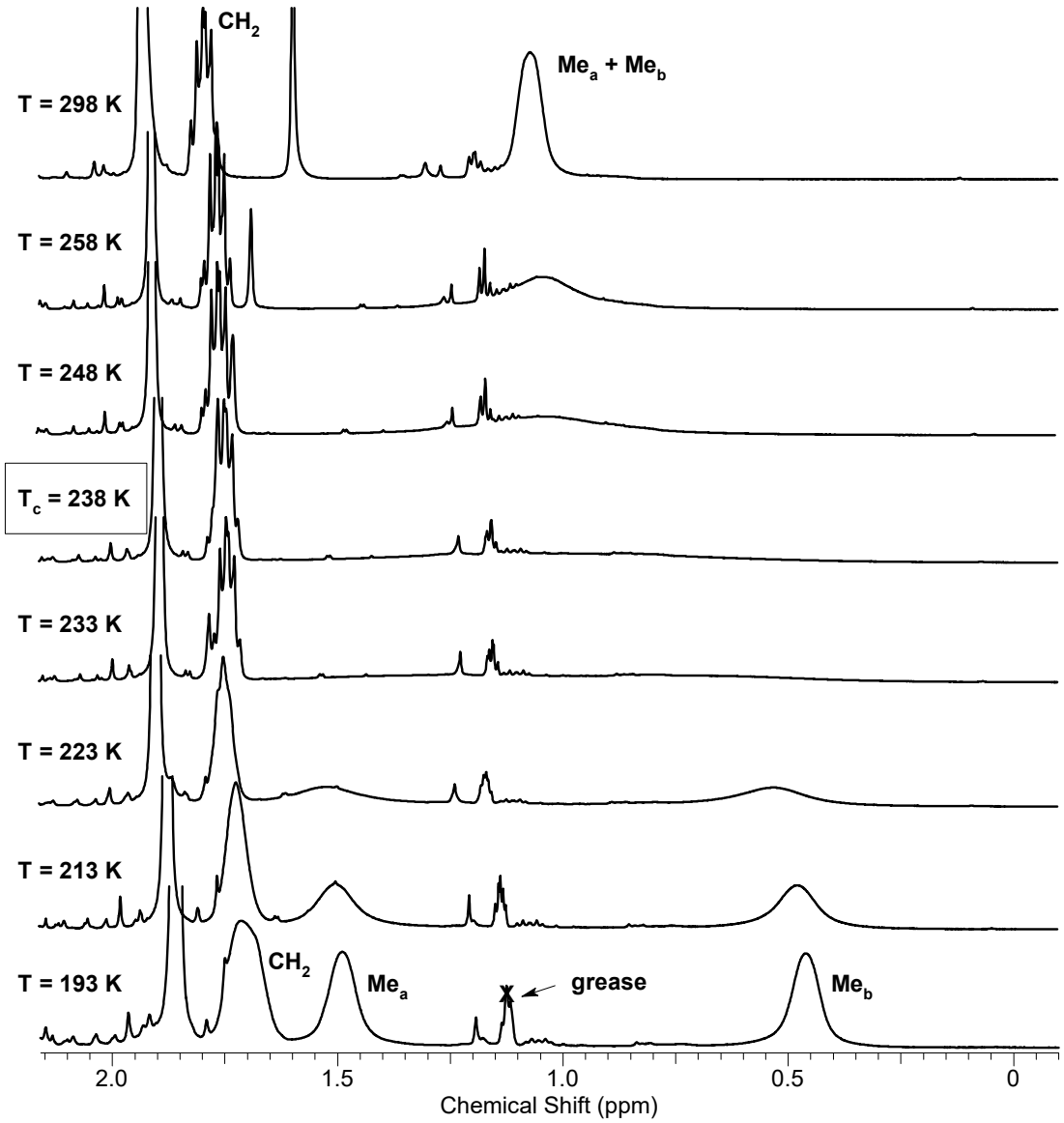

Figure 26. VT NMR spectra of the complex **3b** recorded in CD_2Cl_2 at T = 193 – 298 K.

The rates of slower exchange processes were determined by the 2D ^{1}H EXSY NMR method, which records the exchanging signals in the form of cross-peaks, whose integral intensities allow calculating k_{ex} (Section III). It was shown that even in apolar solvents (benzene, toluene), the chloride complexes **3b,d** undergo a slow exchange of the phosphorus atom substituents. For example, the slow exchange of the ethyl groups for [(η^6-C_6Me_6)RuCl{Et_2P(N-*p*-Tol)$_2$}] **(3b)** in toluene-d_8 (Figure 27A) yielded k_{ex} = 1.4 s^{-1} at 293 K. The activation parameters for the exchange process were obtained from the temperature dependence of the exchange rate constants (k_{ex}) in toluene-d_8 in the range 230 – 315 K from the van't Hoff equation: $\Delta H^{\neq}_{ex}$ = 8.4±0.2 kcal/mol and $\Delta S^{\neq}_{ex}$ = -29±1 cal/(mol•K) (Figure 27B). A large negative value of the activation entropy evidences a highly ordered

transition state in the exchange process, which is caused by the need to reorganize the solvent dipoles for the nonspecific solvation of a charged chloride-ion.

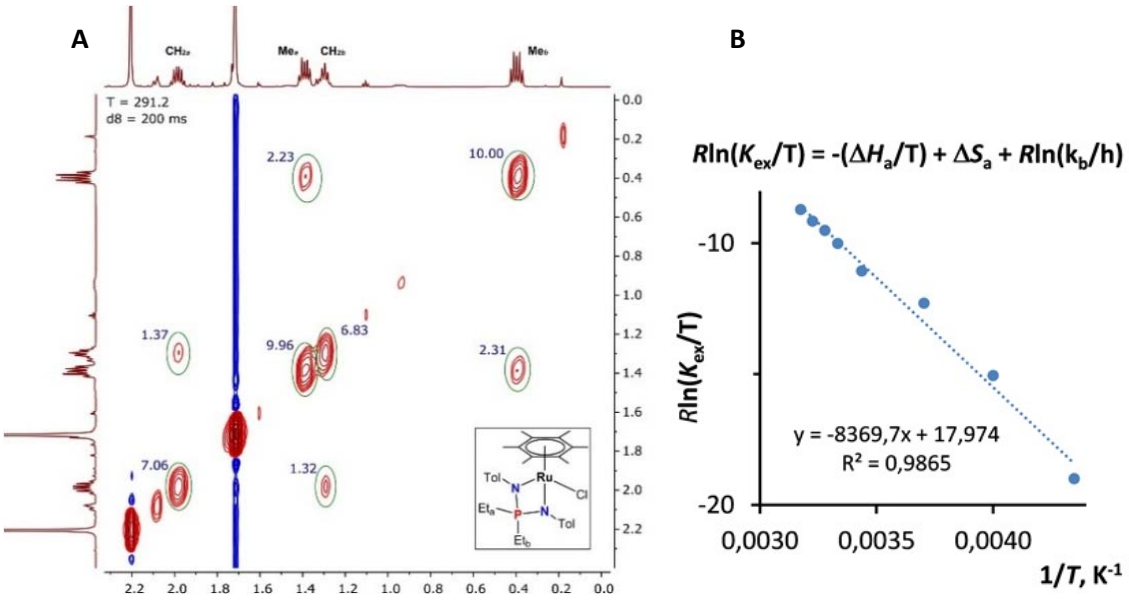

Figure 27. (**A**) 2D EXSY ^{1}H NMR of [(η^6-C_6Me_6)RuCl{Et_2P(N-p-Tol)$_2$}] (**3b)** in toluene-d_8 at 293 K with a mixing time of t_{mix} =200 ms; (**B**) van't Hoff plot of RlnK$_{ex}$ vs 1/T.

The exchange between the R_a and R_b substituents occurs via a configuration inversion at the Ru atom, which can most easily be envisaged by moving the chloride ligand from one coordination side to the opposite one by ligand exchange processes. Generally, such ligand exchange may proceed either via a dissociative mechanism with a cationic 16ē intermediate (Figure 28A) or via a S_N2-like associative mechanism through a 20ē transition state (Figure 28b). In the latter case, however, configuration inversion with exchange of the phosphorus R_a and R_b substituents could take place only when the entering ligand is Cl^-. Given that the NMR studies outlined above were carried out in non-coordinating solvents and coordinating ligands L are not present, the exchange in **3b** most likely takes place via the dissociated complex **[4b]$^+$Cl$^-$** (Figure 28A). We have further confirmed that the exchange rates are independent on the concentration of **3b** (1.6 s^{-1} in both 40 mM and 8 mM toluene-d_8 solutions at 295 K, Table 15, lines 5 and 6).

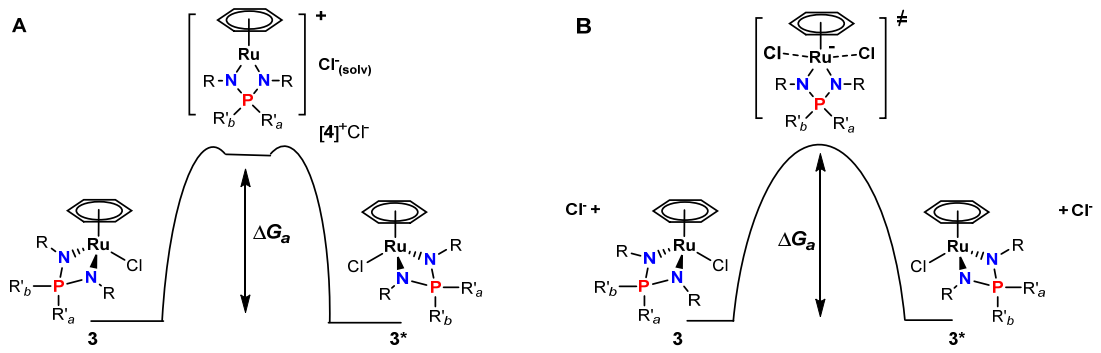

Figure 28. Dissociative (**A**) and associative (**B**) mechanisms for the exchange of the R_a and R_b groups in **3**.

Exchange NMR spectra were also recorded for the **3a**, **3d**, **3f** complexes, but only at room temperature. The exchange rate constants k_{ex} and the calculated free activation energies of the exchange $\Delta G_{ex}^{\neq}$ are presented in Table 15. The P-substituent exchange for complexes **3a** and **3f**, which bear the least electron-donating NPN ligand, is not observed by 2D EXSY ^{1}H NMR even at t_{mix} = 1 s, hence the rates are slower than 0.1 s^{-1} and the activation free energies are greater than 18.5 kcal/mol (Figure 29). In contrast, the exchange rate of complex **3c** in benzene is very high (k_{ex} > 100 s^{-1}).

Table 15. Exchange rate constant (k_{ex}) and activation free energy ($\Delta G^{\neq}_{ex}$) for the P substituent exchange in **3a,b,d,f** from the 2D EXSY ^{1}H NMR investigations.

№	Complex	Solvent	Additives	C(Ru), mM	C(add), mM	*T*, K	k_{ex}, s^{-1}	$\Delta G_{ex}^{\neq}$, kcal/mol
1	**3a**	C_6D_6	-	10		293	<0.1	>18.5
2	**3a**	C_6D_6	H_2O	10	10	294	0.79	17.4
3	**3b**	C_6D_6	-	20		293	1.8	16.8
4	**3b**	C_6D_6	H_2O	20	5	295	>15	<15.7
5	**3b**	toluene-d_8	-	40		295	1.6	17.0
6	**3b**	toluene-d_8	-	8		295	1.6	17.0
7	**3b**	toluene-d_8	-	46		293	1.4	17.0
	3d	C_6D_6	-			294	3.4	16.5
8	**3f**	C_6D_6	-	10		292	<0.1	>18.5
9	**3f**	C_6D_6	H_2O	10	0.7	293	0.72	17.3
10	**3f**	C_6D_6	H_2O	10	2.4	293	2.6	16.6
11	**3f**	C_6D_6	$Et_4N^+Cl^-$	10	0.7	292	>11	<15.7

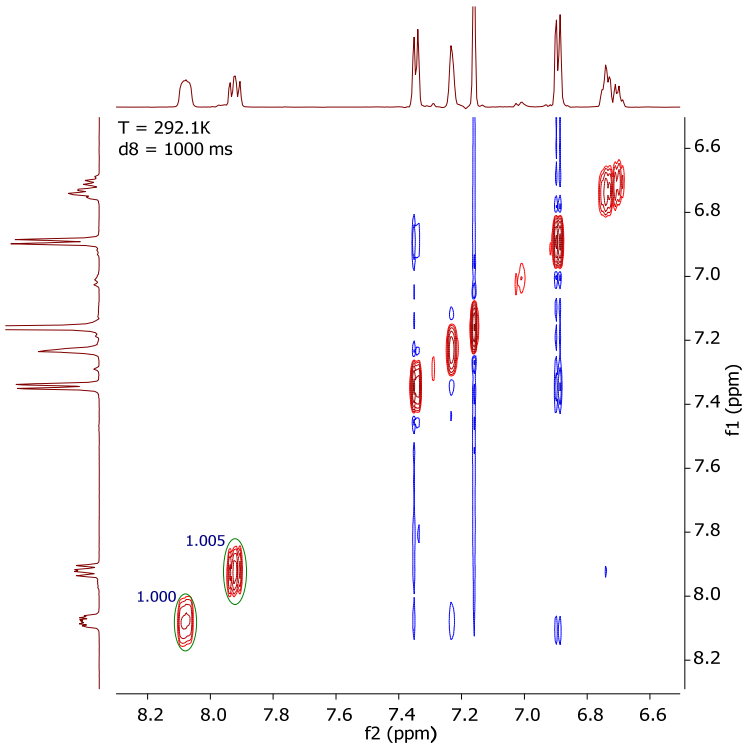

Figure 29. 2D EXSY ^{1}H NMR of [(η^6-C_6Me_6)RuCl{Ph_2P(N-p-Tol)$_2$}] **(3a)** in C_6D_6 at 292 K and the mixing time of t_{mix} =1000 ms.

Interestingly, addition of 0.07 equiv. of $Et_4N^+Cl^-$ to **3f** in C_6D_6 strongly enhances the exchange process (k_{ex} > 11 s^{-1}) (Table 15, line 11; Figure 30). This result strongly suggests that the exchange for this complex may also take place by the associative mechanism. Otherwise, the addition of Cl^- should slow down the exchange processes occurring by the dissociative mechanism. Therefore, it seems that both mechanisms are possible, the former in the absence of added Cl^- and the latter in its presence.

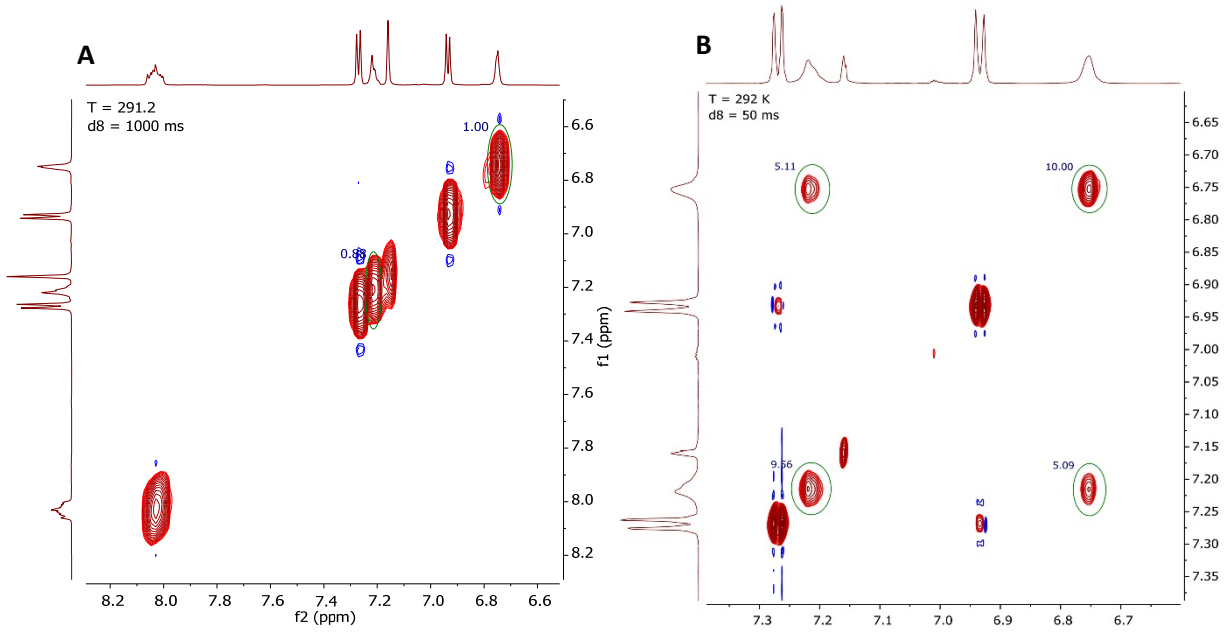

Figure 30. 2D EXSY ^{1}H NMR of [(η^6-*p*-cymene)RuCl{Ph_2P(N-*p*-Tol)$_2$}] (**3f**) (10 mM) in C_6D_6 in the absence of external ligand (**A**) and in the presence of 0.7 mM $Et_4N^+Cl^-$ (**B**) (T = 292 K, t_{mix} = 50 ms).

Assistance by an external ligand L (for example, H_2O) may also result in Cl^- release. While the subsequent attack of the same Ru-L intermediate by Cl^- would not result in any P substituent exchange, attack of another Ru-Cl complex achieves a degenerative self-exchange with configuration inversion the Ru atom and P substituent exchange (Scheme 28). Thus, the P-phenyl group exchange for **3a** and **3f** becomes observable after adding water to the C_6D_6 solutions (Table 15, lines 1,2 for **3a** and lines 8,9 for **3f**) and the rate constants are found to increase with the increase of the water content (Table 15, lines 9,10; Figure 31).

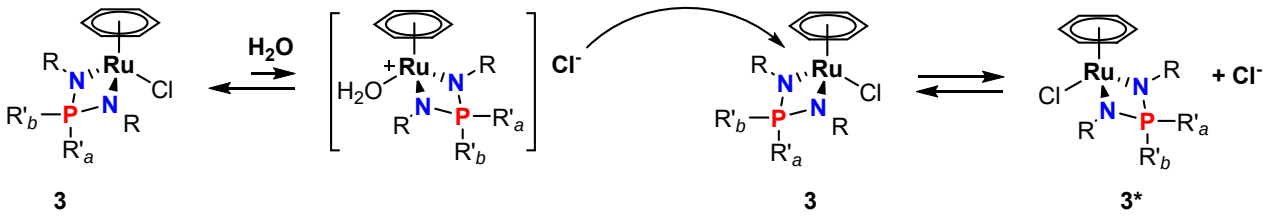

Scheme 28. Associative exchange promoted by water-induced chloride dissociation

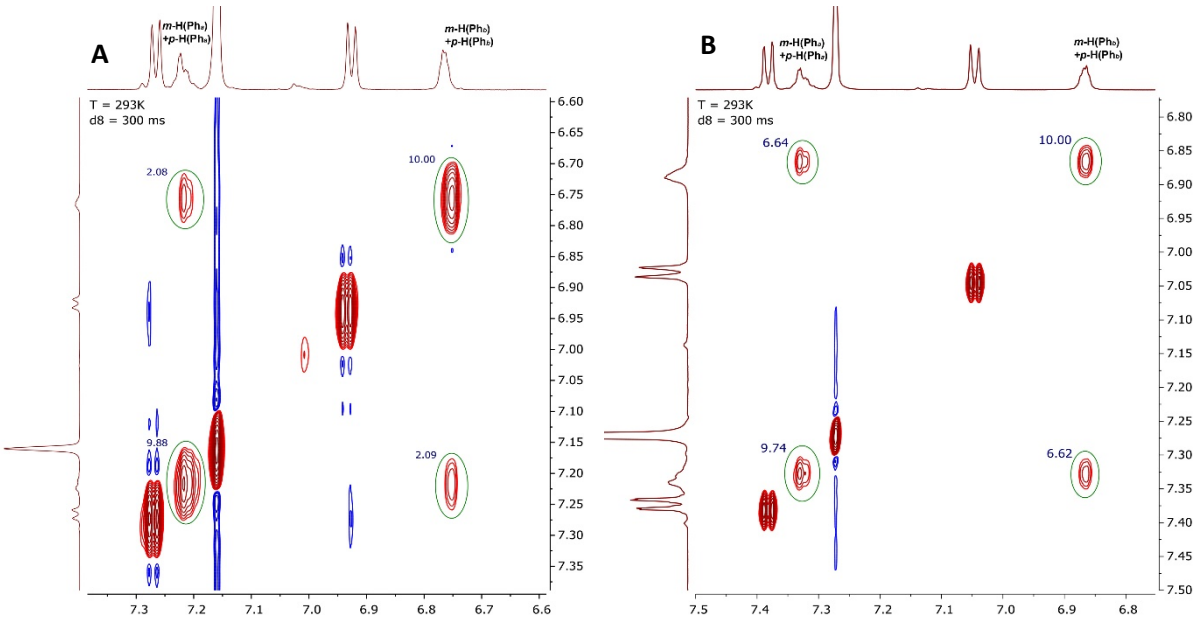

Figure 31. 2D EXSY ^{1}H NMR of **3f** in C_6D_6 at fixed concentration (10 mM), temperature (293 K) and mixing times (300 ms) and different concentration of water: 0.7 mM (**A**) and 2.4 mM (**B**)

For the **3f** sample with [H_2O] = 0.7 mM (0.07 equiv.), the activation parameters could be derived from the temperature dependence (291 – 335 K) of k_{ex} (Figure 32).

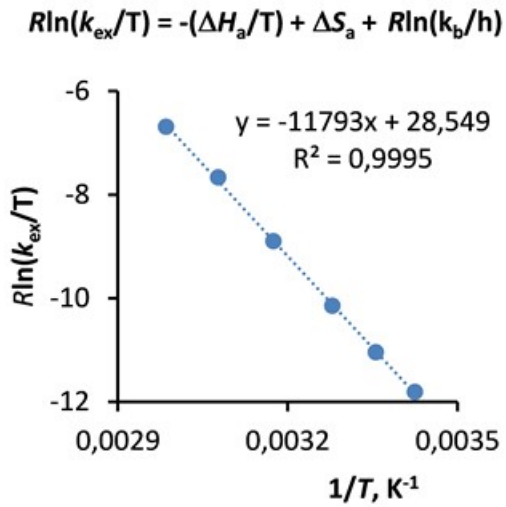

Figure 32. The van't Hoff plot for **3f** (10 mM) in C_6D_6 in the presence of 0.7 mM of water showing dependence of Rln(k_{ex}/T) vs 1/T.

Since associative exchange processes, as a rule, proceed faster than dissociative ones, the calculated activation enthalpy $\Delta H_{ex}^{\neq}$ = 11.8±0.2 kcal/mol of the associative exchange can be used as a lower limit for the $\Delta H_{ex}^{\neq}$ in dissociative exchange of **3f** in the

absence of external ligands. It is pertinent to underline that water may have a double role in the promotion of the associative chloride exchange: as a ligand to replace Cl^- in the coordination sphere of the Ru atom, and as a proton donor to stabilize the dissociated Cl^- by H-bonding. Interestingly, the effect of water for **3a** is much smaller; a rate constant of 0.79 s^{-1} is achieved only in the presence of an equimolar amount of H_2O in C_6D_6 (Table. 15, line 2). Perhaps the sterically bulky C_6Me_6 ligand hampers the Cl^- or external ligand coordination thus increasing the activation free energy.

Thus, we measured (estimated) the rate constants (k_{ex}) and the free activation energies $\Delta G_{ex}^{\neq}$ for the exchange of P-substituents in five complexes **3a-d,f** in benzene-d_6. Assuming that the activation entropy of the exchange process $\Delta S_{ex}^{\neq}$ for all complexes is similar, since the main contribution to it is the solvation of the chloride ion, the activation enthalpies of the exchange process $\Delta H_{ex}^{\neq}$ were calculated (Table 16). For complexes **3a** and **3f** only the lower limits of $\Delta H_{ex}^{\neq} > 10$ kcal/mol were estimated, which in reality can be even higher than 12 kcal/mol – the found activation enthalpy for exchange by the associative mechanism. Obviously, in complex **3e** with the most electron-accepting NPN ligand, the exchange rate of the P-substituents will be even lower, and the activation enthalpy $\Delta H_{ex}^{\neq}$ will be even higher than in **3a** and **3f**. Indeed, as we mentioned earlier, for **3e** this exchange is too slow even in $CDCl_3$.

Table 16. Activation parameters of the dissociation of complexes **3a-d,f**.

	3a	**3b**	**3c**	**3d**	**3f**
k_{ex}, c^{-1} **(293 K)**	<0.1	1.8	380*	3.4	<0.1
$\Delta G_{ex}^{\neq}$, **kcal/mol**	>18.5	17.0±0.2	15.2±0.3*	16.5±0.2	>18.5
$\Delta H_{ex}^{\neq}$, **kcal/mol**	>10	8.4±0.2	5.7±0.3	7.9±0.2	>10
$\Delta S_{ex}^{\neq}$, **kcal/(mol*K)**	*-29***	-29±1	*-29***	*-29***	*-29***

*at T = 328K. ** Estimated value.

With a reasonable degree of confidence, we can assume that the activation enthalpy $\Delta H_{ex}^{\neq}$ for the dissociative exchange process should be very close to the Ru–Cl bond dissociation enthalpy, $\Delta H_d^{\neq}$. As a result, a series of dissociation enthalpies can be established for all chloride complexes: **3e** > **3a**, **3f** (>10 kcal/mol) > **3b** (8.4 kcal/mol) > **3d** (7.9 kcal/mol) > **3c** (5.7 kcal/mol). Thus, the NMR study showed that the tendency of the

ruthenium NPN complexes to dissociate the chloride ligand increases with the introduction of donor substituents at phosphorus and nitrogen atoms. Despite the fact that the influence of the arene ligand could not be revealed, the shortened Ru-Cl bond in the **3f** complex and its inertness with respect to $NaPF_6$ indicate a greater dissociation enthalpy with respect to **3a**.

B) UV-vis spectroscopic studies.

The equilibrium dissociation of complexes **3a-c** was studied in solvents of different polarity using UV-vis spectroscopy. It turns out that complex **3a**, which contains the least donating NPN ligand, does not noticeably dissociate in low-polar solvents, it is not sufficiently soluble in the more polar nitromethane for measurements, and solutions in methanol gradually decompose, which did not allow us to study the dissociation of this complex in solution by electron spectroscopy. Conversely, the dissociation of complexes **3b** and **3c** was successfully demonstrated by this method. Thus, the UV-vis spectra of solutions of complex **3b** in CH_2Cl_2 in the temperature range 190 – 296 K (Figure 33) showed that only the undissociated 18ē complexes is present, as shown by the band centered at 450 nm.

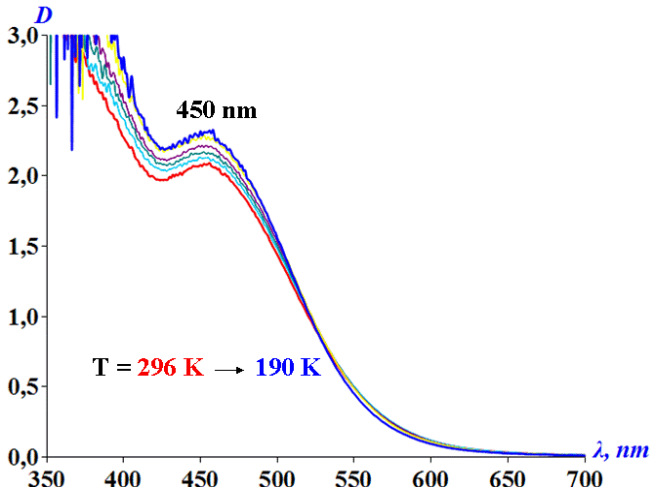

Figure 33. UV-vis of **3b** (c = 2.5*10^{-3} M) in CH_2Cl_2 at 190 – 290 K (cell d = 1.0 cm).

However, the compound predominantly exists as cationic complex **[4b]$^+$Cl$^-$** in solution of the highly polar $MeNO_2$ solvent, exhibiting a band with λ_{max} = 515 nm (Figure 34). Analysis of the temperature dependence of this band in the range 250 – 310 K gave the dissociation enthalpy (ΔH_d = 3.5±0.2 kcal/mol) and entropy (ΔS_d = +0.3±0.6

cal/(mol•K)). Even in nitromethane, this process is endothermic and the good solvating ability of nitromethane leads to a slightly positive entropy and to an increase of the degree of dissociation when heated.

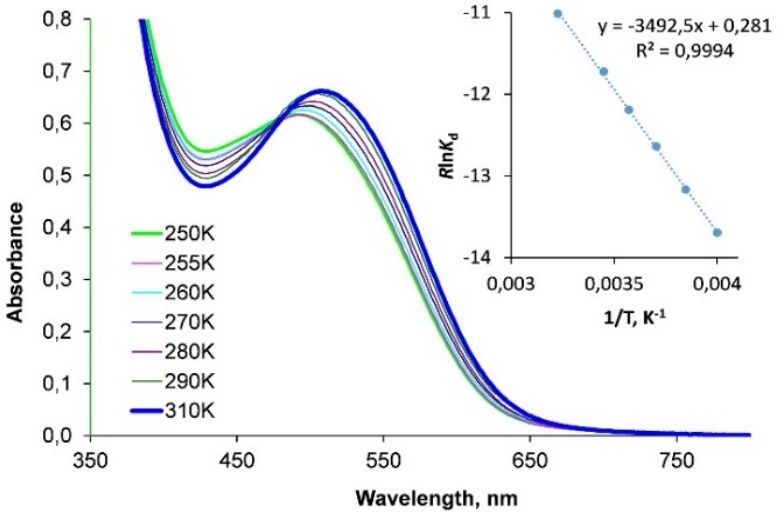

Figure 34. UV-vis spectra of **3b** (c = 2.5*10^{-3} M) in $MeNO_2$ at 250-310 K (cell d = 0.22 cm). The insert shows the van't Hoff plot of $RlnK_d$ vs 1/T.

Complex [(η^6-C_6Me_6)RuCl{Ph_2P(N-Me)$_2$}] (**3c**), bearing the most electron-releasing Me groups, partially dissociates in the relatively polar CH_2Cl_2 solutions. The detailed study by means of UV-vis spectroscopy revealed the distinct absorption bands in toluene for **3c** (at 430 nm; Figure 36B) and in CH_2Cl_2 for **4c** (at 550 nm; Figure 36A). The spectrum of **3c** in CH_2Cl_2 shows a very broad absorption band located in-between these bands (at 520 nm; Figure 35), thus suggesting the coexistence of the dissociated and undissociated forms. The spectra are temperature dependent in the 190-290 K range, showing reversible changes with an isosbestic point at λ = 480 nm (Figure 35). With decreasing temperature, the dissociated form increases and almost complete dissociation is reached at 200 K. The standard enthalpy and entropy for the dissociation process were calculated from the van't Hoff equation (ΔH_d = -5.0±0.2 kcal/mol, $\Delta S_{дис}$ = -27±1 cal/(mol•K)). The unexpectedly large negative entropy change for the dissociation process is attributed to the need to re-organize the solvent dipoles around the charged species formed upon dissociation of **3c**.

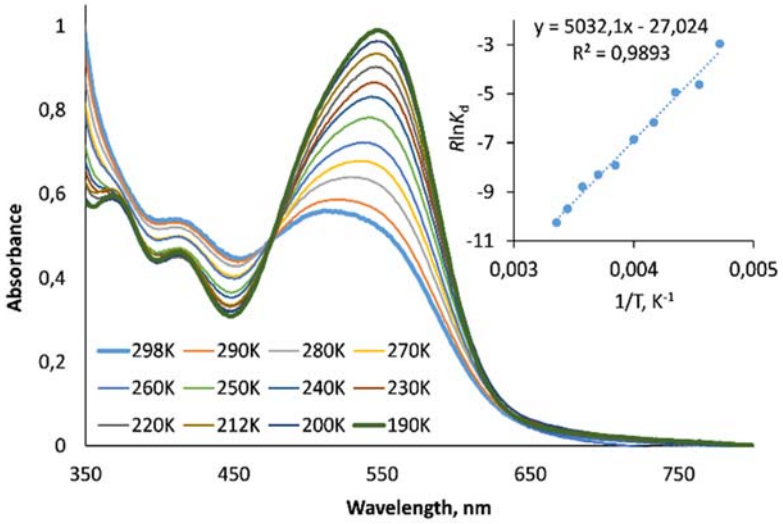

Figure 35. UV-vis spectra of 3c (c = 2.5*10^{-3} M**)** in CH_2Cl_2 at 190-298 K (cell d = 0.22 cm). The insert shows the Van't Hoff plot of $RlnK_d$ vs 1/T.

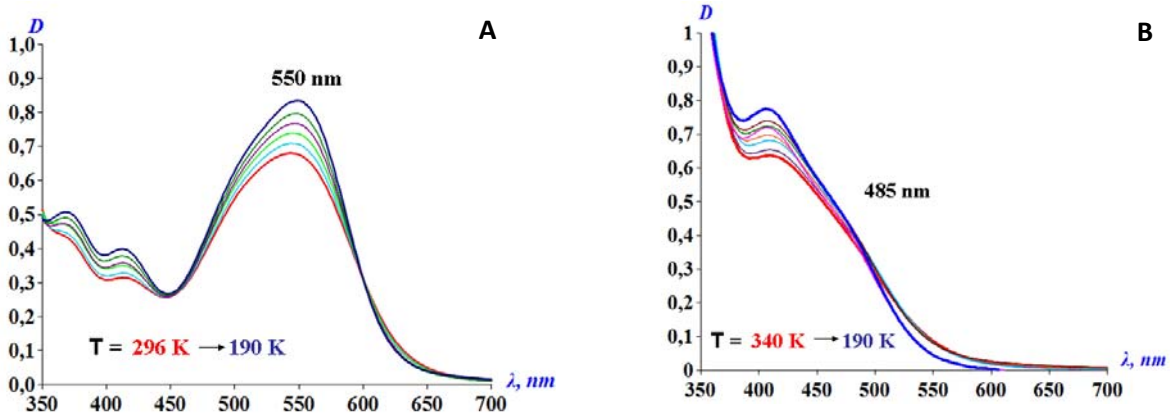

Figure 36. (**A**) UV-vis spectra of **4c** (c = 2.5*10^{-3} M) in CH_2Cl_2 at 190 – 296 K (cell d = 0.22 cm). (**B**) UV-vis spectra of **3c** (c = 2.5*10^{-3} M) in toluene at 190-340 K (cell d = 0.22 cm)

Thus, the UV-vis spectroscopy data confirm the conclusions made on the basis of NMR data that the Ru-Cl bond dissociation in arene iminophosphonamide complexes **3a-f** is facilitated by donor substituents at the nitrogen atoms and with increasing solvent polarity. The complex **3c** with the most donor NPN ligand is able to completely dissociate in dichloromethane at a low temperature.

II.1.4.2. Coordination of external ligands to the 16ē cationic complexes 4.

Cationic NPN complexes **4** are formally electronically unsaturated (16ē). However, the NPN ligand, which can be either a 4ē or a 6ē donor, is able to compensate for the lack of electron density on the metal atom due to additional π-donation from the NPN ligand. In the previous section, we have shown that in complexes **3** even the chloride anion can relatively easily dissociate. In this section, we report our studies of the coordinating ability of 16ē ruthenium complexes **4** with neutral ligands (L) of various nature (L = MeCN, Py, and CO) to yield cationic 18ē [(Arene)Ru(NPN)(L)]$^+$[**4**(L)] complexes (as exemplified for complex **4a** in Scheme 29). All three selected L ligands are 2ē σ-donors with significantly different efficiency for π -back-bonding: MeCN <Py <CO. The interaction with σ-donor ligands, namely acetonitrile and pyridine, has been studied by UV-vis and NMR spectroscopy.

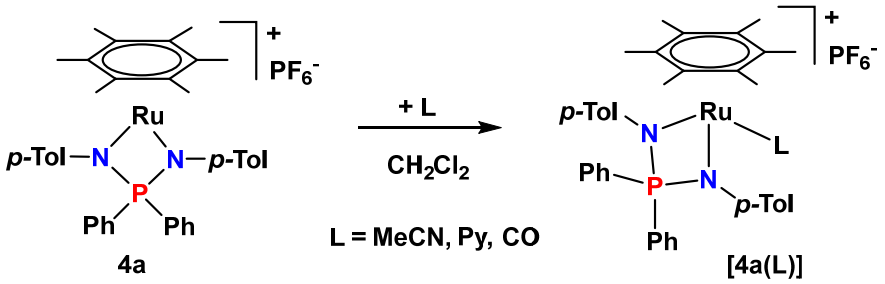

Scheme 29. Coordination of the ligand L to [(η^6-C_6Me_6)Ru{Ph_2P(N-p-Tol)$_2$}]$^+PF_6^-$ (**4a**).

Acetonitrile

When 10 equiv. of MeCN were added to a solution of **4a** in CD_2Cl_2 the colour immediately changed from violet to red and the $^{31}P\{^1H\}$ NMR resonance shifted from δ 72.2 to δ 63.8 indicating the formation of the new complex, presumably the cationic adduct [(η^6-C_6Me_6)Ru(MeCN){Ph_2P(N-*p*-Tol)$_2$}](PF$_6$) [**4a**(MeCN)]. Attempts to isolate it by removing the excess of acetonitrile *in vacuo* returned the starting complex **4a** (violet solution in CD_2Cl_2 with the phosphorus resonance at δ 71.0, no acetonitrile signal in ^1H NMR) which indicates the lability of the acetonitrile ligand and the instability of the corresponding 18ē complex [**4a** (MeCN)].

The binding constant (K_c) of the acetonitrile complex [**4a**(MeCN)] was calculated from the titration of complex **4a** with acetonitrile in dichloromethane using UV-vis spectroscopy (Figure 37). In the spectra of pure complex **4a** in dichloromethane, one band

is observed centered at λ_{max} ~ 535 nm. Adding small amounts of acetonitrile (up to 50 equiv.) does not lead to visible changes in the spectrum. Only in the presence of a significant excesses of MeCN (200 equiv.), the intensity of the band at 535 nm is noticeably reduced and a band at ~ 440 nm, which belongs to the 18ē complex [**4a**(MeCN)], starts to grow.

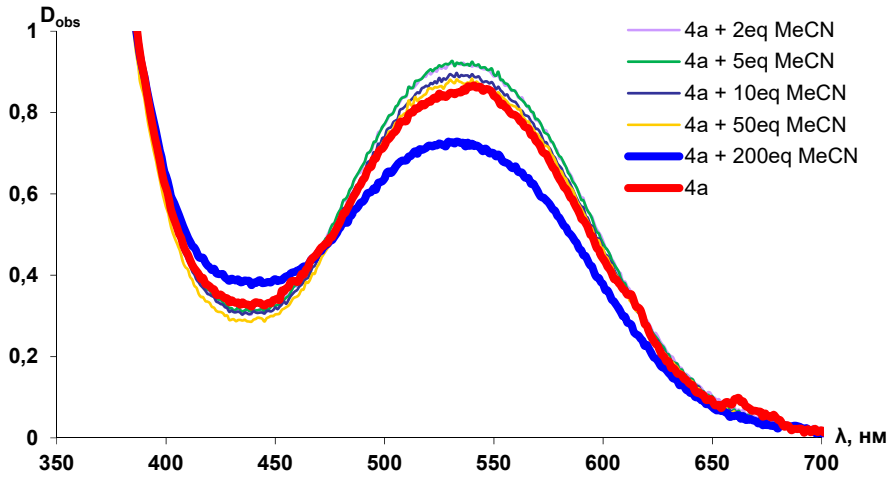

Figure 37. UV-vis monitoring titration of **4a** (c = 0.8 mM) with MeCN in CH_2Cl_2, T = 296 K, cell d = 1 cm.

From the various optical densities at 590 nm (Table 17), we were able to estimate (see Section III, Table 17) the binding constant of [**4a**(MeCN)]: K_c ~ 2.

Table 17. Calculated K_c for the reaction of **4a** with acetonitrile from the UV-vis monitored titration.

V(L), ul	V_{tot}, ml	n(L), eq.	c_0(**4a**), mM	c_0(L), mM	D_0(**4a**)	D_{obs}	c(**4a**), mM	c(**4aL**), M	c(L), mM	K_c, M^{-1}
0	6.00	0	0.8	0	0.533	0.533	0.5	0	0	
2	6.002	8	0.8	6.4	0.533	0.520	0.781	1.9E-05	6.38	3.9
6	6.008	32	0.799	25.6	0.532	0.514	0.771	2.7E-05	25.54	1.4
24	6.032	128	0.796	102.0	0.530	0.457	0.686	0.00011	101.75	1.6

V(L) –volume of added neat MeCN; V_{tot} –total solution volume; c_0(**4a**), c_0(L) – initial **4a** and acetonitrile concentrations; n(L) – amount of added acetonitrile; c(**4a**), c(L), c(**4aL**) – equilibrium concentrations of **4a**, acetonitrile and complex **4a(MeCN)**, D_0(**4a**) –initial absorption of **4a** at 590 nm at a given concentration, D_{obs} – observed absorption for the **4a** + MeCN mixture at 590 nm.

Pyridine

The interaction of complex **4a** with pyridine was studied by NMR spectroscopy at different **4a**/pyridine ratios. The possibility of using high concentrations of the complex allowed the observation of spectral changes with smaller excess amounts of the ligand than in the UV-vis method, in which highly colored compounds must be studied at low concentrations. When pyridine is gradually added to complex **4a** in CD_2Cl_2, the $^{31}P\{^1H\}$ NMR resonance (δ 72.2) shifts upfield to δ 53.2 (Figure 38), which corresponds to the 18ē cationic pyridine complex $[(\eta^6\text{-}C_6Me_6)Ru(Py)\{Ph_2P(N\text{-}p\text{-}Tol)_2\}](PF_6)$ [**4a**(Py)]. This process is also equilibrated. However, compared with acetonitrile, pyridine coordinates more strongly, and strong changes in the spectra are visible even with the addition of 1 equiv. pyridine. The binding constants (K_c) were calculated for each titration point and are presented in Table 18.

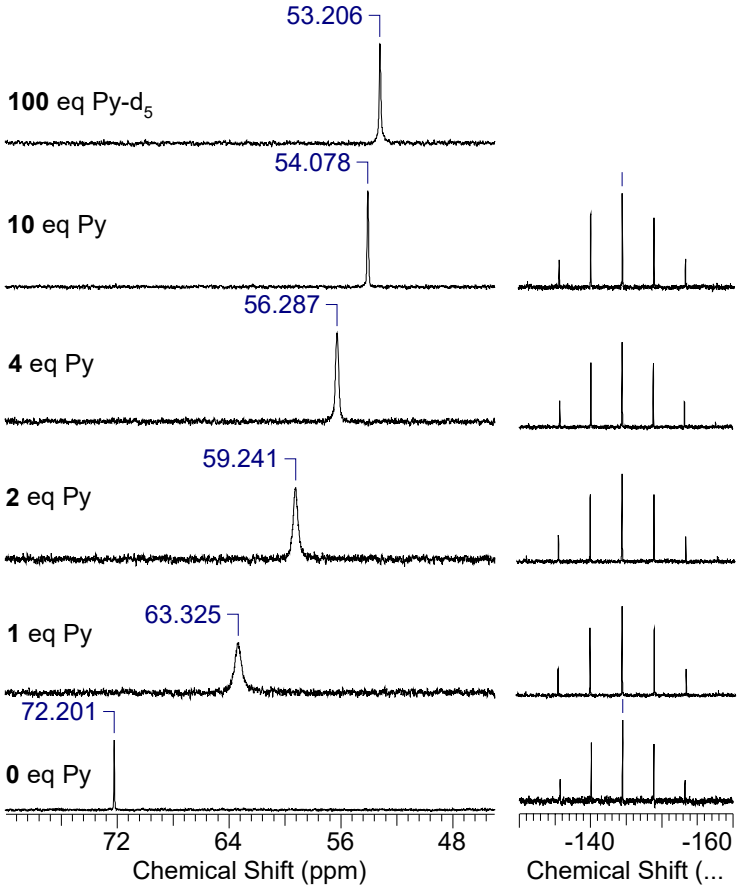

Figure 38. The titration of **4a** (c = 0.04 M) with pyridine monitored by $^{31}P\{^1H\}$ NMR in CD_2Cl_2 (T = 295K).

Table 18. Calculated K_c for the reaction of **4a** with pyridine from the $^{31}P\{^1H\}$ NMR shifts.

c_0(**4a**), M	n(Py), eq.	c_0(Py), M	δ, ppm	δ_1, ppm	δ_2, ppm	c(Py), M	K_c, M^{-1}
0.04	0	0	72.2	52.71	72.2	0	
0.0399	1	0.0399	63.33	52.71	72.2	0.0217	38.4
0.0397	2	0.0794	59.24	52.71	72.2	0.0531	37.4
0.0395	4	0.158	56.29	52.71	72.2	0.1257	35.3
0.0388	10	0.388	54.08	52.71	72.2	0.3515	37.6
0.0303	100	3.025	53.2	52.71	72.2	2.996	12.9
							K_c(av) = 37.2±1.3 M^{-1}

c_0(**4a**) – initial concentration of **4a**, n(Py) – amount of added pyridine, c_0(Py) – initial pyridine concentration, c(Py) – free pyridine concentration, δ – observed chemical shift for the **4a** + Py mixture, δ_1 – estimated chemical shift for the complex **4a**(Py), δ_2 – initial chemical shift of **4a**.

The averaged binding constant, K_c(av) = 37 ± 1 M^{-1}, is significantly greater than for the acetonitrile ligand ($K_c \sim 2$). The δ_1 value (52.71) obtained by least-squares fitting of the binding constant values with 1, 2, 4 and 10 equiv. of pyridine resulted to be close to the chemical shift of the signal measured in the presence of >10 equiv. of pyridine. Note that when adding 100 equiv. pyridine (25 vol.%) the value of K_c is highly understated, since the polarity of the solution significantly changes and it is necessary to adjust the values of δ_1, so this point was not used in the calculation of K_c(av).

A similar titration was carried out using UV-vis spectroscopy (Figure 39). The addition of pyridine to **4a** leads to a decrease in the intensity of the band centered $\lambda_{max} \sim$ 535 nm; at the same time, there is a new band centered $\lambda_{max} \sim$ 445 nm related to the 18ē complex [**4a**(Py)].

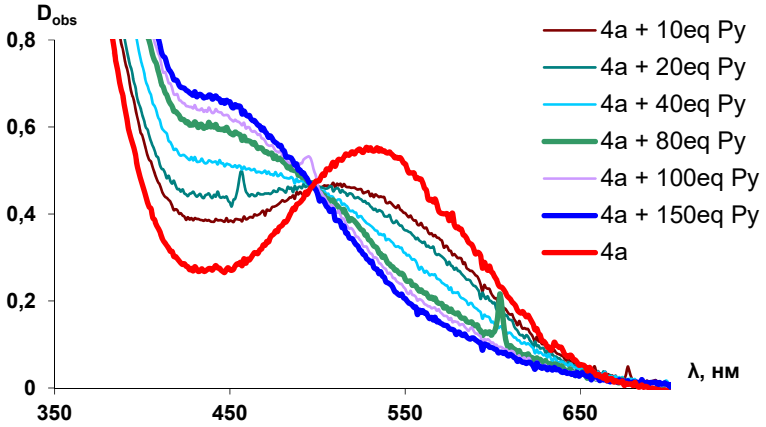

Figure 39. UV-vis titration of **4a** (c = 0.5 mM) with Py in CH_2Cl_2, T = 296 K, cell d = 1 cm.

The binding constants (Table 19) were calculated in accordance with the formulas specified in Section III, using the optical density of the spectrum at 600 nm. As can be seen, the values of K_c differ significantly for different amounts of pyridine, but the average value (K_c(av) ~ 33) is satisfactorily comparable with that obtained from NMR.

Table 19. Calculated K_c for the reaction of **4a** with pyridine from the UV-vis titration.

V(L), ul	V_{tot}, ml	n(L), eq.	c_0(**4a**), mM	c_0(L), mM	D_0(**4a**)	D_{obs}	c(**4a**), mM	c(**4aL**), M	c(L), mM	K_c, M^{-1}
0	4.00	0	0.5	0	0.264	0.264	0.5	0	0	
1.5	4.0015	9.9	0.476	4.76	0.2514	0.212	0.40	7.47E-05	4.687	39.7
1.5	4.003	19.8	0.476	9.42	0.2513	0.200	0.38	9.72E-05	9.323	27.5
3.1	4.0061	40.0	0.476	19.04	0.2512	0.153	0.29	0.000186	18.85	34.0
1.5	4.0076	49.8	0.475	23.68	0.2511	0.143	0.27	0.000205	23.478	32.2
3.1	4.0108	70.0	0.475	33.28	0.2509	0.140	0.26	0.00021	33.067	23.9
1.5	4.0123	79.8	0.475	37.91	0.2508	0.121	0.23	0.000246	37.668	28.5
1.5	4.0138	89.6	0.475	42.55	0.2507	0.113	0.21	0.000261	42.286	28.8
1.5	4.0153	99.4	0.475	47.18	0.2506	0.105	0.20	0.000276	46.901	29.6
8.0	4.0233	151.6	0.474	71.81	0.2501	0.092	0.17	0.000299	71.511	24.0

K_c(av) = 32.2±6.7 M^{-1}

V(L) –volume of added neat pyridine; V_{tot} –total solution volume; c_0(**4a**), c_0(L) – initial **4a** and pyridine concentrations; n(L) – amount of added pyridine; c(**4a**), c(L), c(**4aL**) – equilibrium concentrations of **4a**, pyridine and complex **4a(Py)**, D_0(**4a**) –initial absorption of **4a** at 600 nm at a given concentration, D_{obs} – observed absorption for the mixture of **4a** + Py at 600 nm.

The thermodynamic parameters (ΔH_c, ΔS_c) of the complexation reaction of **4a** with pyridine were calculated by UV-vis spectroscopy at a 1:2 **4a**/pyridine ratio in dichloromethane in the temperature range 296-190 K (Figure 40). Species **4a** dominates at room temperature (λ_{max} ~ 535 nm), while the equilibrium shifts towards the 18ē adduct [**4a**(Py)] at lower temperatures (λ_{max} ~ 445 nm). The conversion becomes essentially complete below 240 K.

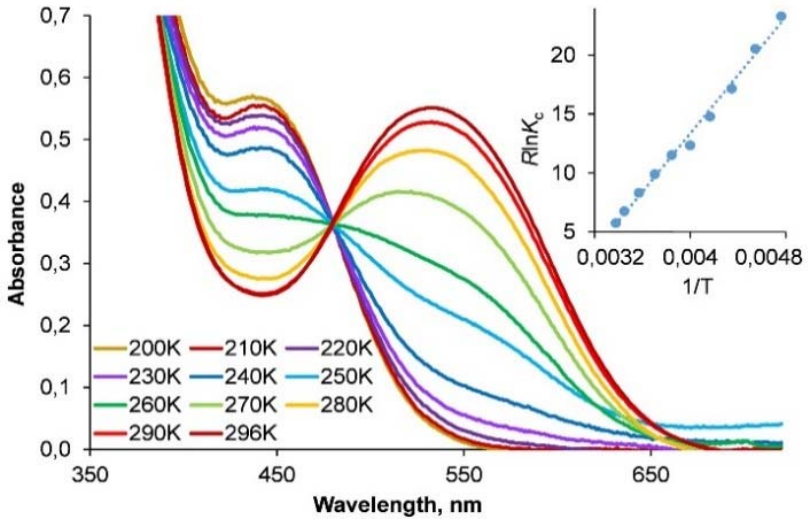

Figure 40. UV-vis spectra of reversible coordination of pyridine to **4a** (c = 2.5*10^{-3} M) in CH_2Cl_2 at 200-296 K (cell d = 0.22 cm). The insert shows the van't Hoff dependence of $RlnK_c$ vs 1/T.

The binding constants and Gibbs free energies (ΔG_c) at each temperature were calculated in accordance with the formulas given in Section III, using the optical density of the spectra at 580 nm. From the temperature dependence of ΔG_c, a van't Hoff analysis gave the thermodynamic parameters ΔH_c = -12.4±0.5 kcal/mol and ΔS_c = -36±2 cal/(mol*K) for the complexation process of **4a** with pyridine.

Thus, pyridine coordination is moderately exothermic, but a large excess of pyridine is required to observe coordination at room temperature because of the high association entropy. This is in sharp contrast with the previously reported irreversible coordination of pyridine to the 16ē arene ruthenium amidinate complex [(C_6H_6)Ru(^{t}BuN-C(Ph)-N^{t}Bu}](BAr$^F{}_4$) (**L23**).[83]

Carbon monoxide

In comparison with acetonitrile and pyridine, carbon monoxide is a stronger π-acceptor and reacts readily with **4a,f** to give the CO adduct **5a,f**. However, the reaction is reversible and facile CO decoordination occurs upon solvent evaporation to give back **4a,f**. Nevertheless, **5a,f** could be isolated by precipitation from its CH_2Cl_2 solution upon addition of excess diethyl ether. Although **5a** and **5f** slowly evolve CO in the solid state under vacuum, satisfactory elemental analyses were obtained for both compounds. It should be noted that **5a** is stable in a CO-saturated solution, whereas **5f** degrades within days to unknown arene-free carbonyl complexes, perhaps similar to the previously observed ones resulting from the decomposition of [(*p*-cymene)Ru(CO)(SXyl)$_2$].[86]

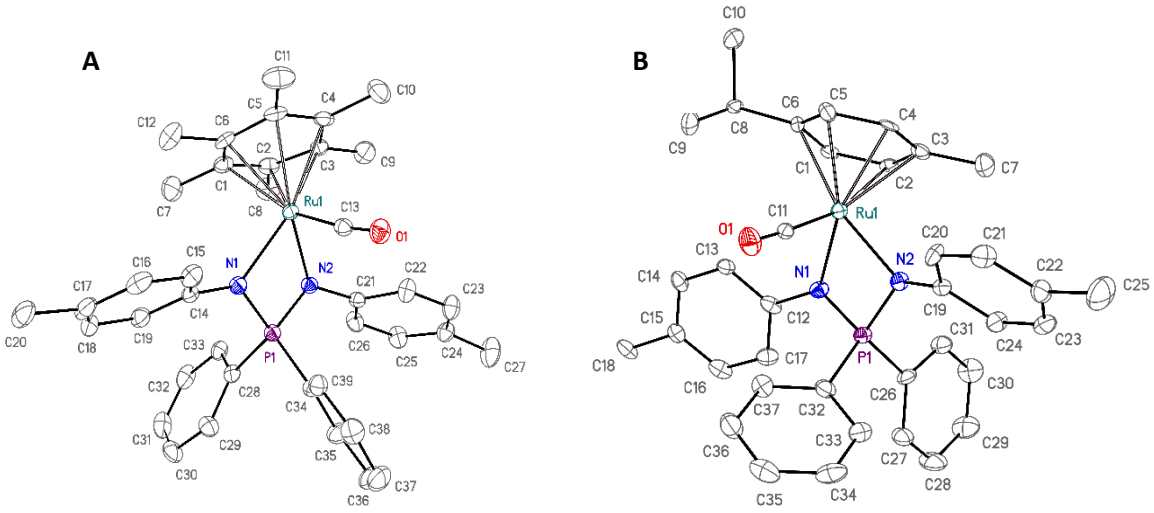

Figure 41. ORTEP diagram of the cation carbonyl complexes **5a** (**A**) и **5f** (**B**). Selected bond lengths (Å) and angles (°):

[(η^6-C_6Me_6)Ru(CO){Ph_2P(N-*p*-Tol)$_2$}]$^+PF_6^-$ (**5a**): Ru-C_6Me_6(centroid) 1.769(1), Ru-C(O) 1.871(3), Ru-N_1 2.112(2), Ru-N_2 2.116(2), C-O 1.145(3), N_1-Ru-N_2 69.20(9), Ru-N_1-P-N_2 164.60(15), Σ(N_1) 348.3(5), Σ(N_2) 359.3(5), Ru-C_{13}-O_1 174;

[(η^6-*p*-cymene)Ru(CO){Ph_2P(N-*p*-Tol)$_2$}]$^+PF_6^-$ (**5f**): Ru-*p*-cymene(centroid) 1.768(3), Ru-C(O) 1.879(9), Ru-N_1 2.095(7), Ru-N_2 2.120(6), C-O_1.145(10), N_1-Ru-N_2 68.9(3), Ru-N_1-P-N_2 165.8(4), Σ(N_1) 353.7(13), Σ(N_2) 355.3(14), Ru-C_{11}-O_1 176.

Complexes **5a** and **5f** are the first crystallographically characterized arene ruthenium carbonyl derivatives with any κ^2-N,N-anionic chelate ligand. Both complexes exhibit a three-legged piano stool geometry with a pseudo octahedral configuration of the ligands

around the ruthenium atom and a linear Ru-C-O geometry (bond angle of 174 – 176°), which is typical of terminal metal carbonyl complexes. The slightly elongated C-O bond (1.145 Å) compared with free CO suggests a noticeable π-acceptance of the electron density from the ruthenium atom. The coordinated arene adopts a nearly staggered (**5a**) or eclipsed (**5f**) conformation relative to the Ru-CO axis, with C_5-Arene(centroid)-Ru-CO dihedral angles of 37.5° and 5.9, respectively. The presence of the CO ligand significantly increases (by ~ 0.1 Å) the Ru-Arene(centroid) distance in both **5a**, **5f** (1.768 – 1.769 Å) relative to **4a, 4f** (1.659 – 1.662 Å). The Ru-C(arene) distances vary in the range 2.208 – 2.333 Å with the longest bonds being *trans* to the CO ligand. The C-C bonds length (1.389 –1.452 Å) in the coordinated arene slightly alternate with the shortest C-C bond (1.389 – 1.403 Å) located *trans* to the CO ligand. Similar Ru-Arene(centroid) (1.810 Å), Ru-C(O) (1.846 Å) and carbonyl C-O (1.133 Å) distances, as well as elongations for the two Ru-C(arene) bonds *trans* to CO (2.389 – 2.396 Å) were previously reported for the arene ruthenium dithiolate carbonyl complex $[(\eta^6\text{-}C_6Me_6)Ru(CO)(S_2C_6H_4)]$[86] (**L24)**. The Ru-N bonds in compounds **5a,f** (2.095 – 2.120 Å) are shorter than those in the neutral 18ē complexes **3a,f** by ca. 0.04 Å, reflecting the presence of the positive charge, but longer (by 0.05 – 0.08 Å) than in the 16ē complexes **4a,f**, in which they are strengthened by π-donation from the NPN ligand. The chelate N_1-Ru–N_2 angles in **5a** and **5f** (68.9 – 69.2°) are similar to those of the other 18ē NPN complexes **3a,f**. However, unlike in the related chloride complexes **3a** and **3f**, the Ru-N_1-P-N_2 metallacycles in **5a** and **5f** are folded by 13 – 15.6° from planarity at the $N_1\cdots N_2$ hinge and the nitrogen atoms (N_1 in **5a**; N_1 and N_2 in **5f**) are noticeably pyramidalized as shown by the Σ(N) parameter (Σ(N_1) = 348.3° and Σ(N_2) = 359.3° for **5a**, Σ(N_1) = 353.7° and Σ(N_2) = 355.3° for **5f**). There are several close H···F contacts between the cation and the PF_6^- anion in both structures, although none of these is shorter than the sum of the van der Waals radii of H and F (2.56 Å).[69]

Complexes **5a** and **5f** are sufficiently stable in concentrated solutions to allow recording their NMR spectra, although the fraction of the corresponding 16ē complexes **4a,f** increases with time. The $^{31}P\{^1H\}$ NMR resonance (δ 61.7 for **5a** and δ 60.2 for **5f**) is downfield shifted by ca. 10 ppm relative to the corresponding 16ē cationic complexes **4a** and **4f**. In the ^1H and $^{13}C\{^1H\}$ NMR spectra recorded in $CDCl_3$ for **5a** and **5f** there are two sets of signals for the magnetically inequivalent phenyl groups at the phosphorus atom, as expected for the C_s-symmetric complexes, hence the decoordination of CO is a slow

process with a relatively high activation barrier. The resonance of the coordinated CO ligand in the $^{13}C\{^1H\}$ NMR spectra is observed at high field (δ 199.2 for **5a**, 193.8 for **5f**), as is typical of terminal linear coordinated CO ligands (cf. to δ 197.8 for **L24**[86] and δ 203-208 reported for the cyclopentadienyl ruthenium complexes with N,N-ligands[87,88].

Both carbonyl adducts **5a** and **5f** exhibit a strong CO stretching vibration band in the IR spectrum at 1984 cm^{-1} (**5a**) and 2012 cm^{-1} (**5f**). The higher ν_{CO} in **5f** evidences weaker Ru→CO π-back-bonding relative to **5a**, which possesses the electron-richer C_6Me_6 arene. These frequencies are substantially lower than those of the more electron-deficient arene ruthenium amidinate carbonylic complex $[(\eta^6\text{-}C_6H_6)Ru(CO)\{PhC(N^tBu)_2\}](BAr^F{}_4)$ (2050 cm^{-1})[83] but closer to those of the arene ruthenium complex with dianionic ditiolate ligands **L24** (ν_{CO} = 1951 cm^{-1})[86], $[(\eta^6\text{-}C_6Me_6)Ru(CO)(SXyl)_2]$ (ν_{CO} = 1965 cm^{-1})[86] and of the cyclopentadienyl complex with neutral κ^2-N,N-ligand $[(\eta^5\text{-}C_5H_5)Ru(CO)(TMEDA)](BAr_4)$ (ν_{CO} = 1968 cm^{-1}).[88] This indicates the intermediate electron-donating ability of the NPN ligand, between the monoanionic and dianionic ligands, which is in good agreement with its zwitterionic structure.

Surprisingly, bubbling CO into the solution of **4c** yielded a stable product, **5c'**, resulting from the addition of two CO molecules, one of which has inserted into one of the two Ru–N bonds forming a carbamoyl metallacycle. The product **5c'** has been fully characterized, including by single crystal X-ray diffractometry (Figure 42). The overall geometry of **5c'** is similar to that of **5a,f** except for the expanded metallacycle with a CO group. The addition of two CO molecules leads to a significant increase of the Ru-Arene(centroid) distance relative to **4c** by ca. 0.18 Å as a result of elongation of the Ru-C(arene) bonds *trans* to the terminal CO (2.299 – 2.312 Å) and to the carbamoyl C=O group (2.373 – 2.381 Å). The arene C-C bonds *trans* to the terminal CO (1.404 Å) and to C=O group (1.392 Å) are shorter than the other four bonds (1.417 – 1.438 Å). Similarly to **5a** and **5f**, the terminal carbonyl group is linear (176°). The carbamoyl C=O and C-N bonds have similar lengths to or are slightly longer than those in organic amides (1.24 and 1.32 Å, respectively). The carbamoyl N_2 atom is planar ($\Sigma(N_2)$ = 359.3°), while N_1 is considerably pyramidalized ($\Sigma(N_1)$ = 349.7°) as in the corresponding 18ē chloride complex **3c**. There are two intermolecular close contacts in the structure of **5c'** that fall below the sum of the van der Waals radii, implicating hydrogen atoms of the C_6Me_6 ligand and either

a PF_6^- F atom or the carbamoyl oxygen atom, H_{8A} ··· F (2.269 Å) and H_{10B} ··· O_2C (2.418 Å), respectively.

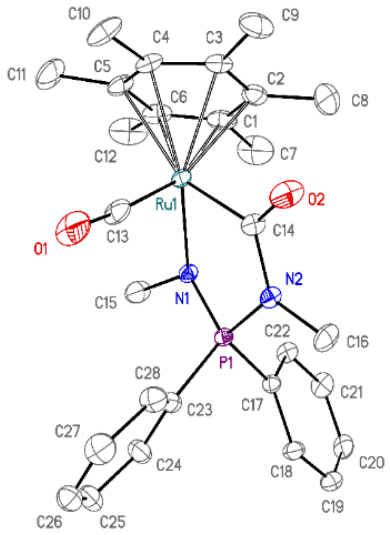

Figure 42. ORTEP diagram of the cation $[(\eta^6\text{-}C_6Me_6)Ru(CO)\{(CONMe)Ph_2P(NMe)\}]^+PF_6^-$ **(5c')**. Selected bond lengths (Å) and angles (°): Ru-C_6Me_6 (centroid) 1.828(1), Ru-N_1 2.107(2), Ru-C(O)N 2.042(3), C=O 1.211(4), N-C(O) 1.414(3), Ru-C(O) 1.859(3), C-O 1.143(4), N_1-Ru-C(O) 83.15(10), Σ(N_1) 349.7(5), Σ(N_2) 359.3(6), Ru-C_{13}–O_1 176 .

The $^{13}C\{^1H\}$ NMR spectrum of **5c'** reveals two signals corresponding to carbonyl C nuclei: a singlet at δ 198.2 and a doublet at δ 192.8 ($^2J_{CP}$ = 19.6 Hz). All the N- and P-substituents in **5c'** are inequivalent and give rise to two sets of signals for both methyl and phenyl groups in the ^1H and $^{13}C\{^1H\}$ spectra. In the IR spectrum, **5c'** (Figure 43) shows two strong carbonyl bands ν_{CO} at 1984 cm^{-1} (metal bound CO) and at 1644 cm^{-1} (carbamoyl C=O), the latter frequency being typical of organic amides.

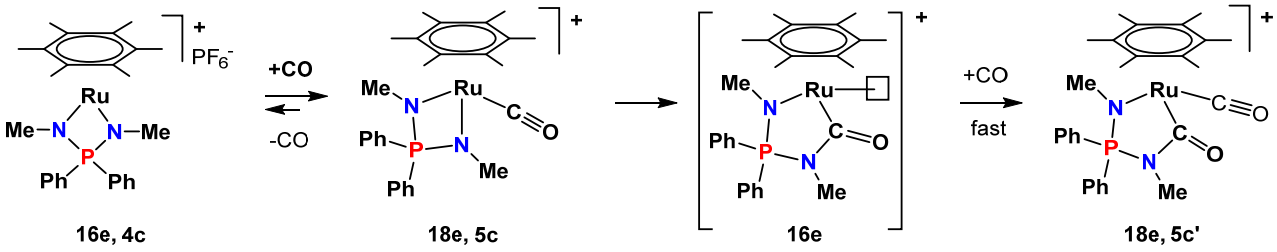

Scheme 30. Reaction of **4c** with carbon monoxide in CH_2Cl_2.

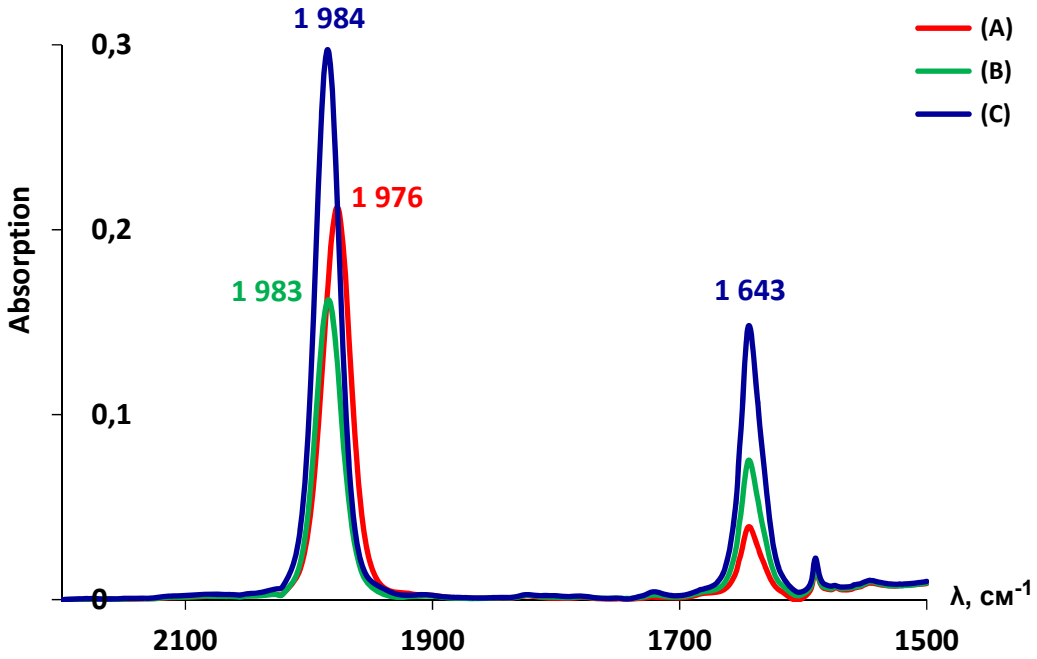

Figure 43. IR monitoring of the reaction of **4c** (c = 2.3*10^{-2} mol/L) with CO (cell d = 0.2 mm). The sample was dissolved in CH_2Cl_2 at -40°C and CO was bubbled for 10 s. The spectra were recorded (**A**) immediately after the preparation, (**B**) after 30 s at room temperature, (**C**) after bubbling CO 1 min at 25°C.

Apparently, the carbonylation of **4c** is a two-step reaction involving a reversible first step (Scheme 30). The initially formed monoadduct **5c** is stable only at low temperatures and when heated to room temperature it disproportionates to the carbonyl-carbamoyl complex **5c'**and the initial complex **4c**. This conclusion is further supported by the results of an IR spectroscopic monitoring at low temperatures (Figure 43). Bubbling CO at -40°C for 10 s fully converts **4c** to the orange mono-adduct **5c**, characterized by a strong CO band at 1975 cm^{-1}. The latter is unstable: even at -40°C and in the absence of additional CO it slowly disappears to be replaced by **5c'**. The coordination of the first CO molecule is reversible, hence dissociation from the mono-adduct **5c** provides the needed CO for the second carbonylation step. The rearrangement is complete within a few minutes at low temperatures and yields a 1:1 mixture of **4c** and **5c'**, which were isolated upon evaporation of the solvent

The peculiarity of the mono-carbonyl intermediate **5c** is the high nucleophilicity of the nitrogen atoms, which is related to the presence of more electron-donating alkyl substituents. Although facile CO-insertion into M–N bonds is a known phenomenon for

certain metal aminopyridinates,[89] triazenides,[90] amidinates,[91-93] and aminophosphines,[94] this reaction has not been previously reported to the best of our knowledge for arene ruthenium complexes. The process that most resembles the formation of **5c'** involves a carbene insertion into a Ru–N bond in the arene ruthenium amidinate complex **L21** [(η^6-C_6Me_6)Ru{(^{i}PrN)$_2$CMe}](PF_6), followed by CO coordination to give [(η^6-C_6Me_6)Ru(CO){(^{i}PrN)CMe(N^{i}Pr)CHSiMe$_3$}](PF_6) (**L25**).[95] The spectral and structural data of **L23** are similar to those of **5c'**: the ν_{CO} is observed at 1963 cm^{-1} and the carbonyl resonance appears at δ_{CO} 203 in the $^{13}C\{^1H\}$ NMR spectrum; the Ru-Arene(centroid) distance is 1.828 Å with the elongation of the Ru-C(arene) bonds *trans* to CO and to the inserted carbene to 2.320 – 2.362 Å; the CO ligand is linear (Ru-C-O is 170.2°), and the Ru-CO and C-O bond lengths are 1.836 Å and 1.159 Å, respectively.

In conclusion, in the first part of the work, two series of new 18ē and 16ē arene ruthenium iminophosphonamide complexes were synthesized, the structures of all ten ruthenium NPN complexes were confirmed and analyzed, the processes of ligand exchange between 18ē and 16ē complexes were studied, and the structures of three cationic arene carbonyl ruthenium complexes were confirmed, which are the first representatives of cationic arene carbonyl complexes with κ^2-N,N-ligand. The structural features of the 18ē and 16ē ruthenium NPN complexes, the increased stability of the 16ē complexes, as well as the vibrational frequencies of the terminal CO groups are in good agreement with the zwitterionic structure of the NPN ligand. The latter indeed appears to be a quite strong σ,π-donor, which is capable to donate either 4ē or 6ē and effectively compete with external ligands for providing complimentary electron density to the unsaturated metal atom, stabilizing the electron-deficient complexes.

II.2. Catalytic activity study of complexes 3 and 4 in the hydrogenation of acetophenone with isopropanol.

The obtained arene ruthenium iminophosphonamides chlorides **3** and cationic complexes **4** were tested as catalysts for the transfer hydrogenation of a model ketone (acetophenone to 1-phenylethanol) by isopropanol (Scheme 31). Initially, this process was studied in detail for the **3f** complex, since the NMR spectra allow facile identification of the *p*-cymene fragment α and β CH-arene signals, which is convenient for identifying the

intermediates implicated in the catalytic cycle. The results of initial tests, aimed at probing the effect of the NPN ligand and of added bases, are listed in Table 20.

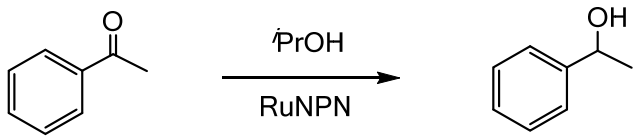

Scheme 31. Transfer hydrogenation of acetophenone by isopropanol with arene ruthenium NPN complexes

Table 20. Results of the catalytic transfer hydrogenation of acetophenone, catalyzed by complexes **3f, 4f** and $[(\eta^6\text{-}p\text{-cymene})RuCl_2]_2$ (**L26**).

№	Complexes	T, °C	NaHMDS	Conversion, %					k_{obs} (h^{-1})	TOF*, h^{-1}
				1 h	2 h	4 h	6 h	24 h		
1	**L26**	60	-	0	-	-	-	<1	-	<1
2	**3f**	60	-	3.8	13.6	27.5	36.2	62.4	0.076 ±0.002	7
3	**4f**	60	-	-	-	1.1	2.5	6.2	-	<1
4	**L26**	60	2	-	4.3	6.6	16.2	57.4	0.034 ±0.002	2
5	**3f**	60	1.5	56.8	79.4	92.1	95.2	-	0.81 ±0.02	78

* TOF – turnover frequency in 1 hour determined by conversion < 30%.

In the absence of base, complex **3f** exhibits low activity at 60°C with a 62.4% yield of product in 24 h (k_{obs} = 0.076 ±0.002 h^{-1}, Table 20, line 2). A run carried out under the same conditions using **4f** in place of **3f** showed no significant activity (less than 6% in 24 h; Table 20 line 3). Addition of 1 equiv. of a strong base (NaHMDS), however, leads to a tenfold increase of the activity of **3f**: (k_{obs} = 0.81±0.02 h^{-1}, Table 20, line 5). The kinetic analysis shows a first order rate law with respect to substrate (more on this later). A control experiment showed that the NPN ligand participates in the catalytic reaction, since in its absence compound $[(\eta^6\text{-}p\text{-cymene})RuCl_2]_2$ (**L26**) does not catalyze the reaction (Table 20, line 1), and still yields a poor activity even in the presence of a base, < 10% yield of the product in 4 h (Table 20, line 4).

It is relevant to point out that other chloride precatalysts are not active unless transformed to the active hydride species by treatment with a strong base in the alcohol solvent.[23,96]

II.2.1 Mechanistic study of acetophenone reduction by 3f.

II.2.1.1. Generation of the hydride complex 6f.

Complex **3f** is poorly soluble in isopropanol at room temperature, therefore benzene/isopropanol mixtures were used for model studies by $^{31}P\{^{1}H\}$ NMR spectroscopy. In a solvent mixture consisting of 0.5 ml of C_6D_6 and 60 µl of ^{i}PrOH (**3f**/^{i}PrOH = 1/40), **3f** is completely soluble and shows long-term stability at room temperature. It is characterized by a $^{31}P\{^{1}H\}$ NMR resonance at δ 43.1 (*vs.* δ 42.9 in pure ^{i}PrOH). Warming to 60°C led to slow and partial decomposition to the phosphine oxide $Ph_2P(O)NHTol$ (NPO, δ 17.9), to free aminoiminophosphoranes **1a** (NPNH, δ -5.1) and to a new complex **6f** (δ 33.05) (Figure 44). The ^{1}H NMR spectra shows the presence of the hydride resonance of **6f** at δ -3.1.

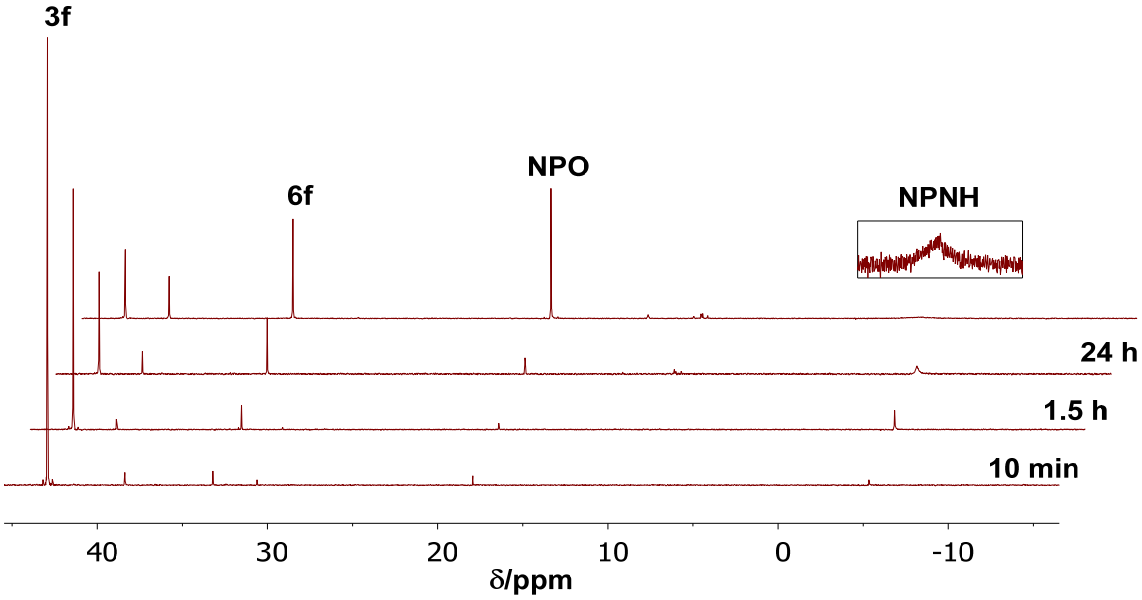

Figure 44. $^{31}P\{^{1}H\}$ monitoring of the heating of **3f** in C_6D_6 in the presence of ^{i}PrOH. Conditions: 0.5 mL of C_6D_6, 13 mg of **3f** (0.02 mmol), 60 µL of ^{i}PrOH (^{i}PrOH/**3f** = 40), T = 60°C.

The generation of **6f** at room temperature is significantly faster in the presence of 5 equiv. a weak base (diazabicycloundecene, DBU). However, a significant decomposition of the initial complex **3f** is observed (Figure 45).

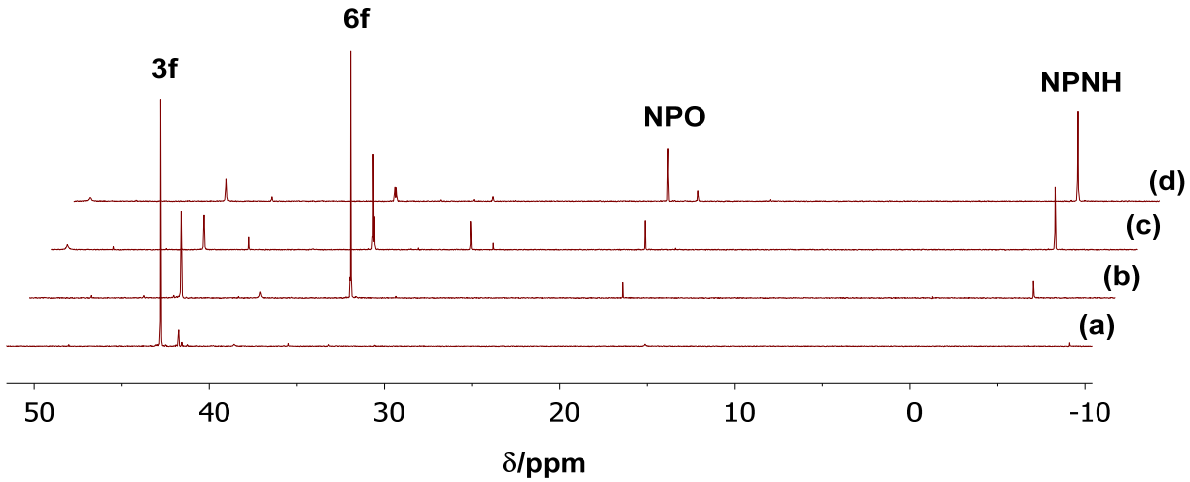

Figure 45. $^{31}P\{^{1}H\}$ monitoring of the reaction of **3f** in C_6D_6 in the presence of ^{i}PrOH and DBU. Conditions: 0.5 mL of C_6D_6, 13 mg of **3f** (0.02 mmol), 60 µL of ^{i}PrOH (^{i}PrOH/**3f** = 40), 15 µL of DBU (0.1 mmol, DBU/**3f** = 5). (**a**) Before DBU addition; (**b**) after 30 min at r.t.; (**c**) after 2 h at 60°C; (**d**) after 24 h at 60°C.

The treatment of **3f** with a strong base (NaHMDS) in C_6D_6/^{i}PrOH leads to the rapid and selective generation of complex **6f** at room temperature, which according to the NMR data corresponds to the hydride complex [(η^6-*p*-cymene)RuH{Ph_2P(N-*p*-Tol)$_2$}] (Scheme 32). The $^{31}P\{^{1}H\}$ resonance is observed at δ 33.2 and the hydride resonance in the ^{1}H NMR spectrum is at δ -3.1 (Figure 46). The other signals have also been identified in the ^{1}H and $^{13}C\{^{1}H\}$ NMR spectra, the assignment being aided by HMQC (^{1}H-^{13}C) and ^{13}C (JMOD-^{1}H) experiments. Both ^{1}H and $^{13}C\{^{1}H\}$ spectra also reveal the simultaneous formation of acetone (see SI, Figures S1 for ^{1}H NMR and S2 for $^{13}C\{^{1}H\}$ NMR). The IR spectra of the hydride complex **6f** in C_6D_6 shows the presence of the ν_{RuH} band at 1882 cm^{-1} and the ν_{CO} band of the acetone co-product at 1716 cm^{-1}.

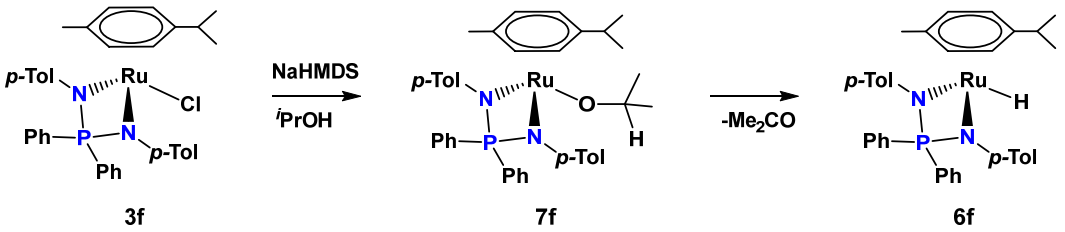

Scheme 32. Generation of arene hydride complex **6f**.

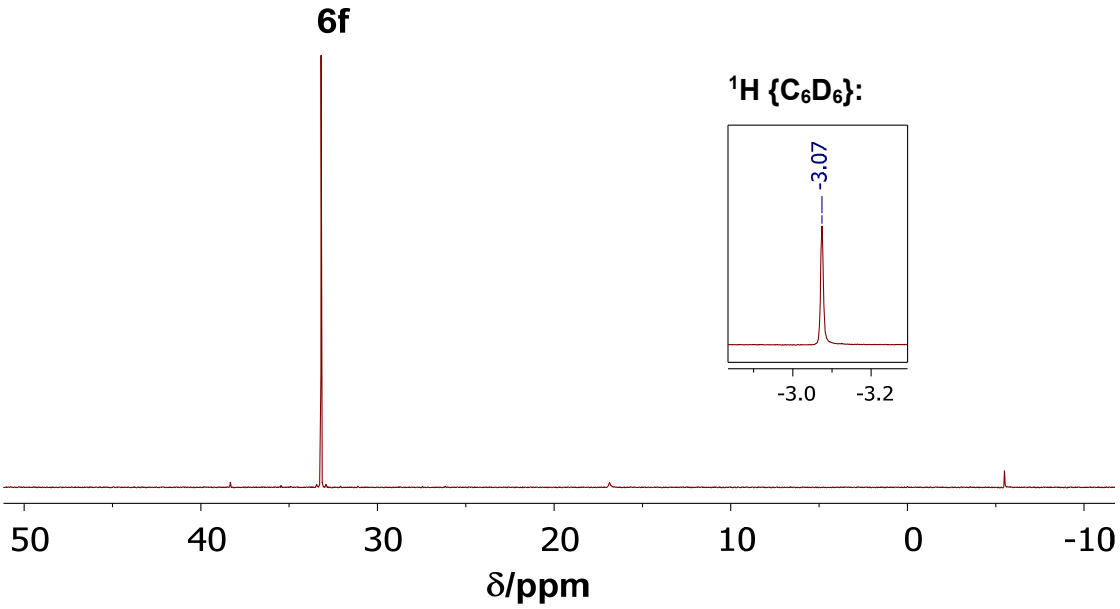

Figure 46. $^{31}P\{^{1}H\}$ NMR spectra of **6f**, generated *in situ* from **3f** in C_6D_6. Conditions: 0.5 mL of C_6D_6, 13 mg of **3f** (0.02 mmol), 60 µL of ^{i}PrOH (^{i}PrOH/**3f** = 40), 15 µL of NaHDMS (2M in THF; HMDS/**3f** = 1.5), 15 min at room temperature.

Monitoring this reaction by $^{31}P\{^{1}H\}$ NMR (Figure 47) shows the presence of an intermediate characterized by a resonance at δ 38.5. In the ^{1}H NMR spectrum (see SI, Figure S3) this compound shows signals close to those of **3f**. It is tentatively assigned to the isopropoxide complex [(η^6-*p*-cymene)Ru(O^{i}Pr){Ph_2P(N-*p*-Tol)$_2$}] (**7f**). This intermediate accumulates in the first few minutes, and then completely turns into the hydride complex **6f** by β-H elimination of acetone within 30 min.

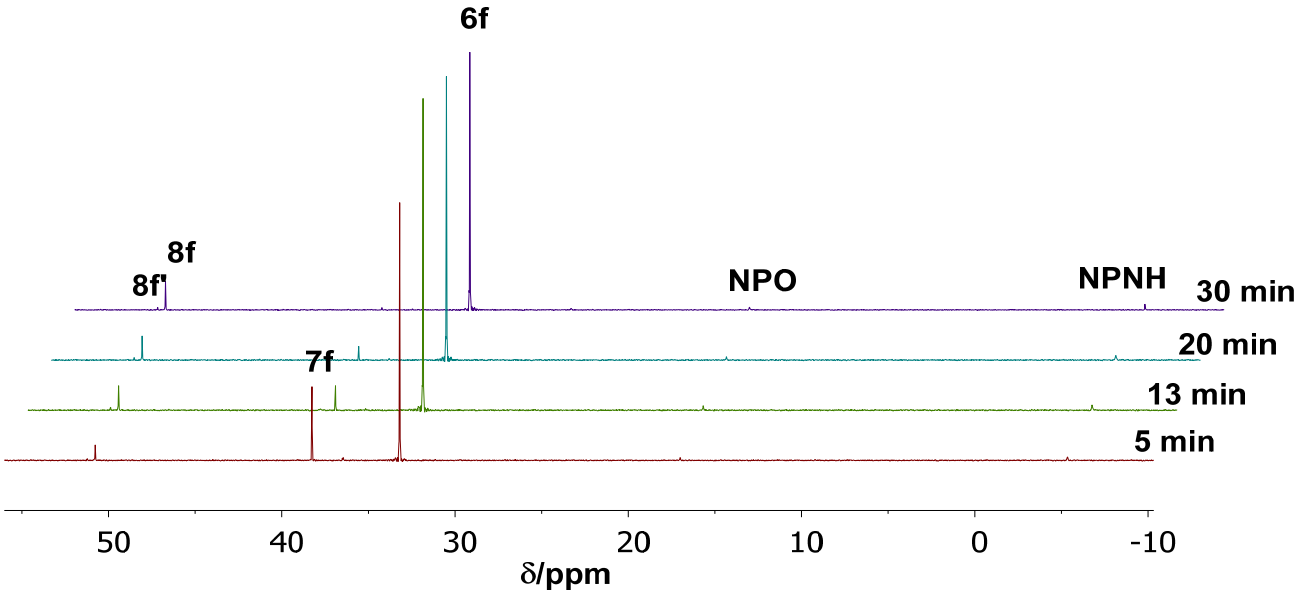

Figure 47. $^{31}P\{^{1}H\}$ NMR monitoring of the generation of **6f** at room temperature: 0.5 mL of C_6D_6, 13 mg of **3f** (0.02 mmol), 60 µL of ^{i}PrOH (^{i}PrOH/**3f** = 40), 15 µL of NaHDMS (2M in THF; HMDS/**3f** = 1.5).

II.2.1.2. Isomerization of 6f to 8f,8f'.

Complex **6f** appears relatively stable at room temperature in the presence of ^{i}PrOH, but two new resonances at δ 50.6 and 51.1 grow over time. These are related to the new complexes **8f** and **8f'** (Figure 47). On a preparative scale, the isolated complex **6f** contains ca. 40% of **8f** and **8f'** according to the NMR spectra in pure C_6D_6 (Figure 48). Analysis of the $^{31}P\{^{1}H\}$, ^{1}H, 2D COZY, $^{13}C\{^{1}H\}$, 2D H-P HMQC and 2D H-C HMQC NMR spectra (see SI, Figure S4-S8) shows that **8f** and **8f'** are isomeric cyclohexadienyl complexes, which are formed by intramolecular migration of the hydride hydrogen atom **6f** to the carbon atom of an arene ring (Scheme 33). It is noteworthy that only one set of signals for the NPN ligand atoms is observed in the ^{1}H NMR spectrum, whereas the cyclohexadienyl ligand signals differ for **8f** and **8f'**.

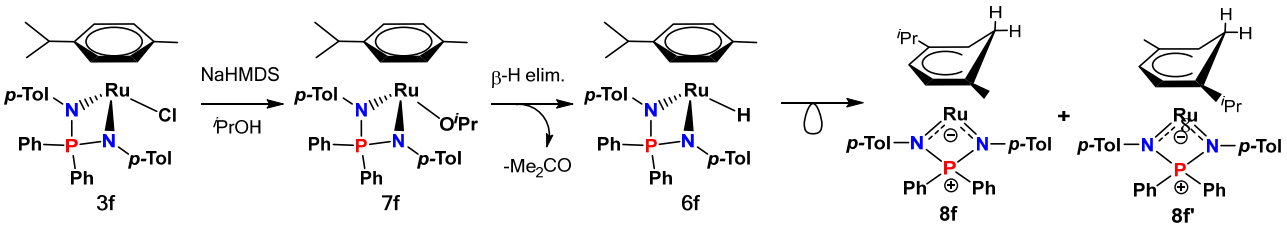

Scheme 33. Rearrangement of hydride complex **6f** to cyclohexadienyl complexes **8f** and **8f'** when trying to isolate **6f**.

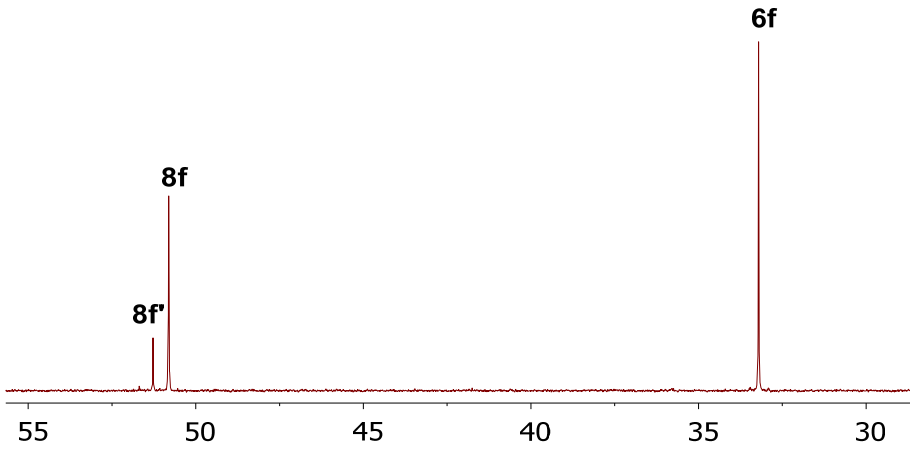

Figure 48. $^{31}P\{^{1}H\}$ NMR spectra of **6f**, prepared from **3f** with isolation and subsequent dissolution in C_6D_6.

The structure of the cyclohexadienyl complex was confirmed by single-crystal X-ray diffraction (Figure 49). The coordination geometry is a typical 2-legged piano stool with the cyclohexadienyl ring approximately orthogonal to the RuN_2P plane. The analysis of the average positions of the ring C atoms indicates that two C atoms (C_{53} and C_{56}) are significantly displaced from the plane of the other four C atoms. This suggests disorder between two conformations that differ in the position of the sp^3 C atom (*ortho* to the C_{iPr} or C_{Me} group). Thus, the crystal appears to derive from the co-crystallization of the two isomers **8f** and **8f'** in a ratio close to 1:1. Therefore, the disorder modelling is difficult, and the exact position of the cyclohexadienyl CH_2-groups cannot be determined.

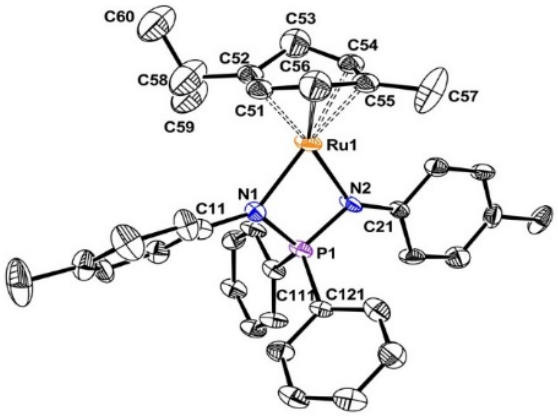

Figure 49. ORTEP diagram of the cyclohexadienyl complexes **8f**/**8f'**.
Selected bond lengths (Å) and angles (°): Ru-C_6Me_6(centroid) 1.743, Ru-N_1 2.061(12), Ru-N_2 2.090(13), N_1-Ru-N_2 70.2(5), N_1-P-N_2 95.8(7), Σ(N_1) 358.9, Σ(N_2) 359.7.

Interestingly, whereas the Cambridge Structural Database (CSD) contains >2300 X-ray structures of (η^6-*p*-cymene) complexes of transition metals, of which nearly all (>2100) are ruthenium complexes, this **8f**/**8f'** mixture is apparently the first reported structure, for any transition metal, with a cyclohexadienyl ligand derived from *p*-cymene. It is also only the second reported structure of a cyclohexadienyl derivative of Ru(II) with a 16ē configuration, the only other precedent being a compound where the cyclohexadienyl ligand is para-disubstituted by CF_3 and by the β-diketiminate -CH(CMe=NAr)$_2$ group (Ar = 2,6-$C_6H_3{}^iPr_2$), in which cyclohexadienyl ligand was formed as a result of the reduction of the coordinated *p*-$(CF_3)_2C_6H_4$ arene by the β-diketiminate as external nucleophile.[78]

The generation of the hydride complex **6f** by an alternative strategy (**3f** and $NaBHEt_3$ in neat C_6D_6, without any ^{i}PrOH), led again to a mixture of the hydride complex **6f** (65%) and the cyclohexadienyl complexes **8f**/**8f'** (35%) and with time the fraction of cyclohexadienyl complexes increased to 60% (Figure 50). Probably, in a apolar solvent, **6f** is less stable than in the presence of isopropanol, and quickly turns into **8f** and **8f'**(Figure 34).

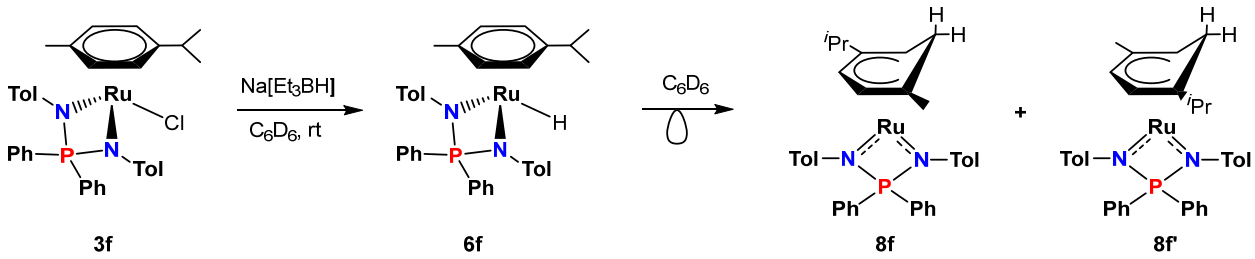

Scheme 34. The reaction of the chloride complex **3f** with $NaBHEt_3$.

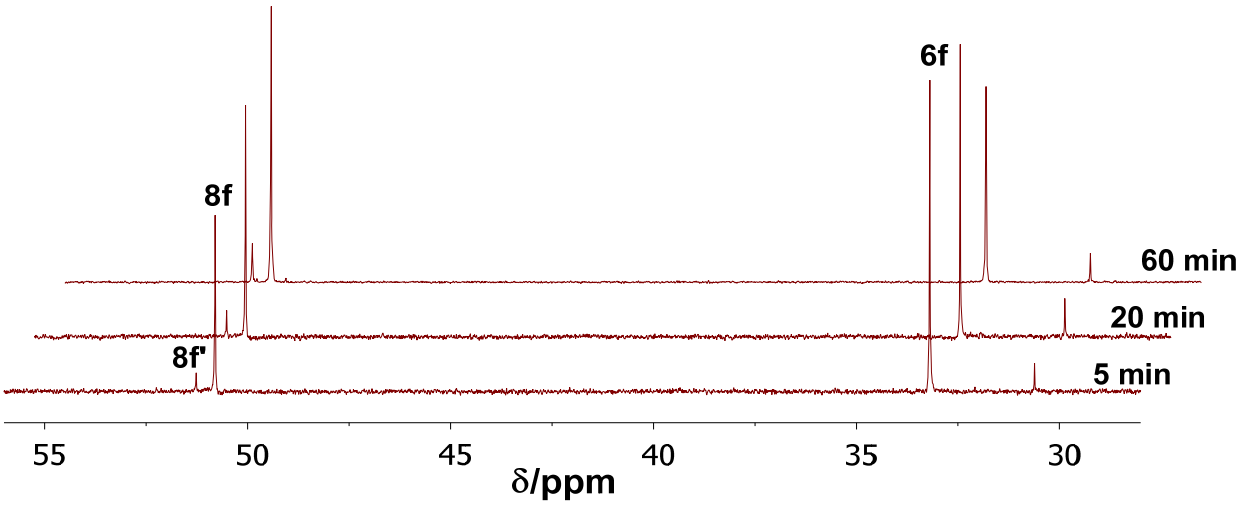

Figure 50. $^{31}P\{^1H\}$ NMR monitoring of the isomerization of **6f** to **8f**/**8f'** in C_6D_6 at room temperature: 0.5 mL of C_6D_6, 13 mg of **3f** (0.02 mmol), 22 μL of $Na[Et_3BH]$ (1M in toluene; $Na[Et_3BH]$/**3f** = 1.2).

The **6f** isomerization to **8f**, **8f'** in apolar (benzene, toluene) solvent is irreversible, or the reversible process is very slow on the NMR timescale. This is suggested by 2D ^1H EXSY NMR experiments carried out in C_6D_6 and toluene-d_8 in the temperature range 25 – 80°C, which did not reveal any cross peak between the hydride resonance of **6f** (δ ^1H at -3.04) and the methylene resonance of the cyclohexadienyl isomer **8f** (δ ^1H at 2.67) (Figure 51).

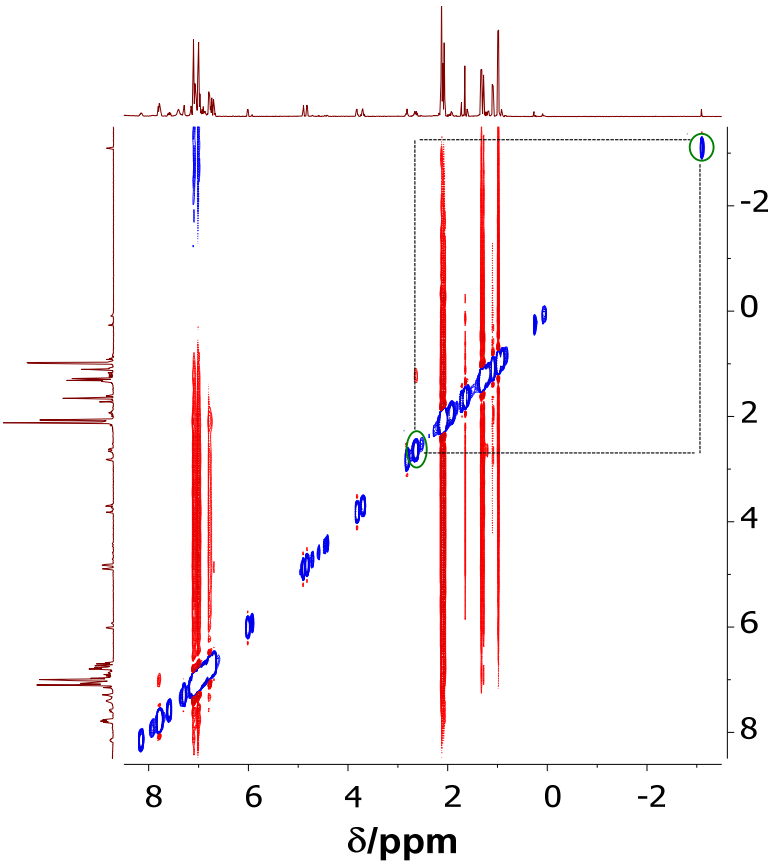

Figure 51. 2D ^{1}H EXSY NMR spectra of **6f**, **8f**, **8f'** in C_6D_6 at 80°C (t_{mix} = 1s).

According to the $^{31}P\{^{1}H\}$ NMR spectra, when the mixture of **6f**/(**8f**+**8f'**) (35/65) is heated from 25°C to 80°C, the thermodynamically more favorable cyclohexadienyl complexes accumulate to ca. 84%. However, when this mixture is subsequently cooled to room temperature, the initial ratio between **6f** and **8f** is not restored (Figure 52).

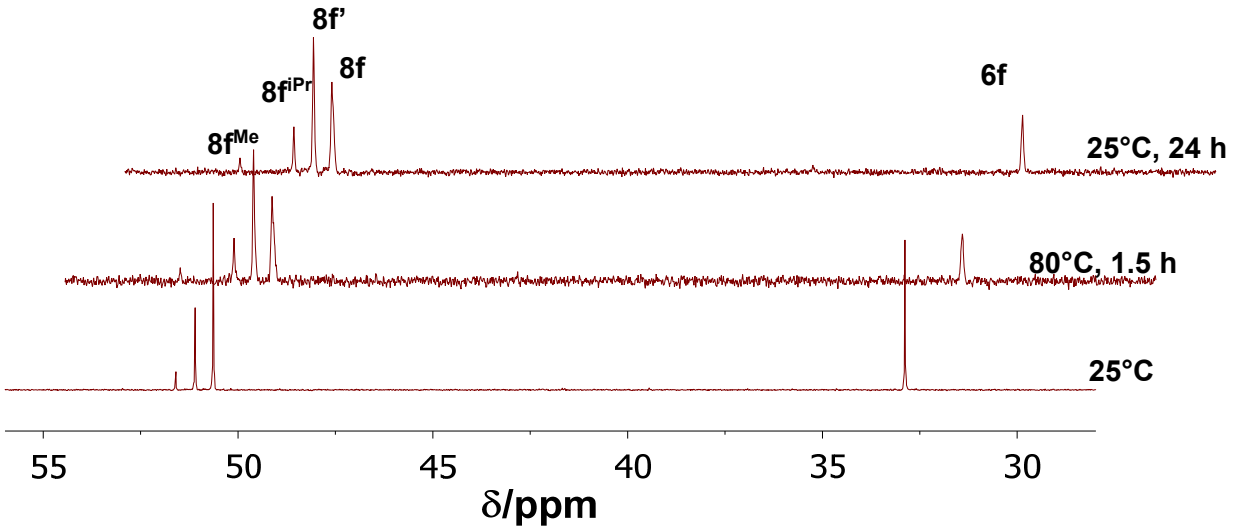

Figure 52. $^{31}P\{^{1}H\}$ NMR spectra of the **6f**/**8f**/**8f'** mixture in toluene-d_8, after being prepared from **3f**/NaHMDS (1/1) in neat ^{i}PrOH.

In addition, the extensive thermal treatment resulted in the appearance of two new resonances in the same region of the cyclohexadienyl isomers, at δ 51.6 and at δ 53.0. It appears reasonable to attribute these peaks to the other possible isomers, **8f^{iPr}** and **8f^{Me}**, respectively (Scheme 35). Before heating, the content of the isomer at δ 51.6 is only 4%, but the relative proportion of this isomer after heating to 80°C for 1.5 h increases to 12% and the signal of the fourth isomer (2%) appears. The structures of all four cyclohexadienyl isomers in solution were confirmed by $P\{^{1}H\}$, ^{1}H, $^{13}C\{^{1}H\}$, ^{1}H-^{1}H COSY and ^{1}H-^{13}C HSQC spectra (see SI, Figure S4 – S8), indicating that the δ 51.6 resonance corresponds to isomer **8f^{iPr}** and that at δ 53.0 is due to **8f^{Me}**. Hence, this thermal treatment resulted not only in the conversion of part of the hydride **6f** to the isomeric cyclohexadienyl structure but also to a redistribution of the cyclohexadienyl isomers among themselves. Although **8f** is the kinetic reaction product, the thermodynamic stability of **8f** and **8f'** are close. The isomers **8f^{iPr}** and **8f^{Me}** resulted from attack of the hydridic atom to sterically more congested carbon atoms are expectedly less thermodynamically favorable.

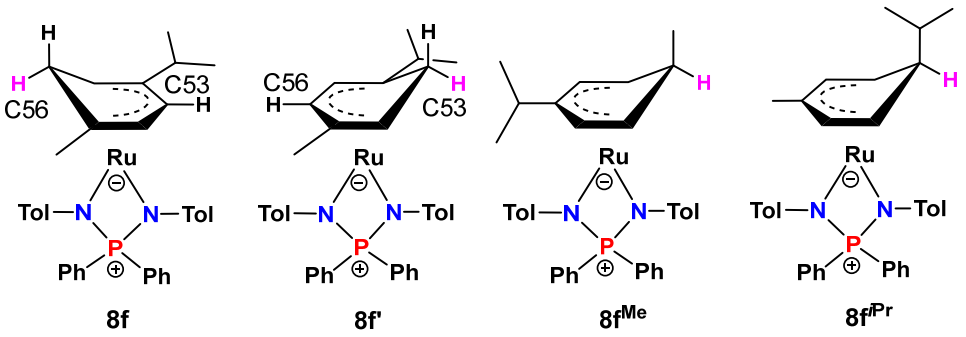

Scheme 35. Possible isomers of the cyclohexadienyl complex **8f**.

II.2.1.3. Quantum chemical calculations of the rearrangement of the complex 6f.

DFT[2] calculations were carried out with two specific objectives in mind: 1) validate the high activation barrier for the **6f/8f** isomerizations; 2) validate the greater stability and kinetic accessibility of the **8f** and **8f'** isomers relative to $\mathbf{8f^{iPr}}$ and $\mathbf{8f^{Me}}$. For the first purpose, the calculations were carried out on a simplified model where *p*-cymene was replaced with a non-substituted benzene ring. The NPN ligand, on the other hand, was kept essentially unchanged, replacing only the tolyl *p*-Me groups, which are both electronically and sterically almost inconsequential, with H atoms: [(η^6-C_6H_6)Ru(PhNPPh$_2$NPh)H] (**6F**) and [(η^5-C_6H_7)Ru(PhNPPh$_2$NPh)] (**8F**). Initial exploration of the relative stability of the **6F** and **8F** isomers were carried out with two standard functionals (M06L and B97D)[96], all geometries being reoptimized with each functional. The calculations with the former functional were corrected for long-range dispersion interactions by Grimme's GD3 method, whereas the B97D functional already considers dispersive forces. The calculations with both functionals were further corrected for the thermal parameters at 298.15 K and for solvation effects in isopropanol using a polarizable continuum model. The overall results were quite similar, therefore only the data of the DFT/B97D calculation will be discussed. The calculations show a slight preference for the cyclohexadienyl structure in terms of electronic energy (ΔE_{iPrOH}). However, the **8F** and **6F** stability is comparable in terms of free energy (ΔG_{iPrOH}, Table 21). For the **6F**/**8F** interconversion, involving H atom transfer between the Ru atom and a ring C atom, energies for the transition state **TSB** were rather high (> 35 kcal/mol) relative to the starting and ending isomers **6F** and **8F**. The transition state is at high energy presumably because of the need to extensively distort the coordination geometry and because there is more extensive bond breaking than bond

[2] The calculation was carried out by Dr. E. Dedier and Prof. R. Poli (LCC CNRS, Toulouse).

forming: the Ru···H and H···C bonds in **TSB** are 1.842 and 1.426 Å compared to 1.575 and 1.098 Å for Ru-H in **6F** and for C-H in **8F**, respectively. The Mulliken charge on the H atom involved in the isomerization process goes from slightly negative in **6F** (-0.111) to slightly positive in **TSB** (0.077) and then more positive in **8F** (0.134). This result justifies the experimental observation of a very slow interconversion between **6f** and the cyclohexadienyl isomers **8f** due to the high activation barrier and between the cyclohexadienyl isomers among themselves. The isomerization of the cyclohexadienyl isomers among themselves would presumably have to transit through the hydride isomer **6f** and is associated with overcoming the same barrier.

Table 21. Relevant geometrical parameters and relative energies of the optimized structures of **6F**, **8F** and of the experimental structures **3f**, **4f**, **8f**.

Parameters	6F	3f	8F	8f/8f'		4f	TSB
			Distances (Å):				
Ru-N	2.164 2.158	2.145(2) 2.126(2)	2.121 2.124	2.06(1) 2.09(1)	2.06(1) 2.12(1)	2.031(2) 2.017(3)	2.132 2.152
Ru-Arene(centroid)	1.809		1.677	1.743	1.689	1.659(1)	1.714
			Angles (°):				
N_1-Ru-N_2	69.03	68.24(9)	70.66	70.2(5)	71.2(5)	72.4(1)	70.07
N_1-P-N_2	96.32	96.7(1)	96.67	95.8(7)	97.7(7)	94.6(1)	97.12
ΣN	355.8 359.1	357.2(6) 358.2(6)	359.1 358.4	358.9 359.7	359.8 353.9	360.0(6) 358.9(5)	357.1 354.7
Arene(centroid)-Ru-P	69.03	68.24(9)	70.66	70.2(5)	71.2(5)	72.4(1)	70.07
			Energies (kcal/mol):				
ΔE_{iPrOH}	0.0		-3.1				36.7
ΔG_{iPrOH}	0.0		0.8				34.9

In terms of optimized geometries, the parameter of greatest interest is the pyramidalization of the N atoms in the NPN ligand, as evaluated by the sum of three bond angles: C(Ar)-N-Ru, Ru-N-P and P-N-N(Ar) (ΣN, Table 21). This provides information on the delocalization of the N lone pair onto the aryl substituent and on the Ru atom (for the electronically unsaturated structures of **8f/8f'**). The calculations indicate that ΣN is close to 360° (planarity) not only for the cyclohexadienyl structure **8F**, but also for 18ē complex

6F, suggesting efficient delocalization of the N lone pair onto the phenyl substituent. This corresponds to the experimental evidence, not only for the 16ē complexes **8f/8f'** and **4f,** but also for the 18ē complex **3f**.

In terms of the second objective, the NPN ligand of **8f** was simplified for computational efficiency by replacing all Ph and *p*-Tol substituents with H atoms (**8f(H)**), since the nature of the NPN substituents should not affect to a great extent the relative stability of the different cyclohexadienyl isomers. The ring, on the other hand, was introduced in the calculations without any simplification. Because the four different isomers contain exactly the same number and type of bonds, only the B97D functional was selected to evaluate their relative energy. The results (Figure 53) show that, in agreement with the experimental evidence, isomers **8f(H)** and **8f'(H)** are more stable that the other two isomers. Their relative energies are quite close, but significantly lower than those of **8f^{iPr}(H)** and **8f^{Me}(H)**. This relative energy ordering is consistent with the isomer ratio in the $^{31}P\{^{1}H\}$ NMR spectra after heating (Figure 52). The small discrepancy in energy for the equimolar **8f** and **8f'**, which is well within the accepted margin of computational error, may in part be related to the simplification of the NPN ligand. The preferred generation at room temperature of the isomer **8f** indicates kinetic control for the H atom transfer from the Ru atom to the ring C atom. The relative barriers for the H atom transfer to all four different types of C atom in the *p*-cymene ligand were not calculated. Steric arguments, however, are consistent with the faster formation of **8f** since the H ligand migrates to the C atom *ortho* to the less hindered C_{Me} group.

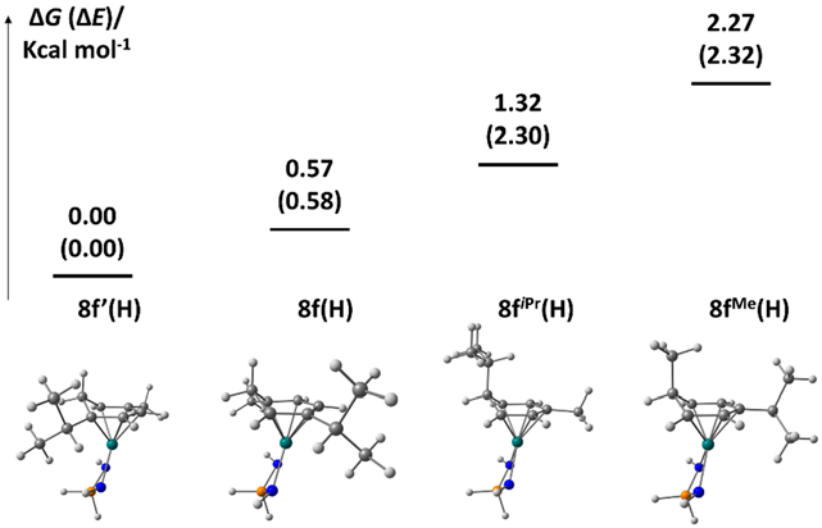

Figure 53. Relative gas phase energies (in kcal/mol) and views of the optimized (DFT/B97D) geometries for the model compounds **8f(H)**, **8f'(H)**, **8f^{iPr}(H)** and **8f^{Me}(H)**.

In terms of optimized geometries, it is of interest to observe that the N atoms are significantly pyramidalized, the ΣN parameter being in the 325.4 – 343.1° range (Table 22). This difference relative to the $PhNPPh_2NPh$ models discussed above (**6F**, **8F** and **TSB**) is related to the inability of the N atoms to delocalize their lone pair onto the H substituent, in spite of the possible partial delocalization to the Ru centre in the 16ē systems.

Table 22. Relevant geometrical parameters of the optimized structures of **8f(H)**, **8f'(H)**, **8f^{iPr}(H)** and **8f^{Me}(H)** using the B97D functional.

Parameters	8f(H)	8f'(H)	8f^{Me}(H)	8f^{iPr}(H)
		Distances (Å):		
Ru-N	2.218	2.215	2.210	2.162
	2.212	2.211	2.204	2.135
Ru-Arene(centroid)	1.747	1.759	1.757	1.654
		Angles (°):		
N-Ru-N	69.38	69.18	69.57	70.95
N-P-N	99.92	99.50	99.71	99.14
ΣN	319.0,	322.7,	320.5,	329.9,
	319.1	317.9	319.1	339.5
Arene(centroid)-Ru-P	159.94	160.99	159.06	165.15

II.2.1.4. Effect of alcohol on 6f.

As noted above, the stabilization of **6f** increases in the presence of ^{i}PrOH. Therefore, we studied the effect of the alcohol concentration and acidity on the ^{1}H NMR spectral properties. The spectral changes observed upon addition of alcohols with different proton-donating strengths, as well as acetone, to a solution of **6f** in C_6D_6, are given in Table 23.

Table 23. NMR resonances for solutions of **6f** in the presence of alcohols and acetone.

№	Solvent	Additive	^{31}P, ppm.	^{1}H (RuH), ppm.
1	C_6D_6	-	33.2	-2.96
2	C_6D_6	^{i}PrOH (2 equiv.)	33.2	-2.98
3	C_6D_6	^{i}PrOH (10 equiv.)	33.2	-3.01
4	C_6D_6	^{i}PrOH (40 equiv.)	33.2	-3.07
5	^{i}PrOH	-	32.9	-3.14
6	C_6D_6	TFE (10 equiv.)	33.4	-3.16
7	C_6D_6	Acetone (10 equiv.)	33.2	-2.98
8	CD_3COCD_3	-	33.9	-3.53

In the ^{1}H NMR spectra in benzene-d_6, an upfield shift of the hydride resonance is observed, proportional to the amount of alcohol added (Table 23, lines 2-5) and to its proton-donating ability (Table 23, lines 3 and 6). Such shift of the hydride resonance indicates the formation of a "dihydrogen bond" [(η^6-*p*-cymene)Ru(NPN)H···HA],[98,99] namely an H-bond between the alcohol as a proton donor (HA) and the hydride ligand of **6f** as a proton acceptor. As expected, this effect is more notable on the ^{1}H hydride resonance and much less on the ^{31}P resonance. Formation of **6f•**iPrOH can be considered as a prerequisite for the observed H_2 evolution from **6f** and iPrOH, to yield **7f**[99] (see below).

The presence of acetone has no effect on the ^{1}H and ^{31}P resonances of **6f** when added in small quantities (Table 23, line 7). A large excess (Table 23, line 8), on the other hand, leads to displacement of the ^{31}P resonance to lower fields and to a strong upfield shift of the hydride ^{1}H resonance. This phenomenon can be rationalized with the establishment of a hydride transfer equilibrium, probably involving an 18ē σ-complex [(η^6-*p*-cymene)Ru^{+}(NPN)···$HCMe_2O^{-}$] (**9f**) (Scheme 36). Such a process should lead to increased shielding for the hydride ligand in the intermediate complex, similar to the dihydrogen

bond.[100,101] Complex **9f** is a presumed intermediate on the way to the isopropoxide complex **7f**. A rapid equilibrium between **6f** and **7f** is excluded because both compounds are independently observed under other conditions (Figure 47), thus their interchange is slow on the NMR timescale.

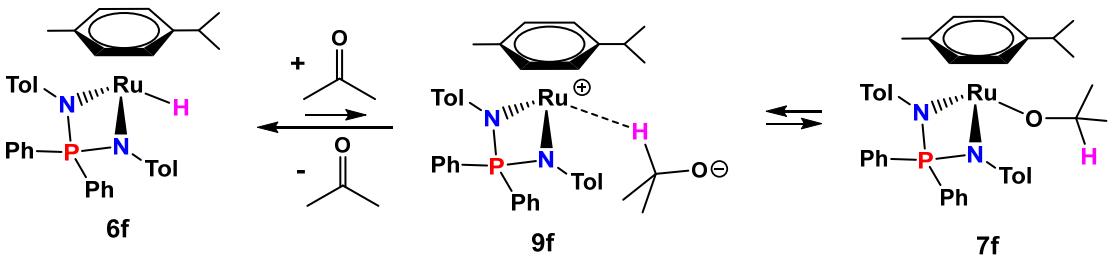

Scheme 36. Formation of 18ē σ-complex **9f**.

The reaction of complex **6f** with proton donors, stronger than ^{i}PrOH, namely trifluoroethanol (TFE) and hexafluoroisopropanol ($(CF_3)_2CHOH$, HFIP) was studied in detail (Scheme 37).

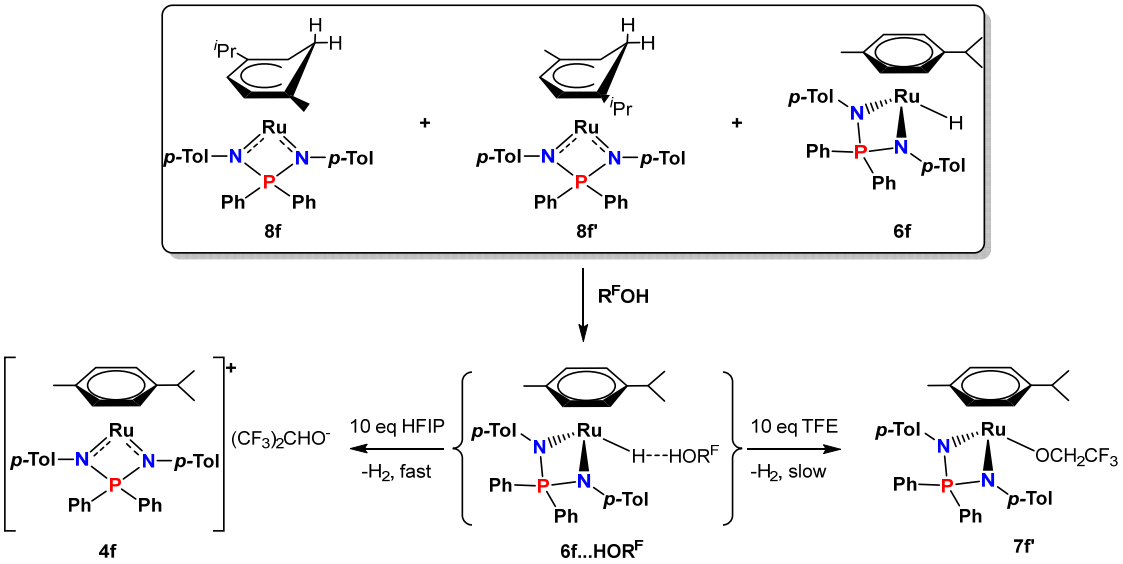

Scheme 37. Reaction of **6f**/**8f**/**8f'** with fluorinated alcohols.

The addition of 10 equiv. of TFE to a C_6D_6 solution of **6f**, **8f** and **8f'** leads to a slow change in the $^{31}P\{^{1}H\}$ NMR spectra (Figure 54). After 15 min at room temperature the (**8f**+**8f'**)/**6f** ratio increases from 42:58% to 66:34%, whereas the **8f**/**8f'** ratio changed slightly in favor of the minor resonance at δ 51.3 from 75:25% to 64:36%. However, a new and broader resonance appears at δ 43.2 (ca. 35% of the total). This is the characteristic

region of the [(η^6-*p*-cymene)Ru(NPN)X] compounds X = Cl (**3f**); H (**6f**); O^{i}Pr (**7f**). We therefore assign this resonance to the alkoxide product [(η^6-*p*-cymene)Ru(NPN)(OCH_2CF_3)] (**7f'**) (Scheme 37). Note that while the ^{1}H and ^{31}P resonances of residual **6f** are slightly shifted (Table 23), because of the formation of the "dihydrogen bonded complex" [(η^6-cymene)Ru(NPN)H···$HOCH_2CF_3$], those of residual **8f** and **8f'** remain at exactly the same chemical shifts – this apparently means that **8f** and **8f'** do not directly interact with TFE. The change of relative intensity for (**8f+8f'**) and **6f** is therefore likely a consequence of the faster reaction of **6f** with TFE to yield **7f'** than the isomerization of **8f** and **8f'** to yield **6f**.

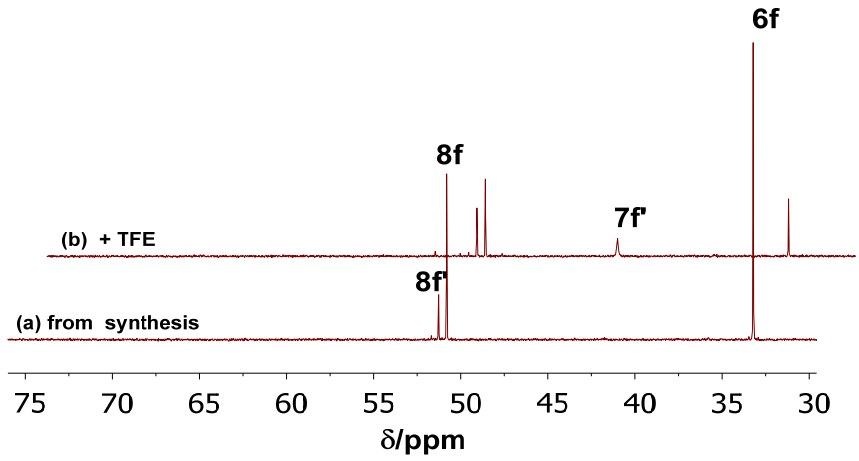

Figure 54. $^{31}P\{^1H\}$ NMR spectra of the reaction between the **6f/8f/8f'** mixture and fluorinated alcohols in C_6D_6. (**a**) Conditions for the synthesis: 13 mg (0.02 mmol) of **3f** in 2 mL of ^{i}PrOH, 10 µL of 2M NaHMDS solution in THF (1 equiv.), followed by drying and dissolution in the NMR solvent. (**b**) From (a), 15 min after adding TFE (14 µL, 0.2 mmol, 10 equiv.) at room temperature.

Treatment of another **6f**/**8f**/**8f'** mixture, prepared in the same manner, in C_6D_6 with 10 equiv of HFIP under the same conditions, on the other hand, resulted in a completely different behavior. The color immediately changed from orange to dark blue and the immediate evolution of H_2 was observed (δ_{H2} 4.51 in the ^{1}H NMR spectrum). The $^{31}P\{^1H\}$ NMR spectrum indicated the total disappearance of **6f** and **8f**/**8f'** within 15 min with generation of a single product characterized by a resonance at δ 72.3 (Figure 55). This clearly suggests the generation of the 16ē cationic complex **[4f]$^+$((CF$_3$)$_2$CHO$^-$)** by

comparison with the resonance of the isolated **[4f]$^{+}$PF$_6^{-}$** (a blue compound), which is reported as δ 71.3 in $CDCl_3$.[62]

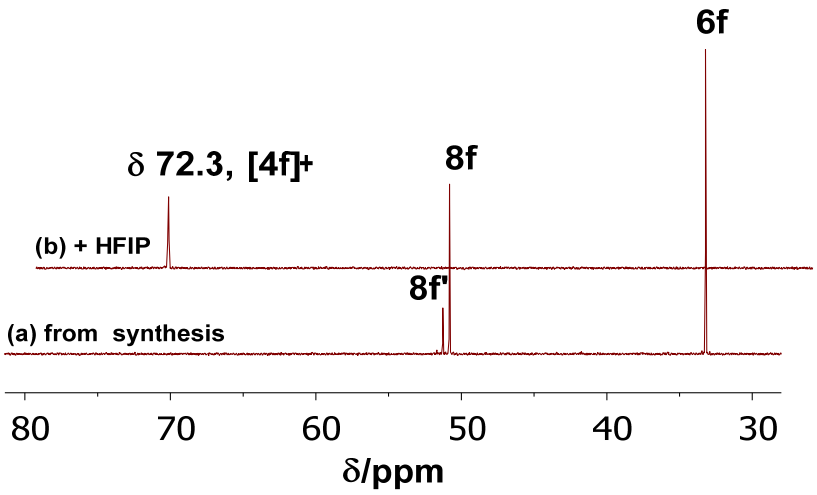

Figure 55. $^{31}P\{^{1}H\}$ NMR spectra of the reaction between the **6f/8f/8f'** mixture and fluorinated alcohols in C_6D_6. (**a**) Conditions for the synthesis: 13 mg (0.02 mmol) of **3f** in 2 mL of ^{i}PrOH, 10 µL of 2M NaHMDS solution in THF (1 equiv.), followed by drying and dissolution in the NMR solvent. (**b**) From (a), 15 min after adding HFIP (20 µL, 0.2 mmol, 10 equiv) at room temperature

The difference between these two reactions is notable in the kinetics, thermodynamics and nature of the product (immediate and quantitative for HFIP to yield **[4f]$^{+}$((CF$_3$)$_2$CHO^{-})**, slow and partial for TFE to yield **7f'** as a result of the different proton donor strength of the two alcohols and of the lower coordinating power of the hexafluoroisopropoxide anion. However, both TFE and HFIP are sufficiently acidic to transfer their proton to the hydride ligand of complex **6f**. We recall here that even the weaker acid ^{i}PrOH has given evidence in favor of the transformation of **6f** to the corresponding alkoxide **7f**.

II.2.1.5. Degradation of complex 6f.

Monitoring the reaction of complex **3f** with NaHMDS/^{i}PrOH in C_6D_6 by ^{1}H NMR spectroscopy shows the formation, in addition to the key compounds (**6f**, **8f**/**8f'**, **7f**), of small amounts of $Ph_2P(O)NH$-*p*-Tol (NPO, δ 16.9) and aminoiminophosphorane **1a**

(NPNH, δ -5.5) (**1a** in $CDCl_3$ δ -3.5), see Figure 56. Generally, aminophosphine oxides $Ph_2P(O)NHAr$ are formed as a result of hydrolytic decomposition of aminoiminophosphoranes $Ph_2P(NAr)(NHAr)$ or haloiminophosphoranes $Ph_2PBr(NHAr)$.[61] After its generation, **6f** slowly decomposes at room temperature (Figure 56). This degradation leads to increased amounts of NPO, NPNH, and the cyclohexadienyl isomers **8f** and **8f'**, as well as to the appearance of two additional compounds characterized by $^{31}P\{^1H\}$ signals at δ 27.4 and 26.2 (**10** and **10'**), which slowly accumulate over several days (Figure 56). These new compounds also form when trying to isolate **6f** (see SI, Figure S9).

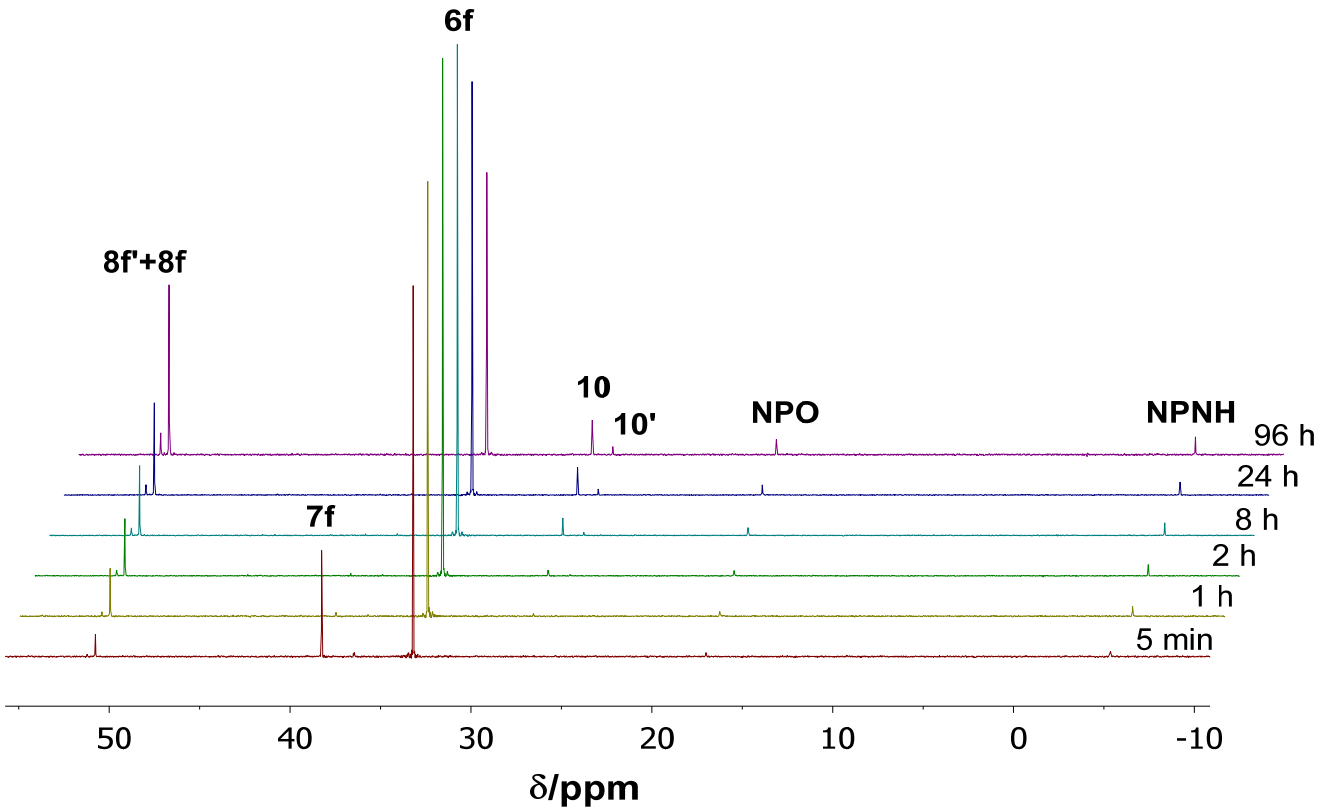

Figure 56. Prolonged monitoring of $^{31}P\{^1H\}$ NMR reaction of **3f** with NaHMDS/^{i}PrOH in C_6D_6 at room temperature (conditions as in Figure 47).

The ^{31}P signals of **10**/**10'** (see SI, Figure S9A) are close to the signals of the corresponding diaminophosphonium salt $Ph_2(NH\text{-}p\text{-}Tol)_2^+Br^-$ (δ 28.0 in $CDCl_3$) and of the palladium complex with the κ^1-NPNH ligand, *trans*-$[PdCl_2\{(p\text{-}C_6H_4{}^iPrN)PPh_2(NH\text{-}p\text{-}$

$C_6H_4{}^iPr)\}_2$] (δ 26.4 in $CDCl_3$).[66] The ^1H NMR spectra for both compound **10** and **10'** contains RuH signals shifted to high field with respect to **6f** (see SI, Figure S9B) and an asymmetric *p*-cymene ligand with four CH aromatic doublets and two nonequivalent methyl groups for ^{i}Pr-substituent.

Presumably, both compounds may correspond to half-sandwich arene ruthenium complexes with three different monodentate ligands, one of which must be a hydride. The above observations allow us to assume that these complexes correspond to [(η^6-*p*-cymene)Ru(H)(κ^1-NPNH)(O^{i}Pr)] with a κ^1-coordinated NPNH ligand. The two isomers **10**/**10'** probably have different types of formed hydrogen bond: either the hydride ligand forms a hydrogen bond with the κ^1-NPNH ligand or with an oxygen atom in the isopropoxide ligand (Scheme 38).

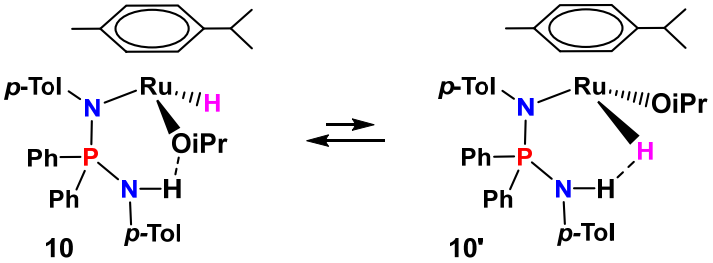

Scheme 38. Possible structures of complexes **10**/**10'**.

The increased amount of **10**,**10'** in the sample of complex **6f** after separation from the solution is probably due to the fact that most of the isopropanol and bases, which can lead the decomposition process, are removed. Prolonged heating of **6f** in the presence of isopropanol leads to the complete decoordination of the NPN ligand to aminoiminophosphorane **1a**, with partial decomposition to NPO.

All observed processes occurring with **3f** and **6f** in isopropanol can be summarized as follows (Scheme 39). In the absence of a base at elevated temperatures, the chloride complex **3f** is prone to self-dissociation with the formation of the 16ē cationic complex **[4f]$^+$Cl$^-$**. Isopropanol reversibly replaces the chloride anion in **3f**, giving the 18ē isopropanol adduct **11f**; these two compounds (**11f** and **[4f]$^+$Cl$^-$**) are present in low concentration and are not detected. The subsequent deprotonation of **11f** leads to the formation of a short-lived isopropoxide intermediate **7f**, which, as a result of the β-hydride shift, gives a relatively stable hydride complex **6f**. Probably, complex **6f** slowly

decomposes due to protonolysis of one Ru-N bond, yielding the observed asymmetric hydride intermediates **10** and **10'**. The subsequent decoordination of NPNH in them with an excess of isopropanol leads to the formation of the expected solvated isopropoxide complex **12**. This product was not detected directly, but it is noted that the related complexes $[(Arene)Ru(\mu\text{-}OR)_3Ru(Arene)]^+$ are formed under similar conditions.[102] It is important to note that the generation of **6f** requires trapping of the released HCl. In the absence of an external base, the proton may bind to the basic nitrogen atoms of the NPN ligand. When it happens, the destruction of the complex and the release of NPNH occur, which can be reused as a deprotonating agent. Thus, in the absence of a base, the generation of hydride **6f** is always accompanied by partial decomposition of the NPN complex.

In the presence of a base, the isopropoxide complex **7f** is formed quantitatively and rapidly from the starting chloride complex **3f** under the action of the isopropoxide anion at room temperature. Further β-H elimination in **7f** occurs easily with the formation of **6f**. However, complex **7f** does not contain a free coordination site, which is necessary for the coordinated intramolecular transformation into **6f**, and the partial decoordination of bidentate NPN or cymene ligands is unlikely. Presumably, this transformation proceeds through ionic dissociation followed by transfer of the hydride from intermediate σ-complex **9f** (see Section II.2.1.4).

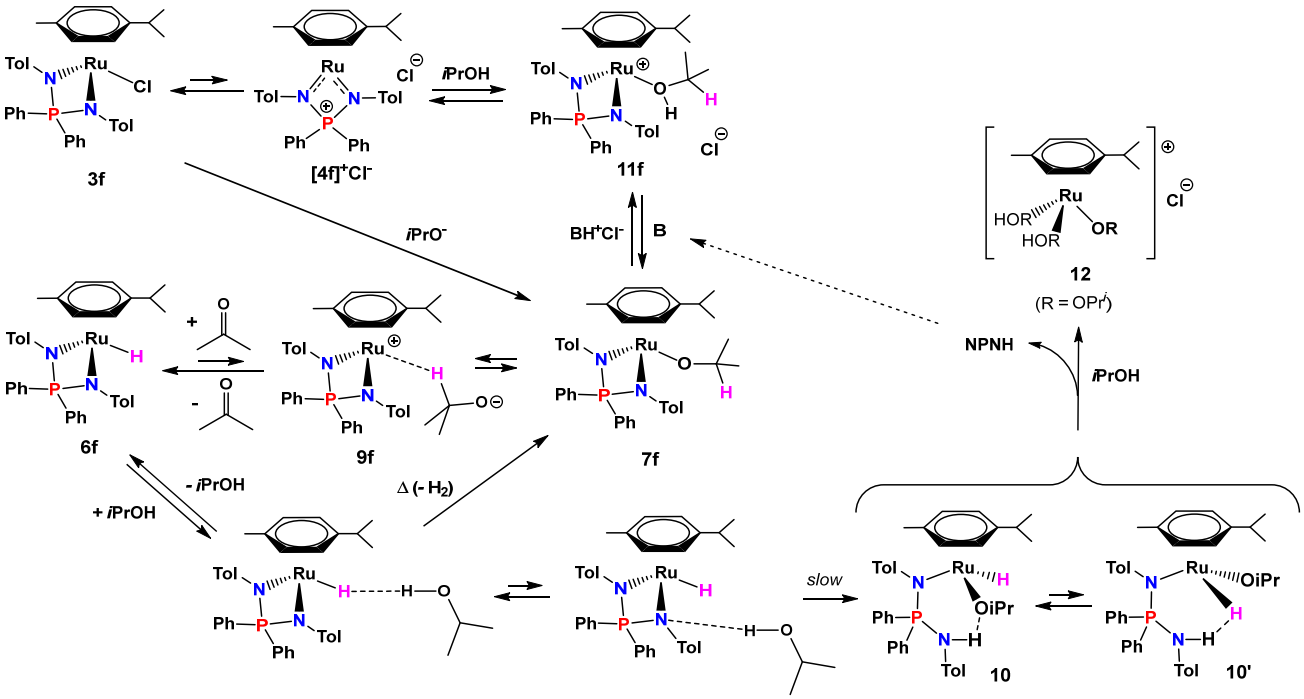

Scheme 39. Proposed mechanism for the generation of hydride **6f** from **3f**, and related chemical processes.

II.2.1.6. Kinetics of the 3f-catalyzed reduction of acetophenone.

As shown earlier, the **3f** chloride complex catalyzes the acetophenone reduction by isopropanol in the absence of a base at elevated temperatures, but the catalytic activity is much greater when a base is present. In the present section, additional results on the reaction rate dependence on the temperature and conditions of the catalytic mixture preparation are reported (Table 24) and discussed.

Table 24. Hydrogenation of acetophenone in the absence of a base catalyzed by **3f**.

№	Complex	T, °C	Conversion, %						k_{obs}, h^{-1}	TOF, h^{-1}
			0.5 h	1 h	2 h	4 h	6 h	24 h		
1	**3f**	80	17.4	40	68.2	92.2	-	-	0.606±0.001	40
2	**3f**	60	1.9	3.8	13.6	27.5	36.2	62.4	0.076±0.002	7
3	**3f***	60	1.6	5.6	14	26.6	36.6	65.9	0.075±0.001	7
4	**3f****	60	-	-	3.4	7.5	15.7	-	<0.03	2

Reaction conditions: complex **3f** (0.02 mmol), acetophenone (233 µl, 2 mmol), dodecane (226 µl), isopropanol (5 ml). [PhCOMe] = $3.7*10^{-1}$ M, [Ru] = $4*10^{-3}$ M. *Solvent ^{i}PrOH/C_6H_6 (1:1). **Keeping the catalyst for 2 hours at 60 °C before adding the substrate.

At 60°C, the kinetic analysis shows the first order behavior of the reaction with respect to substrate during the first 6 hours (Figure 57), but at later stages (24 hours) there is a deviation from linearity, which is a sign of catalyst decomposition. This result agrees with the thermal degradation of the hydride complex **6f** observed in the model experiments. The rate of ketone reduction and catalyst degradation does not have a strong dependence on the solvent polarity, because the observed rate constants in neat ^{i}PrOH and in ^{i}PrOH/C_6H_6 = 1/1 (Table 24, lines 2-3, Figure 58) are identical.

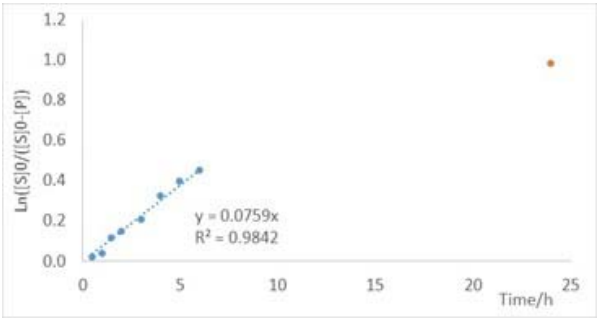

Figure 57. First-order plot for the formation of phenylethanol in ^{i}PrOH (Table 24, line 2).

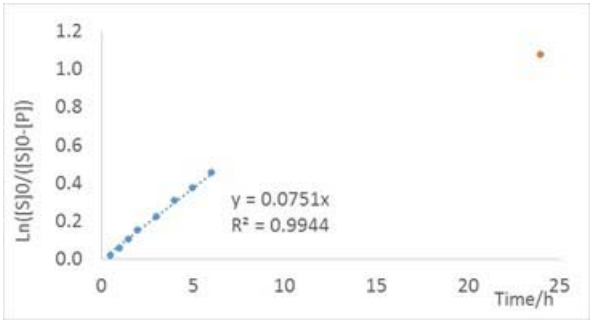

Figure 58. First-order plot for the formation of phenylethanol in ^{i}PrOH/C_6H_6 (Table 24, line 3).

The gradual catalyst decomposition under the reaction conditions is also confirmed by the fact that keeping the catalyst solution at 60°C for 2 hours before the introduction of the substrate leads to the rapid decrease in its activity (Table 24, line 4). Increasing the temperature to 80°C (Table 24, line 1) leads to an increase in the rate constant by almost an order of magnitude, and after 4 hours the yield of the product reached 92%. In this case, the linearity of the kinetic graph is maintained for 5 hours (Figure 59). This suggests that the catalyst degradation rate is much slower and depends on temperature much less than the rate of acetophenone reduction. In turn, this is consistent with the assumption that the catalytically active particle is the **6f** hydride complex, the generation of which in isopropanol in the absence of a base is greatly accelerated with increasing temperature.

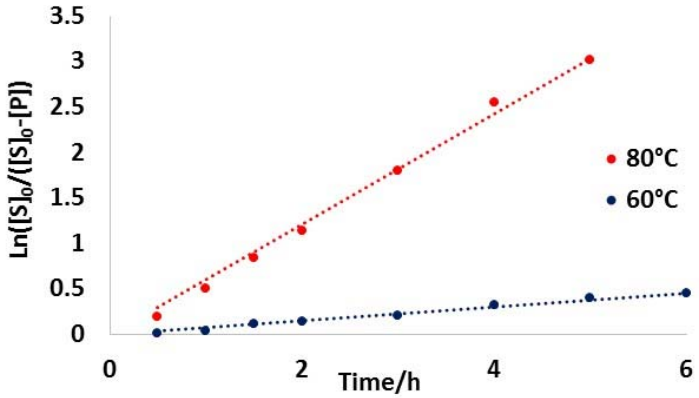

Figure 59. First order kinetic curves of the TH-reaction of acetophenone in isopropanol, catalyzed by **3f** in the absence of base. Blue line (Table 24, line 2); red line (Table 24, line 1).

The rest of catalytic experiments were carried out in the presence of at least one equivalent of NaHMDS, which quantitatively transforms **3f** into the hydride complex **6f**. To explore the order of the reaction in the catalyst, a series of experiments was carried out at a fixed temperature (40°C) and at different catalyst concentrations (Table 25).

Table 25. Hydrogenation of acetophenone with isopropanol, catalyzed by complex **3f** in the presence of a base at 40°C, depending on the catalyst concentration.

№	[3f], M	Ru/ substrate	Conversion, %						k_{obs}, h^{-1}	TOF, h^{-1}
			0.5 h	1 h	2 h	4 h	6 h	24 h		
1	0.001	0.0025	-	8.8	-	28.4	40.8	79.3	0.086±0.002	9
2	0.002	0.005	9.6	14.6	30.1	55.4	71.3	-	0.196±0.004	20
3	0.004	0.01	15.8	26.7	47.9	74.8	86.3	93.7	0.336±0.003	32
4	0.008	0.02	31.6	56.0	89.4	96.4	-	-	1.02±0.09	63

Reaction conditions: complex **3f** (0.005 – 0.04 mmol), NaHMDS/**3f** = 1.5, acetophenone (233 µl, 2 mmol), dodecane (226 µl), isopropanol (5 ml). [PhCOMe] = $3.7*10^{-1}$ M, [Ru] = $1–8*10^{-3}$ M. The catalytic mixture was kept for 15 minutes at the reaction temperature before adding the substrate.

The first-order kinetic curves in the substrate $d[Acp]/[Acp] = -k_{obs}dt$ were constructed for different catalyst concentrations (Figure 60A). The dependence of the observed rate constant k_{obs} on [Ru] is shown in Figure 60 B. This dependence is close to

linear, which confirms the first order dependence of the rate law with respect to the catalyst. The true second-order rate constant is $k = k_{obs}/[Ru] = 0.033 \pm 0.003$ $M^{-1}*s^{-1}$ at 40°C.

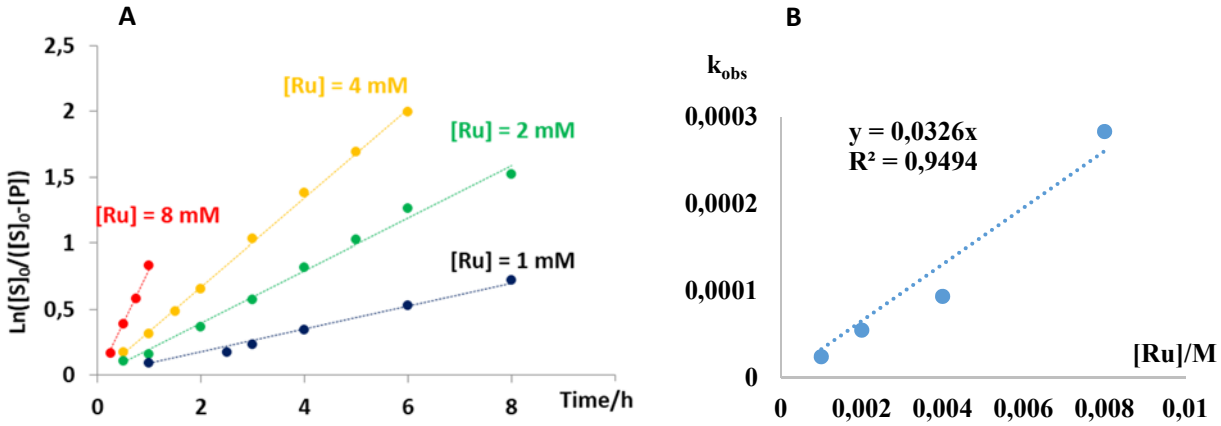

Figure 60. (**A**) Kinetic curves of the 1-phenylethanol formation at different concentrations of catalyst **3f** at 40°C. (**B**) A graph of the observed first-order rate constant k_{obs} as a function of **3f** concentration.

In order to find the activation parameters of the TH-hydrogenation process catalyzed by complex **3f**, a series of catalytic experiments was carried out at different temperatures (Table 26, Figure 61-64).

Table 26. TH of acetophenone by isopropanol, catalyzed by complex **3f** in the presence of a base at different temperatures.

№	T, °C	Conversion, %						k_{obs}, h^{-1}	k, $M^{-1}*s^{-1}$
		0.5 h	1 h	2 h	4 h	6 h	24 h		
1	25	6.8	10.6	19.0	32.6	43.1	81.9	0.095±0.001	0.01
2	40	15.9	26.8	48.0	74.9	86.4	93.8	0.336±0.002	0.05
3	60	38.9	56.8	79.4	92.1	95.2	-	0.81±0.02	0.11
4	80	47.6	78.7	93.9	98.1	-	-	1.46±0.05	0.20

Reaction conditions: complex **3f** (0.02 mmol), NaHMDS/**3f** = 1.5, acetophenone (233 µl, 2 mmol), dodecane (226 µl), isopropanol (5 ml). [PhCOMe] = $3.7*10^{-1}$ M, [Ru] = $4*10^{-3}$ M. Catalytic mixture was kept for 30 minutes at the 25°C, then heated to required temperature, and the substrate was added.

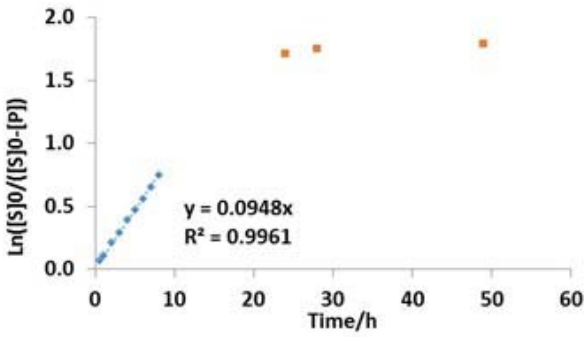

Figure 61. First order plot of the phenylethanol formation at 25°C (Table 26, line 1).

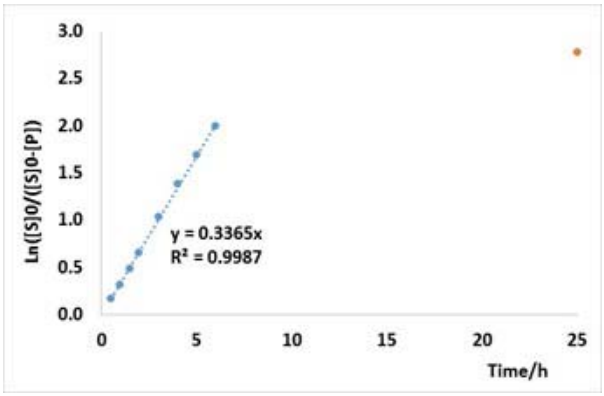

Figure 62. First order plot of the phenylethanol formation at 40°C (Table 26, line 2).

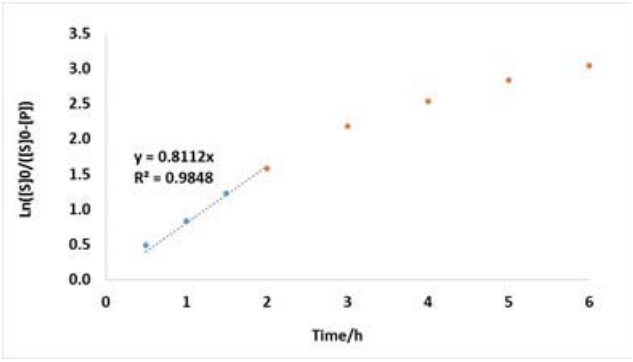

Figure 63. First order plot of the phenylethanol formation at 60°C (Table 26, line 3).

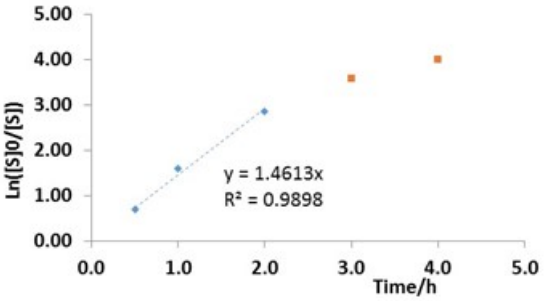

Figure 64. First order plot of the phenylethanol formation at 80°C (Table 26, line 4).

When calculating k_{obs}, only the linear sections of the kinetic curves were used, corresponding to the time periods during which no noticeable degradation of the catalyst occurs: 8 hours at 25°C, 6 hours at 40°C, 2 hours at 60°C and 80°C. Since the degradation rate of **6f** is much less temperature dependent than the rate of its catalyzed reaction, a nearly quantitative conversion of acetophenone into 1-phenylethanol is easily achieved at 80°C.

A generalized graph with the first order kinetic curves at four different temperatures is shown in Figure 65. The analysis of the k values as a function of temperature, according to Eyring relationship (Figure 66), made it possible to determine

the enthalpy and entropy of activation for the acetophenone catalytic hydrogenation: $\Delta H^{\ddagger}$ = 9.7±1.3 kcal/mol and $\Delta S^{\ddagger}$ = -31±4 cal/(mol*K).

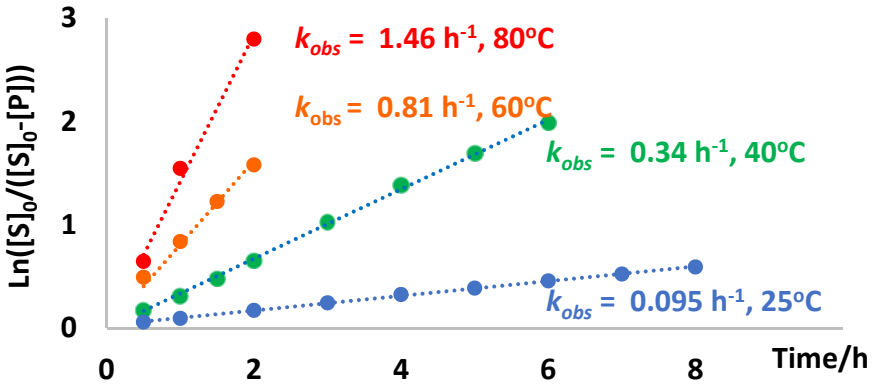

Figure 65. Kinetic curves of 1-phenylethanol formation at different temperatures.

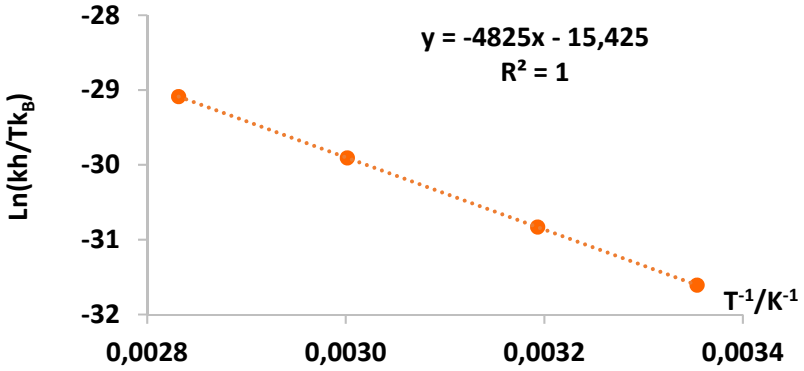

Figure 66. An Eyring analysis of observed second order rate constants *k* of 1/T.

The highly negative activation entropy implies a high level of ordering during the transition from the resting state to the transition state at the rate-limiting step of the catalytic process. Considering that the reaction takes place in a polar solvent, the ordering at the transition state is probably not related to solvation effects, but is rather caused by the coordination of the acetophenone molecule to the hydride complex **6f**, since the concentrations of both are involved in the kinetic equation. An assumption about the nature of such a transition state/intermediate was made by the study with quantum chemistry methods.

II.2.1.7. Quantum-chemical mechanism study of acetophenone hydrogenation with complex 6f.

The purpose of computational investigation was to calculate the relative energies of the intermediates found in model experiments and to establish the transition state of the rate-limiting stage of the process. DFT[3] calculations were carried out with using the same computational level (B97D functional, basis set, thermal and solvation correction) as above in Section II.2.1.3, for model complexes with benzene arene ligand in place of *p*-cymene. The calculations show that the isopropoxide complex **7F** is more stable than **6F** + **acetone** by 11.9 kcal/mol on the E scale in the gas phase, but less stable by 7.2 kcal/mol on the solvation-corrected G scale. Optimization of the benzene model **9F** of the proposed σ-complex **9f** was only possible after explicit introduction of three molecules of MeOH (computational model of the ^{i}PrOH solvent), which stabilize the negative charge of the isopropoxide O atom by H-bonding, to yield structure **9F•3MeOH**. Three MeOH molecules were also added to model complexes **7F** and **6F + acetone**, forming **7F + (MeOH)$_3$** and **6F + Me$_2$CO•3MeOH**, respectively (Figure 67). As can be seen from Figure 67, the Gibbs energy of **9F•(MeOH)$_3$** is rather similar to that of the O-bonded isopropoxide complex (**7F + (MeOH)$_3$**), in fact it is even slightly preferred. Note, however, that the relative energy of **7F** may be lowered by the H-bonding interactions with MeOH molecules, which were not considered in our calculations. Thus, the calculations support the proposition that **9f** is an accessible system and a minimum on the potential energy surface. Isopropoxide dissociation from **9F•(MeOH)$_3$** was probed by calculating the separate ions **[4F]$^+$ + ^{i}PrO$^-$•(MeOH)$_3$** which becomes uphill by 3.8 kcal/mol from **9F•(MeOH)$_3$**, or 2.9 kcal/mol from **7F + (MeOH)$_3$** on the $\Delta G_{iPrOH,298K}$ scale. Without the three H-bonded MeOH molecules, alkoxide dissociation from **7F** to yield **[4f]$^+$ + ^{i}PrO$^-$** becomes uphill by 29.6 kcal/mol. These results clearly show that hydrogen bonding from the alcohol solvent provides the driving force toward alkoxide dissociation.

[3] The calculation was carried out by Dr. E. Dedier and Prof. R. Poli (LCC CNRS, Toulouse).

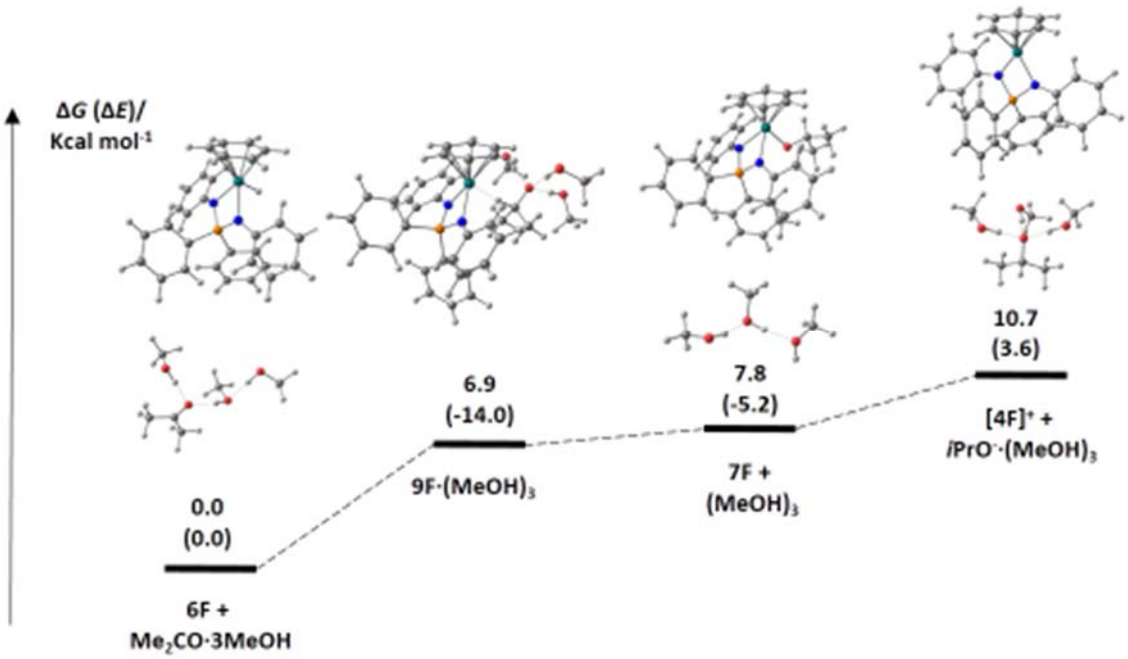

Figure 67. Relative energies ($\Delta G_{iPrOH,298K}$, with gas phase ΔE in parentheses) of systems of relevance for the ketone transfer hydrogenation catalyzed by complex **6f.**

The transition state for the hydride transfer process from **6F** to acetone could not be located/optimized. Thus, the reaction pathway was explored with a series of partial optimizations, keeping the C-H distance at different fixed values. Starting from the optimized **9HF•3MeOH**, the C-H distance was increased stepwise, resulting in an energy increase up to a distance of 1.688 Å, then to a decrease (Figure 68, blue points). Full optimization starting from the final point at C-H = 1.938 Å afforded the van der Waals adduct of **6HF** with the **Me_2CO•3MeOH** cluster, where one MeOH molecule has shifted from the O atom of isopropanolate to another MeOH, giving **6HF•Me_2CO•(2+1)MeOH**. The hydride ligand is located at a distance of 2.56 and 2.58 Å from two H atoms and 2.62 Å from the carbonyl C atom of acetone (Figure 68). This local minimum is set as the zero energy reference point; the highest point along the reaction coordinate is higher by only 5.7 kcal/mol. A new relaxed scan using the final configuration of methanol H-bonds (purple points in Figure 68) showed that the local minimum of **9HF•(2+1)MeOH** has a slightly different relative energy. The highest energy point found at approximately the same C-H distance (1.677 Å), but at even lower energy, 2.5 kcal/mol on the $\Delta G_{iPrOH,298K}$ scale.

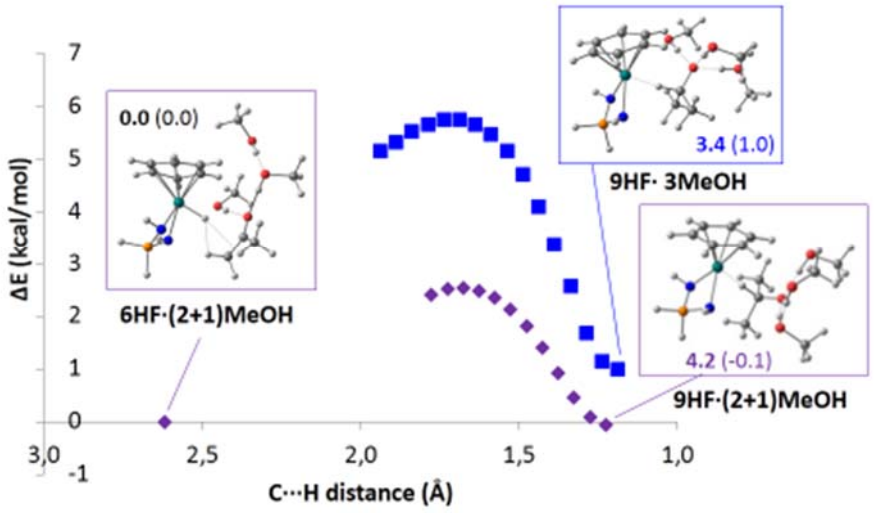

Figure 68. Computational exploration of the hydride transfer from **6HF** to **9HF**. The values indicated for the three local minima are the relative $\Delta G_{iPrOH,298K}$ (in bold characters) and relative gas phase ΔE (in parentheses) in kcal/mol.

The calculations, however, clearly suggest that the transformations of **6f** to **9f** and vice versa require very low activation and should therefore be relatively rapid processes, in agreement with the above given interpretation of the NMR results in acetone-d_6. The other part of the cycle (proton transfer leading from **9f'**+ ^{i}PrOH **9f** + PhCH(Me)OH) was not modelled by DFT, because as a rule processes involving pseudo-degenerate proton transfers between alkoxide anions are not expected to involve high energy barriers.

II.2.1.8. Mechanism of the acetophenone transfer hydrogenation catalyzed by complex 6f.

The combined catalytic, spectroscopic and chemical studies and the DFT calculations point rather firmly to the involvement of the hydride complex **6f** as the catalytically active species. However, it is impossible to envisage either a Noyori-type (bifunctional and concerted outer-sphere proton/hydride transfer from catalyst to substrate)[55] or a coordination/insertion pathway for this species, because the complex does not contain deprotonatable ligands and is coordinatively saturated.

The above described spectroscopic studies suggest facile accessibility of an isopropoxide species from **6f** and acetone, either as a neutral O–bonded complex **7f** or as an isomeric zwitterionic σ-complex **9f**. Hence, it is possible to envisage an outer-sphere

hydride transfer from **6f** to acetophenone via an intermediate **9f'**, similar to **9f**, possibly in equilibrium with the O-bonded 1-phenylethoxide isomer, **7f'**. The 1-phenylethanol product may then be generated by proton exchange with the solvent, which may occur either directly or via the dissociated ion pair (complex $[\mathbf{4f}]^+$ and free alkoxide). The latter is suggested by the observation of free $[\mathbf{4f}]^+$ in the presence of the less coordinating hexafluoroisopropanolate. Complex **9f** then completes the cycle by the reverse hydride transfer process. This catalytic cycle is summarized in Scheme 40. It is pertinent to remark that catalysts devoid of deprotonatable ligands have already been shown to operate by an outer-sphere ionic mechanism with preliminary hydride transfer, followed by subsequent protonation of the alkoxide intermediate, in ionic hydrogenation (the proton coming in this case from activated H_2).[103] Even Noyori's catalyst itself, though containing a deprotonatable ligand, was suggested to have a similar, non-concerted mechanism with the proton delivered in a subsequent step by H_2.[104]

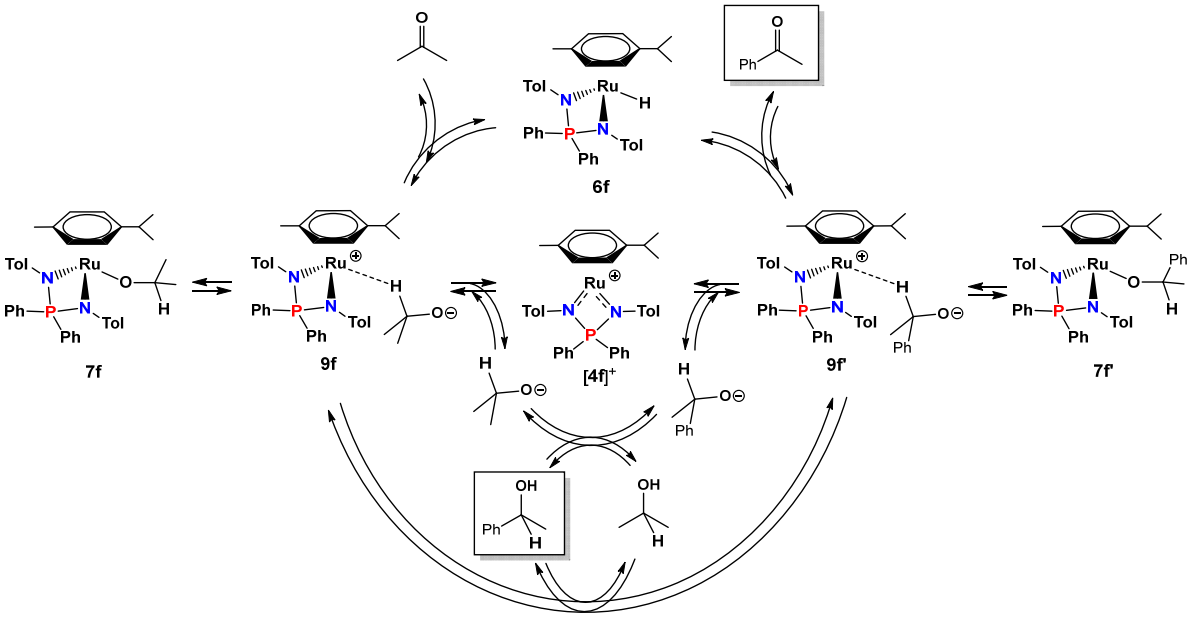

Scheme 40. Proposed mechanism for the catalyzed acetophenone transfer hydrogenation by isopropanol.

According to this mechanism, the ruthenium chloride complex [(η^6-*p*-cymene)RuCl(NPN)] (**3f**) is a precatalyst for the TH reaction of ketone by isopropanol. The active catalytic species is the hydride complex [(η^6-*p*-cymene)RuH(NPN)] (**6f**). Although this hydride complex tends to isomerize into cyclohexadienyl complexes, it is stabilized in isopropanol due to the formation of a dihydrogen bond. The rate-limiting step

of the process is the formation of a zwitterionic σ-complex **9f**, in which the alkoxide anion is linked by a methine carbon atom to a ruthenium atom. As far as we know, this is the first detailed mechanistic study of the TH reaction with the transfer of a hydride in the external sphere of a catalyst, deprived of deprotonated ligands.

II.2.2. Catalytic properties of complexes 3a-e in the TH of acetophenone.

Using the example of complex **3f**, it was shown that during the reduction of acetophenone, the catalytically active particle is the ruthenium hydride complex **6f**, which is generated *in situ* under the action of isopropanol in the presence of a base. A kinetic study has shown that the reaction rate is first-order with respect to both substrate and catalyst, and the strongly negative activation entropy indicates a highly ordered transition state at the rate-limiting step. Based the on model experiments and the DFT calculations, a mechanism was proposed for the reduction of acetophenone, which includes the formation of a zwitterionic intermediate isomeric to the alkoxide complex.

In this section, we compare the catalytic properties of the different arene iminophosphonamide complexes **3a-f**. It is of interest to determine the effect of the arene ligand and of the N,P-substituents in the NPN ligand on the catalyst activity and stability.

II.2.2.1. Generation of ruthenium hydride complexes 6a-e.

It is logical to extrapolate that, for the entire series of **3a-f** complexes, the corresponding hydride complex [(η^6-Arene)RuH(NPN)] (**6a-f**) formed under the reaction conditions is the catalytically active species. In order to optimize the conditions for the generation and stability of these complexes for all chloride complexes **3a-e**, model reactions with isopropanol were studied in the presence of 1–1.5 eq. NaHMDS in a mixture of C_6D_6/^{i}PrOH = 500/40 μL at room temperature using ^{1}H and ^{31}P NMR spectroscopy. The spectral changes that occur after the addition of NaHMDS after a specified period of time are shown in Figures 69-73.

*Generation of **6a** (Figure 69).*

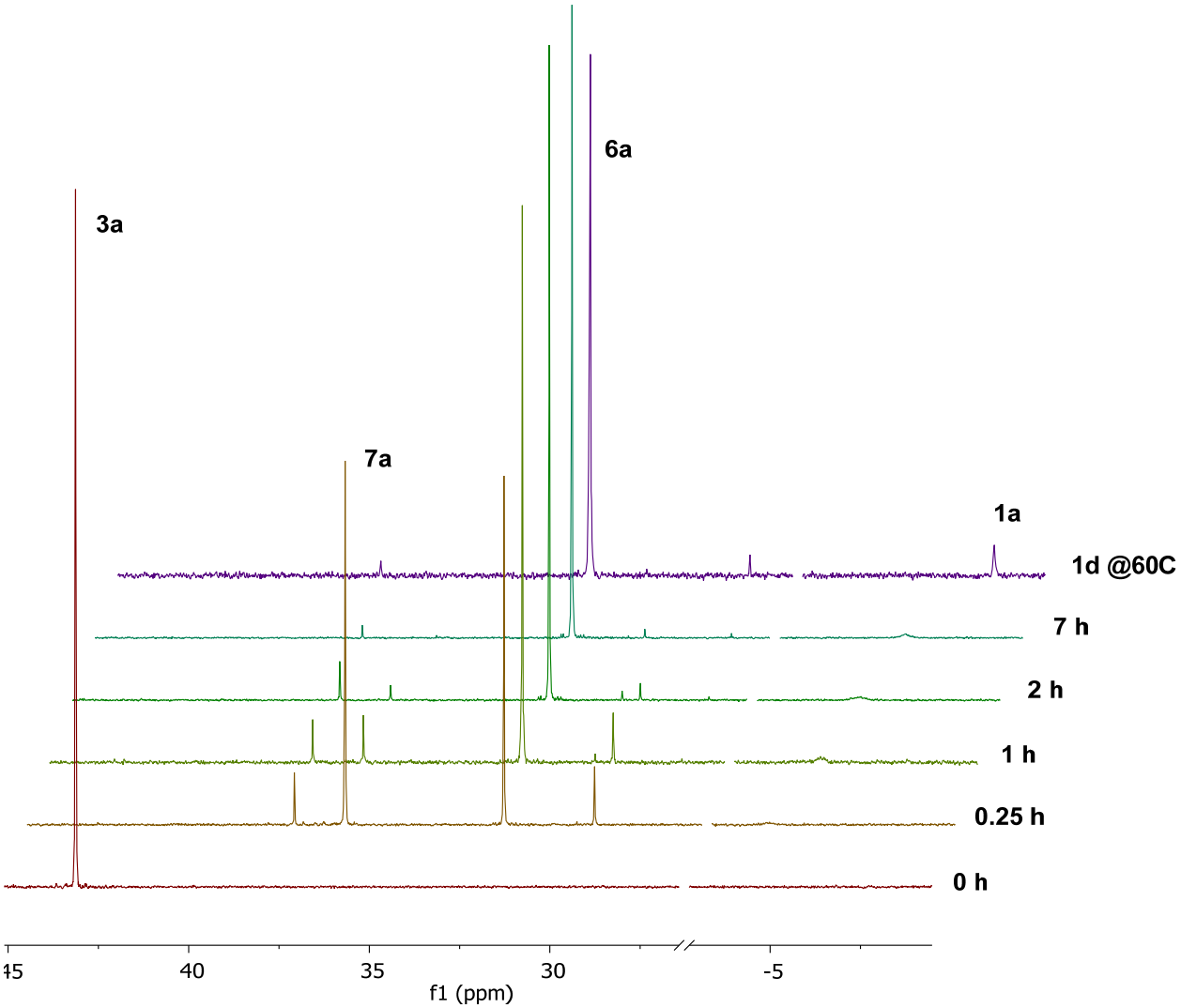

Figure 69. NMR $^{31}P\{^{1}H\}$ monitoring of the reaction of **3a** with NaHMDS/^{i}PrOH in C_6D_6.

This method allows to cleanly obtain the hydride complex $[(C_6Me_6)RuH(Ph_2P(NTol)_2)]$ (**6a**). Initially, the isopropoxide complex $[(C_6Me_6)Ru(O^iPr)(Ph_2P(NTol)_2)]$ (**7a**) (see SI, Figure S13) is predominantly formed and then this gradually turns into **6a** within 2 hours. Unlike the *p*-cymene analogue **6f**, this complex is rather stable, does not decompose, and does not undergo a rearrangement into the cyclohexadienyl complex even with prolonged heating at 60°C. Complex **6a** was isolated from the reaction mixture and characterized by ^{1}H, ^{31}P and ^{13}C NMR spectroscopy (see SI, Figure S10-S12). In the ^{1}H NMR spectra, the RuH signal is observed at δ -3.25 in pure benzene-d_6, and in the presence of 10 equiv. isopropanol it is expectedly upfield shifted to δ -3.30 due to the formation of a dihydrogen bond.

*Generation of **6b** (Figure 70).*

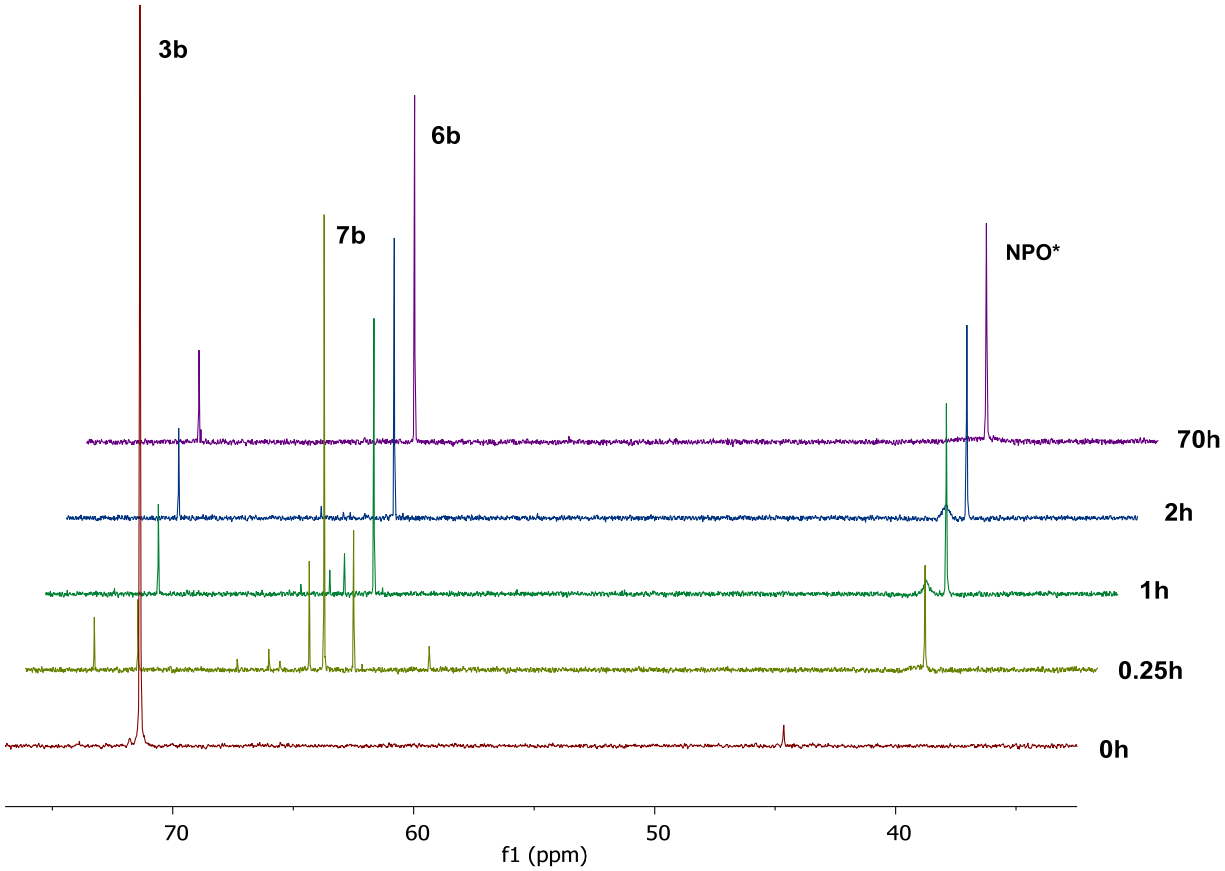

Figure 70. NMR $^{31}P\{^{1}H\}$ monitoring of the reaction of **3b** with NaHMDS/^{i}PrOH in C_6D_6.

In general, the reaction of complex **3b** with sodium isopropoxide occurs similarly to complex **3a**: the isopropoxide complex $[(C_6Me_6)Ru(O^{i}Pr)(Et_2P(NTol)_2)]$ (**7b**) is predominantly formed ($^{31}P\{^{1}H\}$ NMR resonance at δ 64.5 ; ^{1}H NMR signal for the $CHMe_2$ proton at δ 4.59; see SI, Figure S14-S15), which within the hour turns into the $[(C_6Me_6)RuH(Et_2P(NTol)_2)]$ hydride complex (**6b**) with δ 63.3 in the $^{31}P\{^{1}H\}$ NMR (see SI, Figure S14). In this case, in contrast to the **6a** generation reaction, the formation of minor amounts of unknown complexes also occurs, as well as the formation of the aminophosphine oxide **NPO*** (δ 39.8 in the $^{31}P\{^{1}H\}$ NMR spectrum), the amount of which increases simultaneously with the generation of **6b**.

The isopropyl-substituted **NPO***, $Et_2P(O)$-N(^{i}Pr)Tol, has a characteristic doublet of septets at δ 4.53 ($^3J_{PH}$ = 9.2 Hz, $^3J_{CH}$ = 6.0 Hz) (see SI, Figure S15). Its formation is not due to the P-N bond hydrolysis in the ruthenium complex, but, apparently, it is caused by the attack of the electrophilic phosphorus atom by the isopropoxide anion with P-N bond cleavage and subsequent metal atom decoordination and isopropyl group migration to the nitrogen atom (Scheme 41). This side reaction reduces the yield of the hydride complex **6b**, and, as will be seen below, reduces the rate of the catalytic acetophenone reduction.

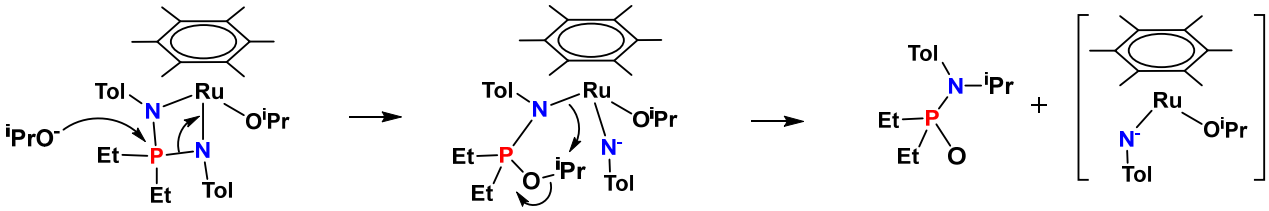

Scheme 41. Proposed mechanism for the formation of *N*-isopropyl-substituted aminophosphine oxide **NPO***.

Generation of ***6c*** *(Figure 71).*

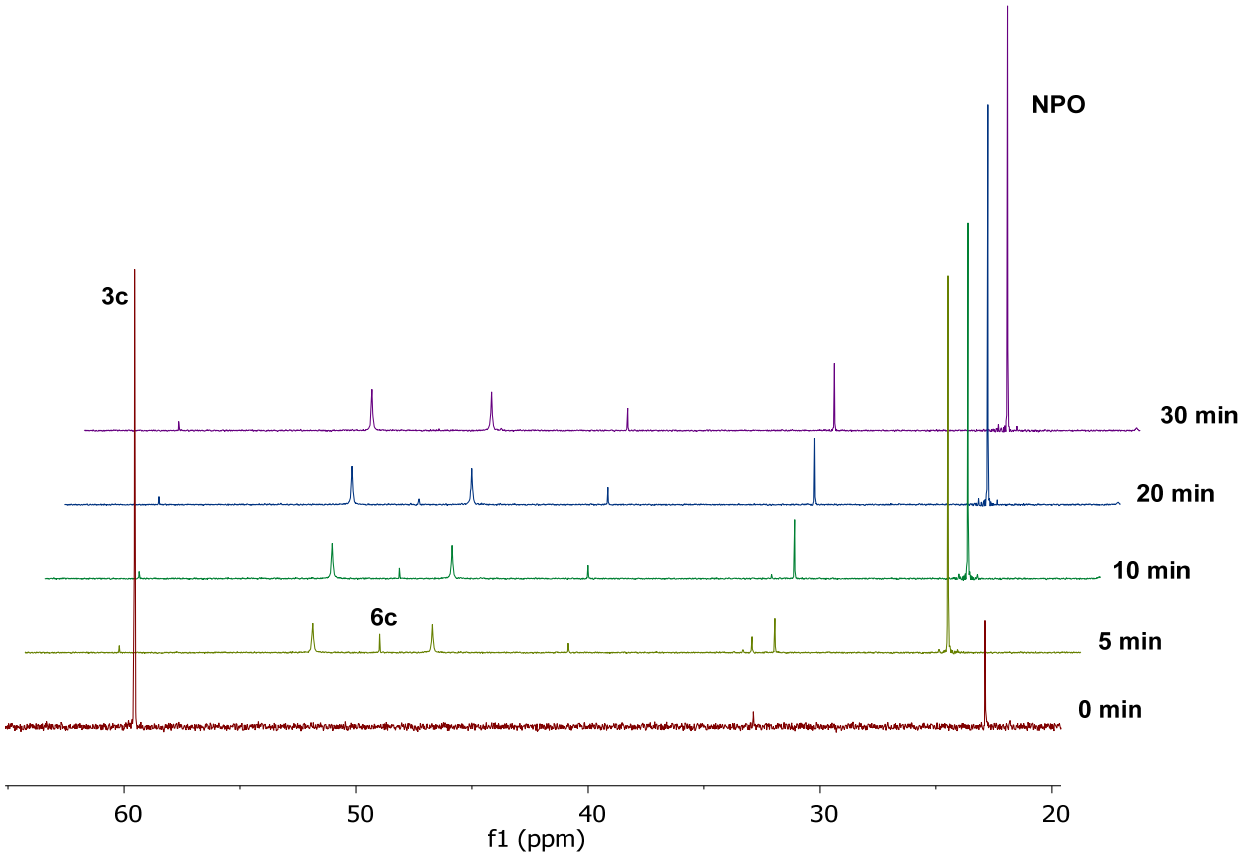

Figure 71. NMR $^{31}P\{^{1}H\}$ monitoring of the reaction of **3c** with NaHMDS/^{i}PrOH in C_6D_6.

The reaction of **3c** with isopropanol in the presence of a strong base proceeds very quickly. According to the NMR $^{31}P\{^{1}H\}$ spectrum, even after 5 minutes the corresponding isopropoxide complex is not observed in the solution. The content of the hydride complex [(C_6Me_6)RuH($Ph_2P(NMe)_2$)] (**6c**), which is characterized by a ^{31}P NMR signal at δ 49.8, does not exceed 5%. The major components are the aminophosphine oxide $Ph_2P(O)(NHMe)$ (**NPO**, δ 25.3) decomposition product and unknown complexes with signals at δ 52.7 and 47.6. A detailed analysis of the spectra was not performed for this reaction, since the yield of the target hydride is very low. The correlation of the signal at δ 49.8 to **6c** was made on the basis of the comparison with the cleaner spectrum of **6c** obtained by an alternative method, namely the interaction of **3c** with a toluene solution of $NaBHEt_3$ in benzene-d_6 (see SI, Figure S16-S17).

It should be noted that the immediate formation of a significant amount of aminophosphine oxide when generating **6c** in isopropanol in the presence of a base is a sign of its mild alcoholysis. Indeed, **3c** slowly decomposes to aminophosphine oxide in isopropanol even in the absence of a base at room temperature (see SI, Figure S18).

*Generation of **6d** (Figure 72).*

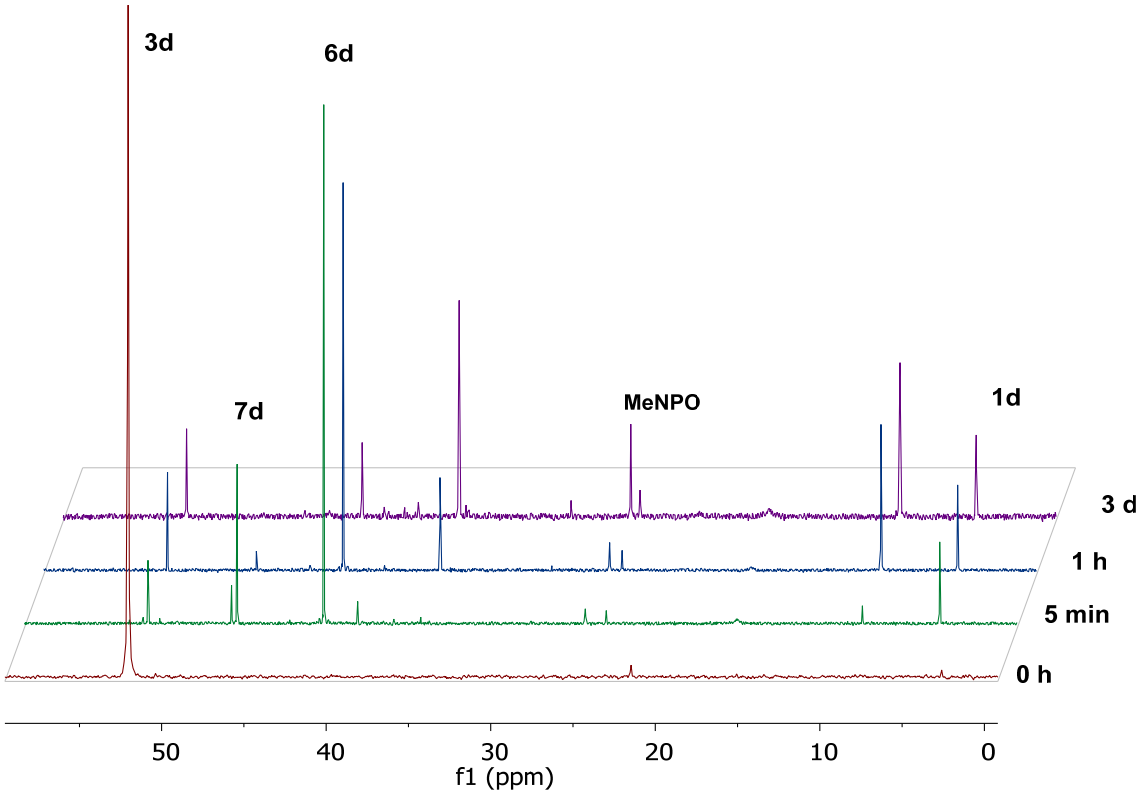

Figure 72. NMR $^{31}P\{^{1}H\}$ monitoring of the reaction of **3d** with NaHMDS/^{i}PrOH in C_6D_6.

Complex **3d** reacts with isopropanol in the presence of a strong base in the same way as **3a** does, but noticeable amounts of the isopropoxide complex **7d** (δ 46.6 in $^{31}P\{^{1}H\}$ NMR) could be detected only in the first few minutes. After 1 hour, **7d** completely turns into the hydride complex [(C_6Me_6)RuH($Ph_2P(NMe)_2$)] (**6d**) with a $^{31}P\{^{1}H\}$ signal at δ 41.3 and a ^{1}H signal at δ -3.72 (see SI, Figure S19). After 3 days, **6d** almost completely decomposes to the aminophosphonoxide $Ph_2P(O)(NHMe)$ (**NPO**, δ 25.3) and unknown complexes with signals at δ 35.5 and 8.7. It can be assumed that the causes of the instability of **6d** under these conditions are similar to those of **6c**, which also has a strongly basic nitrogen atom bonded with a methyl group.

*Generation of **6e** (Figure 73).*

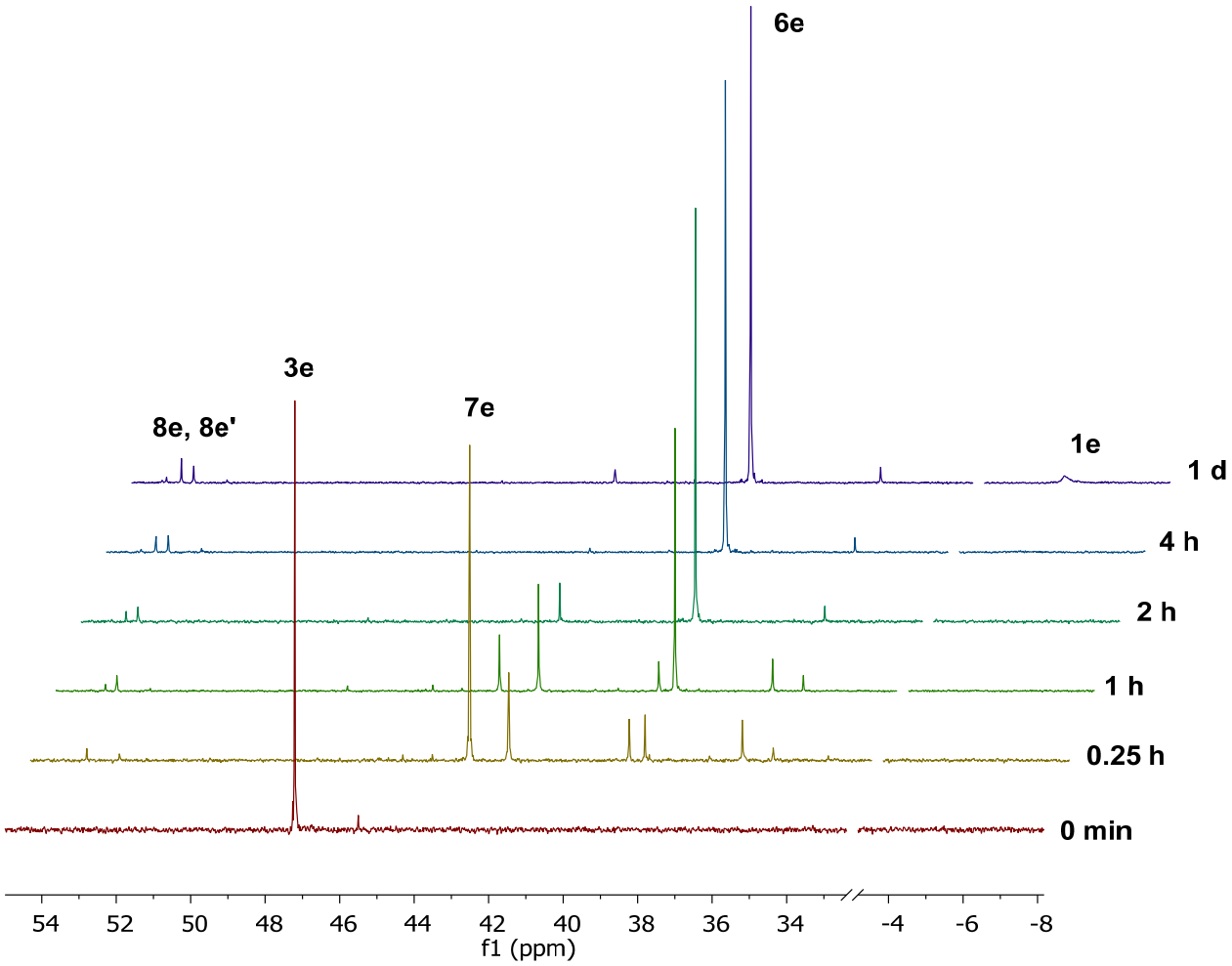

Figure 73. NMR $^{31}P\{^{1}H\}$ monitoring of the reaction of **3e** with NaHMDS/^{i}PrOH in C_6D_6.

Compared to **6f**, the formation of the hydride complex [(η^6-*p*-cymene)RuH($Ph_2P(NC_6H_4COOEt)_2$)] (**6e**) by the action of isopropanol in the presence of 1 equiv. NaHMDS is slower, probably due to the presence of acceptor aryl substituents on the ligand N atoms. The formation of an intermediate isopropoxide complex [(η^6-*p*-cymene)Ru($O^{i}Pr$)($Ph_2P(NC_6H_4COOEt)_2$)] (**7e**) is again evident ($^{31}P\{^{1}H\}$ signal at δ 43.2; ^{1}H NMR signal for C*H*Me_2 at δ 4.68; see SI, Figure S20). This compound forms from the very beginning and turns into the hydride complex **6e** within 2 hours (see SI, Figure S21). Complex **6e** is reasonably stable, but prolonged storage in solution gives slight

isomerization to the mixture of cyclohexadienyl complexes **8e**, **8e'** (^{31}P $\{^{1}H\}$ resonances at δ 53.3, 53.7, see SI, Figure S22), similar to what is observed for **6f.**

It is interesting to note that carrying out the reaction with an excess of base (> 1 equiv. of NaHMDS) simultaneously causes the transesterification of the ethoxy groups to isopropoxy, which leads to a mixture of different esterified hydride complexes [(η^6-*p*-cymene)RuH($Ph_2P(NC_6H_4COOR)_2$)] (R = Et, ^{i}Pr) (see SI, Figure S22). However, such peripheral changes should not have any significant effect on the catalytic activity of the hydride complex.

II.2.2.2. Kinetics of acetophenone transfer hydrogenation catalyzed by complexes 3a-e.

Comparative testing of acetophenone reduction by isopropanol, catalyzed by complexes **3a-f**, was carried out in the presence of a base at 40°C (Table 27). The conditions (temperature, time of incubation after the addition of the base) used for the generation of the catalytically active hydride complexes (**6a-f**) were in accordance with the model experiments shown above.

Table 27. Activity of complexes **3a-f** in the TH reaction of acetophenone by isopropanol in the presence of a base at 40°C.

Complex	*t*, min*	Conversion, %						k_{obs}, h^{-1}	*k*, s^{-1}
		0.5 h	1 h	1.5 h	2 h	3 h	4 h		
3a	120	4.9	8.6	12.8	15	22.6	26.5	0.082	0.0057
3b	60	2.7	4.4	6.1	9.8	13.3	17.3	0.048	0.0033
3c**	5	16.3	27.7	35.5	40.1	44.5	45.4	0.354	0.049
3d	5	6.4	13.3	18.4	22.3	28.4	30.5	0.133	0.0092
3e	30	5.1	9.2	11.1	16.3	24.1	31.7	0.100	0.0070
3f	15	15.9	26.8	38.2	48	64.3	74.9	0.336	0.023

Conditions: complex **3** (0.02 mmol), NaHMDS/**3** = 1.5, acetophenone (233 μl, 2 mmol), dodecane (226 μl), isopropanol (5 ml). [PhCOMe] = $3.7*10^{-1}$ M, [Ru] = $4*10^{-3}$ M. *The catalytic mixture was kept at the reaction temperature for the indicated time before adding the substrate to complete the conversion to the hydride complex **6a-f**. **Used half the amount of catalyst: [Ru] = $2*10^{-3}$ M.

As can be seen from Table 27, the nature of the arene ligand and of the N substituents in the NPN ligand have a large effect on catalyst activity. The catalysts with the *p*-cymene ligand are significantly more active than their hexamethylbenzene analogues (**3f** and **3a**). In this case, acceptor substituents on the nitrogen atom reduce the catalytic activity (**3e**) and more donor substituents increase it (**3c** and **3d**). Donor P-substituents also reduce the activity of complex **3b**. A loss of activity for this catalyst is also caused by the side decomposition during the generation of the active hydride complex **6b** (see above).

For each of the complexes **3a-e**, the temperature dependence of the hydrogenation reaction rate constant was analyzed (Figure 74A-78A) and the activation parameters for the rate-determining step of catalytic hydrogenation (Figure 74B-78B) were determined using the Eyring equation. The activation enthalpy $\Delta H^{\neq}$ and entropy $\Delta S^{\neq}$ data are summarized in Table 28. Unfortunately, it was not possible to determine the activation parameters for complex **3c**, since it decomposes significantly at temperatures above 40°C.

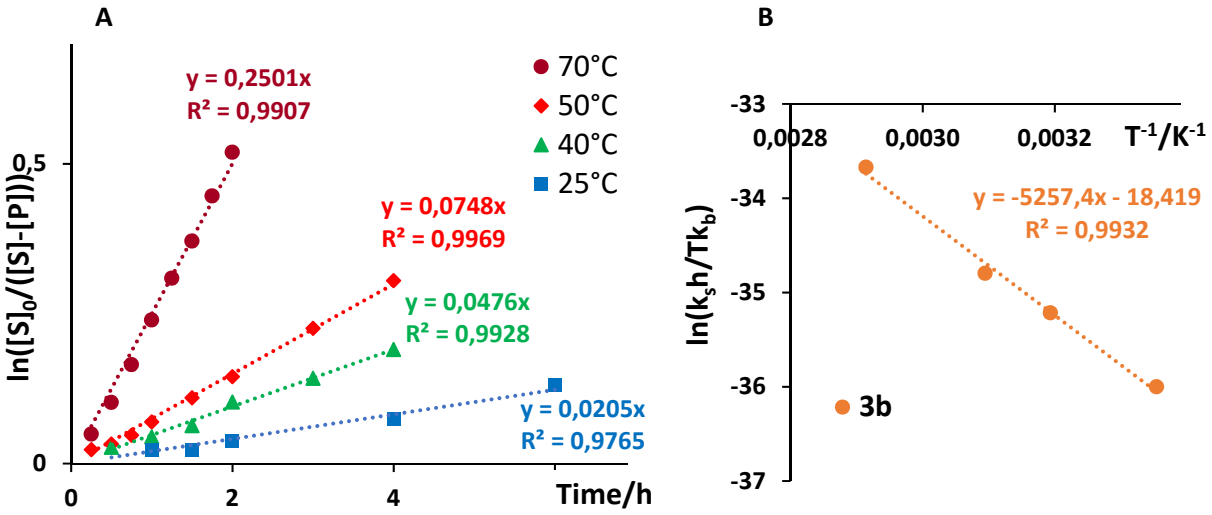

Figure 74. A) Kinetic curves for the formation of phenylethanol in ^{i}PrOH at different temperatures for complex **3a**. **B**) Eyring analysis of the second order rate constant *k*. Reaction conditions as in Table 27.

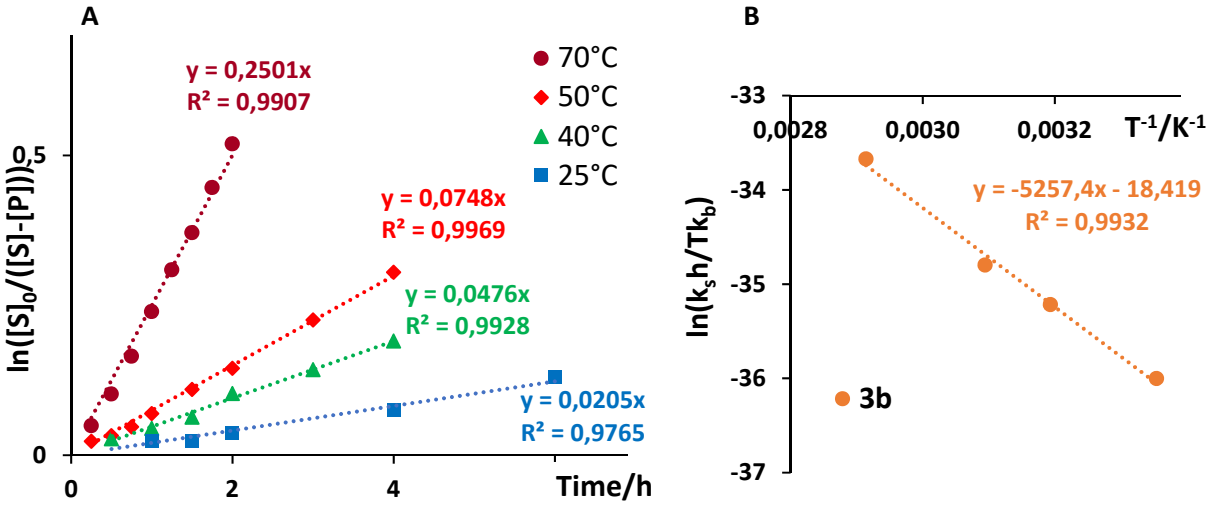

Figure 75. **A**) Kinetic curves for the formation of phenylethanol in ^{i}PrOH at different temperatures for complex **3b**. **B)** Eyring analysis of the second order rate constant *k*. Reaction conditions as in Table 27.

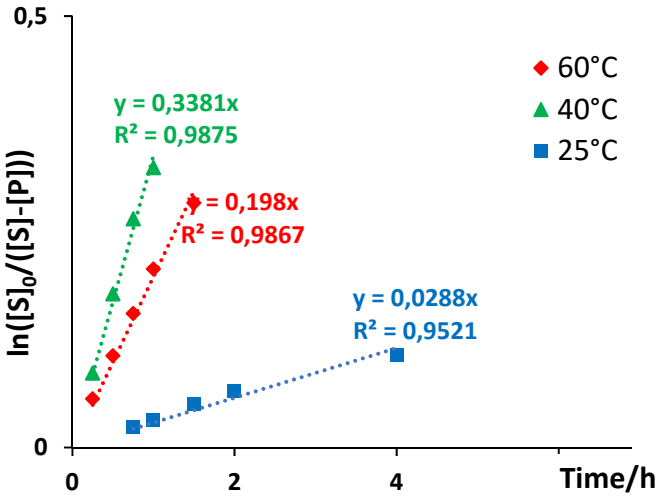

Figure 76. Kinetic curves for the formation of phenylethanol in ^{i}PrOH at different temperatures for complex **3c**. Reaction conditions as in Table 27.

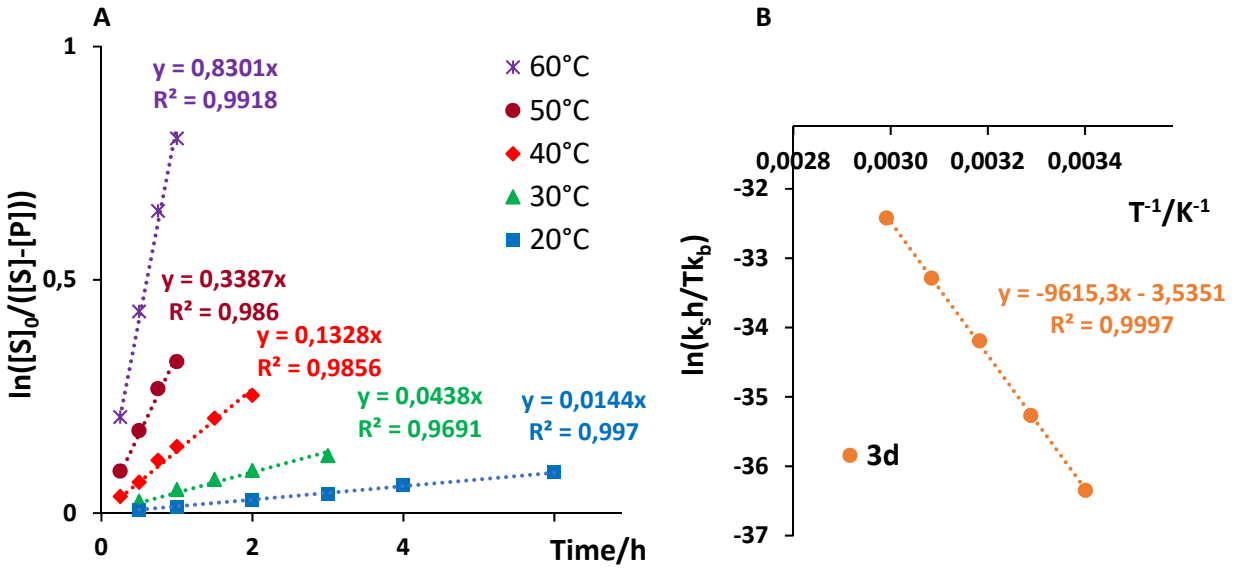

Figure 77. **A**) Kinetic curves for the formation of phenylethanol in ^{i}PrOH at different temperatures for complex **3d**. **B**) Eyring analysis of the second order rate constant *k*. Reaction conditions as in Table 27.

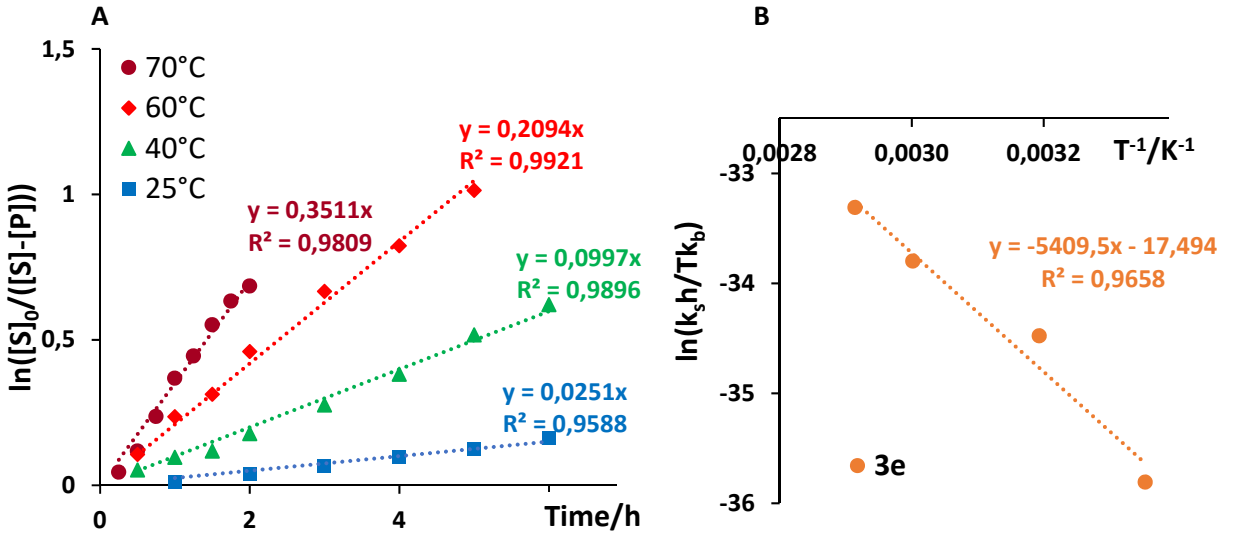

Figure 78. **A**) Kinetic curves for the formation of phenylethanol in ^{i}PrOH at different temperatures for complex **3e**. **B**) Eyring analysis of the second order rate constants *k*. Reaction conditions as in Table 27.

Table 28. Activation parameters of acetophenone hydrogenation with complexes **3a-f**.

	3a	**3b**	**3c**	**3d**	**3e**	**3f**
$\Delta H^{\neq}$, kcal/mol	11.7±1.0	10.5±1.2	-	19.1±0.6	10.8±1.4	9.7±1.0
$\Delta S^{\neq}$, kcal/(mol*K)	-32±4	-37±5	-	-7±3	-35±5	-31±4

The activation parameters of the catalytic reaction suggest that for all NPN complexes with only N aryl substituents (**3a**, **3b**, **3e**, **3f**) the reaction proceeds according to the same mechanism, through the formation of a catalytically active hydride complex. For these complexes, the $\Delta H^{\neq}$ and $\Delta S^{\neq}$ values are in a narrow range of 9.7–11.7 kcal/mol and 31–37 kcal/(mol*K), respectively. Within this series, an accordance is observed between the enthalpy of activation and the activity of the catalyst: *p*-cymene complexes with more donor N-substituents are more active. However, according to these data, the activity of the P-ethyl complex **3b** should be significantly higher than the activity of the P-phenyl analogue **3a**, but that was not confirmed by the test experiments (Table 27). Obviously, the reason for this is the reduced stability of **3b**, as observed in the model experiment.

The activation parameters for complex **3d** with one N-methyl substituent are significantly different from the others: $\Delta H^{\neq}$ is almost twice as high (19.1 kcal/mol) and the activation entropy is much smaller, which clearly indicates that the rate-determining transition state is not highly ordered in this case. Apparently, the N-methyl-substituted complexes **3c** and **3d** promote another catalytic mechanism.

Additional investigations suggest that the catalytically active species, when using the **3c** and **3d** precatalysts, are not the hydride complexes **6c** and **3d**. Indeed, these precatalysts demonstrate high activity also in the absence of a base. The acetophenone hydrogenation kinetic curves with **3c** and **3d** complexes in pure isopropanol are shown in Figure 79–80.

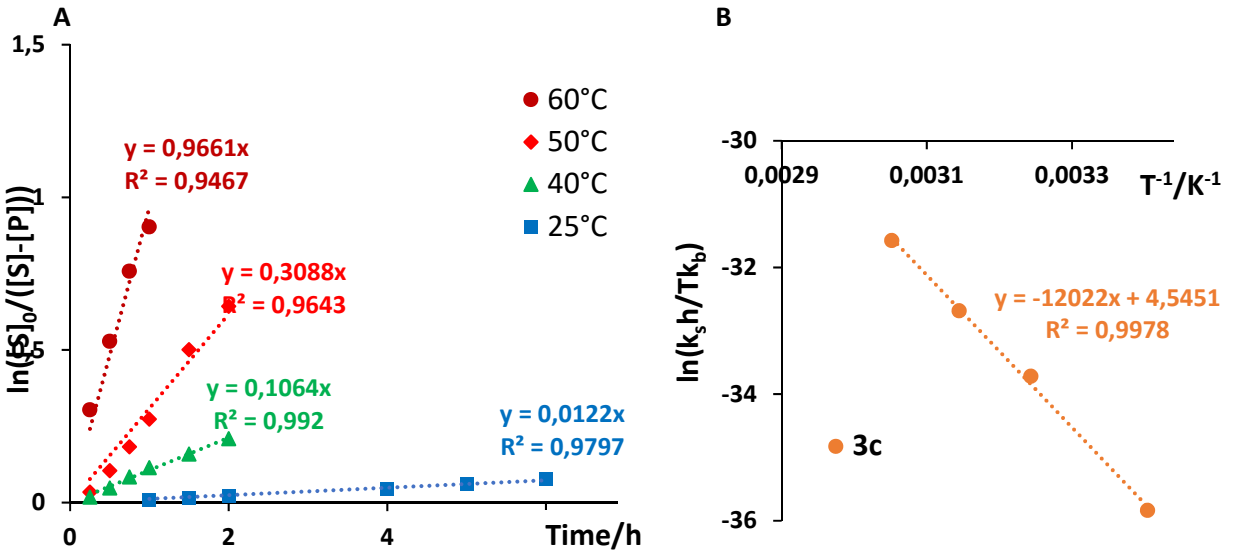

Figure 79. **A**) Kinetic curves for the formation of phenylethanol in ^{i}PrOH at different temperatures for complex **3c**. **B**) Eyring analysis of the second order rate constant *k*.

Reaction conditions: complex **3c** (0.01 mmol), acetophenone (233 μl, 2 mmol), isopropanol (5 ml). [PhCOMe] = $3.7*10^{-1}$ M, [Ru] = $2*10^{-3}$ M.

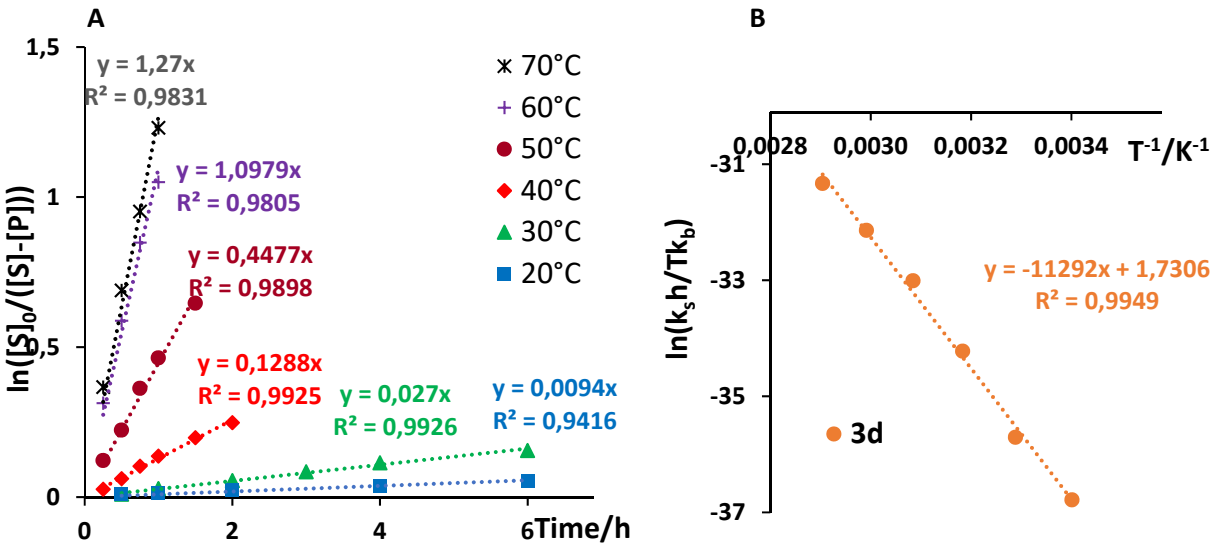

Figure 80. **A**) Kinetic curves for the formation of phenylethanol in ^{i}PrOH at different temperatures for complex **3d**. **B**) Eyring analysis of the second order rate constant *k*. Reaction conditions: complex **3d** (0.02 mmol), acetophenone (233 μl, 2 mmol), isopropanol (5 ml). [PhCOMe] = $3.7*10^{-1}$ M, [Ru] = $4*10^{-3}$ M.

The $\Delta H^{\neq}$ and $\Delta S^{\neq}$ values found are 24±2 (**3c**), 22.4±0.8 (**3d**) kcal/mol and 9±6 (**3c**), 4±3 (**3d**) kcal/(mol*K), respectively. The obtained activation parameters are close to each other and to that for **3d** in the presence of a base. It is important to note that, in the absence of a base, these complexes are much more stable and able to catalyze the reaction at higher temperatures without noticeable decomposition.

Dissolving both **3c** and **3d** complexes in isopropanol leads to an immediate color change from red to purple, which corresponds to the formation of the dissociated 16ē form $[(\eta^6\text{-}C_6Me_6)Ru(NPN)]^+Cl^-$ (see Section II.1.4.1). In the $^{31}P\{^1H\}$ NMR spectra, the expected downfield shift of the phosphorus atom signal from δ 59.8 to δ 77.8 for **3c** and from δ 52.0 to δ 68.4 for **3d** occurs. During catalysis, the violet color does not change until the end of the reaction – this probably means that the cationic 16ē complex $[(\eta^6\text{-}C_6Me_6)Ru(NPN)]^+Cl^-$ is the resting state of the catalyst in the catalytic cycle.

Unfortunately, the establishment of the acetophenone hydrogenation mechanism with **3c** and **3d** complexes in isopropanol requires additional model experiments and quantum-chemical calculations that do not fit into the time frame of this thesis. However,

at this stage, we can propose a mechanism that would satisfy the established facts: a) high enthalpy and weakly positive activation entropy, b) the cationic 16ē complex is the resting state of the catalyst. We assume that the reaction proceeds through a path related to the classical Noyori-Ikaria mechanism:[55] the rate-determining transition state for the isopropanol dehydrogenation step is a pericyclic structure in which the isopropanol methine hydrogen atom is transferred to the ruthenium atom and the hydroxyl proton is simultaneously transferred to the basic nitrogen atom (Scheme 42). The transfer of H_2 to the acetophenone substrate occurs

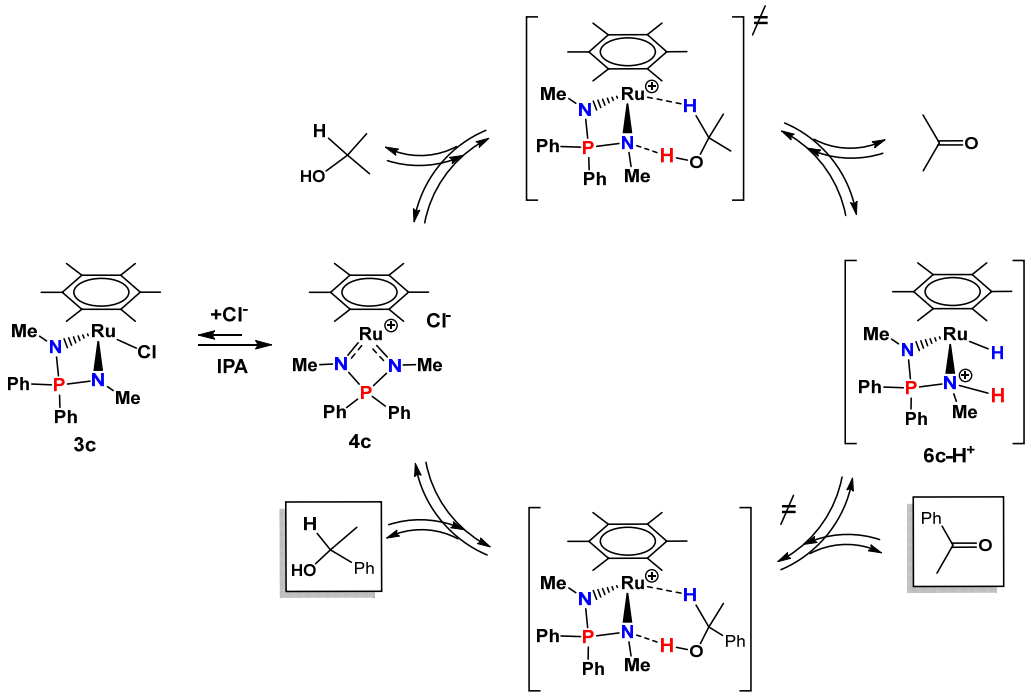

Scheme 42. Proposed mechanism of the TH reaction, catalyzed by arene ruthenium NPN complexes **3c,d** in the absence of a base.

We assume that the catalytically active species is the **6c-H**$^+$ hydride complex protonated at the nitrogen atom, the stationary concentration of which in the catalytic system is low. It should be noted that in the presence of a base, this complex may also be a catalytically active species. However, the resting state of the catalyst in that case would be the hydride complex **6c**, which decomposes much faster than the stabilized complex **4c**.

In the 16ē cationic complexes **4**, the nitrogen atom lone pairs are involved in π-donation to a ruthenium atom. Therefore, their basicity is reduced (Section II.1.4.2.). However, coordination of an external ligand to the ruthenium center makes the complex

again 18ē and the nitrogen atoms become highly basic again, as it was demonstrated by the example of the carbonylation of compound **3c**. Possibly, the nitrogen lone pair activation in complex **4c** is promoted by the reversible coordination of the isopropanol molecule during the catalytic acetophenone reduction (Scheme 43).

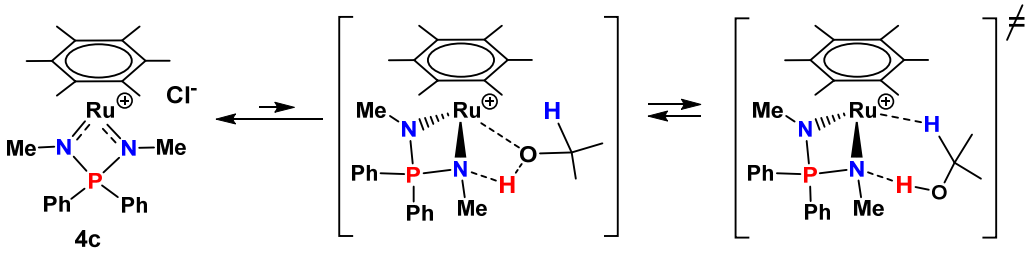

Scheme 43.

In this case, a change in the type of coordination of the ruthenium atom with the alcohol molecule from κ-O to κ-H may be the rate-limiting step, which is a transition with low entropy. The proposed mechanism of the catalytic cycle by complexes **3c** and **3d** is in good agreement with the experimental data obtained so far.

III. Experimental part.

General procedures. All manipulations were carried out using standard Schlenk techniques under an atmosphere of dry argon. Solvents were purified by standard methods and distilled prior to use. Conditions for NMR and UV-vis spectral studies are described in detail in Section II.1.4.1. The IR spectra were obtained on a Fourier spectrometer Nicolet 6700. Elemental analyses were performed on a Carlo Erba 1106 CHN analyzer.

The following compounds were prepared according to described procedures: $[(\eta^6\text{-}C_6Me_6)Ru(\mu\text{-}Cl)Cl]_2$[105], $[(\eta^6\text{-}p\text{-cymene})Ru(\mu\text{-}Cl)Cl]_2$[106], $[(\eta^6\text{-}C_7H_8)Ru(\mu\text{-}Cl)Cl]_2$[107], $Ph_2P(NH\text{-}p\text{-}C_6H_4Me)_2]Br$ (**2a**)[61], $[Ph_2P(NH\text{-}p\text{-}C_6H_4\text{-}CO_2Et)_2]Br$ (**2e**)[61]. Methylamine gas was obtained by solid-state reaction of $[MeNH_3]$ Cl with an excess of NaOH, dried by passing through an alkali tube, and dissolved in CH_2Cl_2 at –40 ° C, the concentration of methylamine was determined by titration. The diphenylchlorophosphine (Ph_2PCl) was distilled under high vacuum, prior to use, fraction collected at 130-140°C. The diethylchlorophosphine (Et_2PCl), previously synthesized in our laboratory [108], was distilled under at ambient pressure prior to use, collecting the fraction at 133-134°C. Other commercially available compounds were used as received.

Synthesis of $[Et_2P(NH\text{-}p\text{-}C_6H_4Me)_2]Br$ (2b). To a solution of Et_2PCl (2.67 g, 21.5 mmol) in CH_2Cl_2 (30 mL) cooled to 0°C a solution of Br_2 (1.10 mL, 21.5 mmol) in CH_2Cl_2 (30 mL) was added dropwise. The reaction mixture was warmed to 20°C, stirred for 1.5 h and cooled again to 0°C. A solution of *p*-toluidine (9.2 g, 86 mmol) in CH_2Cl_2 (50 mL) was added to the reaction mixture and the resulting suspension was stirred overnight at 20°C. The precipitate was filtered off and washed with CH_2Cl_2 (3x20 mL). The filtrate was evaporated to dryness and the oily product was stirred with ethyl acetate (150 mL) for 2 h. The fine crystalline solid formed was filtered off, washed with ethyl acetate (3x10 mL) and dried *in vacuo* to yield 5.80 g of **2b**. The filtrate was concentrated to 30 mL and left overnight. The crystalline precipitate was filtered off, washed with ethyl acetate (3x3 mL) and dried *in vacuo* to give an additional 0.92 g of the product. The total yield was 6.72 g (82%). Anal. calcd for $C_{18}H_{26}BrN_2P$: C, 56.70; H, 6.87; N, 7.35 %. Found: C, 56.92; H, 6.96; N, 7.33 %. $^{31}P\{^1H\}$ NMR ($CDCl_3$): δ 50.4. ^1H NMR ($CDCl_3$): δ 8.77 (d, $^2J_{HP}$ = 13.6, 2H, NH), 7.28 (d, $^3J_{HH}$ = 8.0, 4H, C_6H_4), 6.85 (d, $^3J_{HH}$ = 8.0, 4H, C_6H_4), 2.62 (dq, $^2J_{HP}$ =

14.0, $^{3}J_{HH}$ = 7.6, 4H, C$\underline{H_2}$CH$_3$), 2.15 (s, 6H, Me$_{Tol}$), 1.04 (dt, $^{3}J_{HP}$ = 21.1, $^{3}J_{HH}$ = 7.6, 6H, CH$_2$C$\underline{H_3}$). ^{13}C{^{1}H} NMR (CDCl$_3$): δ 135.6 (br.s, *i*-C$_{Tol}$(N)), 133.3 (s, *i*-C$_{Tol}$(Me)), 130.1 (s, β-C$_{Tol}$), 119.7 (br. s, α-C$_{Tol}$), 20.6 (s, Me$_{Tol}$), 14.7 (d, $^{1}J_{CP}$ = 80, $\underline{C}$H$_2$Me), 4.8 (s, CH$_2\underline{Me}$).

Synthesis of [Ph$_2$P(NHMe)$_2$]Br (2c). To a solution of Ph$_2$PCl (4.35 mL, 24.0 mmol) in CH$_2$Cl$_2$ (50 mL) at room temperature a solution of Br$_2$ (1.23 mL, 24.0 mmol) in CH$_2$Cl$_2$ (15 mL) was added dropwise. The reaction mixture was stirred for 1.5 h and cooled to -50°C. A freshly prepared cold solution of dimethylamine in CH$_2$Cl$_2$ (3M, 75 mL, 225 mmol) was added to the reaction mixture and the resulting suspension was stirred overnight at 20°C. The precipitate was filtered off and washed with CH$_2$Cl$_2$ (3x40 mL). The filtrate was evaporated to dryness and then washed with benzene (5x20 mL) and acetone (5x20 mL). The white crystalline residue was dried *in vacuo* to yield 6.25 g of **2c** (80%). Anal. calcd for C$_{14}$H$_{18}$BrN$_2$P: C, 51.71; H, 5.58; N, 8.61 %. Found: C, 51.89; H, 5.74; N, 8.69 %. ^{31}P{^{1}H} NMR (CDCl$_3$): δ 40.2. ^{1}H NMR (CDCl$_3$): δ 7.97 (dd, $^{3}J_{HP}$ = 13.0, $^{3}J_{HH}$ = 8.2, 4H, *o*-H$_{Ph}$), 7.51 (dt, $^{3}J_{HH}$ = 7.6, $^{5}J_{HP}$ = 1.0, 2H, *p*-H$_{Ph}$), 7.40 (dt, $^{3}J_{HH}$ = 8.0, $^{4}J_{HP}$ = 3.6, 4H, *m*-H$_{Ph}$), 6.61 (dq, $^{2}J_{HP}$ = 16.2, $^{3}J_{HH}$ = 5.4, 2H, NH), 2.57 (dd, $^{3}J_{HP}$ = 13.0, $^{3}J_{HH}$ = 5.4, 6H, NMe). ^{13}C{^{1}H} NMR (CDCl$_3$): δ 123.0 (d, $^{1}J_{CP}$ = 126.0, *i*-C$_{Ph}$), 132.4 (d, $^{2}J_{CP}$ = 11.2, *o*-C$_{Ph}$), 129.5 (d, $^{3}J_{CP}$ = 13.7, *m*-C$_{Ph}$), 133.9 (d, $^{4}J_{CP}$ = 2.7, *p*-C$_{Ph}$), 26.1 (s, NMe).

Synthesis of Ph$_2$P(NH-*p*-C$_6$H$_4$Me)(N-*p*-C$_6$H$_4$Me) (1a). To a suspension of **2a** (2.00 g, 4.19 mmol) in benzene (50 mL) at room temperature neat Et$_2$NH (0.45 mL, 4.35 mmol) was added. The mixture was stirred for 4 h. The fine microscrystalline solid was filtered off, washed with benzene (2x20 mL) and discarded. The filtrate was evaporated to dryness, the residue was washed with 10 mL of Et$_2$O/hexane = 1/2 (v:v) and finally redissolved in benzene. The resulting hazy solution was filtered to remove the traces of the ammonium salts and then evaporated to give an off-white powder. Yield 1.62 g (97%). Anal. calcd for C$_{26}$H$_{25}$N$_2$P: C, 78.77; H, 6.36; N, 7.06 %. Found: C, 78.94; H, 6.49; N, 6.95 %. ^{31}P{^{1}H} NMR (CDCl$_3$): δ -3.5. ^{1}H NMR (CDCl$_3$): δ 7.93 (ddd, $^{3}J_{HP}$ = 12.4, $^{3}J_{HH}$ = 8.1, $^{4}J_{HH}$ = 1.8, 4H, *o*-H$_{Ph}$), 7.39-7.51 (m, 6H, *(m+p)*-H$_{Ph}$), 6.96 (d, $^{3}J_{HH}$ = 7.5, 4H, C$_6$H$_4$), 6.92 (d, $^{3}J_{HH}$ = 7.5, 4H, C$_6$H$_4$), 5.55 (br. s, 1H, NH), 2.21 (s, 6H, CH$_3$). ^{13}C{^{1}H} NMR (C$_6$D$_6$): δ 132.7 (d, $^{1}J_{CP}$ = 130.6, *i*-C$_{Ph}$), 132.2 (d, $^{2}J_{CP}$ = 9.1, *o*-C$_{Ph}$), 131.3 (s, *p*-C$_{Ph}$), 129.8 (s, β-C$_{Tol}$), 128.9 (br. s, *i*-C$_{Tol}$(Me)), 128.5 (d, $^{3}J_{CP}$ = 12.9, *m*-C$_{Ph}$), 121.3 (br. d, $^{3}J_{CP}$ = 11.8, α-C$_{Tol}$), 20.5 (s, Me$_{Tol}$).

Synthesis of $Et_2P(NH\text{-}p\text{-}C_6H_4Me)(N\text{-}p\text{-}C_6H_4Me)$ (1b). To a solution of **2b** (0.76 g, 2.20 mmol) in benzene (30 mL) at room temperature a 2.0 M solution of NaHMDS (1.0 mL, 2.0 mmol) in THF was added and the mixture was stirred for 2 h. The precipitate of NaBr was filtered off and washed with benzene (3x5 mL). The filtrate was evaporated to dryness and the oily residue was washed with hexane (2x3 mL) to give quantitatively the product. For an analytical purity the product was recrystallized from warm diethyl ether. Yield 0.55 g (92%). Anal. calcd for $C_{18}H_{25}N_2P$: C, 71.97; H, 8.39; N, 9.33 %. Found: C, 71.95; H, 8.41; N, 9.27 %. $^{31}P\{^1H\}$ NMR ($CDCl_3$): δ 23.3. ^1H NMR ($CDCl_3$): δ 6.96 (br. s, 8H, C_6H_4), 3.85 (br. s, 1H, NH), 2.24 (s, 6H, CH_3), 2.07 (dq, $^2J_{HP}$ = 14.4, $^3J_{HH}$ = 7.6, 4H, $C\underline{H_2}CH_3$), 1.12 (dt, $^3J_{HP}$ = 18.5, $^3J_{HH}$ = 7.6, 6H, $CH_2C\underline{H_3}$). $^{13}C\{^1H\}$ NMR (C_6D_6): δ 144.5 (br. s, *i*-C_{Tol}(N)), 128.6 (s, *i*-C_{Tol}(Me)), 129.9 (s, β-C_{Tol}), 121.1 (d, $^3J_{CP}$ = 12, α-C_{Tol}), 20.5 (s, Me_{Tol}), 18.9 (d, $^1J_{CP}$ = 87, $\underline{C}H_2Me$), 6.4 (d, $^2J_{CP}$ = 3, $CH_2\underline{Me}$).

Synthesis of $Ph_2P(NHMe)(NMe)$ (1c). To a suspension of **2c** (1.00 g, 3.05 mmol) in THF (50 mL) at room temperature a 2.0 M solution of NaHMDS (1.5 mL, 3.0 mmol) in THF was added and the mixture was stirred for 18 h. The precipitate of NaBr was filtered off and washed with THF (3x5 mL). The filtrate was evaporated to dryness and the oily residue was washed with hexane (2x5 mL) and dried *in vacuo* to give a colorless glassy solid. Yield 0.72 g (96%). Compound **1c** is extremely sensitive to moisture in the air, therefore it was characterized only by the NMR ^1H and $^{31}P\{^1H\}$. $^{31}P\{^1H\}$ NMR ($CDCl_3$): δ 12.4. ^1H NMR (THF-d_8): δ 7.95 (ddd, $^3J_{HP}$ = 11.2, $^3J_{HH}$ = 7.6, $^4J_{HH}$ = 2.0, 4H, *o*-H_{Ph}), 7.45-7.52 (m, 6H, *(m+p)*-H_{Ph}), 2.81 (d, $^3J_{HP}$ = 18.0, 6H, CH_3).

Synthesis of $(Ph_2P)(NH\text{-}p\text{-}C_6H_4\text{-}CO_2Et)(N\text{-}p\text{-}C_6H_4\text{-}CO_2Et)$ (1e). To a suspension of **2e** (1.25 g, 2.10 mmol) in benzene (40 mL) at room temperature Et_3N (0.3 mL, 2.1 mmol) was added and the mixture was stirred for 1.5 h. The precipitate was filtered off. The filtrate was evaporated to dryness and the residue was reprecipitated from ether (20 mL) by addition of hexane (40 mL). The white crystalline precipitate was dried *in vacuo* to yield 1.06 g of **1e** (98%). Anal. calcd for $C_{30}H_{29}N_2O_4P$: C, 70.30; H, 5.70; N, 5.47%. Found: C, 70.59; H, 5.87; N, 5.34%. $^{31}P\{^1H\}$ NMR ($CDCl_3$): δ -2.4 (broad). $^{31}P\{^1H\}$ NMR (C_6D_6): δ -5.3. ^1H NMR ($CDCl_3$): δ 7.90 (ddd, $^3J_{HP}$ = 12.6, $^3J_{HH}$ = 7.8, $^4J_{HH}$ = 1.4, 4H, *o*-H_{Ph}), 7.80 (d, $^3J_{HH}$ = 8.4, 4H, $C_6\underline{H_4}(CO_2Et)$), 7.54 (td, $^3J_{HH}$ = 7.4, $^4J_{HH}$ = 1.4, 2H, *p*-H_{Ph}), 7.45 (td, $^3J_{HH}$ = 7.4, $^4J_{HP}$ = 3.6, 4H, *m*-H_{Ph}), 7.03 (d, $^3J_{HH}$ = 8.8, 4H, $C_6\underline{H_4}(CO_2Et)$), 4.28 (q, $^3J_{HH}$ = 7.2, 4H, $C\underline{H_2}CH_3$), 1.32 (t, $^3J_{HH}$ = 7.2, 6H, $CH_2C\underline{H_3}$). ^1H NMR (C_6D_6): δ 8.01 (d, $^3J_{HH}$ = 8.4, 4H,

$C_6\underline{H_4}(CO_2Et)$), 7.91 (ddd, $^3J_{HP}$ = 12.8, $^3J_{HH}$ = 8.0, $^4J_{HH}$ = 1.8, 4H, *o*-H_{Ph}), 7.22 (d, $^3J_{HH}$ = 8.4, 4H, $C_6\underline{H_4}(CO_2Et)$), 6.97 (m, 6H, (*m*+*p)*-H_{Ph}), 6.29 (s, 1H, NH), 4.07 (q, $^3J_{HH}$ = 7.2, 4H, $C\underline{H_2}CH_3$), 0.99 (t, $^3J_{HH}$ = 7.2, 6H, $CH_2C\underline{H_3}$). $^{13}C\{^1H\}$ NMR ($CDCl_3$): δ 166.8 (s, $\underline{C}O_2Et$), 145.0 (s, *i*-$C_6H_4(CO_2Et)$), 132.0 (d, $^2J_{CP}$ = 9.9, *o*-C_{Ph}), 132.7 (d, $^4J_{CP}$ = 2.8, *p*-C_{Ph}), 131.3 (s, *m*-$C_6H_4(CO_2Et)$), 130.1 (d, $^1J_{CP}$ = 130.4, *i*-C_{Ph}), 129.3 (d, $^3J_{CP}$ = 13.2, *m*-C_{Ph}), 122.3 (br. s, *p*-$C_6H_4(CO_2Et)$), 120.2 (br. s, *o*-$C_6H_4(CO_2Et)$), 60.6 (s, $\underline{C}H_2CH_3$), 14.5 (s, $CH_2\underline{C}H_3$). $^{13}C\{^1H\}$ NMR (C_6D_6): δ 166.7 (s, $\underline{C}O_2Et$), 145.4 (s, *i*-$C_6H_4(CO_2Et)$), 131.9 (d, $^2J_{CP}$ = 9.8, *o*-C_{Ph}), 131.8 (d, $^4J_{CP}$ = 2.8, *p*-C_{Ph}), 131.2 (s, *m*-$C_6H_4(CO_2Et)$), 130.9 (d, $^1J_{CP}$ = 131.9, *i*-C_{Ph}), 128.6 (d, $^3J_{CP}$ = 12.3, *m*-C_{Ph}), 122.1 (br. s, *p*-$C_6H_4(CO_2Et)$), 120.2 (d, $^3J_{CP}$ = 18.3, *o*-$C_6H_4(CO_2Et)$), 59.9 (s, $\underline{C}H_2CH_3$), 13.9 (s, $CH_2\underline{C}H_3$).

Synthesis of (Ph_2P)(NH-Me)(N-*p*-Tol) (1d). To a solution of Ph_2PCl (3.6 mL, 20 mmol) in CH_2Cl_2 (15 mL) at room temperature a solution of Br_2 (1.0 mL, 20.0 mmol) in CH_2Cl_2 (15 mL) was added dropwise. The reaction mixture was warmed to 22°C, stirred for 1.5 h and cooled again to 0°C. A solution of *p*-toluidine (4.3 g, 40 mmol) in CH_2Cl_2 (40 mL) was added to the reaction mixture and the resulting suspension was stirred overnight at 20°C. The precipitate of ammonium salt was filtered off and washed with CH_2Cl_2 (3x20 mL). The filtrate was cooled to -30°C and a cold (0°C) solution of $MeNH_2$ (80 mmol) in CH_2Cl_2 (30 mL) was added dropwise. The reaction mixture was warmed to room temperature and stirred overnight. The precipitate was filtered off and washed with CH_2Cl_2 (3x10 mL). The filtrate was concentrated to 7 mL and the precipitated was filtered and washed with CH_2Cl_2 (3x2 mL). The white crystalline solid was dried *in vacuo* to yield 4.63 g of **1d** (72%). Anal. calcd for $C_{20}H_{21}N_2P$: C, 74.98; H, 6.61; N, 8.74%. Found: C, 74.85; H, 6.69; N, 8.58%. $^{31}P\{^1H\}$ NMR (C_6D_6): δ 2.91. ^1H NMR (C_6D_6): δ 7.92 (m, 4H, *o*-H_{Ph}), 7.24 (dd, $^3J_{HH}$ = 8.2, $^4J_{HP}$ = 1.0, 2H, *o*-H_{Tol}), 7.11 (d, $^3J_{HH}$ = 8.0, 2H, m-H_{Tol}), 7.03 (m, 6H, *(m+p)*-H_{Ph}), 2.28 (s, 3H, Me_{Tol}), 2.23 (d, $^3J_{HP}$ = 11.6, 3H, Me(N)), 2.16 (br. s, 1H, NH). $^{13}C\{^1H\}$ NMR (C_6D_6): δ 149.5 (d, $^2J_{CP}$ = 3.0, *i*-C(N)), 132.9 (d, $^1J_{CP}$ = 128.2, *i*-C_{Ph}), 132.6 (d, $^2J_{CP}$ = 9.2, *o*-C_{Ph}), 131.2 (d, $^4J_{CP}$ = 2.7, *p*-C_{Ph}), 129.9 (d, $^4J_{CP}$ = 0.6, *m*-C_{Tol}), 128.6 (d, $^3J_{CP}$ = 12.3, *m*-C_{Ph}), 126.5 (d,$^5J_{CP}$ = 0.6, *p*-C_{Tol}), 124.0 (d, $^3J_{CP}$ = 18.3, *o*-C_{Tol}), 26.5 (s, Me(N)), 21.0 (s, Me_{Tol}).

Synthesis of [(η^6-C_6Me_6)RuCl{Ph_2P(N-*p*-$C_6H_4Me)_2$}] (3a). To a solution of **1a** (0.80 g, 2.02 mmol) in benzene (60 mL) a 2.0 M solution of NaHMDS in THF (1.10 mL, 2.20 mmol) was added and the resulting solution was stirred for 1 h. Then solid [(η^6-

$C_6Me_6)Ru(\mu\text{-}Cl)Cl]_2$ (0.67 g, 1.00 mmol) was added and the reaction mixture was stirred overnight. The solvent was removed *in vacuo*, the residue was washed with hexane (2x10 mL) and extracted with CH_2Cl_2 (100 mL). The filtrate was concentrated to 10 mL and diluted with 10 mL of benzene, then slowly evaporated to 3-5 mL. The brick-red crystalline precipitate was filtered off, washed with benzene (2 mL), Et_2O (10 mL) and dried in vacuum. Yield 1.20 g (86%). Anal. calcd for $C_{38}H_{42}ClN_2PRu$: C, 65.74; H, 6.10%. Found: C, 65.87; H, 6.29%. $^{31}P\{^1H\}$ NMR ($CDCl_3$): δ 43.9. $^{31}P\{^1H\}$ NMR (C_6D_6): δ 43.3. ^1H NMR ($CDCl_3$): δ 7.76 (br. dd, $^3J_{HP}$ = 12, $^3J_{HH}$ = 8, 4H, *o*-H_{Ph}), 7.44 (br. t, 2H, *p*-H_{Ph}), 7.33 (br. m, 4H, *m*-H_{Ph}), 6.88 (d, $^3J_{HH}$ = 8.0, 4H, C_6H_4), 6.78 (d, $^3J_{HH}$ = 8.0, 4H, C_6H_4), 2.10 (s, 6H, Me_{Tol}), 1.95 (s, 18H, C_6Me_6). ^1H NMR (C_6D_6): δ 8.07 (m, 2H, *o*-H_{Ph}), 7.91 (ddd, $^3J_{HP}$ = 11.2, $^3J_{HH}$ = 8.0, $^4J_{HH}$ = 1.6, 2H, *o'*-H_{Ph}), 7.35 (dd, $^3J_{HH}$ = 8.0, $^4J_{HP}$ = 1.2, 4H, C_6H_4), 7.23 (m, 3H, *(p'+m)*-H_{Ph}), 6.89 (d, $^3J_{HH}$ = 8.0, 4H, C_6H_4), 6.73 (m, 3H, *(p+m')*-H_{Ph}), 2.10 (s, 6H, Me_{Tol}), 1.80 (s, 18H, C_6Me_6). $^{13}C\{^1H\}$ NMR ($CDCl_3$): δ 144.6 (d, $^2J_{CP}$ = 4.4, *i*-C_{Tol}(N)), 133.2 (d, $^2J_{CP}$ = 10.9, *o*-C_{Ph}), 131.4 (d, $^4J_{CP}$ = 2.0, *p*-C_{Ph}), 128.5 (s, β-C_{Tol}), 127.9 (s, *i*-C_{Tol}(Me)), 127.6 (d, $^3J_{CP}$ = 12.7, *m*-C_{Ph}), 125.1 (d, $^3J_{HH}$ = 9.3, α-C_{Tol}), 89.2 (s, C_6Me_6), 20.5 (s, Me_{Tol}), 16.2 (s, C_6Me_6). UV-vis (CH_2Cl_2; λ_{max}, nm; ε, M^{-1} cm^{-1}): 450 (900).

Synthesis of [(η^6-C_6Me_6)RuCl{Et_2P(N-*p*-$C_6H_4Me)_2$}] (3b). To a solution of **1b** (0.51 g, 1.70 mmol) in THF (50 mL) a 2.0 M solution of NaHMDS in THF (0.90 mL, 1.80 mmol) was added and the resulting solution was stirred for 1 h. Then solid [(η^6-C_6Me_6)Ru(μ-Cl)Cl]$_2$ (0.56 g, 0.85 mmol) was added and the reaction mixture was stirred overnight. The solvent was removed *in vacuo*, the residue was washed with hexane (2x10 mL) and extracted with benzene (50 mL). The filtrate was concentrated to 3-5 mL and diluted with 10 mL of Et_2O. The red-brown crystalline precipitate was filtered off, washed with Et_2O (5 mL) and dried in vacuum. Yield 0.74 g (73%). Anal. calcd for $C_{30}H_{42}ClN_2PRu$: C, 60.24; H, 7.08%. Found: C, 60.37; H, 7.11%. $^{31}P\{^1H\}$ NMR ($CDCl_3$): δ 72.4. $^{31}P\{^1H\}$ NMR (C_6D_6): δ 71.1. ^1H NMR ($CDCl_3$): δ 7.04 (d, $^3J_{HH}$ = 8.0, 4H, C_6H_4), 6.89 (d, $^3J_{HH}$ = 8.0, 4H, C_6H_4), 2.23 (s, 6H, Me_{Tol}), 1.89 (s, 18H, C_6Me_6), 1.77 (dq, $^2J_{HP}$ = 11.7, $^3J_{HH}$ = 7.6, 4H, $C\underline{H_2}CH_3$), 1.05 (dt, $^3J_{HP}$ = 16.2, $^3J_{HH}$ = 7.6, 6H, $CH_2C\underline{H_3}$). ^1H NMR (C_6D_6): δ 7.48 (d, $^3J_{HH}$ = 7.7, 4H, C_6H_4), 7.11 (d, $^3J_{HH}$ = 7.7, 4H, C_6H_4), 2.33 (s, 6H, Me_{Tol}), 2.17 (br. dq, $^2J_{HP}$ = 14.4, $^3J_{HH}$ = 7.2, 2H, $C\underline{H_2}'CH_3$), 1.86 (s, 18H, C_6Me_6), 1.47 (br. dt, $^3J_{HP}$ = 15.6, $^3J_{HH}$ = 7.2, 3H, $CH_2C\underline{H_3}$), 1.31 (br. dq, $^2J_{HP}$ = 14.4, $^3J_{HH}$ = 7.2, 2H, $C\underline{H_2}CH_3$), 0.54 (br. dt, $^3J_{HP}$ = 15.6, $^3J_{HH}$ = 7.8, 3H, $CH_2C\underline{H_3}'$). $^{13}C\{^1H\}$ NMR ($CDCl_3$): δ 145.1 (d, $^2J_{CP}$ = 4.0, *i*-C_{Tol}(N)), 128.9

(s, *i*-C_{Tol}(Me)), 128.8 (s, β-C_{Tol}), 126.1 (d, $^3J_{CP}$ = 6.7, α-C_{Tol}), 88.7 (s, C_6Me_6), 25.7 (d, $^1J_{CP}$ = 54.8, $\underline{C}H_2Me$), 20.6 (s, Me_{Tol}), 15.9 (s, C_6Me_6), 6.5 (d, $^2J_{CP}$ = 4.8, $CH_2\underline{Me}$). UV-vis (CH_2Cl_2; λ_{max}, nm; ε, M^{-1} cm^{-1}): 450 (940).

Synthesis of [(η^6-C_6Me_6)RuCl{$Ph_2P(NMe)_2$}] (3c). To a solution of **2c** (0.76 g, 2.3 mmol) in THF (50 mL) a 2.0 M solution of NaHMDS in THF (1.20 mL, 2.40 mmol) was added and the resulting mixture was stirred for 3 h. The precipitate of NaBr was filtered off and washed with THF (10mL). The filtrate was treated again with 2.0 M solution of NaHMDS (1.2 mL, 2.4 mmol) and stirred for an extra 3 h. Then solid [(η^6-C_6Me_6)Ru(μ-Cl)Cl]$_2$ (0.77 g, 1.15 mmol) was added and the reaction mixture was stirred overnight. The solvent was removed *in vacuo*, the residue was washed with hexane (2x10 mL) and extracted with benzene (40 mL). The filtrate was diluted with 40 mL of hexane and the resulting flocculated black impurities were filtered off. The solution was evaporated to 5-7 mL and set for crystallization in a fridge at -20 °C. The dark-red crystalline precipitate was filtered off, washed with cold hexane (5 mL) and dried in vacuum. Yield 0.77 g (62%). Anal. calcd for $C_{26}H_{34}ClN_2PRu$: C, 57.61; H, 6.32%. Found: C, 57.40; H, 6.38%. $^{31}P\{^1H\}$ NMR ($CDCl_3$): δ 76.9. $^{31}P\{^1H\}$ NMR (C_6D_6): δ 59.8. ^1H NMR ($CDCl_3$): δ 7.55 (td, $^3J_{HH}$ = 7.2, $^5J_{HP}$ = 1.2, 2H, *p*-H_{Ph}), 7.44 (td, $^3J_{HH}$ = 8.0, $^4J_{HP}$ = 2.8, 4H, *m*-H_{Ph}), 7.26 (dd, $^3J_{HP}$ = 10.4, $^3J_{HH}$ = 8.0, 4H, *o*-H_{Ph}), 2.71 (d, $^3J_{HP}$ = 19.2, 6H, NMe), 2.27 (s, 18H, C_6Me_6). ^1H NMR (C_6D_6): δ 8.00 (br. s, 2H, *o*-H_{Ph}), 7.69 (br. s, 2H, *o*-H_{Ph}), 7.21 (br. s, 3H, *(m+p)*-H_{Ph}), 7.12 (br. s, 1H, *p'*-H_{Ph}), 7.05 (br. s, 2H, *m'*-H_{Ph}), 2.74 (d, $^3J_{HP}$ = 19.2, 6H, NMe), 1.84 (s, 18H, C_6Me_6). $^{13}C\{^1H\}$ NMR (C_6D_6): δ 140.6 (d, $^1J_{CP}$ = 104.0, *i*-C_{Ph}), 132.2 (d, $^1J_{CP}$ = 58.2, *i*-C_{Ph}'), 134.9 (br. s, *o*-C_{Ph}), 131.3 (br. s, *p*-C_{Ph}), 130.5 (br. s, *(m+m')*-C_{Ph}), 130.2 (br. s, *(o'+p')*-C_{Ph}), 88.7 (s, C_6Me_6), 32.9 (s, NMe), 15.6 (s, C_6Me_6). UV-vis (toluene; λ_{max}, nm; ε, M^{-1} cm^{-1}): 430 (1550).

Synthesis of (η^6-C_6Me_6)RuCl(Ph_2P)(N-Me)(N-*p*-Tol) (3d). To a solution of **1d** (0.32 g, 1.0 mmol) in benzene (50 mL) a 0.64 M solution of NaHMDS in toluene (1.87 mL, 1.20 mmol) was added and the resulting solution was stirred for 2 h at room temperature. Then solid [(η^6-C_6Me_6)Ru(μ-Cl)Cl]$_2$ (0.30 g, 0.50 mmol) was added and the reaction mixture was stirred overnight. The precipitated was filtered off and the solvent was removed *in vacuo*. The residue was dried and dissolved in toluene (50 ml), the precipitate was filtered off. The solution was evaporated to 3-5 mL, then diluted with 30 mL of pentane and set for crystallization in a fridge at -20 °C. The resulting orange-red crystals were filtered off,

washed with hexane (5 mL) and dried in vacuum. Yield 0.47 g (77%). Anal. calcd for $C_{32}H_{38}ClN_2PRu$: C, 62.18; H, 6.20%. Found: C, 62.54; H, 6.58%. $^{31}P\{^1H\}$ NMR (C_6D_6): δ 52.04. ^1H NMR (C_6D_6): δ 7.92 (m, 4H, *(o+o')*-H_{Ph}), 7.23 (br. s, 3H, *(m+p)*-H_{Ph}), 7.15 (dd, $^3J_{HH}$ = 8.0, $^4J_{HP}$ = 1.2, 2H, *o*-H_{Tol}), 6.91 (d, $^3J_{HH}$ = 8.0, 2H, *m*-H_{Tol}), 6.87 (br. s, 3H, *(m+p)'*-H_{Ph}), 2.74 (d, $^3J_{HP}$ = 20.0, 3H, MeN), 2.14 (s, 3H, Me_{Tol}), 1.82 (s, 18H, C_6Me_6). $^{13}C\{^1H\}$ NMR (C_6D_6): δ 146.2 (d, $^2J_{CP}$ = 3.2, *i*-C_{Tol}(N)), 135.1 (br. d, $^2J_{CP}$ = 10.4, *o*-C_{Ph}), 131.7 (br. d, $^2J_{CP}$ = 10.6, *o'*-C_{Ph}), 131.4 (br. s, *p*-C_{Ph}), 131.0 (br. s, *p'*-C_{Ph}), 127.8-128.0 (overlapped, *(m+m')*-C_{Ph}), 129.1 (s, *m*-C_{Tol}), 127.0 (d, $^5J_{CP}$ = 1.3, *p*-C_{Tol}), 124.6 (d, $^3J_{CP}$ = 10.0, *o*-C_{Tol}), 89.3 (s, $\underline{C_6}Me_6$), 32.8 (s, MeN), 20.8 (s, Me_{Tol}), 16.0 (s, $C_6\underline{Me_6}$).

Synthesis of [(η^6-*p*-cymene)RuCl{Ph_2P(N-*p*-$C_6H_4Me)_2$}] (3f). To a solution of **1a** (0.79 g, 2.0 mmol) in benzene (60 mL) a 2.0 M solution of NaHMDS in THF (1.10 mL, 2.20 mmol) was added and the resulting solution was stirred for 2 h at room temperature. Then solid $[(\eta^6\text{-}C_6Me_6)Ru(\mu\text{-}Cl)Cl]_2$ (0.61 g, 1.00 mmol) was added and the reaction mixture was stirred overnight. The precipitated was filtered off and was washed with benzene (2x5 mL). The filtrate was evaporated to dryness and the residue was washed with hexane (2x10 mL), Et_2O (3x5 mL) and then recrystallized from hot benzene (20 mL). The dark-red crystalline solid was filtered off, washed with Et_2O (5 mL) and dried *in vacuo*. Yield 1.00 g of **3f** (88%). Anal. calcd for $C_{36}H_{38}ClN_2PRu$: C, 64.90; H, 5.75%. Found: C, 64.85; H, 5.84%. $^{31}P\{^1H\}$ NMR ($CDCl_3$): δ 43.8. $^{31}P\{^1H\}$ NMR (C_6D_6): δ 42.9. ^1H NMR ($CDCl_3$): δ 7.87 (dd, $^3J_{HP}$ = 10.8, $^3J_{HH}$ = 8.0, 4H, *o*-H_{Ph}), 7.50 (m, 2H, *p*-H_{Ph}), 7.39 (m, 4H, *m*-H_{Ph}), 6.90 (d, $^3J_{HH}$ = 8.0, 4H, C_6H_4), 6.82 (d, $^3J_{HH}$ = 8.4, 4H, C_6H_4), 6.31 (d, $^3J_{HH}$ = 5.6, 2H, C_6H_4(Cym)), 5.41 (d, $^3J_{HH}$ = 5.6, 2H, C_6H_4(Cym)), 2.89 (sept, $^3J_{HH}$ = 6.8, 1H, C$\underline{H}Me_2$), 2.19 (s, 6H, Me_{Tol}), 2.11 (s, 3H, Me_{Cym}), 1.21 (d, $^3J_{HH}$ = 6.8, 6H, CH$\underline{Me_2}$). ^1H NMR (C_6D_6): δ 8.03 (m, 4H, *o*-H_{Ph}), 7.27 (d, $^3J_{HH}$ = 7.8, 4H, C_6H_4), 7.22 (m, 3H, *(m+p)*-H_{Ph}), 6.93 (d, $^3J_{HH}$ = 7.8, 4H, C_6H_4), 6.75 (m, 3H, *(m+p)*-H_{Ph}'), 5.05 (d, $^3J_{HH}$ = 6.0, 2H, C_6H_4(Cym)), 4.87 (d, $^3J_{HH}$ = 6.0, 2H, C_6H_4(Cym)), 2.88 (sept, $^3J_{HH}$ = 6.6, 1H, C$\underline{H}Me_2$), 2.15 (s, 6H, Me_{Tol}), 1.86 (c, 3H, Me_{Cym}), 1.05 (d, $^3J_{HH}$ = 6.8, 6H, CH$\underline{Me_2}$). $^{13}C\{^1H\}$ NMR ($CDCl_3$): δ 145.8 (d, $^2J_{CP}$ = 4.4, *i*-C_{Tol}(N)), 133.4 (br. s, *o*-C_{Ph}), 131.9 (d, $^4J_{CP}$ = 2.7, *p*-C_{Ph}), 129.0 (s, β-CH_{Tol}), 128.2 (d, $^3J_{CP}$ = 11.2, *m*-C_{Ph}), 127.5 (s, *i*-C_{Tol}), 122.9 (d, $^3J_{CP}$ = 9.7, α-CH_{Tol}), 102.0 (s, *i*-C_{Cym}), 94.8 (s, *i*-C_{Cym}), 80.5 (s, CH_{Cym}), 79.6 (s, CH_{Cym}), 30.9 (s, $\underline{C}HMe_2$), 22.5 (s, CH$\underline{Me_2}$), 20.5 (s, Me_{Tol}), 18.9 (s, Me_{Cym}). $^{13}C\{^1H\}$ NMR (C_6D_6): δ 146.9 (s, $^2J_{CP}$ = 4.2, *i*-C_{Tol}(N)), 136.5 (d, $^1J_{CP}$ = 95.1, *i*-C_{Ph}), 135.0 (d, $^2J_{CP}$ = 11.0, *o*-C_{Ph}), 132.6 (d, $^2J_{CP}$ = 9.8, *o*-C_{Ph}'),

132.0 (d, $^4J_{CP}$ = 2.7, *p*-C_{Ph}), 131.8 (d, $^4J_{CP}$ = 2.9, *p*-C_{Ph}'), 130.2 (d, $^1J_{CP}$ = 84.0, *i*-C_{Ph}'), 129.4 (s, β-CH_{Tol}), 128.6 (d, $^3J_{CP}$ = 12.5, *m*-C_{Ph}), 128.5 (s, *i*-C_{Tol}(Me)), ~127.7 (overlapped, *m*-C_{Ph}'), 123.9 (d, $^3J_{CP}$ = 9.7, α-CH_{Tol}), 102.4 (s, *i*-C_{Cym}), 94.8 (s, *i*-C_{Cym}), 80.7 (s, CH_{Cym}), 79.4 (s, CH_{Cym}), 31.2 (s, C<u>H</u>Me_2), 22.5 (s, CH<u>Me</u>$_2$), 20.7 (s, Me_{Tol}), 18.8 (s, Me_{Cym}). UV-vis (CH_2Cl_2; λ_{max}, nm; ε, M^{-1} cm^{-1}): 450 (450, shoulder).

Синтез [(η^6-*p*-cymene)RuCl{Ph_2P(N-*p*-C_6H_4-$CO_2Et)_2$}] (3e). To a suspension of **1e** (0.49 g, 0.96 mmol) in benzene (40 mL) a solid [(η^6-*p*-cymene)$RuCl_2$]$_2$ (0.29 g, 0.48 mmol) was added, then Et_2NH (0.12 mL, 1.16 mmol, 1.2 эquiv.) was added and the resulting mixture was stirred overnight at room temperature. The solution was evaporated to dryness and the residue was dried *in vacuo*. Then the residue was dissolved in benzene (30 ml) and the precipitate was filtered off. The filtrate was evaporated to 3-5 mL, then diluted with 30 mL of Et_2O. The orange crystalline precipitate was filtered off and washed with Et_2O (3x5 mL), then dried *in vacuo*. Yield of **3e** 0.69 g (88%). Anal. calcd for $C_{40}H_{42}ClN_2O_4PRu$: C, 61.42; H, 5.41%. Found: C, 61.55; H, 5.54%. $^{31}P\{^1H\}$ NMR (C_6D_6): δ 47.2. ^1H NMR (C_6D_6): δ 8.12 (dd, $^3J_{HH}$ = 8.8, $^5J_{HP}$ = 0.8, 4H, $C_6H_4(CO_2Et)$), 7.98 (ddd, $^3J_{HP}$ = 12.4, $^3J_{HH}$ = 8.2, $^4J_{HH}$ = 1.4, 2H, *o*-H_{Ph}), 7.87 (ddd, $^3J_{HP}$ = 12.0, $^3J_{HH}$ = 8.2, $^4J_{HH}$ = 1.4, 2H, *o'*-H_{Ph}), 7.23 (td, $^3J_{HH}$ = 7.2, $^4J_{HP}$ = 1.6, 1H, *p*-H_{Ph}), 7.19 (td, $^3J_{HH}$ = 7.2, $^4J_{HP}$ = 2.8, $^4J_{HH}$ = 1.6, 2H, *m*-H_{Ph}), 7.13 (dd, $^3J_{HH}$ = 8.8, $^4J_{HP}$ = 0.8, 4H, $C_6H_4(CO_2Et)$), 6.76 (td, $^3J_{HH}$ = 7.6, $^4J_{HP}$ = 1.6, 1H, *p*'-H_{Ph}), 6.69 (td, $^3J_{HH}$ = 7.6, $^4J_{HP}$ = 2.8, 2H, *m*'-H_{Ph}), 4.98 (d, $^3J_{HH}$ = 6.0, 2H, C_6H_4(Cym)), 4.82 (d, $^3J_{HH}$ = 6.0, 2H, C_6H_4(Cym)), 4.17 (q, $^3J_{HH}$ = 7.2, 4H, C<u>H</u>$_2$$CH_3$), 2.67 (sept, $^3J_{HH}$ = 6.8, 1H, C<u>H</u>Me_2), 1.69 (s, 3H, Me_{cym}), 1.04 (t, $^3J_{HH}$ = 7.2, 6H, CH_2C<u>H</u>$_3$), 0.95 (d, $^3J_{HH}$ = 6.8, 6H, CH<u>Me</u>$_2$). $^{13}C\{^1H\}$ NMR (C_6D_6):δ 166.5 (s, <u>C</u>O_2Et), 153.7 (d, $^2J_{CP}$ = 5.4, *i*-<u>C</u>N(CO_2Et)), 135.8 (d, $^1J_{CP}$ = 116.6, *i*'-C_{Ph}), 134.8 (d, $^2J_{CP}$ = 11.3, *o'*-C_{Ph}), 133.3 (d, $^1J_{CP}$ = 99.3, *i*-C_{Ph}), 133.0 (d, $^4J_{CP}$ = 2.7, *p'*-C_{Ph}), 132.6 (d, $^4J_{CP}$ = 2.5, *p*-C_{Ph}), 132.4 (d, $^2J_{CP}$ = 10.9, *o*-C_{Ph}), 130.9 (s, *m*-$C_6H_4(CO_2Et)$), 129.1 (d, $^3J_{CP}$ = 12.1, *m*-C_{Ph}), 128.6 (d, $^3J_{CP}$ = 12.3, *m'*-C_{Ph}), 122.2 (d, $^3J_{CP}$ = 12.2, *o*-$C_6H_4(CO_2Et)$), 120.6 (s, *p*-$C_6H_4(CO_2Et)$), 104.1 (s, *i*-C_{Cym}), 95.7 (s, *i*-C_{Cym}), 81.1 (s, CH_{Cym}), 78.9 (s, CH_{Cym}), 60.1 (s, <u>C</u>H_2CH_3), 31.5 (s, <u>C</u>HMe_2), 22.4 (s, CH<u>Me</u>$_2$), 18.6 (s, Me_{Cym}), 14.5 (s, CH_2<u>C</u>H_3).

Synthesis of [(η^6-C_6Me_6)Ru{R_2P(N-R')$_2$}]X (4a, X = PF_6; 4b, X = BF_4; 4c, X = PF_6). General procedure. (**a**, R = Ph, R' = *p*-Tol). To a solution of **3a** (0.46 g, 0.66 mmol) in CH_2Cl_2 (30 ml), solid $NaPF_6$ (0.20 g, 1.2 mmol) was added, causing an immediate color change from red to deep violet. The reaction suspension was stirred for 3 h and then filtered

through a plug of Celite. The solution was concentrated to 2 mL and further addition of Et_2O (10 mL) resulted in precipitation of a product, which was filtered off, washed with Et_2O (2x5 mL) and dried in vacuum. Yield of **4a** 0.51 g (96%). Anal. calcd for $C_{38}H_{42}F_6N_2P_2Ru$: C, 56.78; H, 5.27%. Found: C, 56.69; H, 5.12%. $^{31}P\{^1H\}$ NMR ($CDCl_3$): 71.9, -144.4 (sept, J_{PF} = 707, PF_6^-). ^1H NMR ($CDCl_3$): δ 7.64 (td, $^3J_{HH}$ = 7.6, $^5J_{HP}$ = 1.2, 2H, *p*-H_{Ph}), 7.49 (td, $^3J_{HH}$ = 7.6, $^4J_{HP}$ = 3.2, 4H, *m*-H_{Ph}), 7.38 (dd, $^3J_{HP}$ = 12.0, $^3J_{HH}$ = 7.2, 4H, *o*-H_{Ph}), 7.02 (d, $^3J_{HH}$ = 7.6, 4H, C_6H_4), 6.68 (d, $^3J_{HH}$ = 7.6, 4H, C_6H_4), 2.28 (s, 6H, Me_{Tol}), 2.08 (s, 18H, C_6Me_6). $^{13}C\{^1H\}$ NMR (CD_2Cl_2): δ 141.6 (d, $^2J_{CP}$ = 2, *i*-C_{Tol}(N)), 135.3 (s, *p*-C_{Tol}(Me)), 134.2 (d, $^4J_{CP}$ = 2.3, *p*-C_{Ph}), 132.0 (d, $^2J_{CP}$ = 10.6, *o*-C_{Ph}), 130.1 (s, *m*-C_{Tol}), 129.3 (d, $^3J_{CP}$ = 12.4, *m*-C_{Ph}), 126.3 (d, $^3J_{нн}$ = 6.2, *o*-C_{Tol}), 126.2 (d, $^1J_{HH}$ = 90.5, *i*-C_{Ph}), 89.9 (s, $\underline{C_6}Me_6$), 20.8 (s, Me_{Tol}), 16.5 (s, $C_6\underline{Me_6}$). UV-vis (CH_2Cl_2; λ_{max}, nm; ε, M^{-1} cm^{-1}): 540 (1320).

(**4b**, R = Et, R' = *p*-Tol). Analogously, from **3b** (0.45 g, 0.75 mmol) and $NaBF_4$ (0.085 g, 0.77 mmol), complex **4b** was obtained (0.46 g, 93%). Anal. calcd for $C_{30}H_{42}BF_4N_2PRu$: C, 55.48; H, 6.52%. Found: C, 55.61; H, 6.44%. UV-vis (CH2Cl2; λmax, nm; ε, M-1 cm-1): 540 (1410). $^{31}P\{^1H\}$ NMR ($CDCl_3$): δ 102.3. ^1H NMR ($CDCl_3$): δ 7.14 (d, $^3J_{HH}$ = 6.0, 4H, C_6H_4), 6.91 (d, $^3J_{HH}$ = 6.0, 4H, C_6H_4), 2.31 (s, 6H, Me_{Tol}), 2.02 (s, 18H, C_6Me_6), 1.59 (br. dq, $^2J_{HP}$ = 10, $^3J_{HH}$ = 8, 4H, $C\underline{H_2}CH_3$), 0.99 (br. dt, $^3J_{HP}$ = 16, $^3J_{HH}$ = 8, 6H, $CH_2C\underline{H_3}$). $^{13}C\{^1H\}$ NMR ($CDCl_3$): δ 141.4 (d, $^2J_{CP}$ = 4.0, *i*-C_{Tol}(N)), 134.9 (d, $^5J_{CP}$ = 2.0, *p*-C_{Tol}(Me)), 130.3 (s, *m*-C_{Tol}), 125.7 (d, $^3J_{CP}$ = 5.2, *o*-C_{Tol}), 89.2 (s, $\underline{C_6}Me_6$), 20.6 (s, Me_{Tol}), 19.8 (d, $^1J_{CP}$ = 53.6, $\underline{C}H_2Me$), 16.3 (s, $C_6\underline{Me_6}$), 5.2 (d, $^2J_{CP}$ = 5.4, $CH_2\underline{Me}$). UV-vis (CH_2Cl_2; λ_{max}, nm; ε, M^{-1} cm^{-1}): 540 (1410).

(**4c**, R = Ph, R' = Me). Analogously, from **3c** (0.14 g, 0.26 mmol) and $NaPF_6$ (0.10 g, 0.6 mmol), complex **4c** was obtained (0.16 g, 96%). Anal. calcd for $C_{26}H_{34}F_6N_2P_2Ru$: C, 47.93; H, 5.26%. Found: C, 48.25; H, 5.41%. $^{31}P\{^1H\}$ NMR($CDCl_3$): δ 80.6, -144.5 (sept, J_{PF} = 711, PF_6^-). ^1H NMR ($CDCl_3$): δ 7.60 (ttd, $^3J_{HH}$ = 7.5, $^4J_{HH}$ = 1.5, $^5J_{HP}$ = 1.4, 2H, *p*-H_{Ph}), 7.46 (td, $^3J_{HH}$ = 7.5, $^4J_{HP}$ = 3.0, 4H, *m*-H_{Ph}), 7.25 (dd, $^3J_{HP}$ = 12.9, $^3J_{HH}$ = 7.2, 4H, *o*-H_{Ph}), 2.74 (d, $^3J_{HP}$ = 18.3, 6H, NMe), 2.27 (s, 18H, C_6Me_6). $^{13}C\{^1H\}$ NMR($CDCl_3$): δ 133.8 (d, $^4J_{CP}$ = 2.4, *p*-C_{Ph}), 131.1 (d, $^2J_{CP}$ = 9.9, *o*-C_{Ph}), 129.3 (d, $^3J_{CP}$ = 11.6, *m*-C_{Ph}), 124.9 (d, $^1J_{HH}$ = 87.5, *i*-C_{Ph}), 89.3 (s, C_6Me_6), 33.2 (s, NMe), 16.4 (s, C_6Me_6). UV-vis (CH_2Cl_2; λ_{max}, nm; ε, M^{-1} cm^{-1}): 550 (1300).

Synthesis of [(η^6-*p*-cymene)Ru{$Ph_2P(N$-*p*-$C_6H_4Me)_2$}](PF$_6$) (4f). To a solution of **3a** (0.39 g, 0.59 mmol) in CH_2Cl_2 (15 ml), solid $AgPF_6$ (0.16 g, 0.62 mmol) was added, causing the color to immediately change from red to deep violet. The reaction suspension was stirred for 2 h and then filtered through a bed of Celite. The solvent was removed under reduced pressure and the residue was washed with Et_2O (2x5 mL). The product was dried *in vacuo* to give violet-black **4f**. Yield 0.41 g (91%). Anal. calcd for $C_{36}H_{38}F_6N_2P_2Ru$: C, 55.74; H, 4.94%. Found: C, 55.47; H, 4.99%. $^{31}P\{^1H\}$ NMR($CDCl_3$): δ 71.3 (s, PPh_2), -144.1 (sept, J_{PF} = 712, PF_6^-). ^1H NMR ($CDCl_3$): δ 7.65 (m, 2H, *p*-H_{Ph}), 7.52 (m, 4H, *m*-H_{Ph}), 7.47 (m, 4H, *o*-H_{Ph}), 7.02 (d, $^3J_{HH}$ = 8.0, 4H, C_6H_4), 6.84 (dd, $^3J_{HH}$ = 8.0, $^4J_{HP}$ = 1.2, 4H, C_6H_4), 5.88 (d, $^3J_{HH}$ = 6.8, 2H, C_6H_4(Cym)), 5.84 (d, $^3J_{HH}$ = 6.8, 2H, C_6H_4(Cym)), 2.68 (sept, $^3J_{HH}$ = 6.8, 1H, C<u>H</u>Me_2), 2.26 (s, 3H, Me_{Cym}), 2.25 (s, 6H, Me_{Tol}), 1.31 (d, $^3J_{HH}$ = 6.8, 6H, CH<u>Me_2</u>). $^{13}C\{^1H\}$ NMR ($CDCl_3$): δ 144.1 (d, $^2J_{CP}$ = 3.6, *i*-C_{Tol}(N)), 134.4 (d, $^4J_{CP}$ = 2.2, *p*-C_{Ph}), 134.1 (s, *p*-C_{Tol}(Me)), 132.4 (d, $^2J_{CP}$ = 10.3, *o*-C_{Ph}), 130.2 (s, *m*-CH_{Tol}), 129.5 (d, $^3J_{CP}$ = 12.5, *m*-C_{Ph}), 124.7 (d, $^1J_{CP}$ = 89.4, *i*-C_{Ph}), 123.7 (d, $^3J_{CP}$ = 8.0, *o*-CH_{Tol}), 99.6 (s, *i*-C_{Cym}), 89.6 (s, *i*-C_{Cym}), 81.0 (s, CH_{Cym}), 78.7 (s, CH_{Cym}), 31.8 (s, <u>C</u>HMe_2), 22.8 (s, CH<u>Me_2</u>), 20.9 (s, Me_{Tol}), 19.7 (s, Me_{Cym}). UV-vis (CH_2Cl_2; λ_{max}, nm; ε, M^{-1} cm^{-1}): 590 (1880).

Reaction of 4a, 4c and 4f with CO.

General procedure. (For **5a**): A stream of CO was slowly bubbled through a stirred solution of **4a** (0.12 g, 0.15 mmol) in CH_2Cl_2 (5 mL) for 10 min. The color quickly changed from deep violet to orange. The product was precipitated with Et_2O (20 ml) as a yellow-orange crystalline solid, which was filtered off and dried *in vacuo* for 1 h. Yield 0.12 g (96%). Anal. calcd for $C_{39}H_{42}F_6N_2OP_2Ru$: C, 56.32; H, 5.09%. Found: C, 56.34; H, 4.95%. $^{31}P\{1H\}$ NMR (CD_2Cl_2): δ 61.7 (s, PPh_2), -144.5 (sept, $^1J_{PF}$ = 713, PF_6^-). ^1H NMR (CD_2Cl_2): δ 7.84 (t, $^3J_{HH}$ = 8.6, 1H, *p*-H_{Ph}), 7.81 (dd, $^3J_{HP}$ = 12.8, $^3J_{HH}$ = 8.0, 2H, *o*-H_{Ph}), 7.69 (dt, $^3J_{HH}$ = 7.2, $^4J_{HP}$ = 3.2, 2H, *m*-H_{Ph}), 7.48 (dt, $^3J_{HH}$ = 7.2, $^5J_{HP}$ = 1.6, 1H, *p'*-H_{Ph}), 7.24 (dt, $^3J_{HH}$ = 8.0, $^4J_{HP}$ = 3.2, 2H, *m'*-H_{Ph}), 7.19 (dd, $^3J_{HP}$ = 10.8, $^3J_{HH}$ = 8.0, 2H, *o'*-H_{Ph}), 6.90 (d, $^3J_{HH}$ = 8.0, 4H, C_6H_4), 6.46 (dd, $^3J_{HH}$ = 8.0, $^4J_{HP}$ = 2.0, 4H, C_6H_4), 2.21 (s, 6H, Me_{Tol}), 2.11 (s, 18H, C_6Me_6). $^{13}C\{^1H\}$ NMR (CD_2Cl_2): δ 199.2 (s, Ru-CO), 140.8 (d, $^2J_{CP}$ = 2.2, *i*-C_{Tol}(N)), 135.8 (d, $^1J_{CP}$ = 97.2, *i*-C_{Ph}), 134.9 (d, $^4J_{CP}$ = 2.6, *p*-C_{Ph}), 133.6 (d, $^4J_{CP}$ = 2.7, *p'*-C_{Ph}), 132.9 (d, $^2J_{CP}$ = 9.3, *o*-C_{Ph}), 132.7 (d, $^2J_{CP}$ = 11.0, *o'*-C_{Ph}), 132.8 (s, *p*-C_{Tol}(Me)), 130.4 (d, $^4J_{CP}$ = 1.3, *m*-CH_{Tol}), 130.0 (d, $^3J_{CP}$ = 12.1, *m*-C_{Ph}), 128.9 (d, $^3J_{CP}$ =

11.4, *m'*-C_{Ph}), 128.3 (d, $^{1}J_{CP}$ = 83.3, *i'*-C_{Ph}), 126.0 (d, $^{3}J_{CP}$ = 7.0, *o*-CH_{Tol}), 110.3 (s, C_6Me_6), 20.8 (s, Me_{Tol}), 17.1 (s, C_6Me_6). UV-vis (CH_2Cl_2; λ_{max}, nm; ε, M^{-1} cm^{-1}): 450 (100, shoulder). IR (CH_2Cl_2, ν, cm^{-1}): 1984 (RuCO).

(For **5c**) Analogously, from **4c** (0.10 g, 0.15 mmol) in CH_2Cl_2 (3 ml), complex **5c** was obtained as a stable yellow crystalline solid. Yield 0.10 g (95%). Anal. calcd for $C_{28}H_{34}F_6N_2O_2P_2Ru*H_2O$: C, 46.35; H, 5.00%. Found: C, 46.49; H, 5.00%. $^{31}P\{^{1}H\}$ NMR (CD_2Cl_2): δ 55.2 (s, PPh_2), -144.5 (csept, $^{1}J_{PF}$ = 713, PF_6^-). ^{1}H NMR (CD_2Cl_2): δ 7.83 (ttd, $^{3}J_{HH}$ = 7.8, $^{4}J_{HH}$ = 1.8, $^{5}J_{HP}$ = 1.2, 1H, *p*-H_{Ph}), 7.75 (ttd, $^{3}J_{HH}$ = 7.8, $^{4}J_{HH}$ = 1.2, $^{5}J_{HP}$ = 1.2, 1H, *p'*-H_{Ph}), 7.71 (dt, $^{3}J_{HH}$ = 7.8, $^{4}J_{HP}$ = 3.6, 2H, *m*-H_{Ph}), 7.63 (ddd, $^{3}J_{HP}$ = 12.6, $^{3}J_{HH}$ = 7.8, $^{4}J_{HH}$ = 1.2, 2H, *o*-H_{Ph}), 7.60 (dt, $^{3}J_{HH}$ = 7.8, $^{4}J_{HP}$ = 3.6, 2H, *m'*-H_{Ph}), 7.42 (ddd, $^{3}J_{HP}$ = 12.6, $^{3}J_{HH}$ = 7.8, $^{4}J_{HH}$ = 1.2, 2H, *o*-H_{Ph}), 2.73 (d, $^{3}J_{HP}$ = 8.4, 3H, NMe(CO)), 2.64 (d, $^{3}J_{HP}$ = 17.4, 3H, NMe), 2.24 (s, 18H, C_6Me_6). $^{13}C\{^{1}H\}$ NMR (CD_2Cl_2): δ 198.2 (s, Ru-CO), 192.8 (d, $^{2}J_{CP}$ = 19.6, NC=O), 135.1 (d, $^{4}J_{CP}$ = 2.4, *p*-C_{Ph}), 135.0 (d, $^{4}J_{CP}$ = 2.4, *p'*-C_{Ph}), 133.6 (d, $^{2}J_{CP}$ = 10.6, *o'*-C_{Ph}), 132.6 (d, $^{2}J_{CP}$ = 10.6, *o*-C_{Ph}), 130.3 (d, $^{3}J_{CP}$ = 12.8, *m*-C_{Ph}), 130.2 (d, $^{3}J_{CP}$ = 12.6, *m'*-C_{Ph}), 124.2 (d, $^{1}J_{CP}$ = 112.2, *i*-C_{Ph}), 122.2 (d, $^{1}J_{CP}$ = 98.6, *i'*-C_{Ph}), 113.4 (s, $\underline{C_6}Me_6$), 39.3 (d, $^{3}J_{CP}$ = 4.2, NMe), 29.3 (d, $^{3}J_{CP}$ = 8.4, NMe(CO)), 17.0 (s, $C_6\underline{Me_6}$). IR (CH_2Cl_2, ν, cm^{-1}): 1983 (RuCO), 1644 (RuC(O)N).

(For **5f**) Analogously, carbonylation of **4f** (0.11 g, 0.14 mmol) gave a red solution of **5f**. The product was precipitated by Et_2O (20 ml) saturated with CO, filtered and dried *in vacuo* for 30 min. Yield 0.09 g (82%). Anal. calcd for $C_{37}H_{38}F_6N_2OP_2Ru$: C, 55.29; H, 4.77%. Found: C, 55.05; H, 4.86%. $^{31}P\{^{1}H\}$ NMR($CDCl_3$): δ 60.2 (s, PPh_2), -144.2 (sept, $^{1}J_{PF}$ = 713, PF_6^-). ^{1}H NMR ($CDCl_3$): δ 7.93 (dd, $^{3}J_{HP}$ = 12.4, $^{3}J_{HP}$ = 7.2, 2H, *o*-H_{Ph}), 7.80 (t, $^{3}J_{HH}$ = 7.2, 1H, *p*-H_{Ph}), 7.73 (dt, $^{3}J_{HH}$ = 7.6, $^{4}J_{HP}$ = 2.8, 2H, *m*-H_{Ph}), 7.50 (t, $^{3}J_{HH}$ = 7.2, 1H, *p'*-H_{Ph}), 7.35 (dd, $^{3}J_{HP}$ = 10.2, $^{3}J_{HH}$ = 7.2, 2H, *o'*-H_{Ph}), 7.30 (dt, $^{3}J_{HH}$ = 7.6, $^{3}J_{HH}$ = 3.2, 2H, *m'*-H_{Ph}), 6.87 (d, $^{3}J_{HH}$ = 8.0, 4H, C_6H_4(Tol)), 6.51 (d, $^{3}J_{HH}$ = 8.0, 4H, C_6H_4(Tol)), 6.29 (br. s, 4H, C_6H_4(Cym)), 2.65 (sept, $^{3}J_{HH}$ = 6.8, 1H, C$\underline{H}Me_2$), 2.18 (s, 6H, Me_{Tol}), 2.11 (s, 3H, Me_{Cym}), 1.22 (d, $^{3}J_{HH}$ = 6.8, 6H, CH$\underline{Me_2}$). $^{13}C\{^{1}H\}$ NMR ($CDCl_3$): δ 193.8 (s, Ru-CO), 143.1 (d, $^{2}J_{CP}$ = 3.4, *i*-C_{Tol}(N)), 134.5 (d, $^{4}J_{CP}$ = 2.6, *p*-C_{Ph}), 133.7 (d, $^{4}J_{CP}$ = 2.4, *p'*-C_{Ph}), 132.7 (d, $^{2}J_{CP}$ = 10.3, *o*-C_{Ph}), 132.2 (d, $^{2}J_{CP}$ = 11.3, *o'*-C_{Ph}), 131.1 (d, $^{5}J_{CP}$ = 0.8, *p*-C_{Tol}-Me), 130.0 (s, *m*-CH_{Tol}), 129.9 (d, $^{3}J_{CP}$ = 12.3, *m*-C_{Ph}), 129.0 (d, $^{3}J_{CP}$ = 11.7, *m'*-C_{Ph}), 128.6 (d, $^{1}J_{CP}$ = 105.2, *i*-C_{Ph}), 126.8 (d, $^{1}J_{CP}$ = 80.6, *i'*-C_{Ph}), 123.4 (d, $^{3}J_{CP}$ = 8.6, *o*-CH_{Tol}), 121.2 (s, *i*-C_{Cym}), 119.5 (s, *i*-C_{Cym}), 97.8 (s, CH_{Cym}), 95.2 (s, CH_{Cym}), 32.1 (s, $\underline{C}HMe_2$), 22.7 (s,

CH<u>Me$_2$</u>), 20.6 (s, Me$_{Tol}$), 19.5 (s, Me$_{Cym}$). IR (CH_2Cl_2, ν, cm^{-1}): 2012 (RuCO). UV-vis (CH_2Cl_2; λ_{max}, nm; ε, M^{-1} cm^{-1}): 480 (140).

***In situ* generation of hydride complexes.**

General procedure. (For **6f**). The hydride complex **6f** was generated *in situ* in a NMR tube. To a solution of the chloride complex **3f** (0.013 g, 0.020 mmol) in C_6D_6 (0.5 mL) a NaHMDS solution (2.0 M in THF, 0.015 mL, 0.030 mmol) and isopropanol (0.06 mL, 0.80 mmol,) were added. The resulting suspension was vigorously shaken for 15 min at room temperature to complete the dissolution of **3f** yielding a yellow solution. According to the NMR spectra, the yield of complex **6f** is 95-98%. $^{31}P\{^1H\}$ NMR (C_6D_6): δ 33.2. ^1H NMR (C_6D_6): δ 8.16 (m, 2H, *o*-H$_{Ph}$), 7.61 (ddd, $^3J_{HP}$ = 11.0, $^3J_{HH}$ = 8.0, $^4J_{HH}$ = 1.6, 2H, *o'*-H$_{Ph}$), 7.25 (m, 3H, *(p+m)*-H$_{Ph}$), 6.82 (m, 3H, *(p+m)'*-H$_{Ph}$), 6.79 (d, $^3J_{HH}$ = 8.0, 4H, C_6H_4(Tol)), 6.73 (dd, $^3J_{HH}$ = 8.0, $^4J_{HP}$ = 1.2, 4H, C_6H_4(Tol)), 4.89 (d, $^3J_{HH}$ = 5.6, 2H, C_6H_4(Cym)), 4.82 (d, $^3J_{HH}$ = 5.6, 2H, C_6H_4(Cym)), 2.65 (sept, $^3J_{HH}$ = 6.8, 1H, C<u>H</u>Me$_2$), 2.08 (s, 3H, Me$_{cym}$), 2.08 (s, 6H, Me$_{Tol}$), 1.29 (d, $^3J_{HH}$ = 6.8, 6H, CH<u>Me$_2$</u>), -3.07 (s, Ru-H). $^{13}C\{^1H\}$ NMR (C_6D_6): δ 148.7 (d, $^2J_{CP}$ = 5.1, *i*-C$_{Tol}$), 135.9 (d, $^1J_{CP}$ = 92.4, *i*-C$_{Ph}$), 133.1 (d, $^2J_{CP}$ = 9.2, *o'*-C$_{Ph}$), 132.6 (d, $^2J_{CP}$ = 10.4, *o*-C$_{Ph}$), 131.8 (d, $^4J_{CP}$ = 2.7, *p*-C$_{Ph}$), 131.4 (d, $^4J_{CP}$ = 2.7, *p'*-C$_{Ph}$), 129.1 (s, *m*-C$_{Tol}$), 128.9 (d, $^3J_{CP}$ = 11.5, *m*-C$_{Ph}$), 126.5 (d, $^5J_{CP}$ = 1.1, *p*-C$_{Tol}$), 123.5 (d, $^3J_{CP}$ = 11.1, *o*-C$_{Tol}$), 106.5 (s, C$_{Cym}$), 99.7 (s, C$_{Cym}$), 80.3 (s, CH$_{Cym}$), 76.2 (s, CH$_{Cym}$), 32.7 (s, <u>C</u>HMe$_2$), 24.0 (s, CH<u>Me</u>), 20.6 (s, Me$_{Tol}$), 20.1 (s, Me$_{Cym}$). IR (C_6D_6, ν, cm^{-1}): 1880 (RuH).

(For **6a**). Analogously, from **3a** (0.014 g, 0.02 mmol), a NaHMDS solution (2.0 M in THF, 0.015 mL, 0.030 mmol) and isopropanol (0.06 mL, 0.80 mmol,) in C_6D_6 (0.5 ml), complex **6a** was generated *in situ*. According to the NMR spectra, the yield of complex **6a** is 94-97%. $^{31}P\{^1H\}$ NMR (C_6D_6): δ 31.9. ^1H NMR (C_6D_6): δ 8.25 (m, 2H, *o*-H$_{Ph}$), 7.43 (m, 2H, *o'*-H$_{Ph}$), 7.29 (m, 3H, (*m+p)*-H$_{Ph}$), 6.73 (m, 3H, (*m+p)'*-H$_{Ph}$), 6.82 (d, $^3J_{HH}$ = 8.8, 4H, C_6H_4(Tol)), 6.79 (d, $^3J_{HH}$ = 9.2, 4H, C_6H_4(Tol)), 2.07 (s, 6H, Me$_{Tol}$), 1.95 (s, 18H, C_6Me_6), -3.30 (RuH). $^{13}C\{^1H\}$ NMR (C_6D_6): δ 147.5 (d, $^2J_{CP}$ = 3.8, *i*-C$_{Tol}$(N)), 138.8 (d, $^1J_{CP}$ = 101.3, *i*-C$_{Ph}$), 133.2 (d, $^2J_{CP}$ = 8.6, *o'*-C$_{Ph}$), 132.7 (d, $^2J_{CP}$ = 10.6, *o*-C$_{Ph}$), 131.6 (d, $^4J_{CP}$ = 2.7, *p*-C$_{Ph}$), 131.1 (d, $^4J_{CP}$ = 2.6, *p'*-C$_{Ph}$), 130.5 (d, $^1J_{CP}$ = 77.3, *i*'-C$_{Ph}$), 128.8 (s, *m*-C$_{Tol}$), 128.6 (d, $^3J_{CP}$ = 11.7, *m*-C$_{Ph}$), 128.2 (d, *m'*-C$_{Ph}$), 127.0 (d, $^5J_{CP}$ = 2.3, *p*-C$_{Tol}$), 125.9 (d, $^3J_{CP}$ = 9.2, *o*-C$_{Tol}$), 90.1 (s, <u>C$_6$</u>Me$_6$), 20.7 (s, Me$_{Tol}$), 17.2 (s, C$_6$<u>Me$_6$</u>).

(For **6e**). Analogously, from **3e** (0.011 g, 0.014 mmol), a NaHMDS solution (2.0 M in THF, 0.014 mL, 0.008 mmol) and isopropanol (0.011 mL, 0.14 mmol,) in C_6D_6 (0.5 ml),

complex **6e** was generated *in situ*. According to the NMR spectra, the yield of complex **6e** is 91-93%. $^{31}P\{^{1}H\}$ NMR (C_6D_6): δ 38.4. ^{1}H NMR (C_6D_6): δ 8.09 (ddd, $^{3}J_{HP}$ = 12.0, $^{3}J_{HH}$ = 8.0, $^{4}J_{HH}$ = 1.6, 2H, *o*-H_{Ph}), 8.00 (d, $^{3}J_{HH}$ = 8.4, 4H, $C_6\underline{H_4}(CO_2Et)$), 7.48 (dd, $^{3}J_{HP}$ = 11.2, $^{3}J_{HH}$ = 7.6, 2H, *o'*-H_{Ph}), 7.24 (m, 3H, *(m+p)*-H_{Ph}), 6.82 (t, $^{3}J_{HH}$ = 6.8, 1H, *p'*-H_{Ph}), 6.74 (td, $^{3}J_{HH}$ = 7.4, $^{4}J_{HP}$ = 2.4, 2H, *m'*-H_{Ph}), 6.67 (d, $^{3}J_{HH}$ = 8.4, 4H, $C_6\underline{H_4}(CO_2Et)$), 4.81 (d, $^{3}J_{HH}$ = 5.6, 2H, C_6H_4(Cym)), 4.74 (d, $^{3}J_{HH}$ = 6.0, 2H, C_6H_4(Cym)), 4.13 (q, $^{3}J_{HH}$ = 6.6, 4H, $C\underline{H_2}CH_3$), 2.54 (sept, $^{3}J_{HH}$ = 6.8, 1H, $C\underline{H}Me_2$), 1.88 (s, 3H, Me_{cym}), 1.23 (d, $^{3}J_{HH}$ = 6.8, 6H, $CH\underline{Me}_2$), 1.01 (t, $^{3}J_{HH}$ = 6.6, 6H, $CH_2\underline{CH_3}$), -2.98 (s, 1H, RuH). $^{13}C\{^{1}H\}$ NMR (C_6D_6): δ 166.7 (s, $\underline{C}O_2Et$), 156.0 (d, $^{2}J_{CP}$ = 6.3, *i*-$C_N(CO_2Et)$), 132.8 (d, $^{2}J_{CP}$ = 10.0, *o*-C_{Ph}), 132.6 (d, $^{4}J_{CP}$ = 3.0, *p*-C_{Ph}), 132.5 (d, $^{1}J_{CP}$ = 94.6, *i*-C_{Ph}), 132.5 (d, $^{4}J_{CP}$ = 2.5, *p'*-C_{Ph}), 132.4 (d, $^{2}J_{CP}$ = 10.8, *o'*-C_{Ph}), 130.6 (s, *m*-$C_6H_4(CO_2Et)$), 129.3 (d, $^{3}J_{CP}$ = 11.9, *m*-C_{Ph}), 127.9 (d, $^{1}J_{CP}$ = 103.5, *i'*-C_{Ph}), 128.8 (d, $^{3}J_{CP}$ = 11.8, *m'*-C_{Ph}), 121.9 (d, $^{3}J_{CP}$ = 12.3, *o*-$C_6H_4(CO_2Et)$), 119.6 (s, *p*-$C_6H_4(CO_2Et)$), 107.2 (s, *i*-C_{Cym}), 101.1 (s, *i'*-C_{Cym}), 81.2 (s, CH_{Cym}), 76.1 (s, CH_{Cym}), 60.0 (s, $\underline{C}H_2CH_3$), 32.7 (s, $\underline{C}HMe_2$), 23.9 (s, $CH\underline{Me}_2$), 19.8 (s, Me_{Cym}), 14.5 (s, $CH_2\underline{CH_3}$).

(For **6d**). Analogously, from **3d** (0.012 g, 0.019 mmol), a NaHMDS solution (2.0 M in THF, 0.015 mL, 0.028 mmol) and isopropanol (0.015 mL, 0.19 mmol,) in C_6D_6 (0.5 ml), complex **6d** was generated *in situ*. According to the NMR spectra, the yield of complex **6d** is 60-63%. $^{31}P\{^{1}H\}$ NMR (C_6D_6): δ 41.33. ^{1}H NMR (C_6D_6): δ 7.98 (m, 2H, *o*-H_{Ph}), 7.59 (m, 2H, *o'*-H_{Ph}), 7.25 (br. s, 3H, *(m+p)*-H_{Ph}), 6.92 (br. s, 3H, *(m+p)'*-H_{Ph}), 6.83 (d, $^{3}J_{HH}$ = 8, 2H, *o*-C_6H_4(Tol)), 6.78 (d, $^{3}J_{HH}$ = 7.6, 2H, *m*-C_6H_4(Tol)), 2.52 (d, $^{3}J_{HP}$ = 20.4, 3H, Me(N)), 2.08 (s, 3H, Me_{Tol}), 2.03 (s, 18H, Me_{Cym}), -3.72 (s, 1H, RuH).

Transformation of 6f into a mixture of [(η^5-C_6H_5-1-Me-4-^{i}Pr)Ru{Ph_2P(N-*p*-Tol)$_2$}] (8f) and [(η^5-C_6H_5-1-^{i}Pr-4-Me)Ru{Ph_2P(N-*p*-Tol)$_2$}] (8f'). In a Schlenk tube containing a solution of NaHMDS (2.0 M in THF, 0.045 mL, 0.09 mmol) in isopropanol/toluene (2.5/2.5 mL), the chloride complex **3f** (0.050 g, 0.075 mmol) was added and the resulting suspension was stirred for 40 min at room temperature. The solvent was removed under reduced pressure, the solid residue was dried and then extracted with deuterated benzene (2 mL). The precipitate was filtered off and the filtrate was kept at 40°C for 1 day. According to the NMR spectra in C_6D_6, the product consists of a mixture of two regioisomers **8f** and **8f'** and residual complex **6f** in a ratio **8f**:**8f'**:**6f** = 55:15:30. $^{31}P\{^{1}H\}$ NMR (C_6D_6): δ 50.6 (**8f**), 51.1 (**8f'**). The assignment of the resonances to compounds **8f** and **8f'** was based on the detailed analysis of $^{31}P\{^{1}H\}$, ^{1}H, $^{13}C\{^{1}H\}$, ^{1}H-^{1}H COSY and ^{1}H-

^{13}C HSQC NMR spectra (see details in the Supporting Information, Figure S4-S8). In the ^{1}H NMR spectrum, the aromatic P-phenyl and N-tolyl resonances of the NPN ligands of compounds **8f** and **8f'** overlap and are observed at δ 7.80 (m, 4H, *o*-H), 6.97 (m, 6H, *(m+p)*-H), 7.09 (d, $^{3}J_{HH}$ = 7.8, 4H, *o'*-H), 6.85 (d, $^{3}J_{HH}$ = 7.8, 4H, *m'*-H). ^{1}H NMR for **8f** (C_6D_6): δ 6.03 (d, $^{3}J_{HH}$ = 4.8, 1H, H_b), 3.93 (d, $^{3}J_{HH}$ = 4.8, 1H, H_a), 2.92 (d, $^{3}J_{HH}$ = 6.0, 1H, H_j), 2.67 (dd, $^{2}J_{HH}$ = 13.2, $^{3}J_{HH}$ = 6.6, 1H, H_{en}), 2.05 (s, 6H, Me_h), 1.94 (sept, $^{3}J_{HH}$ = 6.6, 1H, CH_f), 1.38 (d, $^{3}J_{HH}$ = 6.6, 3H, Me_g), 1.36 (s, 3H, Me_e), 1.28 (d, $^{2}J_{HH}$ = 13.2, 1H, H_{ex}), 1.13 (d, $^{3}J_{HH}$ = 6.6, 3H, $Me_{g'}$). ^{1}H NMR for **8f'** (C_6D_6): δ 5.93 (d, $^{3}J_{HH}$ = 4.8, 1H, H_b), 3.88 (d, $^{3}J_{HH}$ = 4.8, 1H, H_a), 2.96 (d, $^{3}J_{HH}$ = 6.0, 1H, H_j), 2.72 (dd, $^{2}J_{HH}$ = 13.2, $^{3}J_{HH}$ = 6.6, 1H, H_{en}), 2.04 (s, 6H, Me_h), 1.78 (s, 3H, Me_e), 1.74 (m, 1H, CH_f), 1.71 (d, $^{3}J_{HH}$ = 6.6, 3H, $Me_{g'}$), 1.02 (d, $^{2}J_{HH}$ = 13.2, 1H, H_{ex}), 0.90 (d, $^{3}J_{HH}$ = 6.6, 3H, Me_g). ^{13}C{^{1}H} NMR for **8f** (C_6D_6): δ 147.2 (d, $^{2}J_{CP}$ = 5.3, *i'*-C), 132.4 (d, $^{2}J_{CP}$ = 9.6, *o*-C), 131.9 (d, $^{4}J_{CP}$ = 2.0, *p*-C), 131.8 (d, $^{1}J_{CP}$ = 86.4, *i*-C), 129.2 (s, *m'*-C), 128.5 (d, $^{3}J_{CP}$ = 11.0, *m*-C), 126.6 (s, *p'*-C), 125.0 (d, $^{3}J_{CP}$ = 9.8, *o'*-C), 92.4 (s, C_d), 76.4 (s, CH_a), 70.2 (s, CH_b), 38.4 (s, $CH_{2(k)}$), 37.5 (s, *i*-C_c), 32.7 (s, CH_f), 29.2 (s, CH_j), 25.3 (s, Me_e), 24.9 (s, $Me_{g'}$), 22.4 (s, Me_g), 20.8 (s, Me_h). ^{13}C{^{1}H} NMR for **8f'** (C_6D_6): δ 147.0 (d, $^{2}J_{CP}$ = 5.1, *i'*-C), 132.5 (d, $^{2}J_{CP}$ = 9.6, *o*-C), 131.9 (overlapped, *p*-C), 129.3 (s, *m'*-C), 128.4 (d, overlapped, *m*-C), 126.6 (s, overlapped, *p'*-C), 125.1 (d, $^{3}J_{CP}$ = 9.8, *o'*-C), 82.6 (s, C_d), 75.4 (s, CH_a), 73.1 (s, CH_b), 47.8 (s, C_c), 35.2 (s, CH_f), 30.8 (s, CH_j), 30.4 (s, $CH_{2(k)}$), 22.1 (s, $Me_{g'}$), 20.9 (s, Me_e), 20.3 (s, Me_g), 20.6 (s, overlapped, Me_h).

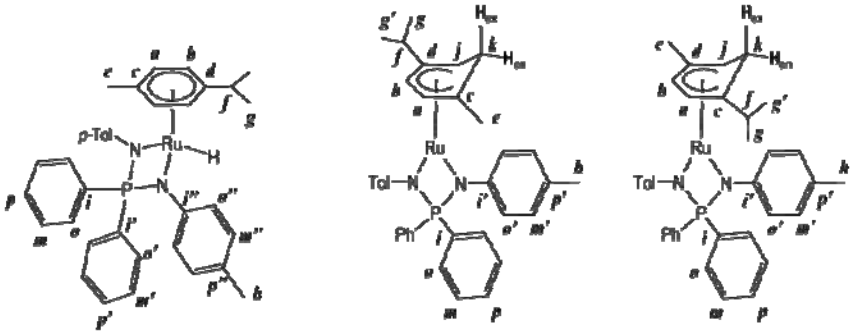

6f (30%) 8f (55%) 8f' (15%)

Alternative method for generation of 6f. To a Schlenk tube containing a suspension of **3f** (0.020 g, 0.030 mmol) in toluene (3 mL), $NaEt_3BH$ (1.0 M in toluene, 0.036 mL, 0.036 mmol) was added, and the resulting mixture was stirred for 1 h at room temperature. The precipitate was filtered off, the filtrate was evaporated to dryness under reduced pressure and the residue was dried *in vacuo*. According to ^{31}P{^{1}H} NMR (C_6D_6) the final product contains **6f**, **8f** and **8f'** in a 35:57:8 ratio.

Physico-chemical methods.

NMR-spectroscopy. The ^{1}H, $^{31}P\{^{1}H\}$ and $^{13}C\{^{1}H\}$ NMR spectra were obtained on Bruker AMX 300, Bruker AMX 400, Bruker AMX 600, Bruker Avance 600, Bruker Avance 400 and Bruker Avance 300 spectrometers and referenced to the residual signals of deuterated solvent (^{1}H and ^{13}C), and to 85% H_3PO_4 (^{31}P, external standard). If necessary, complementary 2D NMR COSY and HSQC experiments were carried out to establish the structure.

2D ^{1}H-^{1}H EXSY NMR spectra were collected on a Bruker Avance 600 spectrometer in a wide range of temperatures using the standard Bruker library noesygpph pulse program. At least three experiments with different values of the mixing time tm were performed to find an optimum mixing time, resulting in sufficiently large exchange cross-peaks without significant relaxation contribution. The calculation of the rate constants from the 2D EXSY ^{1}H NMR spectra was performed as described in the literature.[109] The rate constants $\boldsymbol{k} = \boldsymbol{k_{AB}} + \boldsymbol{k_{BA}}$ for the A ↔ B exchange reactions were calculated using simple two-site model using Equations (1), (2), where $\boldsymbol{k_{AB}}$ and $\boldsymbol{k_{BA}}$ are the rate constants of the direct and inverse reactions, $\boldsymbol{I_{AB}}$, $\boldsymbol{I_{BA}}$ and $\boldsymbol{I_{AA}}$, $\boldsymbol{I_{BB}}$ are the cross-peak and the diagonal peak integral intensities, respectively. In case of exchange between equally populated states ($\boldsymbol{k_{AB}} = \boldsymbol{k_{BA}}$), the exchange rate constant is $\boldsymbol{k_{ex}} = \boldsymbol{k}/2$.

$$\boldsymbol{k} = \frac{\boldsymbol{1}}{\boldsymbol{t_m}} \boldsymbol{\ln}\left(\frac{\boldsymbol{r+1}}{\boldsymbol{r-1}}\right) \qquad (1)$$

$$\boldsymbol{r} = \frac{\boldsymbol{I_{AA}+I_{BB}}}{\boldsymbol{I_{AB}+I_{BA}}} \qquad (2)$$

In the variable temperature NMR experiments, the rate constant of the exchange process ($\boldsymbol{k_{ex}}$) at the coalescence temperature ($\boldsymbol{T_c}$) of the exchanging signals was calculated using Equation (3), where Δν is the difference between the centers of the exchanging signals (in Hz) at a temperature other than $\boldsymbol{T_c}$.

$$\boldsymbol{kex} = \frac{\boldsymbol{\pi(\Delta\nu)}}{\sqrt{\boldsymbol{2}}} \qquad (3)$$

The temperature ranges used were: 298-193 K (CD_2Cl_2), 273-353 K (toluene-d_8) for **3b** and 298-338 K (C_6D_6) for **3c**, with temperature steps of 10 K. The temperature $\boldsymbol{T_c}$ was found as an average between two adjacent points, at which the separation of exchange signals occurred. Thus, the accuracy on the $\boldsymbol{T_c}$ values is ±5 K.

From the exchange rate constants ($\boldsymbol{k_{ex}}$) at $\boldsymbol{T_c}$ or $\boldsymbol{T_{EXSY}}$, the activation free energy $\Delta G^{\neq}$ was calculated from the Eyring equation (4) and the activation enthalpy $\Delta H^{\neq}$ and

entropy $\Delta S^{\neq}$ were derived by linear fitting of $R\ln(k_{ex}/T)$ plotted vs. 1/T according to the equation (5).

$$\Delta G^{\neq} = -RT\ln\frac{k_{ex}h}{k_bT} \quad (4)$$

$$R\ln\frac{k_{ex}}{T} = -\frac{\Delta H^{\neq}}{T} + \Delta S^{\neq} + R\ln\frac{k_b}{h} \quad (5)$$

UV-Vis spectroscopic study. The UV spectra were recorded on a Varian Cary 50 WinUV spectrometer. The UV-vis monitored titrations were performed in a 10 mm quartz cell, while the spectra at low temperatures were recorded in a 2.2 mm quartz cell. In most experiments the initial concentrations of ruthenium complex (c^0_{Ru}) were 2.5x10^{-3} M, while in other cases c^0_{Ru} was in the range 5–8x10^{-4} M. Neat MeCN and pyridine were used for the titrations. To calculate the dissociation constants K_d for **3b,c** (Eq. 6) and the constant K_c for the ligand coordination to **4a** (Eq. 7), the equilibrium concentrations of the 16ē ($c_{16ē}$) and 18ē ($c_{18ē}$) complexes were obtained from the UV-vis spectra according to the Beer-Lambert law. The absorption of the equilibrium mixture $D(\lambda_i)$ was measured at a wavelength λ_i (Eq. 8), at which the absorption coefficient $\varepsilon_{18ē}$ for 18ē complexes (**3** or **4a(L)**) is close to zero, while the $\varepsilon_{16ē}$ for 16ē species (**4a-c**) is still high enough. Particularly, at the chosen λ_i = 600 nm, $\varepsilon_{16ē}$ is in the range 550 – 650 M^{-1} cm^{-1}, whereas $\varepsilon_{18ē}$ is < 30 M^{-1} cm^{-1}. Therefore, the equilibrium concentration $c_{16ē}$ can be approximated as in Equation (9).

$$K_d = \frac{c_{Ru+}c_{Cl-}}{c_{RuCl}} \quad (6)$$

$$K_c = \frac{c_{RuL+}}{c_{Ru+}c_L} \quad (7)$$

$$D(\lambda_i) = \varepsilon_{16ē}(\lambda_i)c_{16ē}l + \varepsilon_{18ē}(\lambda_i)c_{18ē}l \quad (8)$$

$$c_{16ē} \sim \frac{D(\lambda_{600})}{\varepsilon_{16ē}(\lambda_{600})l} \quad (9)$$

In the titration of **4a** with L, the initial concentrations $c^0_{16ē}$ of **4a** for every *i*-titration point was corrected for the dilution factor ($c^0_{16ē}(i)$) according to Equation (10).

$$c^0_{16ē}(i) = c^0_{16ē}\frac{V^0_{16ē}}{V^0_{16ē}+V_L} \quad (10)$$

where $V^0_{16ē}$ and V_L are the initial volume of **4a** solution and the added volume of **L**, correspondingly.

The Gibbs free energies for each point were calculated by the formula $\Delta G = -RT\ln K_c$, and the enthalpy and entropy of complexation were found from the temperature dependence according to the Van't Hoff equation $-\Delta G/T = -\Delta H/T + \Delta S$.

X-ray crystallography. Single crystals of the complexes were obtained by slow diffusion of hexane to a solution of a complexes (**3b, 3c**) in benzene, or by slow diffusion of Et_2O to a solution of complexes (**3a, 3f, 4a-c, 4f, 5a, 5c, 5f)** in CH_2Cl_2. Single crystals of the compositionally disordered **8f/8f'** mixture were obtained by slow crystallization a freshly prepared mixture of **6f**, **8f** and **8f'** in neat ^{i}PrOH. The data collection, structure solution and refinement for compounds **3a**, **3b**, **3c**, **3f**, **4a-c**, **4f**, **5a**, **5c** and **5f** were carried out by Dr. Ivan V. Fedyanin of the INEOS RAS Moscow. The structure of the **8f**/**8f'** was solved by Dr. Jean-Claude Daran of the LCC Toulouse.

The asymmetric unit **8f** contains two independent Ru complexes with roughly similar geometry. The crystal was poorly diffracting and no significant intensities could be detected above 24° in theta. Moreover, the crystal is a mixture of two isomers as shown by NMR (see Discussion of the result).

Computational details. The geometry optimizations for **3a,f** and **4a,f** were carried out by Dr. Oleg A. Filippov at the INEOS RAS Moscow, with the PBE functional and def2-TZVP[110] basis set for all atoms without any symmetry restrictions in the gas phase using the Gaussian09 package.[111] The obtained stationary points were confirmed to have no imaginary frequencies. The orbital energies were computed with the SMD[112] solvent model using the gas phase optimized geometry.

The geometry optimizations for **6f**, **8f** were carried out by Dr. Eric Deydier and prof. Rinaldo Poli at the LCC Toulouse within DFT approach with M06L[113] and 97D[114] functionals in Gaussian 09.[111] All geometry optimizations were carried out using the LANL2DZ basis set and ECP for the Ru atom,[115] augmented with an f polarization function ($\alpha = 1.235$),[116] and the 6-311G(d,p)[117] basis sets for all other atoms. Calculations were corrected for dispersion interactions by Grimme's D3 method for M06L whereas the B97D functional already considers dispersion. The effect of the solvent was included by the SMD polarisable continuum[112] in isopropanol (ε = 19,264). All of the energies presented in the text are Gibbs energies in isopropanol (ΔG_{iPrOH}).

Catalytic studies. A series of experiments on the reduction of acetophenone (Acp) by isopropanol (^{i}PrOH) in a temperature range 25 ˚C – 80˚C catalyzed by the ruthenium hydride NPN complexes was carried out. The catalytic data are presented in Table 20. 24 – 27. Dodecane was used as an internal standard, aliquots (0.1 mL) were taken at the times specified, diluted with diethyl ether (0.8 mL) and filtered through a silica bed. The reaction

samples were analyzed by GC equipped with J&W GC Column with a DB-1MS stationary phase (program: 20 min at 50°C, with further heating rate 10˚C/min to 170˚C; retention times : τ_{Acp} = 24 min, τ_{AcpH2} = 25 min, $\tau_{dodecane}$ = 31 min). In a typical experiment the hydride complexes **6a-f** were generated *in situ* from the chloride NPN complexes **3a-f** (0.02 mmol), ^{i}PrOH (5 ml) or ^{i}PrOH/toluene (2.5/2.5 mL) by treatment with 2M solution of NaHMDS in THF (0.02 mmol, 10 μL, 1 equiv.). The mixture was preliminarily stirred at room temperature for 40 minutes, then it was warmed to the desired temperature followed by the addition of dodecane (1 mmol, 0.225 ml) and acetophenone (2 mmol, 0.233 ml), with catalyst/Acp ratios of 1/50, 1/100, 1/200 or 1/400, as specified. Additional control experiments were performed with ruthenium chloride complex $[(\eta^6\text{-}p\text{-cymene})RuCl_2]_2$ (**7**), with chloride NPN complex **3a-f**.

Catalytic tests for each sample were carried out 2-3 times to verify reproducibility. The catalytic activity is expressed in terms of *TOF* (turnover number per time unit). $TOF = (1/t)^*(N_{substrate}/N_{kt})$, where $N_{substrate}$ is the number of moles of substrate that a mole of catalyst can convert before becoming inactivated, N_{kt} is a mole of catalyst, t is reaction time, h^{-1}.

IV. Conclusions.

1. A series of new arene ruthenium 18ē and 16ē NPN complexes **3a-f**, **4a-c**, **f**, with different substituents at the nitrogen and phosphorus atoms, was obtained. All ruthenium complexes were completely characterized spectroscopically, their composition was confirmed by elemental analysis, and their structures were established by single-crystal X-ray diffraction.
2. It has been established that neutral ruthenium chloride 18ē NPN complexes can dissociate the chloride ligand with the formation of formally 16ē cationic complexes. This process proceeds more easily in more polar solvents and in the presence of more electron-donating substituents on the NPN ligand. The Ru-Cl bond dissociation enthalpies for compounds **3a-f** were determined.
3. The interaction of the 16ē NPN complex **4a** with the labile acetonitrile and pyridine ligands was studied by NMR and UV-vis spectroscopies. The more stable carbonyl adducts of the cationic **4a**,**c**,**f** complexes were isolated, spectroscopically characterized, and their structures were established by single-crystal X-ray diffraction. Complexes **4a**,**f** give monocarbonyl adducts **5a**,**f**, and complex **4c** with the stronger electron-donating N methyl substituents forms a carbonyl-carbamoyl adduct **5c'**. Thus, the physico-chemical properties of the ruthenium NPN complexes confirm the zwitterionic structure of the NPN ligand and its strong ($4\sigma/2\pi$) donor properties.
4. For the first time, it has been shown that ruthenium iminophosphonamide complexes **3a-f** are active catalysts for the transfer hydrogenation of ketones in the presence of a strong base. The catalytic activity increases with the introduction of the *p*-cymene arene ligand and more electron-donating N substituents.
5. Using the example of the ruthenium *p*-cymene complex **3f**, a series of model reactions was carried out to establish the key intermediates of ketone hydrogenation. It was found that, in the presence of a base, a previously unknown ruthenium hydride complex **6f** is formed in isopropanol. This hydride complex is able to form dihydrogen-bonded adducts with alcohols of various nature (isopropanol, TFE, HFIP), which can then be dehydrogenated to produce hydrogen and form cationic

16ē complexes of type **4**. Complex **6f** undergoes rearrangement with the formation of a mixture of isomeric η^5-cyclohexadienyl complexes **8f** and **8f'**, which are catalytically inactive, the structure of which was established by X-ray diffraction.

6. The kinetics of acetophenone reduction by complexes **3a-f** in the presence of a base has been studied in detail. For **3f**, it was shown that the rate law is first-order in substrate and catalyst. The measured activation parameters $\Delta H^{\neq}$ and $\Delta S^{\neq}$ indicate a highly organized transition state for the rate-limiting step of the catalytic cycle when using the N-aryl-substituted complexes **3a**, **3b**, **3e**, **3f** as precatalysts. Conversely, the $\Delta H^{\neq}$ and $\Delta S^{\neq}$ parameters for the reaction catalyzed by the N-methyl-substituted complexes **3c**, **3d**, in addition to the observed activity of the latter in the absence of a base, indicate the occurrence of an alternative mechanism.
7. On the basis of the experimental work done, as well as the DFT calculations for N-aryl-substituted complexes, a mechanism was proposed for the transfer hydrogenation of acetophenone in isopropanol catalyzed by the NPN complexes **3** in the presence of a base, in which the hydride complex **6** is catalytically active and the rate-determining step is the transfer reaction of the hydride atom from the ruthenium atom to the carbonyl carbon atom of the ketone with the formation of the zwitterionic intermediate **9**.

V. References.

1. Evans, D., Osborn, J.A., Jardine, F.H., Wilkinson, G. Homogeneous Hydrogenation and Hydroformylation using Ruthenium Complexes // *Nature* – **1965 –** 208 (5016), 1203-1204.
2. Halpern, J., Harrod, J.F., James, B.R. Homogeneous Catalysis of the Hydrogenation of Olefinic Compounds by Ruthenium(II) Chloride // *J. Am. Chem. Soc.* – **1966 –** 88 (22), 5150-5155.
3. Noyori, R., Takaya, R. BINAP: an efficient chiral element for asymmetric catalysis // *Acc. Chem. Res.* – **1990** – 23 (10), 345-350.
4. James, B.R. Synthesis of chiral amines catalyzed homogeneously by metal complexes // *Catal. Today* – **1997** – 37, 209-221.
5. Fache, F., Schulz, E., Tommasino, M.L., Lemaire, M. Nitrogen-containing ligands for asymmetric homogeneous and heterogeneous catalysis // *Chem. Rev.* – **2000** – 100 (6), 2159-2232.
6. Noyori, R. Asymmetric catalysis: science and opportunities // *Angew. Chem. Int. Ed. Engl.* – **2002** – 41 (12), 2008-2022.
7. Blaser, H.-U., Malan, C., Pugin, B., Spindler, F., Steiner, H., Studer, M. Selective Hydrogenation for Fine Chemicals: Recent Trends and New Developments // *Adv. Synth. Catal.* – **2003** – 345 (1-2), 103-151.
8. Noyori, R., Ohkuma, T. Asymmetric Catalysis by Architectural and Functional Molecular Engineering: Practical Chemo- and Stereoselective Hydrogenation of Ketones // *Angew. Chem. Int. Ed.* – **2001** – 40 (1), 40-73.
9. Meerwein, H., Schmidt, R. Ein neues Verfahren zur Reduktion von Aldehyden und Ketonen // *Justus Liebigs Ann. Chem.* – **1925** – 444 (1), 221-238.
10. Verley, A. Sur l'échange de groupements fonctionnels entre deux molécules. Passage de la fonction alcool à la fonction aldehyde et inversement // *Bull. Soc. Chim. Fr.* – **1925** – 37, 537-542.
11. Ponndorf, W. Der reversible Austausch der Oxydationsstufen zwischen Aldehyden oder Ketonen einerseits und primären oder sekundären Alkoholen anderseits // *Angew. Chem.* – **1926** – 39 (5), 138-143.

12. Oppenauer, R.V. Eine Methode der Dehydrierung von Sekundären Alkoholen zu Ketonen. I. Zur Herstellung von Sterinketonen und Sexualhormonen // *Recl. Trav. Chim. Pays-Bas Belg.* – **1937** – 56, 137-144.

13. de Graauw, C.F., Peters, J.A., van Bekkum, H., Huskens, J. Meerwein-Ponndorf-Verley Reductions and Oppenauer Oxidations: An Integrated Approach // *Synthesis* – **1994**, 10, 1007-1017.

14. Haddad, Y.M.Y., Henbest, H.B., Husbands, J., Mitchell, T.R.B. Reduction of Cyclohexanones to Axial Alcohols via Iridium Containing Catalysts // *Proc. Chem. Soc (London)* – **1964**, 361-365.

15. Trochagr, J., Henbest, H.B. Catalysis of the Transfer of Hydrogen from Propan-2-ol to α,β-Unsaturated Ketones by Organo-iridium Compounds. A Carbon-Iridium Compound Containing a Chelate Keto-group // *Chem. Commun.* – **1967** – 544-544.

16. Sasson, Y., Blum, J., Dunkelblum, E. $RuCl_2(PPh_3)_3$ – Catalyzed transfer hydrogenation of cyclohexane-1,3-diones // Tetrahedron Lett. – **1973** – 14 (34), 3199-3202.

17. Sasson, Y., Blum, J. Dichlorotris(triphenylphosphine)ruthenium-catalyzed hydrogen transfer from alcohols to saturated and .alpha.,.beta.-unsaturated ketones // J. *Org. Chem.* – **1975 –** 40 (13), 1887-1896.

18. Palmer, M.J., Wills, M. Asymmetric transfer hydrogenation of C=O and C=N bonds // *Tetrahedron: Asymmetry* – **1999** – 10 (11), 2045-2061.

19. Blum, Y., Czarkie, D., Rahamim, Y., Shvo, Y. (Cyclopentadienone)ruthenium carbonyl complexes – a new class of homogeneous hydrogenation catalysts // *Organometallics* – **1985** – 4 (8), 1459-1461.

20. Samec, J.S.M., Bäckvall, J.-E. Ruthenium-Catalyzed Transfer Hydrogenation of Imines by Propan-2-ol in Benzene // *Chem. Eur. J* – **2002** – 8 (13), 2955-2961.

21. Samec, J.S.M., Mony, L, Bäckvall, J.-E. Efficient ruthenium catalyzed transfer hydrogenation of functionalized imines by isopropanol under controlled microwave heating // *Can. J. Chem.* – **2005** – 83, 909-916.

22. Menashe, N., Salant, E., Shvo, Y. Efficient catalytic reduction of ketones with formic acid and ruthenium complexes // *J. Organomet. Chem.* – **1996** – 514 (1-2) 97-102.

23. Samec, J.S M., Bäckvall, J.-E., Andersson, P.G., Brandt, P. Mechanistic aspects of transition metal-catalyzed hydrogen transfer reactions // *Chem. Soc. Rev.* – **2006 –** 35, 237-248.

24. Danopoulos, A.A., Winston, S., Motherwell, W.B. Stable N-functionalised 'pincer' bis carbene ligands and their ruthenium complexes; synthesis and catalytic studies // *Chem. Commun.* – **2002**, 1376-1377.

25. Poyatos, M., Mata, J.A., Falomir, E., Crabtree, R.H., Peris, E. New Ruthenium(II) CNC-Pincer Bis(carbene) Complexes: Synthesis and Catalytic Activity // *Organometallics* – **2003** – 22 (5), 1110-1114.

26. Zeng, F., Yu, Z. Ruthenium(II) Complexes Bearing a Pyridyl-Supported Pyrazolyl−N-Heterocyclic Carbene (NNC) Ligand and Their Catalytic Activity in the Transfer Hydrogenation of Ketones // *Organometallics* – **2008 –** 27 (22), 6025- 6028.

27. Poyatos, M., Maisse-François, A., Bellemin-Laponnaz, S., Peris, E., Gade, L.H. Synthesis and structural chemistry of arene-ruthenium half-sandwich complexes bearing an oxazolinyl–carbene ligand // *J. Organomet. Chem.* – **2006** – 691 (12), 2713-2720.

28. Baratta, W., Da Ros, P., Del Zotto, A., Zangrando, E., Rigo, P. Cyclometalated Ruthenium (II) Complexes as Highly Active Transfer Hydrogenation Catalysts // *Angew. Chem. Int. Ed.* – **2004** – 43 (27), 3584-3588.

29. Baratta, W., Schütz, J., Herdtweck, E., Herrmann, W.A, Rigo, P. Fast transfer hydrogenation using a highly active orthometalated heterocyclic carbene ruthenium catalyst // *J. Organomet. Chem.* – **2005** – 690 (24-25), 5570-5575.

30. Baratta, W., Chelucci, G., Magnolia, S., Siega, K., Rigo, P. Highly Productive CNN Pincer Ruthenium Catalysts for the Asymmetric Reduction of Alkyl Aryl Ketones // *Chem. Eur. J.* – **2009** – 15 (3), 726-732.

31. Fujii, A., Hashiguchi, S., Uematsu, N., Ikariya, T., Noyori, R. Ruthenium(II)-Catalyzed Asymmetric Transfer Hydrogenation of Ketones Using a Formic Acid−Triethylamine Mixture // *J. Am. Chem. Soc* – **1996** – 118 (10), 2521-2522.

32. Hashiguchi, S., Fujii, A., Takehara, J., Ikariya, T., Noyori, R. Asymmetric Transfer Hydrogenation of Aromatic Ketones Catalyzed by Chiral Ruthenium (II) Complexes // *J. Am. Chem. Soc* – **1995** – 117 (28), 7562-7563.

33. Noyori, R., Hashiguchi, S. Asymmetric Transfer Hydrogenation Catalyzed by Chiral Ruthenium Complexes // *Acc. Chem. Res*. – **1997** – 30 (2), 97-102.

34. Uematsu, N., Fujii, A., Hashiguchi, S., Ikariya, T., Noyori, R. Asymmetric Transfer Hydrogenation of Imines // *J. Am. Chem. Soc.* – **1996** – 118 (20), 4916-4917.

35. Haack, K.-J., Hashiguchi, S., Fujii, A., Ikariya, T., Noyori, R. The Catalyst Precursor, Catalyst, and Intermediate in the Ru(II)-Promoted Asymmetric Hydrogen Transfer between Alcohols and Ketones // *Angew. Chem. Int. Ed. Engl.* – **1997** – 36 (3), 285-288.

36. Murata, K., Okano, K., Miyagi, M., Iwane, H., Noyori, R., Ikariya, T. A Practical Stereoselective Synthesis of Chiral Hydrobenzoins via Asymmetric Transfer Hydrogenation of Benzils // *Org. Lett*. – **1999** – 1 (7), 1119-1121.

37. Watanabe, M., Murata, K., Ikariya, T. Practical Synthesis of Optically Active Amino Alcohols via Asymmetric Transfer Hydrogenation of Functionalized Aromatic Ketones // *J. Org. Chem.* – **2002** – 67 (5), 1712-1715.

38. Canivet, J., Labat, G., Stoeckli-Evans, H., Süss-Fink, G. Water-Soluble Arene Ruthenium Complexes Containing a *trans*-1,2-Diaminocyclohexane Ligand as Enantioselective Transfer Hydrogenation Catalysts in Aqueous Solution // *Eur. J. Inorg. Chem.* – **2005** – 2005 (22) 4493-4500.

39. Canivet, J., Süss -Fink, G. Water-soluble arene ruthenium catalysts containing sulfonated diamine ligands for asymmetric transfer hydrogenation of α-aryl ketones and imines in aqueous solution // *Green Chem.* – **2007 –** 9, 391-397.

40. Hannedouche, J., Clarkson, G.J., Wills, M. A New Class of "Tethered" Ruthenium (II) Catalyst for Asymmetric Transfer Hydrogenation Reactions // *J. Am. Chem. Soc.* – **2004 –** 126 (4), 986-987.

41. Hayes, A.M., Morris, D.J., Clarkson, G.J., Wills, M. A Class of Ruthenium (II) Catalyst for Asymmetric Transfer Hydrogenations of Ketones // *J. Am. Chem. Soc.* – **2005** – 127 (20), 7318-7319.

42. Cheung, F.K., Lin, C., Minissi, F., Lorente Crivillé, A., Graham, M.A., Fox, D.J., Wills, M. An Investigation into the Tether Length and Substitution Pattern of Arene-Substituted Complexes for Asymmetric Transfer Hydrogenation of Ketones // *Org. Lett*. – **2007** – 9 (22), 4659-4662.

43. Morris, D.J., Hayes, A.M., Wills, M. The "Reverse-Tethered" Ruthenium (II) Catalyst for Asymmetric Transfer Hydrogenation: Further Applications // *J. Org. Chem.* – **2006 –** 71 (18), 7035-7044.

44. Martins, J.E.D., Morris, D.J., Tripathi, B., Wills, M. Further ‘tethered’ Ru (II) catalysts for asymmetric transfer hydrogenation (ATH) of ketones; the use of a benzylic linker and a cyclohexyldiamine ligand // *J. Organomet. Chem.* – **2008** – 693 (23), 3527-3532.

45. Cheung, F.K., Hayes, A.M., Hannedouche, J., Yim, A.S.Y., Wills, M. “Tethered” Ru (II) Catalysts for Asymmetric Transfer Hydrogenation of Ketones // *J. Org. Chem.* – **2005 –** 70 (8), 3188-3197.

46. Nedden, H.G., Zanotti-Gerosa, A., Wills, M. The Development of Phosphine-Free Tethered Ruthenium (II) Catalysts for the Asymmetric Reduction of Ketones and Imines // *Chem. Rec.* – **2016** – , 16, 2623-2643.

47. Soni, R., Hall, T.H, Mitchell, B.P., Owen, M.R., Wills, M. Asymmetric Reduction of Electron-Rich Ketones with Tethered Ru(II)/TsDPEN Catalysts Using Formic Acid/Triethylamine or Aqueous Sodium Formate // *J. Org. Chem.* – **2015** – 80 (13), 6784-6793

48. Wakeham, R.J., Morris, J.A., Williams, J.M.J. Alternative Hydrogen Source for Asymmetric Transfer Hydrogenation in the Reduction of Ketones // *ChemCatChem* – **2015** – 7 (24), 4039–4041.

49. Takehara, J., Hashiguchi, S., Fujii, A., Shin-ichi, I., Ikariya, T., Noyori, R. Amino alcohol effects on the ruthenium(II)-catalysed asymmetric transfer hydrogenation of ketones in propan-2-ol // *Chem. Commun.* – **1996** – 233-234.

50. Newkome, G.R. Pyridylphosphines // *Chem. Rev.* – **1993** – 93 (6), 2067-2089.

51. Thoumazet, C., Melaimi, M., Ricard, L., Mathey, F., Le Floch, P. A Cationic 1-(2-Methylpyridine)Phosphole Cymene Ruthenium Chloride Complex as an Efficient Catalyst in the Transfer Hydrogenation of Ketones // *Organometallics* – **2003** – 22 (8), 1580-1581.

52. Lundgren, R.L., Rankin, M.A., McDonakd, R., Schatte, G., Stradiotto, M. A Formally Zwitterionic Ruthenium Catalyst Precursor for the Transfer Hydrogenation of Ketones that Does Not Feature an Ancillary Ligand N-H Functionality // *Angew. Chem. Int. Ed.* – **2007** – 46 (25), 4732-4735.

53. Pàmies, O., Bäckvall, J.-E. Studies on the Mechanism of Metal-Catalyzed Hydrogen Transfer from Alcohols to Ketones // *Chem. Eur. J.* – **2001** – 7 (23), 5052-5058.

54. Laxmi, Y.R.S., Bäckvall, J.-E. Mechanistic studies on ruthenium-catalyzed hydrogen transfer reactions // *Chem. Commun.* – **2000** – 611-612.

55. Yamakawa, M., Ito, H., Noyori, R. The Metal−Ligand Bifunctional Catalysis: A Theoretical Study on the Ruthenium(II)-Catalyzed Hydrogen Transfer between Alcohols and Carbonyl Compounds // *J. Am. Chem. Soc.* – **2000** – 122 (7) 1466-1478.

56. Mizushima, E., Yamaguchi, M., Yamagishi, T. Effective transfer hydrogenation of unsaturated compounds by ruthenium dihydride complex in propan-2-ol // *J. Mol. Catal. A: Chem.* – **1999** – 148 (1-2), 69-75.

57. Mizushima, E., Yamaguchi, M., Yamagishi, T. Effective Catalysts for Transfer Hydrogenation of Ketones and Imines by Propan-2-ol: Ruthenium-Hydride or Ruthenium-Dihydride Complexes // *Chem. Lett.* – **1997** – 26 (3), 237-238.

58. Bryndza, H.E., Fong, L.K., Paciello, R.A., Tam, W., Bercaw, J.E. Relative metal-hydrogen, -oxygen, -nitrogen, and -carbon bond strengths for organoruthenium and organoplatinum compounds; equilibrium studies of $Cp^*(PMe_3)_2RuX$ and (DPPE)MePtX systems // *J. Am. Chem. Soc.* – **1987** – 109 (5), 1444-1456.

59. Alonso, D.A., Brandt, P., Nordin, S.J.M., Andersson, P.G. Ru(arene)(amino alcohol)-Catalyzed Transfer Hydrogenation of Ketones: Mechanism and Origin of Enantioselectivity // *J. Am. Chem. Soc.* – **1999** – 121 (41), 9580-9588.

60. Petra, D.G.I., Reek, J.N.H., Handgraaf, J.-W., Meijer, E.J., Dierkes, P., Kamer, P.C.J., Brusse, J., Schoemaker, H.E., van Leeuwen, P.W.N.M. Chiral Induction Effects in Ruthenium (II) Amino Alcohol Catalysed Asymmetric Transfer Hydrogenation of Ketones: An Experimental and Theoretical Approach // *Chem. Eur. J.* – **2000** – 6 (15), 2818-2829.

61. Gusev, O.V., Peganova, T.A., Gonchar, A.V., Petrovskii, P.V., Lyssenko, K.A., Ustynyuk, N.A. Synthesis of Diaminophosphonium Salts $[Ph_2(ArNH)_2P]^+Br^-$ (Ar = *o*-MeC_6H_4, *p*-MeC_6H_4, *p*-Pr^i C_6H_4, *p*-$EtO_2CC_6H_4$, *p*-$MeOC_6H_4$) // *Phosphorus Sulfur and Silicon and the Related Elements* – **2009 –** 184 (2), 322-331.

62. Sinopalnikova, I.S., Peganova, T.A., Novikov, V.V., Fedyanin, I.V., Filippov, O.A., Belkova, N.V., Shubina, E.S., Poli, R., Kalsin, A.M. Coordinatively labile 18-electron arene ruthenium iminophosphonamide complexes // *Chem. Eur. J.* – 2017 – 23 (61), 15424-15435.

63. Валяева, А.В. *Синтез аминоиминофосфоранатных комплексов переходных металлов, изучение их строения и каталитических свойств* // дис. канд. хим. наук, 02.00.08, ИНЭОС РАН, Москва, **2009.**

64. Scherer, O.J., Klusmann, P. Elementorganische Amin/Imin-Verbindungen. VIII. Synthese metallorganischer Diaminophosphine und deren Überführung in Aminohalogenphosphinimine // *Z. Anorg. Allg. Chem.* – **1969 –** 370 (3-4), 171-184.

65. Prashanth, B., Singh, S. Bulky iminophosphonamines for N–P–N coordination: Synthesis and structural characterization of lithium iminophosphonamides and homoleptic *bis*-chelates of Co(II), Ni(II) and Cu(II) // *J. Chem. Sci.,* – **2015** – 127 (2), 315-325.

66. Peganova, T.A., Valyaeva, A.V., Kalsin, A.M., Petrovskii, P.V., Borissova, A O., Lyssenko, K.A., Ustynyuk, N.A. Synthesis of Aminoiminophosphoranate Complexes of Palladium and Platinum and X-ray Diffractional Investigation of the Weak C−H···Pd Interactions Affecting the Geometry of the PdNPN Metallacycles // *Organometallics* – **2009 –** 28 (10), 3021–3028.

67. Düppmann, M., Kuchen, W., Peters, W. Preparation and NMR-data of some new phosphonium bromides $[R_2P(NHR')_2]Br$ and of iminophosphinic acid amides $R_2P(NR')(NHR')$ // *Phosphorus, Sulfur Silicon Relat. Elem.* – **1997** – 129, 53-58.

68. Bondi, A. Van der Waals Volumes and Radii // *J. Phys. Chem.* – **1964** – 68 (3), 441-451.

69. Rowland, R.S., Taylor, R. Intermolecular Nonbonded Contact Distances in Organic Crystal Structures: Comparison with Distances Expected from van der Waals Radii //*J. Phys. Chem.* – **1996 –** 100 (18), 7384-7391.

70. Phillips, A.D., Laurenczy, G., Scopelliti, R., Dyson, P.J. Facile, Thermoreversible Cycloaddition of Small Molecules to a Ruthenium(II) Arene β-Diketiminate // *Organometallics* – **2007** – 26 (5), 1120-1122.

71. Peganova, T.A., Filippov, O.A., Belkova, N.V., Fedyanin, I.V., Kalsin, A.M. The Origin of the MNXN Metallacycle Flexibility in the Chelate Iminophosphonamide and Amidinate Transition Metal Complexes // *Eur. J. Inorg Chem.* – **2018** – 2018 (47), 5098-5107.

72. Singh, T., Kishan, R., Nethaji, M., Thirupathi, N. Synthesis, Reactivity Studies, Structural Aspects, and Solution Behavior of Half Sandwich Ruthenium(II) *N,N′,N″*-Triarylguanidinate Complexes // *Inorg. Chem.* – **2012** – 51 (1), 157-169.

73. Hayashida, T., Nagashima, H. Access to Novel Ruthenium−Amidinate Complexes, $(\eta^6\text{-arene})Ru(\eta^2\text{-amidinate})X$ and $[Ru(\eta^2\text{-amidinate})(MeCN)_4]^+PF_6^-$ by Photochemical

Displacement of the Benzene Ligand in (η^6-C_6H_6)Ru(η^2-amidinate)X // *Organometallics* – **2002** – 21 (19), 3884-3888.

74. Bailey, P.J., Mitchell, L.A., Parsons, S. Guanidine anions as chelating ligands; syntheses and crystal structures of [Rh(η-C_5Me_5){η^2-$(NPh)_2CNHPh$}Cl] and [Ru(η-$MeC_6H_4Pr^i$-*p*)-{η^2-$(NPh)_2CNHPh$}Cl] // *J. Chem. Soc., Dalton Trans.* – **1996 –** (13), 2839-2841.

75. Seidel, W.W., Dachtler, W., Pape, T. Synthesis, Structure, and Reactivity of Ru^{II} Complexes with Trimethylsilylethinylamidinate Ligands // *Z. Anorg. Allg. Chem.* – **2012 –** 638 (1), 116-121.

76. Munslow, I.J., Wade, A.R., Deeth, R.J., Scott, P. Aminooxazolinate; a chiral amidinate analogue // *Chem. Commun.* – **2004** – (22), 2596-2597.

77. Barboza da Silva, C.F., Schwarz, S., Galceran Mestres, M., Teijelo López, S., Strähle, J. Synthese und Struktur von Ruthenium(II)-Komplexen mit Triazenido- und Pentaazadienido-Liganden // *Z. Anorg. Allg. Chem.* – **2004** – 630 (12), 1919-1923.

78. Phillips, A.D., Zava, O., Scopelitti, R., Nazarov, A.A., Dyson, P.J. Rational Design of Highly Cytotoxic η^6-Arene β-Diketiminato−Ruthenium Complexes // *Organometallics* – **2010** – 29 (2), 417-427.

79. Phillips, A.D., Thommes, K., Scopelliti, R., Gandolfi, C., Albrecht, M., Severin, K., Schreiber, D.F., Dyson, P.J. Modulating the Steric, Electronic, and Catalytic Properties of Cp* Ruthenium Half-Sandwich Complexes with β-Diketiminato Ligands // *Organometallics* – **2011** – 30 (22), 6119-6132.

80. Glöge, T., Petrovic, D., Hrib, C., Jones, P.G., Tamm, M. 16-Electron (Arene)ruthenium Complexes with Superbasic Bis(imidazolin-2-imine) Ligands and Their Use in Catalytic Transfer Hydrogenation // *Eur. J. Inorg. Chem.* – **2009** – 2009 (29-30), 4538-4546.

81. Hayashida, T., Kondo, H., Terasawa, J.I., Kirchner, K., Sunada, Y., Nagashima, H. Trifluoromethanesulfonate (triflate) as a moderately coordinating anion: Studies from chemistry of the cationic coordinatively unsaturated mono- and diruthenium amidinates // *J. Organomet. Chem.* – **2007 –** 692 (1-3), 382-394.

82. Bailey, P.J., Grant, K.J., Parsons, S. The Anion of a Phenyltris(alkylamino)phosphonium (PhTAP) Salt as a Chelating Ligand: Synthesis and

X-ray Crystal Structure of a 16-Electron Ruthenium(II) Organometallic Complex // *Organometallics* – **1998** – 17 (4), 551-555.

83. Hayashida, T., Yamaguchi, Y., Kirchner, K., Nagashima, H. Isolable Yet Highly Reactive Cationic Organoruthenium(II) Amidinates, $[Ru(\eta^6\text{-}C_6R_6)(\eta\text{-amidinate})]^+X^-$, Showing Signs of Coordinative Unsaturation: Isoelectronic Complexes of $Ru(\eta^5\text{-}C_5Me_5)(\eta\text{-amidinate})$ // *Chem. Lett*. – **2001 –** 30 (10), 954-955.

84. Kondo, H., Sue, T., Kageyama, A., Yamaguchi, Y., Sunada, Y., Nagashima, H. Two coordination modes of TCNE in the ruthenium amidinates: The first example providing experimental evidence for κ^1-N to η^2-C rearrangement // *J. Organomet. Chem.* – **2009** – 694 (5), 795-800.

85. Mashima, K., Kaneyoshi, H., Kaneko, S., Mikami, A., Tani, K., Nakamura, A. Chemistry of Coordinatively Unsaturated Bis(thiolato)ruthenium(II) Complexes (η^6-arene)$Ru(SAr)_2$ [SAr = 2,6-Dimethylbenzenethiolate, 2,4,6-Triisopropylbenzenethiolate; $(SAr)_2$ = 1,2-Benzenedithiolate; Arene = Benzene, *p*-Cymene, Hexamethylbenzene] // *Organometallics* – **1997** – 16 (5), 1016-1025.

86. Bain, A.D. Chemical exchange in NMR // *Progress in Nuclear Magnetic Resonance Spectroscopy* – 2003 – 43 (3–4), 63-103.

87. Yamaguchi, Y., Nagashima, H. (η^5-C_5Me_5)Ru(amidinate): Highly Reactive Ruthenium Complexes Formally Bearing 16 Valence Electrons Showing Signs of Coordinative Unsaturation // *Organometallics* – **2000 –** 19 (5), 725-727.

88. Gemel, C., Huffman, J.C., Caulton, K.G., Mauthner, K., Kirchner, K. Solution and solid–gas reactivity of unsaturated $[RuCp(tmeda)]^+$ (tmeda=$Me_2NC_2H_4NMe_2$) // *J. Organomet. Chem.* – **2000** – 593–594, 342-353.

89. Zamorano, A., Rendón, N., Valpuesta, J.E.V., Álvarez, E., Carmona, E. Synthesis and Reactivity toward H_2 of (η^5-C_5Me_5)Rh(III) Complexes with Bulky Aminopyridinate Ligands // *Inorg. Chem.* – **2015 –** 54 (13), 6573-6581.

90. Adams, C.J., Baber, R.A., Connelly, N.G., Harding, P., Hayward, O.D., Kandiah, M., Orpen, A.G. Iodination of triazenide-bridged rhodium and iridium complexes: oxidative addition vs. one-electron oxidation // *Dalton Trans.* – **2007 –** 1325-1333.

91. Jones, C., Schulten, C., Rose, R.P., Stasch, A., Aldridge, S., Woodul, W.D., Murray, K.S., Moubaraki, B., Brynda, M., La Macchia, G., Gagliardi, L. Amidinato- and

Guanidinato-Cobalt(I) Complexes: Characterization of Exceptionally Short Co-Co Interactions // *Angew. Chem. Int. Ed.* – **2009** – 48 (40), 7406-7410.

92. Sciarone, T.J.J., Nijhuis, C.A., Meetsma, A., Hessen, B. Neutral and Cationic Paramagnetic Amino-amidinate Iron(II) Complexes: ^{19}F NMR Evidence for Interactions with Weakly Coordinating Anions // *Organometallics* – **2008** – 27 (9), 2058-2065.

93. Jellema, E., Sciarone, T.J.J., Navarrete, N.M., Hettinga, M.J., Meetsma, A., Hessen, B. Reactivity of Paramagnetic Fe^{II}–Bis(amidinate) Complexes // *Eur. J. Inorg. Chem.* – **2011 –** 2011 (1), 91-100.

94. Öztopcu, Ö., Stöger, B., Mereiter, K., Kirchner, K. Reactivity of iron complexes containing monodentate aminophosphine ligands – Formation of four-membered carboxamido-phospha-metallacycles // *J. Organomet. Chem.* – **2013 –** 735, 80-87.

95. Hayashida, T., Nagashima, H. Ruthenium Amidinato−Carbene Complexes Containing a Ru−Si Bond: Formation and Reversible α-Silyl Group Migration from the Metal to the Carbene Ligand // *Organometallics* – **2001 –** 20 (24), 4996-4998.

96. Clapham, S.E., Hadzovic, A., Morris, R.H. Mechanisms of the H_2-hydrogenation and transfer hydrogenation of polar bonds catalyzed by ruthenium hydride complexes // *Coord. Chem. Rev.* – **2004** – 248 (21-24), 2201-2237.

97. Sinopalnikova, I.S., Peganova, T.A., Belkova, N.V., Deydier, E., Daran, J.C., Shubina, E.S., Kalsin, A.M., Poli, R. Ruthenium *p*-cymene iminophosphonamide complexes: activation under basic conditions and transfer hydrogenation catalysis // *Eur. J. Inorg. Chem.* – **2017 –** 2018 *(20-21),* 2285-2299.

98. Epstein, L.M., Belkova, N.V., Shubina, E.S. Dihydrogen Bonded Complexes and Proton Transfer to Hydride Ligands by Spectral (IR, NMR) Studies // Recent Advances in Hydride Chemistry / Peruzzini, M., Poli, R. – Amsterdam: Elsevier, **2001** – 391-418.

99. Belkova, N.V., Epstein, L.M., Shubina, E.S. Dihydrogen Bonding, Proton Transfer and Beyond: What We Can Learn from Kinetics and Thermodynamics // *Eur. J. Inorg. Chem.* – **2010 –** 2010 (23), 3555-3565.

100. Belkova, N.V., Epstein, L.M., Filippov, O.A., Shubina, E.S. Hydrogen and Dihydrogen Bonds in the Reactions of Metal Hydrides // *Chem. Rev.* – **2016 –** 116 (15), 8545-8587.

101. Belkova, N.V., Filippov, O.A., Shubina, E.S Z−H Bond Activation in (Di)hydrogen Bonding as a Way to Proton/Hydride Transfer and H_2 Evolution // *Chem. Eur. J.* – **2018 –** 24 (7),1464-1470.

102. Arthur, T., Robertson, D.R., Tocher, D.A., Stephenson, T.A. Synthesis of binuclear hydroxo- and alkoxo-bridged arene complexes of ruthenium(II) and osmium(II) // *J. Organomet. Chem.* – **1981 –** 208 (3), 389-400.

103. Hayes, J.M., Deydier, E., Ujaque, G., Lledós, A., Malacea-Kabbara, R., Manoury, E., Vincendeau, S., Poli, R. Ketone Hydrogenation with Iridium Complexes with "non N–H" Ligands: The Key Role of the Strong Base // *ACS Catal.* – **2015 –** 5 (7), 4368–4376.

104. Dub, P.A., Henson, N.J., Martin, R.J., Gordon, J.C. Unravelling the Mechanism of the Asymmetric Hydrogenation of Acetophenone by [RuX_2(diphosphine)(1,2-diamine)] Catalysts // *J. Am. Chem. Soc.* – **2014** – 136 (9), 3505-3521.

105. Bennett, M.A., Huang, T.-N., Matheson, T.W., Smith, A.K. 16. (η^6-Hexamethylbenzene)Ruthenium Complexes // *Inorg. Synth.* – **1982 –** 21, 74-78.

106. Jensen, S.B., Rodger, S.J., Spicer, M.D. Facile preparation of η^6-*p*-cymene ruthenium diphosphine complexes. Crystal structure of [(η^6-*p*-cymene)Ru(dppf)Cl]PF_6 // *J. Organomet. Chem.* – **1998 –** 556 (1-2), 151-158.

107. Johnson, B.F.G., Lewis, J., Ryder, I.E. Some reactions of co-ordinated cycloheptatriene and cyclo-octa-1,5-diene in ruthenium (d^6) complexes // *J. Chem. Soc. Dalton Trans.* – **1977 –** 719-724.

108. Issleib, K., Seidel, W. Darstellung und chemisches Verhalten aliphatischer und cycloaliphatischer Diphosphine, R_2P-PR_2 // *Chem. Ber.* – **1959 –** 92 (11), 2681-2694.

109. Perrin, C.L., Dwyer, T.J. Application of two-dimensional NMR to kinetics of chemical exchange // *Chem. Rev*. – **1990 –** 90 (6), 935-967.

110. Weigend, F., Ahlrichs, R. Balanced basis sets of split valence, triple zeta valence and quadruple zeta valence quality for H to Rn: Design and assessment of accuracy // *Phys. Chem. Chem. Phys.* – **2005** – 7 (18), 3297-3305.

111. Frisch, M.J., Trucks, G.W., Schlegel, H.B., Scuseria, G.E., Robb, M.A., Cheeseman, J.R., Scalmani, G., Barone, V., Mennucci, B., Petersson, G.A., Nakatsuji, H., Caricato, M., Li, X., Hratchian, H.P., Izmaylov, A.F., Bloino, J., Zheng, G., Sonnenberg, J.L., Hada, M., Ehara, M., Toyota, K., Fukuda, R., Hasegawa, J., Ishida, M., Nakajima, T., Honda, Y., Kitao, O., Nakai, H., Vreven, T., Montgomery, J., J.A., Peralta, J.E.,

Ogliaro, F., Bearpark, M., Heyd, J.J., Brothers, E., Kudin, K.N., Staroverov, V.N., Kobayashi, R., Normand, J., Raghavachari, K., Rendell, A., Burant, J.C., Iyengar, S.S., Tomasi, J., Cossi, M., Rega, N., Millam, N.J., Klene, M., Knox, J.E., Cross, J.B., Bakken, V., Adamo, C., Jaramillo, J., Gomperts, R., Stratmann, R.E., Yazyev, O., Austin, A.J., Cammi, R., Pomelli, C., Ochterski, J.W., Martin, R.L., Morokuma, K., Zakrzewski, V.G., Voth, G.A., Salvador, P., Dannenberg, J.J., Dapprich, S., Daniels, A.D., Farkas, Ö., Foresman, J.B., Ortiz, J.V., Cioslowski, J., Fox, D.J. *Gaussian 09, Revision D.01* // Gaussian, Inc., Wallingford CT, **2009**.

112. Marenich, A.V., Cramer, C.J., Truhlar, D.G. Universal solvation model based on solute electron density and on a continuum model of the solvent defined by the bulk dielectric constant and atomic surface tensions. // *J. Phys. Chem.* – **2009** – 113 (18), 6378-6396.

113. Zhao, Y., Truhlar, D.G. A new local density functional for main-group thermochemistry, transition metal bonding, thermochemical kinetics, and noncovalent interactions // *J. Chem. Phys.* – **2006 –** 125 (19), 194101(1)-194101(18).

114. Grimme, S. Semiempirical GGA-type density functional constructed with a long-range dispersion correction // *J. Comput. Chem.* – **2006 –** 27 (15), 1787-1799.

115. Dolg, M., Wedig, U., Stoll, H., Preuss, H. *Ab initio* pseudopotential study of the first row transition metal monoxides and iron monohydride// *J. Chem. Phys.* – **1987** – 86 (4), 866-872.

116. Ehlers, A.W., Böhme, M., Dapprich, S., Gobbi, A., Hoellwarth, A., Jonas, V., Koehler, K.F., Stegmann, R. Veldkamp, A., Frenking, G. A set of f-polarization functions for pseudo-potential basis sets of the transition metals Sc-Cu, Y-Ag and La-Au // *Chem. Phys. Lett.* – **1993** – 208 (1-2), 111-114.

117. Krishnan, R., Binkley, J.S., Seeger, R., Pople, J. Self-consistent molecular orbital methods. XX. A basis set for correlated wave functions // *A. J. Chem. Phys.* – **1980** – 72 (1), 650-654.

Supporting information.

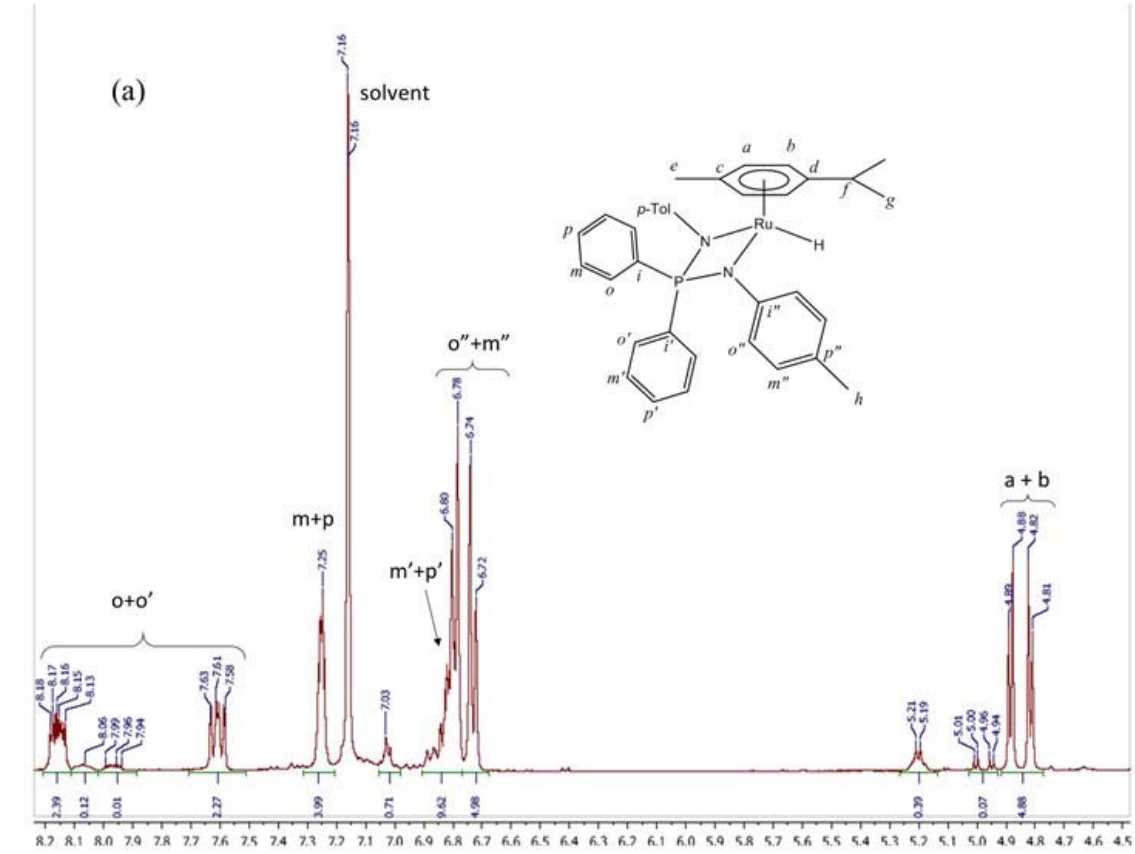

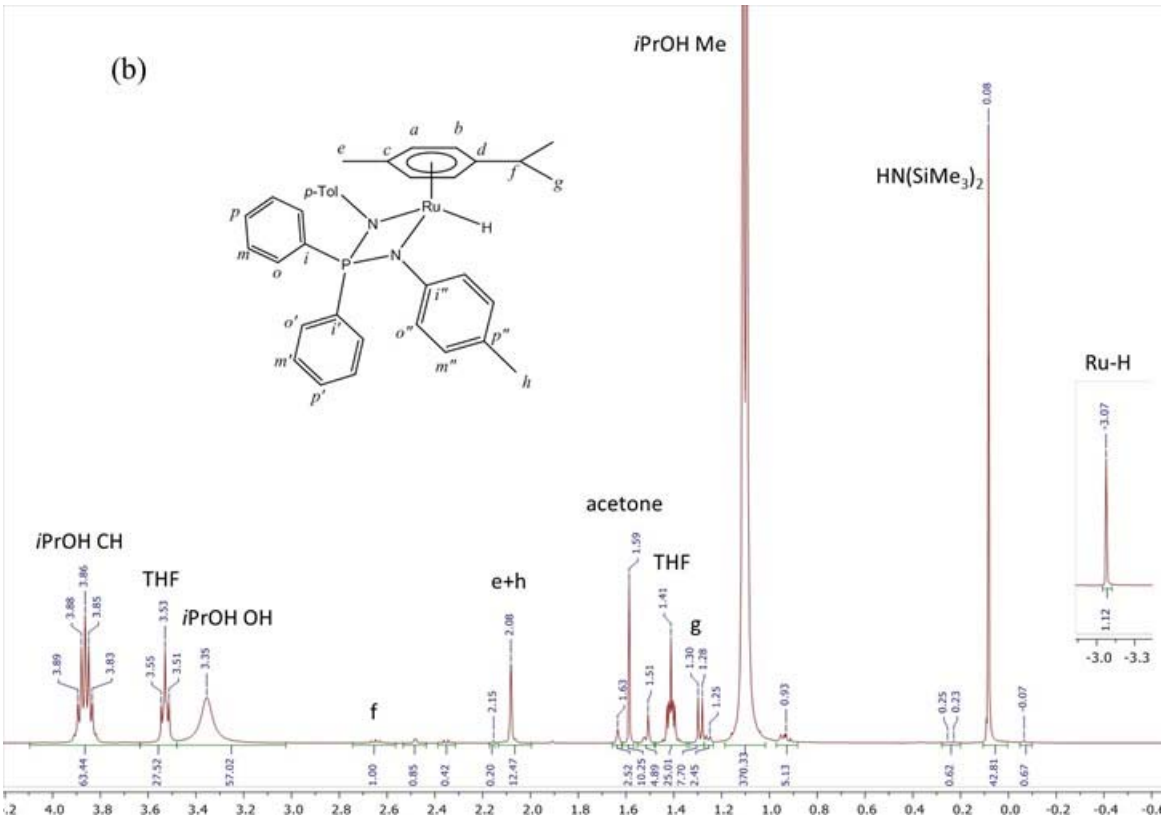

Figure S1. ^{1}H NMR spectra of **6f**, generated *in situ* from **3f** in C_6D_6. Conditions: 0.5 mL of C_6D_6, 13 mg of **3f** (0.02 mmol), 60 µL of ^{i}PrOH (^{i}PrOH/1 = 40), 15 µL of NaHDMS (2M in THF; HMDS/**3f** = 1.5).

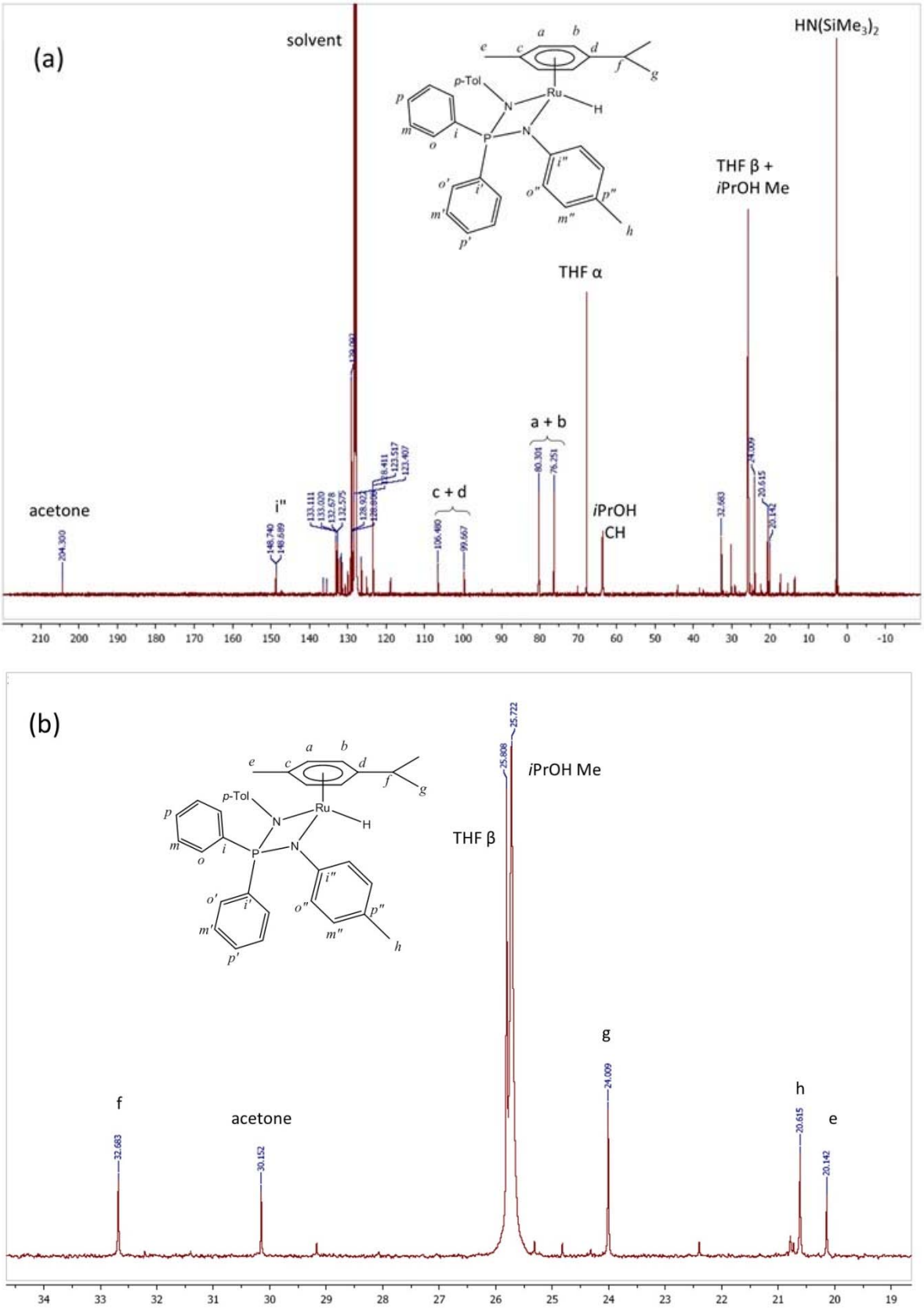

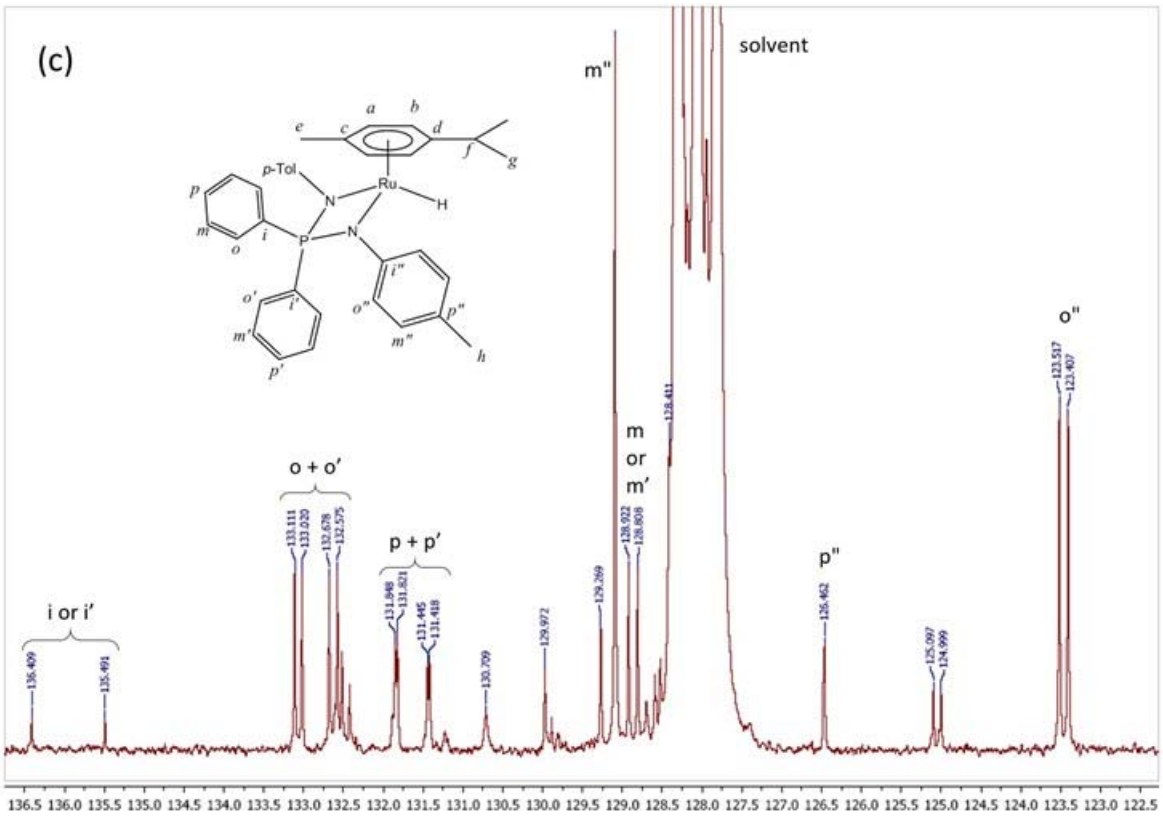

Figure S2. $^{13}C\{^{1}H\}$ NMR spectra of **6f**, obtained from **3f** and HMDS in ^{i}PrOH. Conditions: 0.5 mL of C_6D_6, 11 mg of **3f** (0.016 mmol), 18 μL of ^{i}PrOH (^{i}PrOH/**3f** = 15), 22 μL of NaHDMS (1.9M in THF; HMDS/**3f** = 2.6). (**a**) Full spectrum. (**b**) Expansion of the 34-19 ppm region. (**c**) Expansion of the 137-122 ppm region.

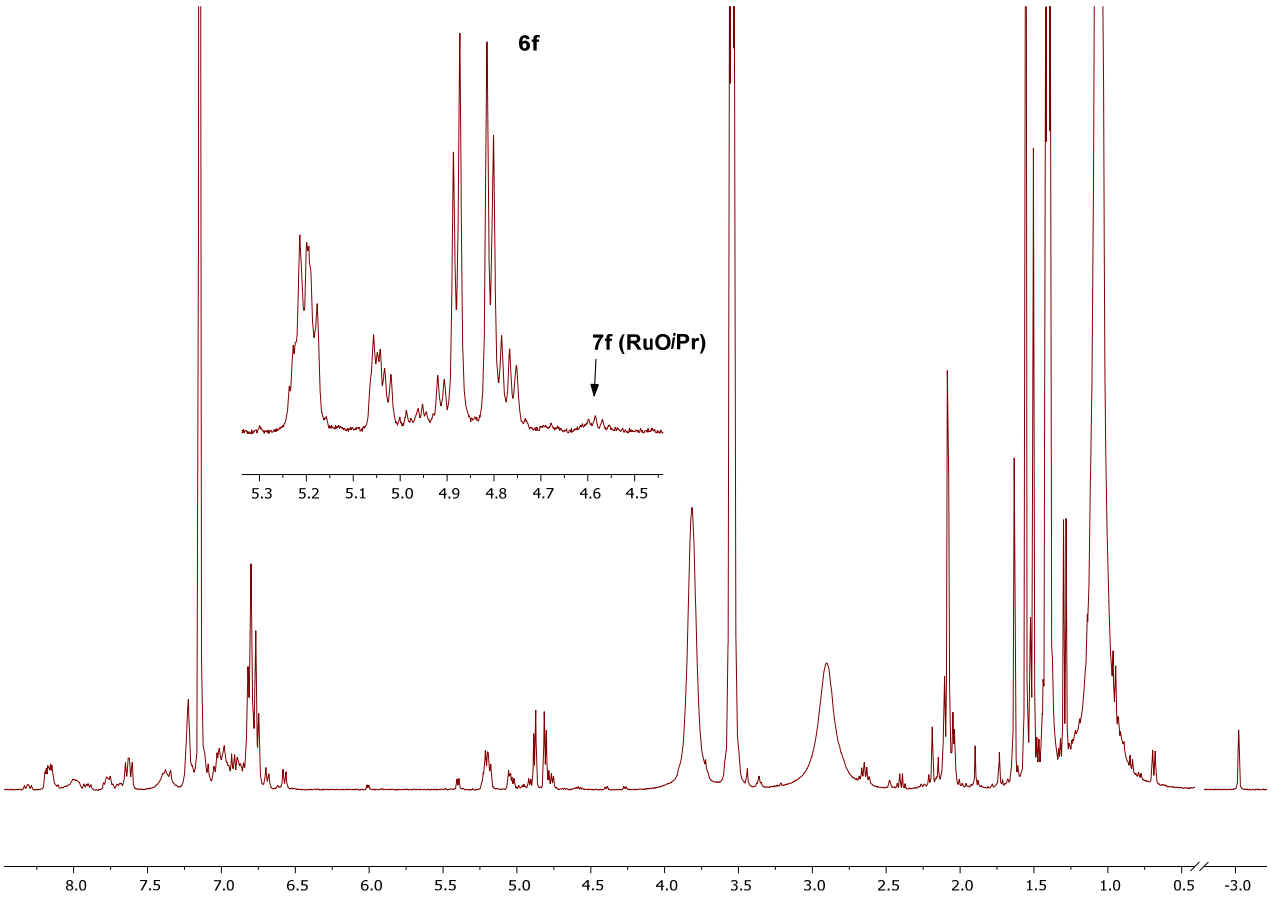

Figure S3. ^{1}H NMR spectrum of **3f** in C_6D_6/^{i}PrOH (500/40 µL) recorded 15 minutes after adding NaHMDS (1.5 equiv.). The characteristic signal for the **7f** is marked.

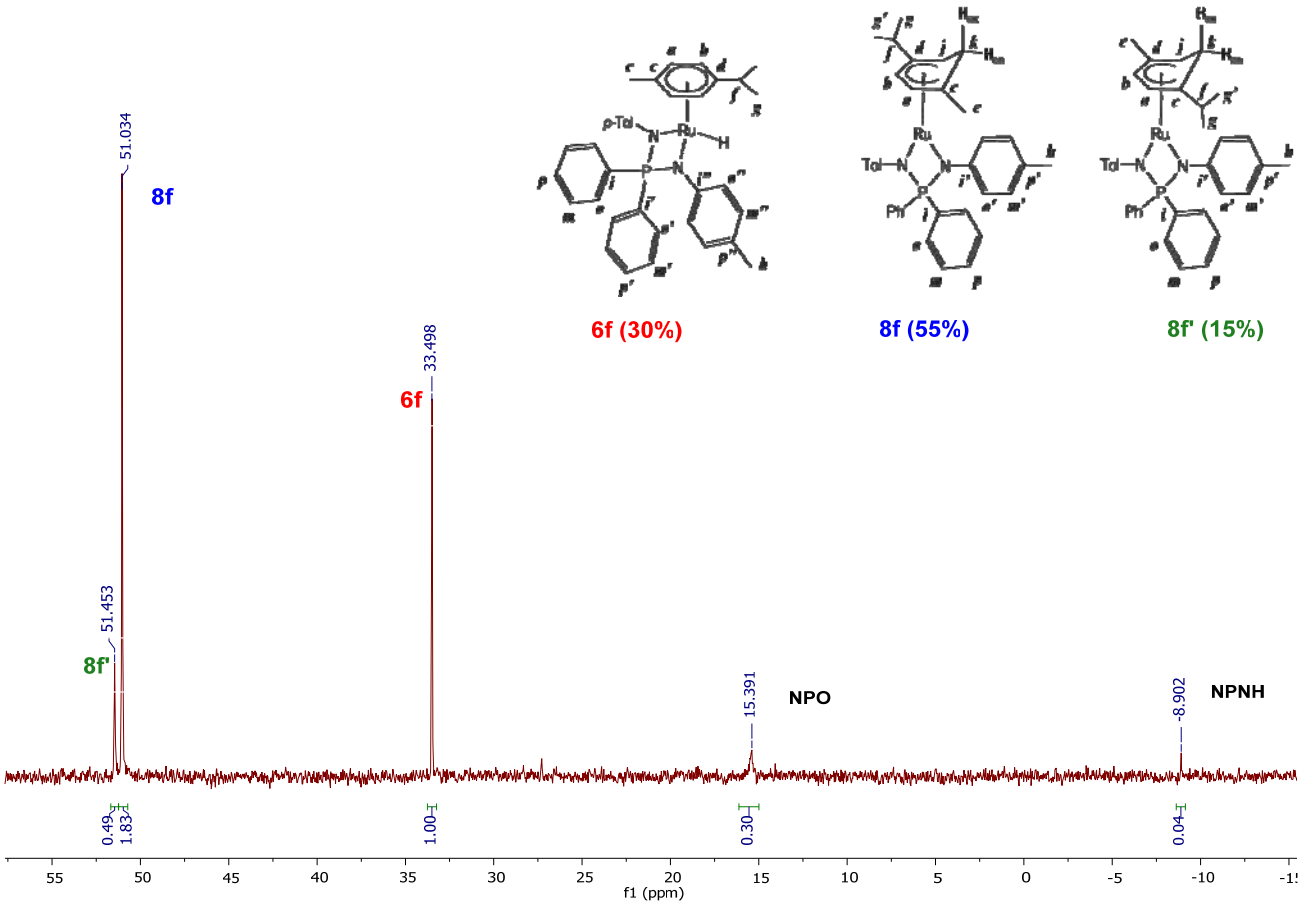

Figure S4. $^{31}P\{^{1}H\}$ NMR spectrum of the **6f/8f/8f'** mixture in a 30/55/15 ratio in C_6D_6, prepared as described in the experimental section.

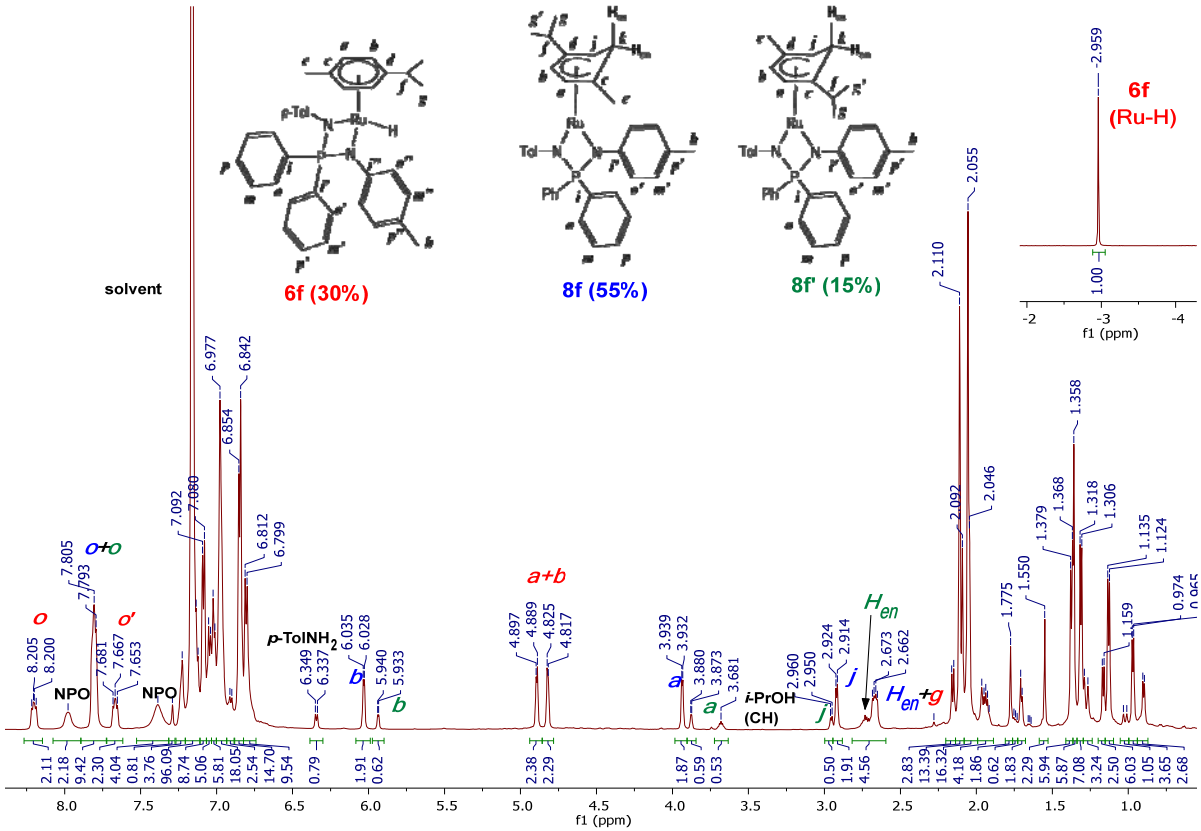

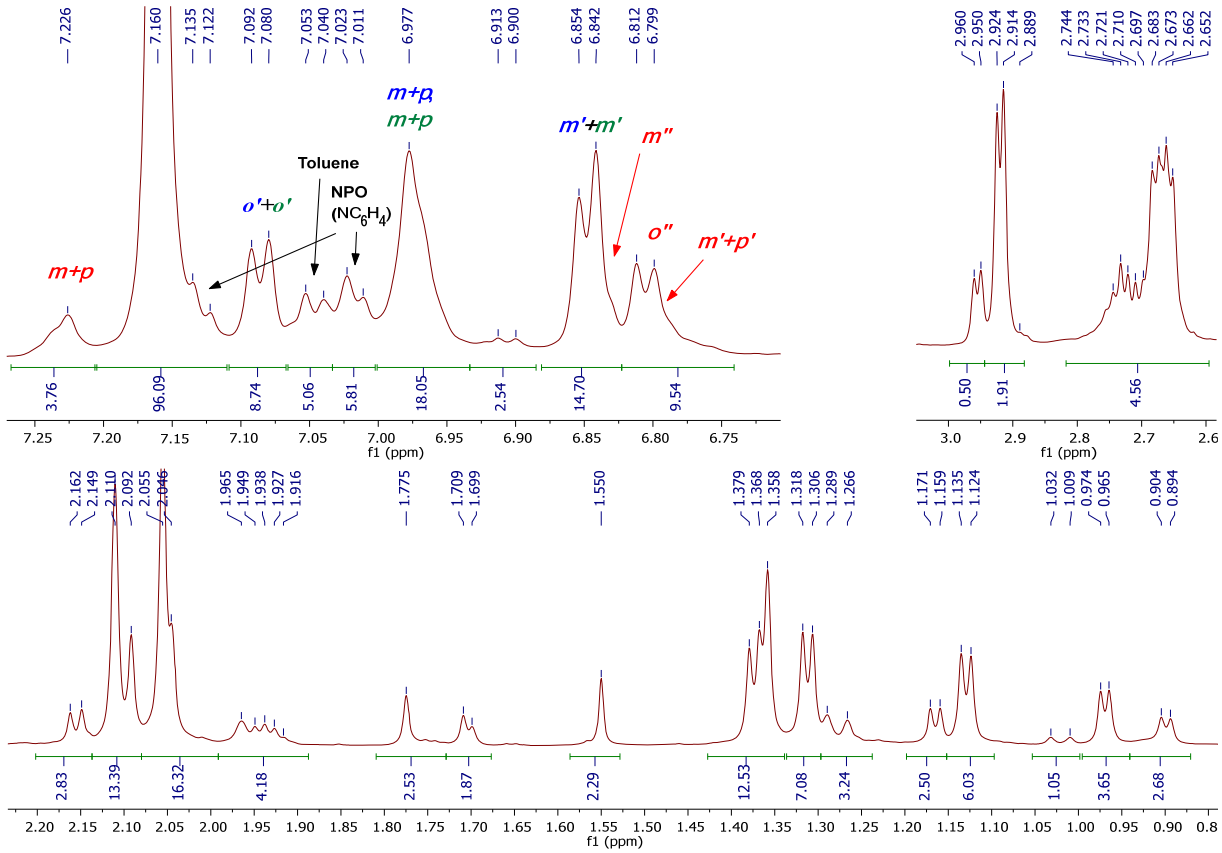

Figure S5. ^{1}H NMR spectrum of the **6f/8f/8f'** mixture in a 30/55/15 ratio in C_6D_6. The "X" labelled resonances corresponds to *p*-cymene in an unknown Ru complex formed as a result of NPN ligand decoordination, tentatively assigned to a solvated species [(η^6-*p*-cymene)Ru(L)$_x$].

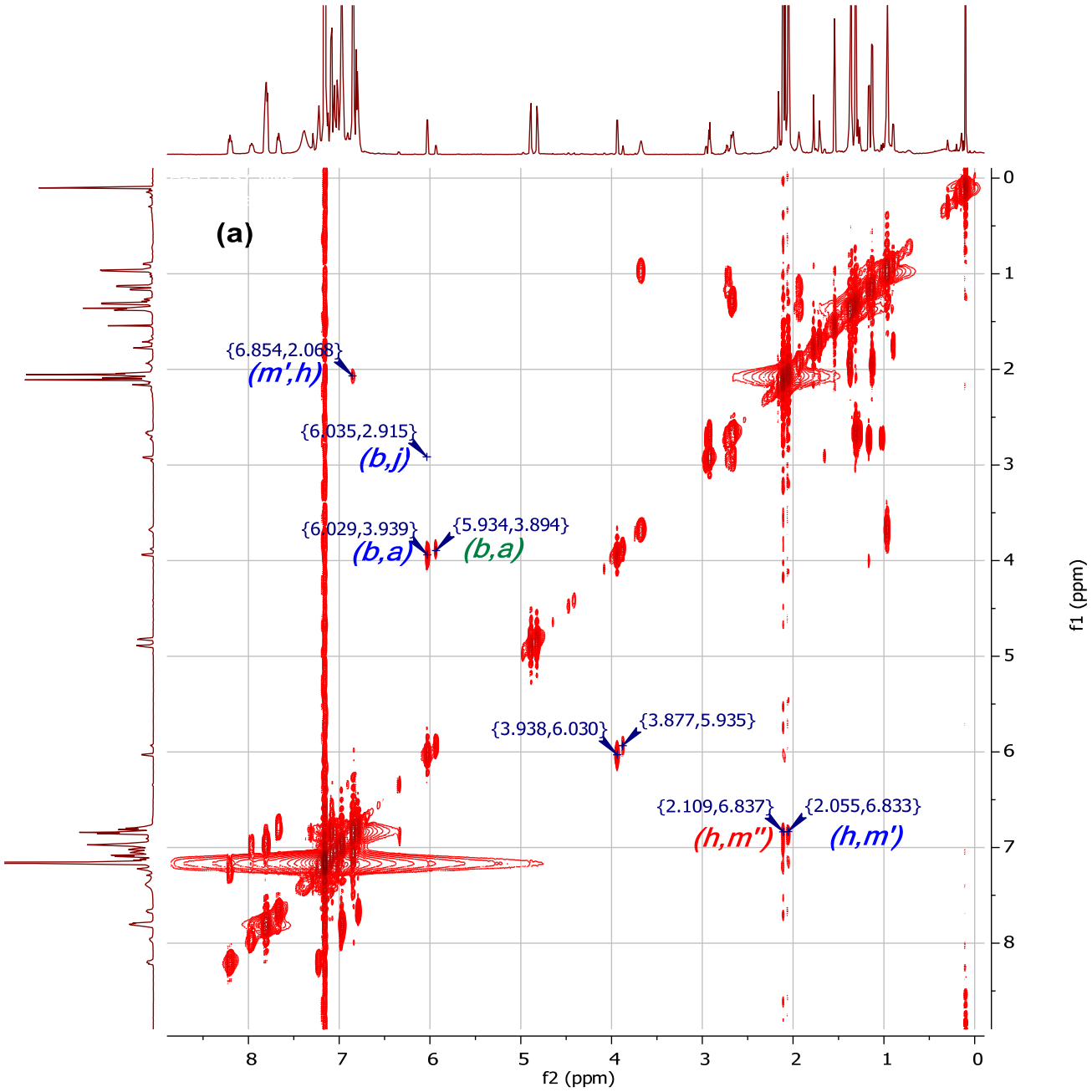
(a)
{6.854,2.068}
(m',h)
{6.035,2.915}
(b,j)
{6.029,3.939}
(b,a)
{5.934,3.894}
(b,a)
{3.938,6.030}
{3.877,5.935}
{2.109,6.837}
(h,m'')
{2.055,6.833}
(h,m')
f2 (ppm)
f1 (ppm)

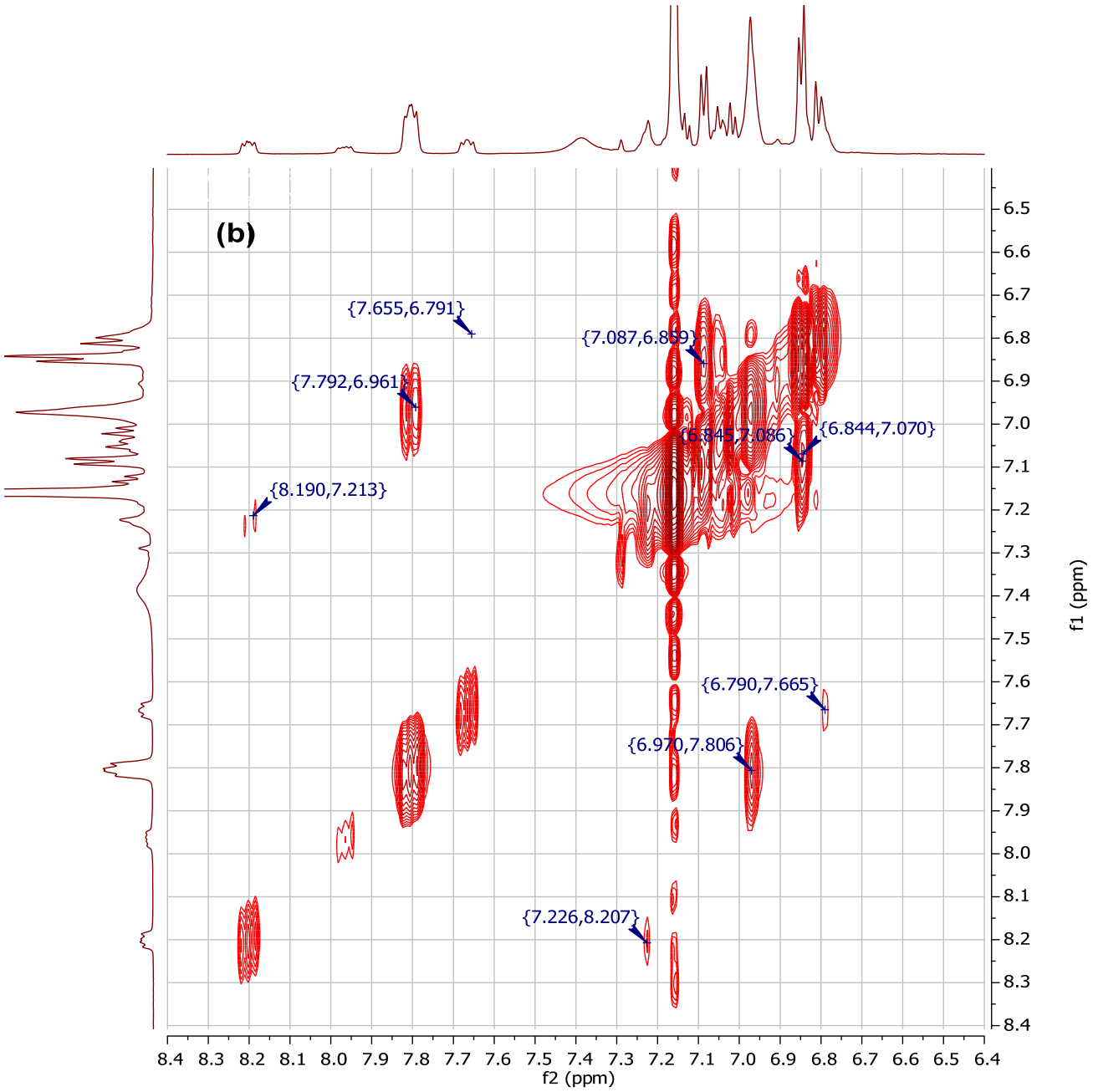
(b)
{7.655,6.791}
{7.792,6.961}
{8.190,7.213}
{7.087,6.859}
{6.845,7.086}
{6.844,7.070}
{6.790,7.665}
{6.970,7.806}
{7.226,8.207}
f2 (ppm)
f1 (ppm)

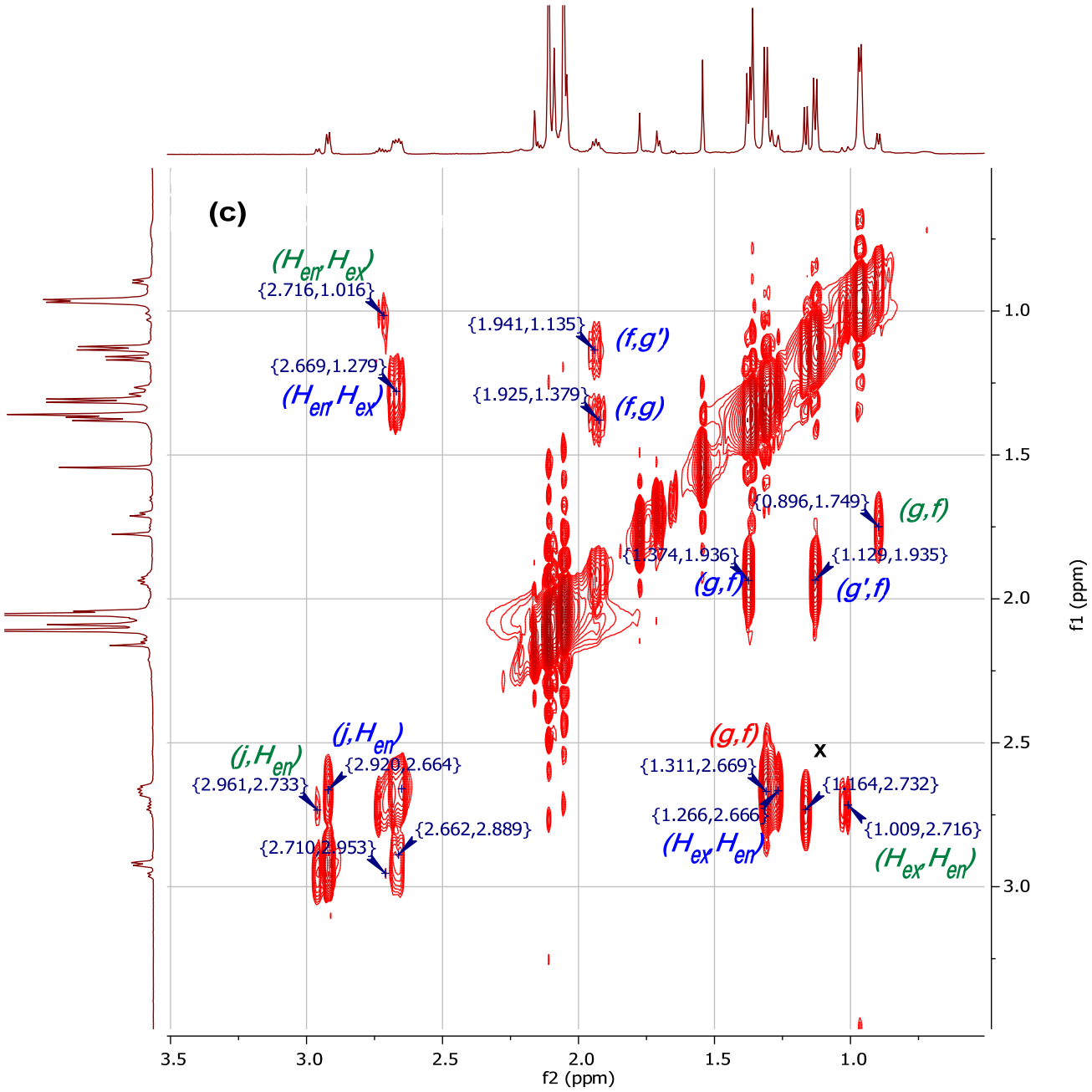

Figure S6. ^{1}H-^{1}H COSY NMR spectrum of the **2f/8f/8f'** mixture in a 30/55/15 ratio in C_6D_6. (**a**) Full spectrum. (**b**) Expansion of the δ 6.40-8.40 region. (**c**) Expansion of the δ 0.5-3.5 region. Designations as in Figure S5.

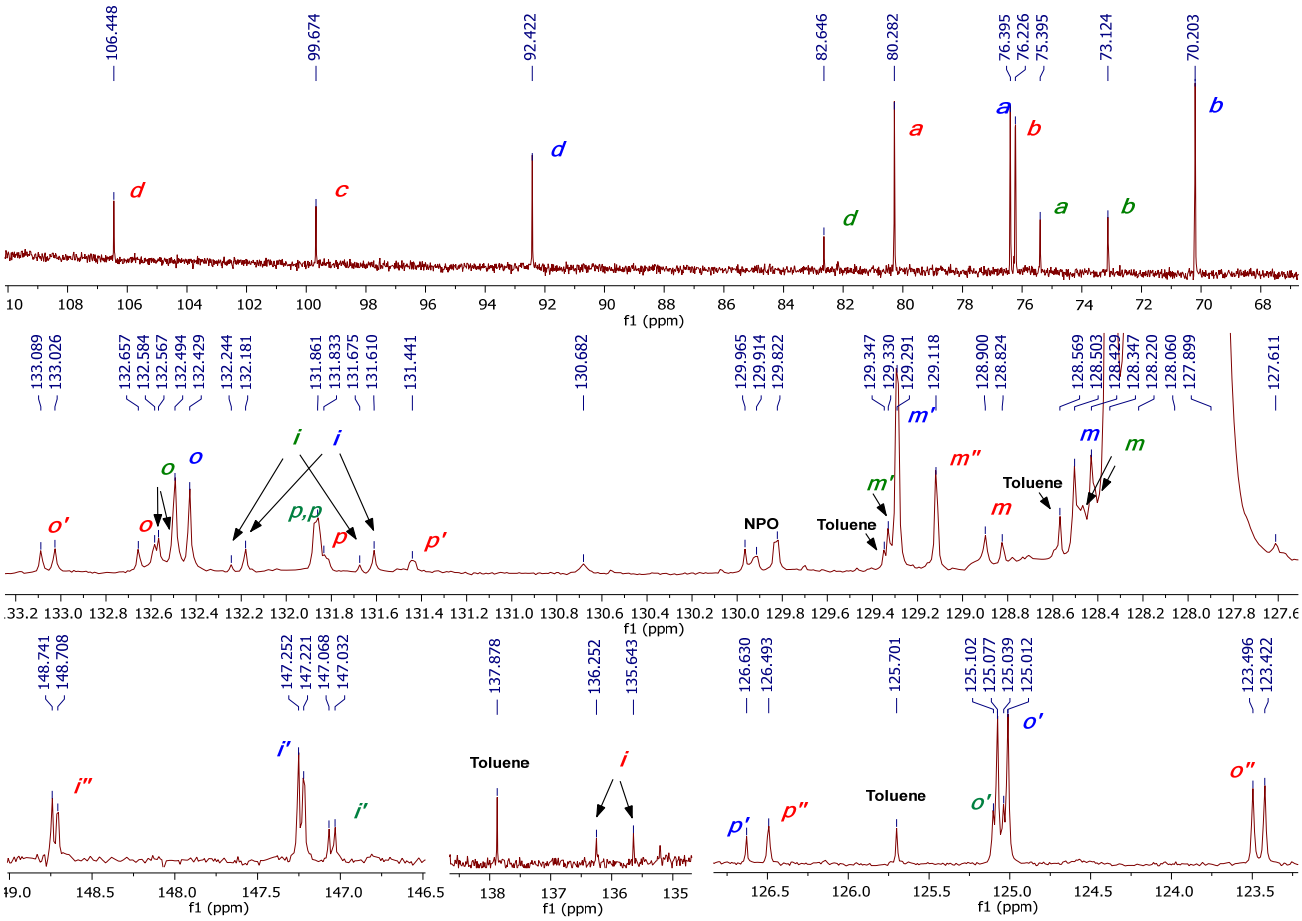

Figure S7. $^{13}C\{^{1}H\}$ NMR spectrum of the **6f/8f/8f'**mixture in a 30/55/15 ratio in C_6D_6. Designations as in Figure S5.

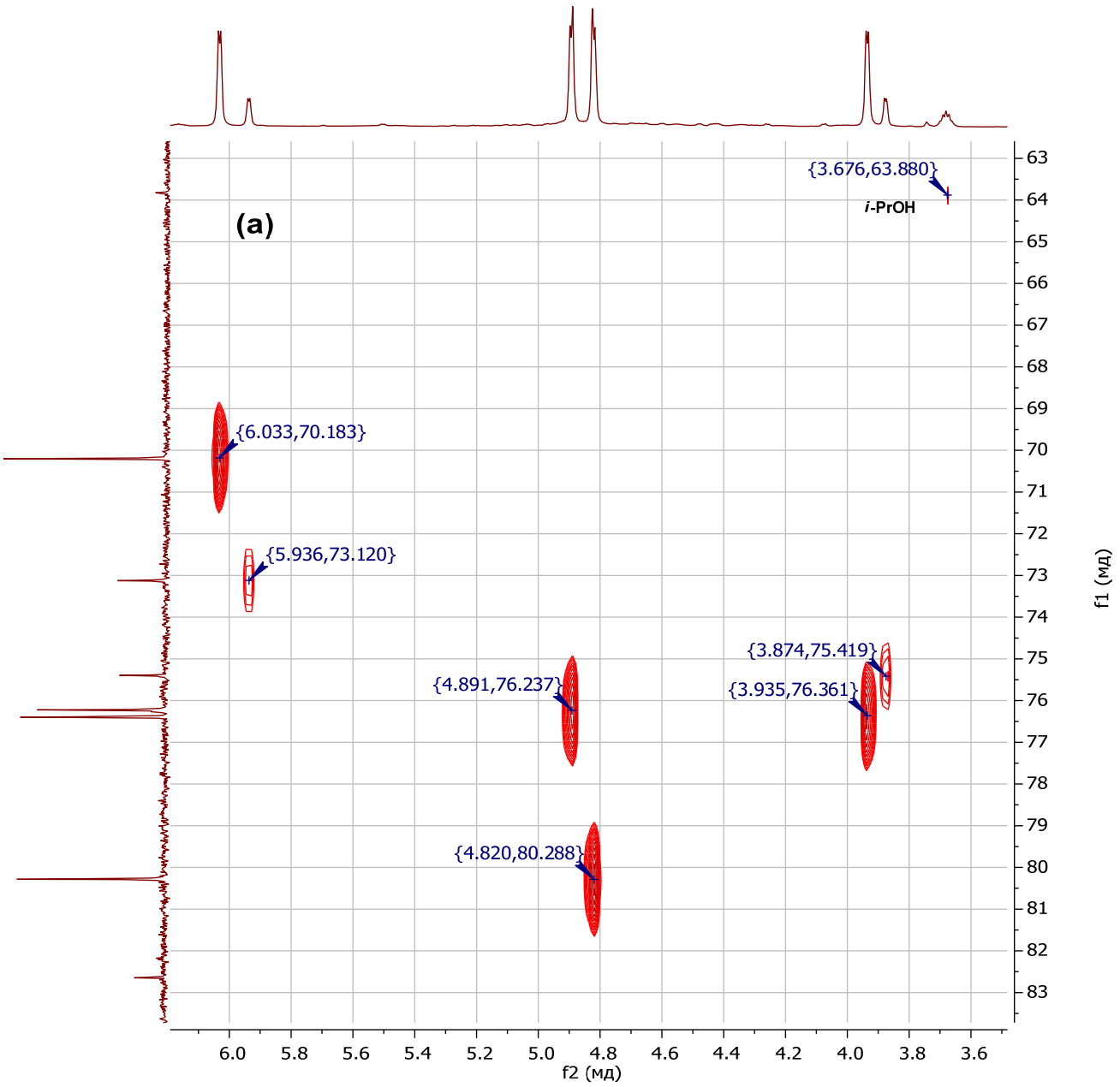
(a)
{3.676,63.880}
i-PrOH
{6.033,70.183}
{5.936,73.120}
{4.891,76.237}
{3.874,75.419}
{3.935,76.361}
{4.820,80.288}
f2 (мд)
f1 (мд)

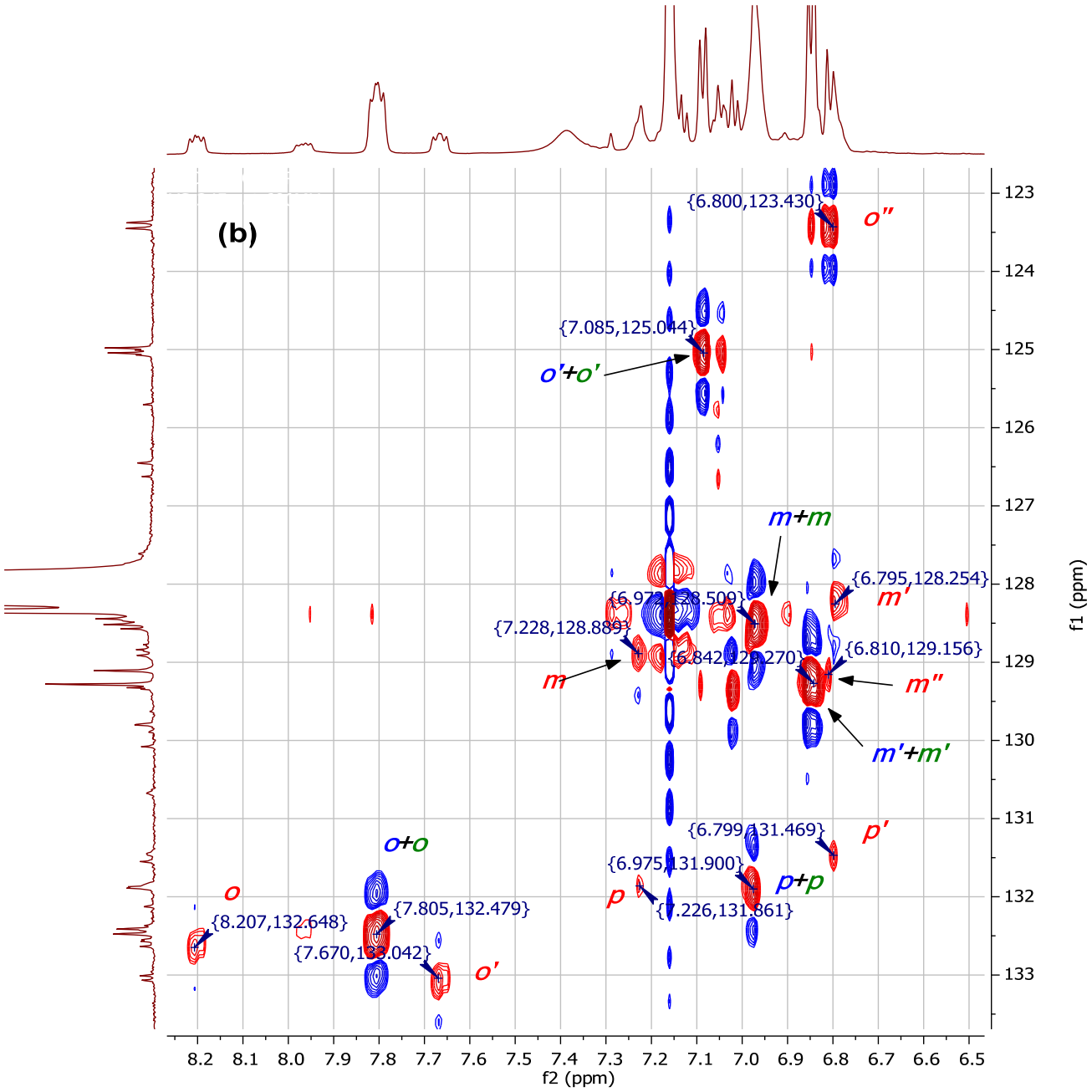
(b)
{6.800,123.430}
o''
{7.085,125.044}
o'+o'
m+m
{6.795,128.254}
m'
{7.228,128.889}
{6.810,129.156}
m
m''
m'+m'
{6.799,131.469}
p'
{6.975,131.900}
p+p
p
{7.226,131.861}
o+o
o
{8.207,132.648}
{7.805,132.479}
{7.670,132.042}
o'
f2 (ppm)
f1 (ppm)

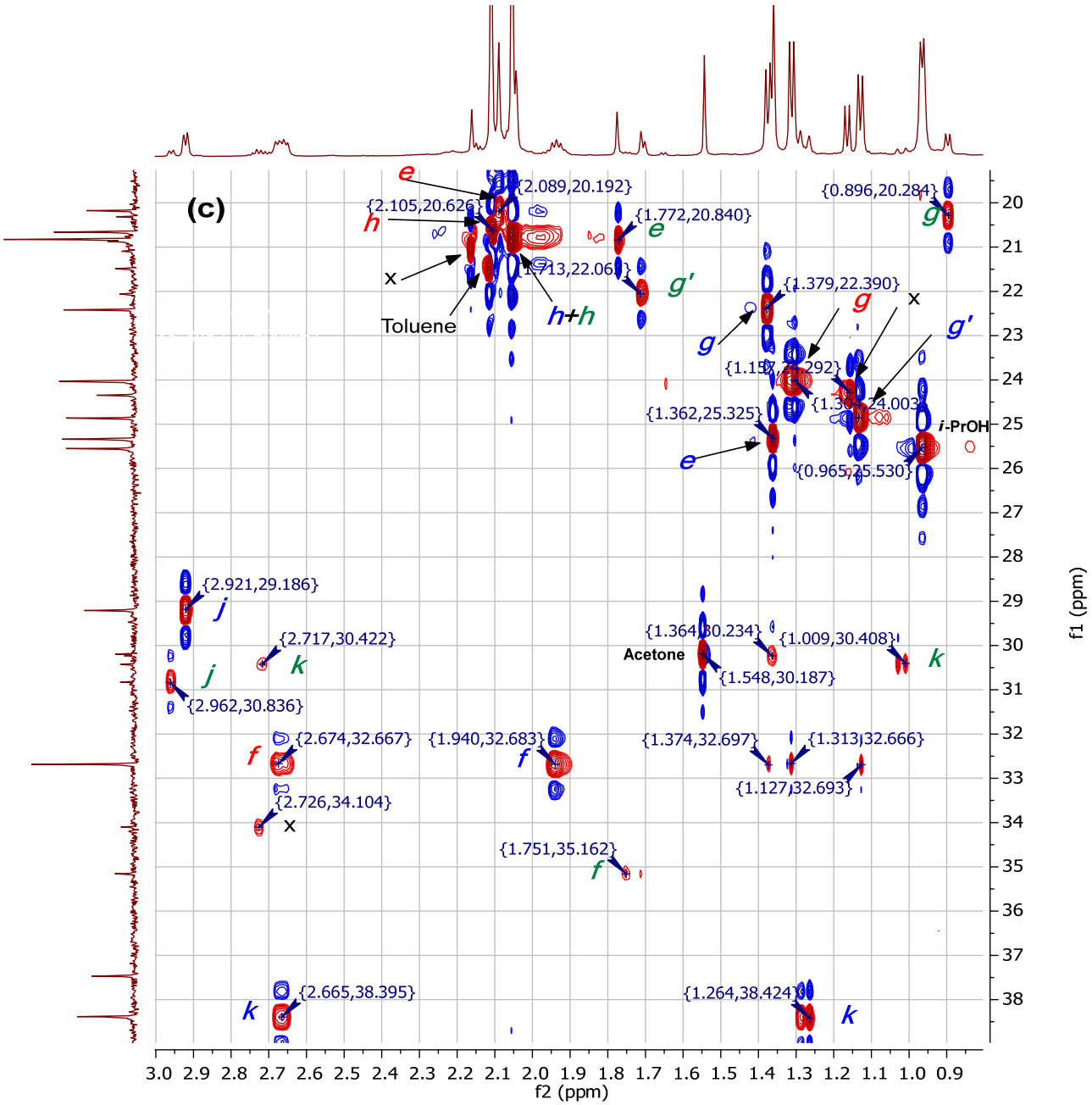

Figure S8. ^{1}H-^{13}C HSQC NMR spectrum of the **6f**/**8f**/**8f'** mixture in a 30/55/15 ratio in C_6D_6. (**a**) Expansion of the *p*-cymene aromatic resonance region. (**b**) Expansion of the PPh and NTol resonance region**.** (**c**) Expansion of aliphatic resonance region**.** Designations as in Figure S5.

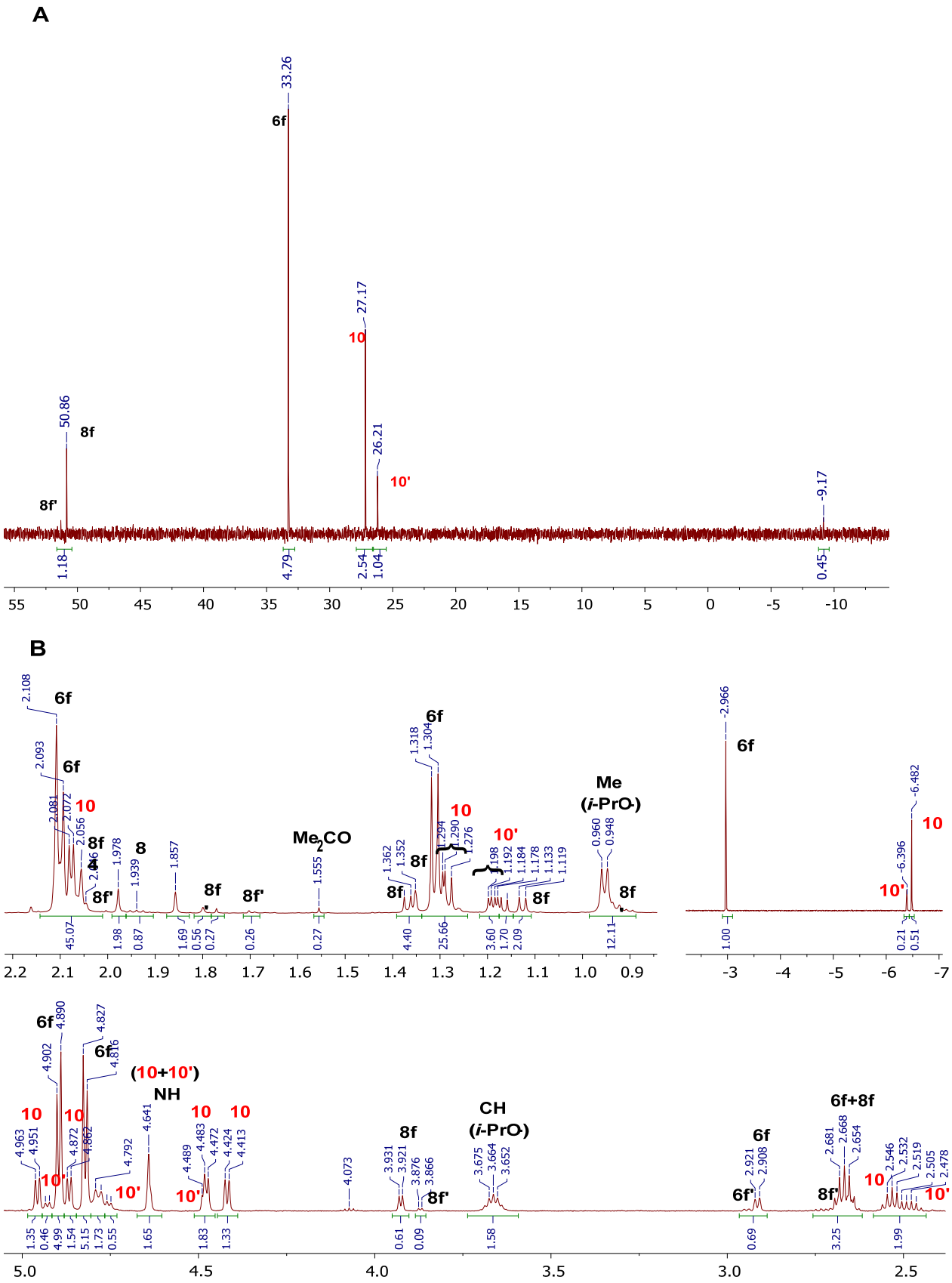

Figure S9. $^{31}P\{^{1}H\}$ (**A**) and ^{1}H (**B**) NMR spectra of compound **6f** prepared from **3f** and NaHMDS in neat ^{i}PrOH, followed by evaporation, extraction in Et_2O, filtration, evaporation and analysis in C_6D_6.

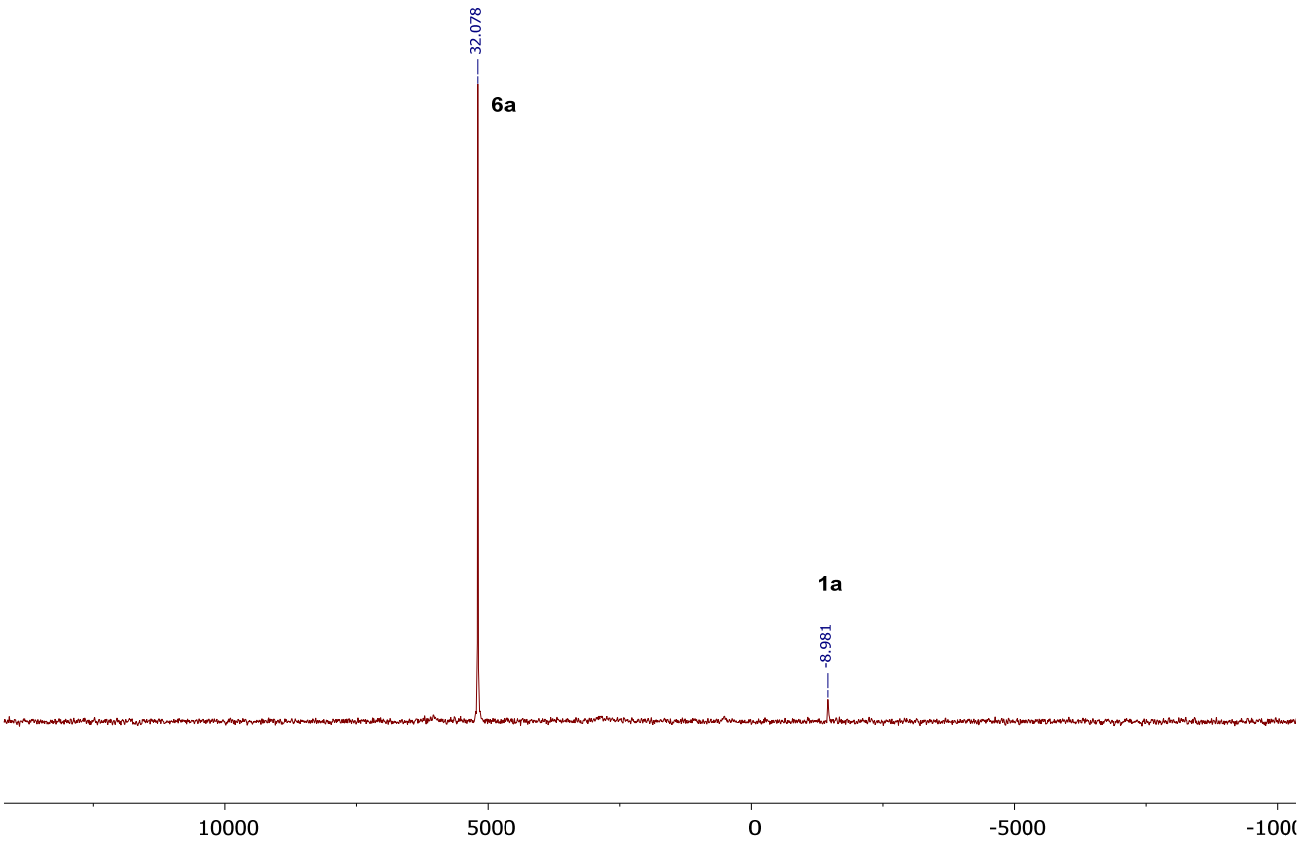

Figure S10. $^{31}P\{^{1}H\}$ NMR spectrum of compound **6a** prepared from **3a** and NaHMDS (1.5 equiv.) in $C_6D_6/^{i}PrOH$ (500/40 µL), followed by evaporation, extraction in Et_2O, filtration, evaporation and analysis in C_6D_6. About 10% of **1a** is present as an impurity.

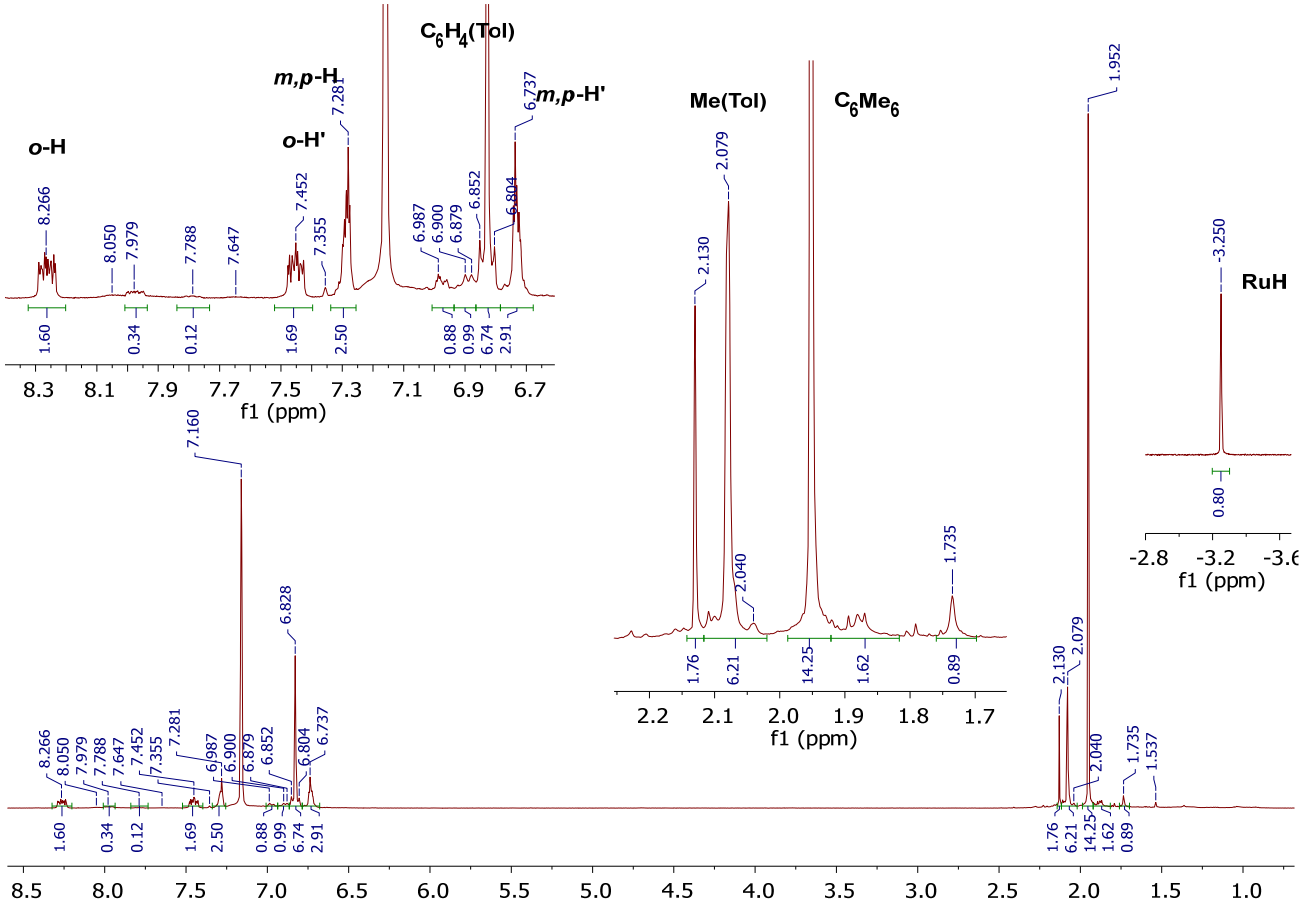

Figure S11. ^{1}H NMR spectrum of compound **6a** prepared from **3a** and NaHMDS (1.5 equiv.) in C_6D_6/^{i}PrOH (500/40 µL), followed by evaporation, extraction in Et_2O, filtration, evaporation and analysis in C_6D_6. About 10% of **1a** is present as an impurity.

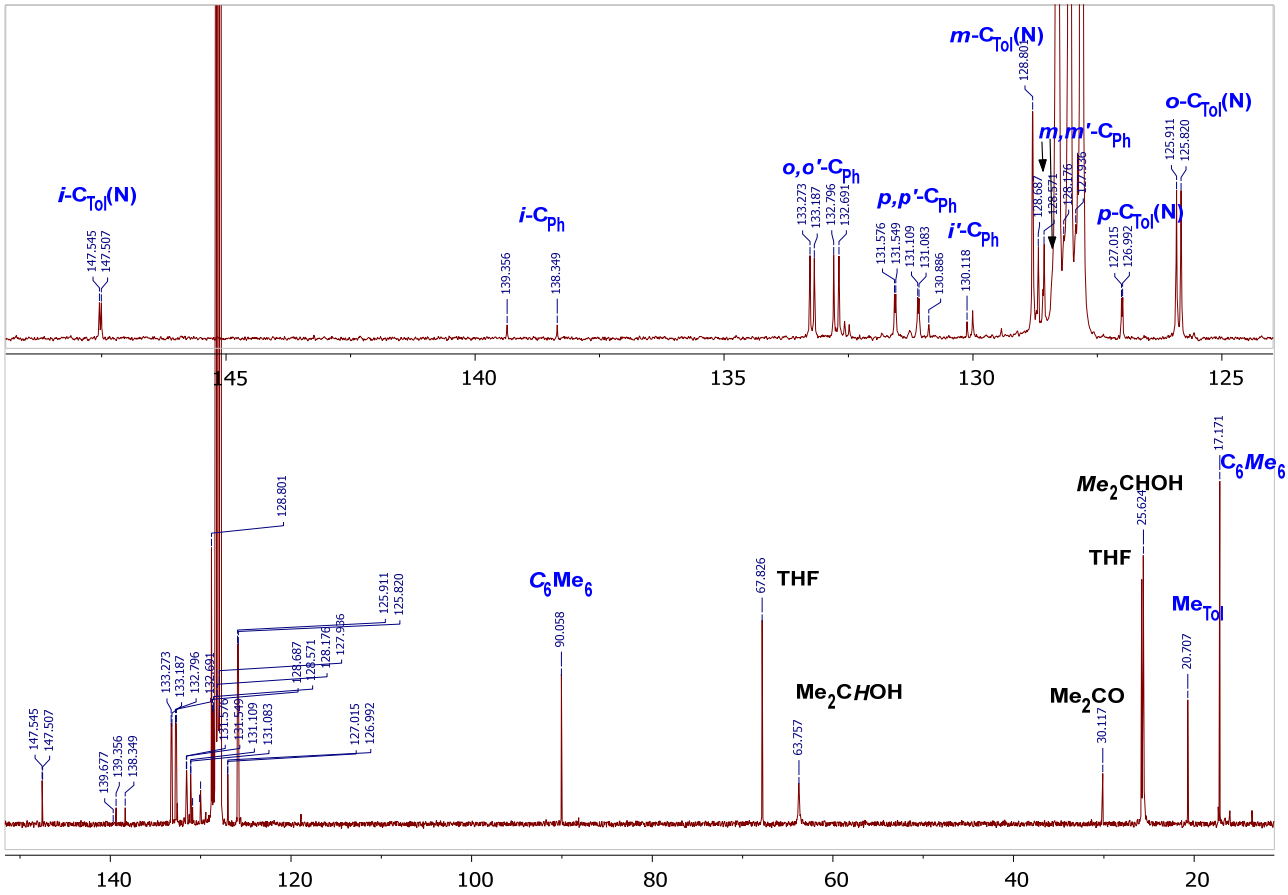

Figure S12. $^{13}C\{^{1}H\}$ NMR spectrum of compound **6a** prepared from **3a** and NaHMDS (1.5 equiv.) in C_6D_6/^{i}PrOH (500/40 μL) without isolation.

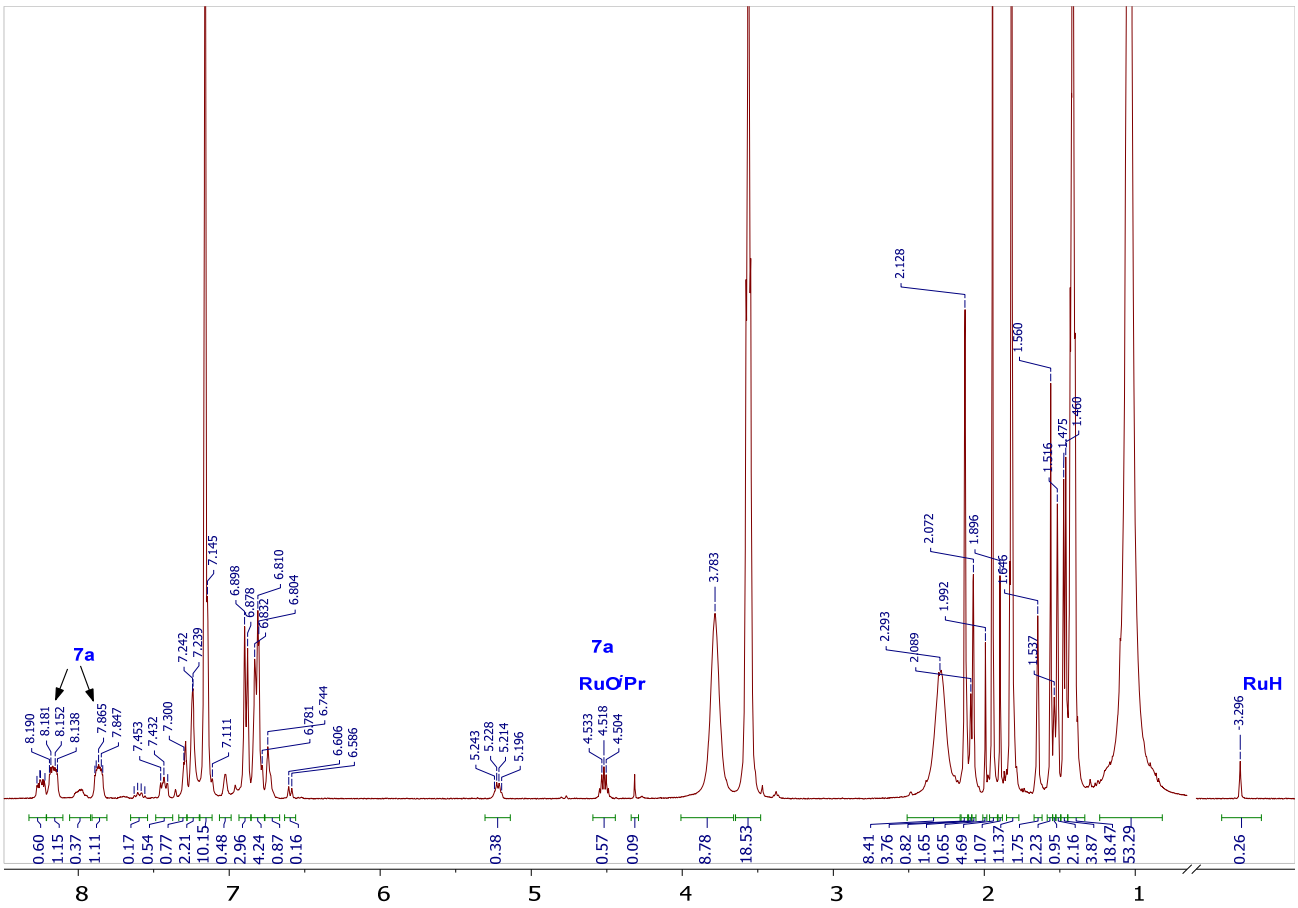

Figure S13. ^{1}H NMR spectrum of **3a** in C_6D_6/^{i}PrOH (500/10 µL), recorded 15 minutes after adding NaHMDS (1.5 equiv.). The characteristic signal for the **7a** is marked.

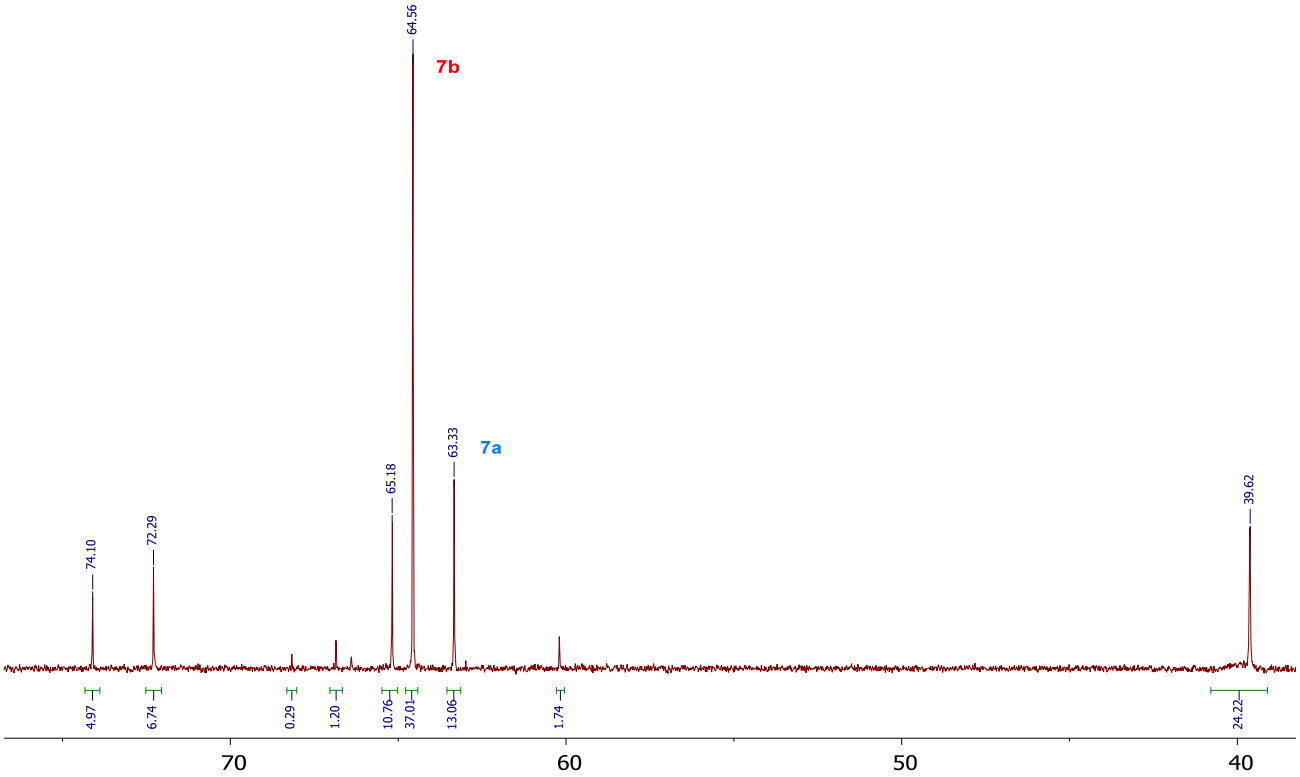

Figure S14. $^{31}P\{^{1}H\}$ NMR spectrum of **3b** in $C_6D_6/^{i}PrOH$ (500/10 µL), recorded 10 minutes after adding NaHMDS (1.5 equiv.).

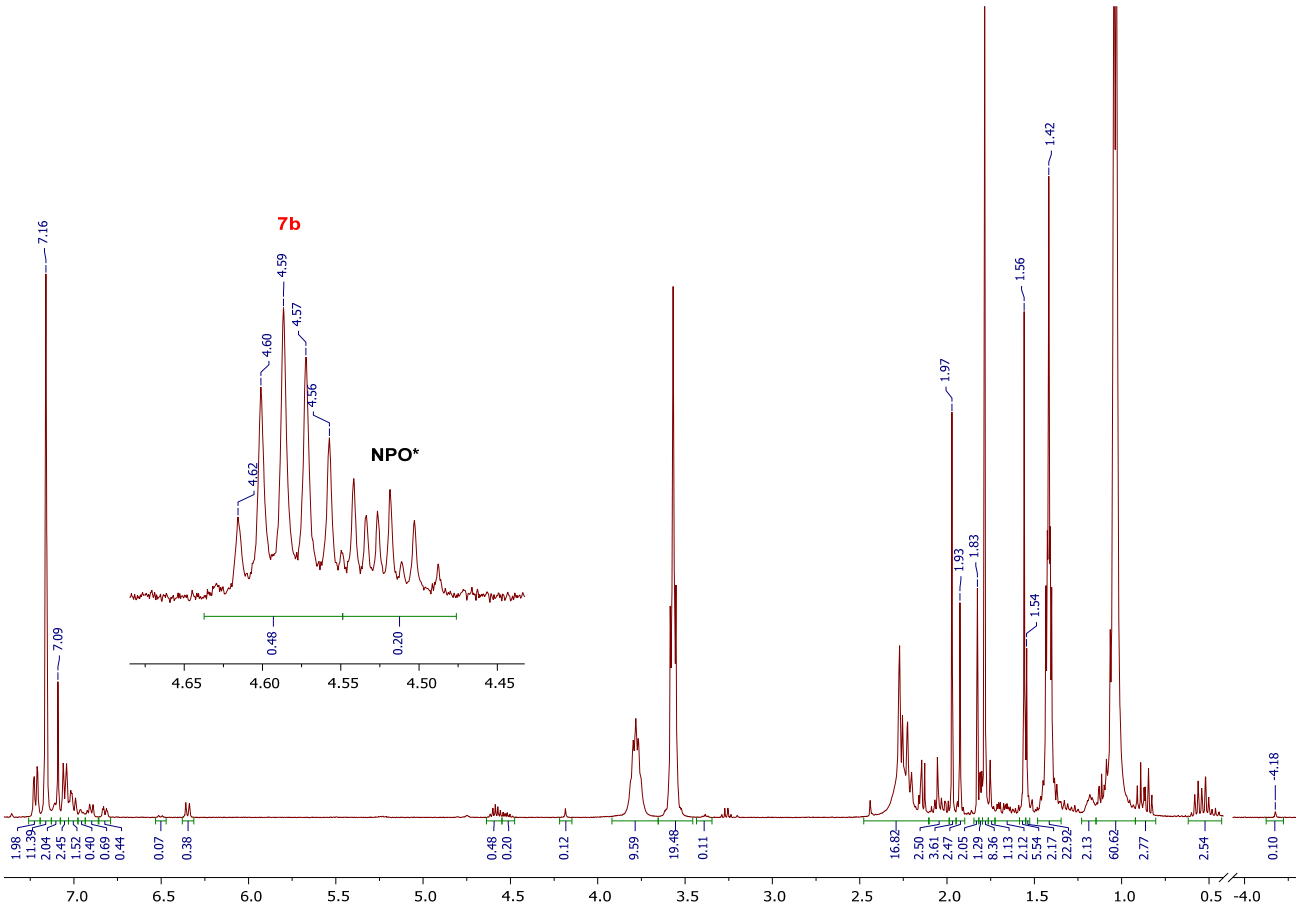

Figure S15. ^{1}H NMR spectrum of **3b** in C_6D_6/^{i}PrOH (500/10 µL), recorded 5 minutes after adding NaHMDS (1.5 equiv.). The characteristic signals for the **7b** and **NPO*** are marked.

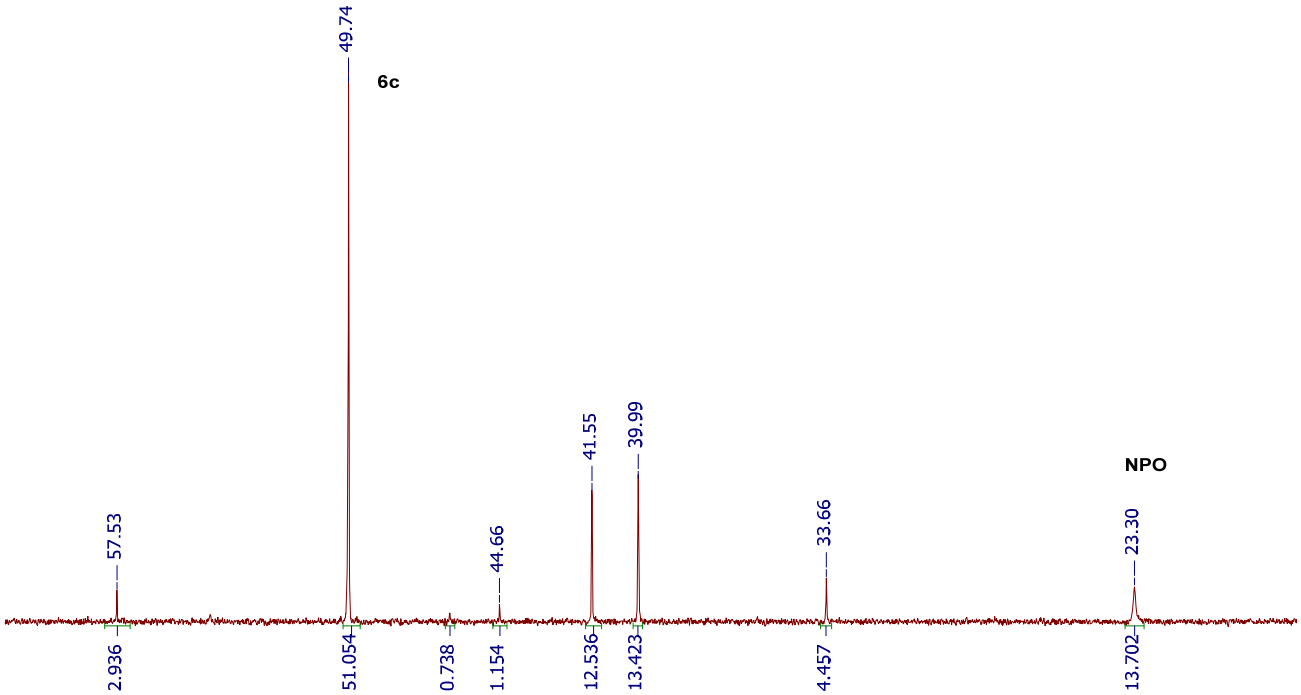

Figure S16. $^{31}P\{^{1}H\}$ NMR spectrum of **3c** in C_6D_6 recorded 20 minutes after adding $NaHBEt_3$ (1 equiv.).

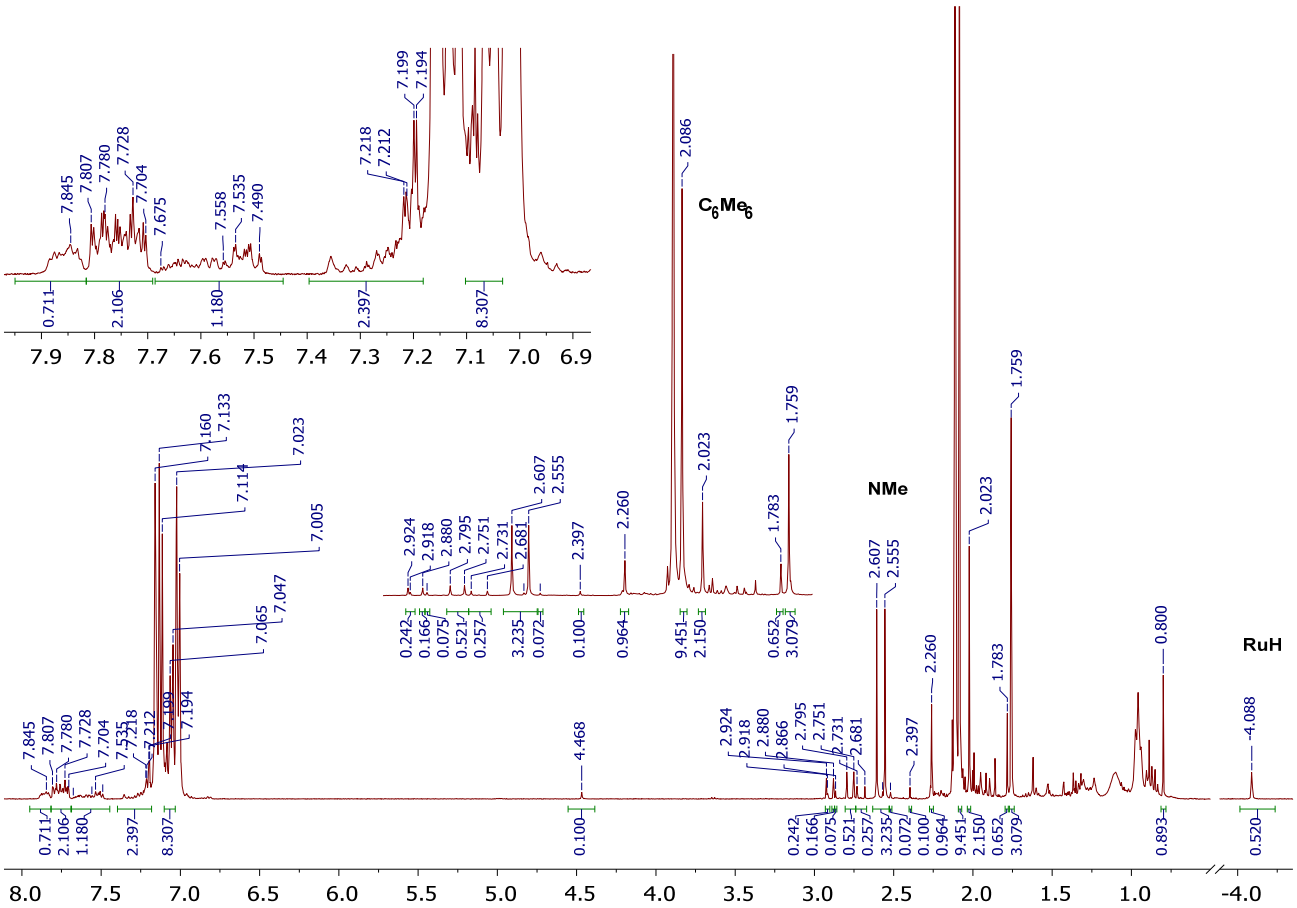

Figure S17. ^{1}H NMR spectrum of **3c** in C_6D_6 recorded 20 minutes after adding $NaHBEt_3$ (1 equiv.).

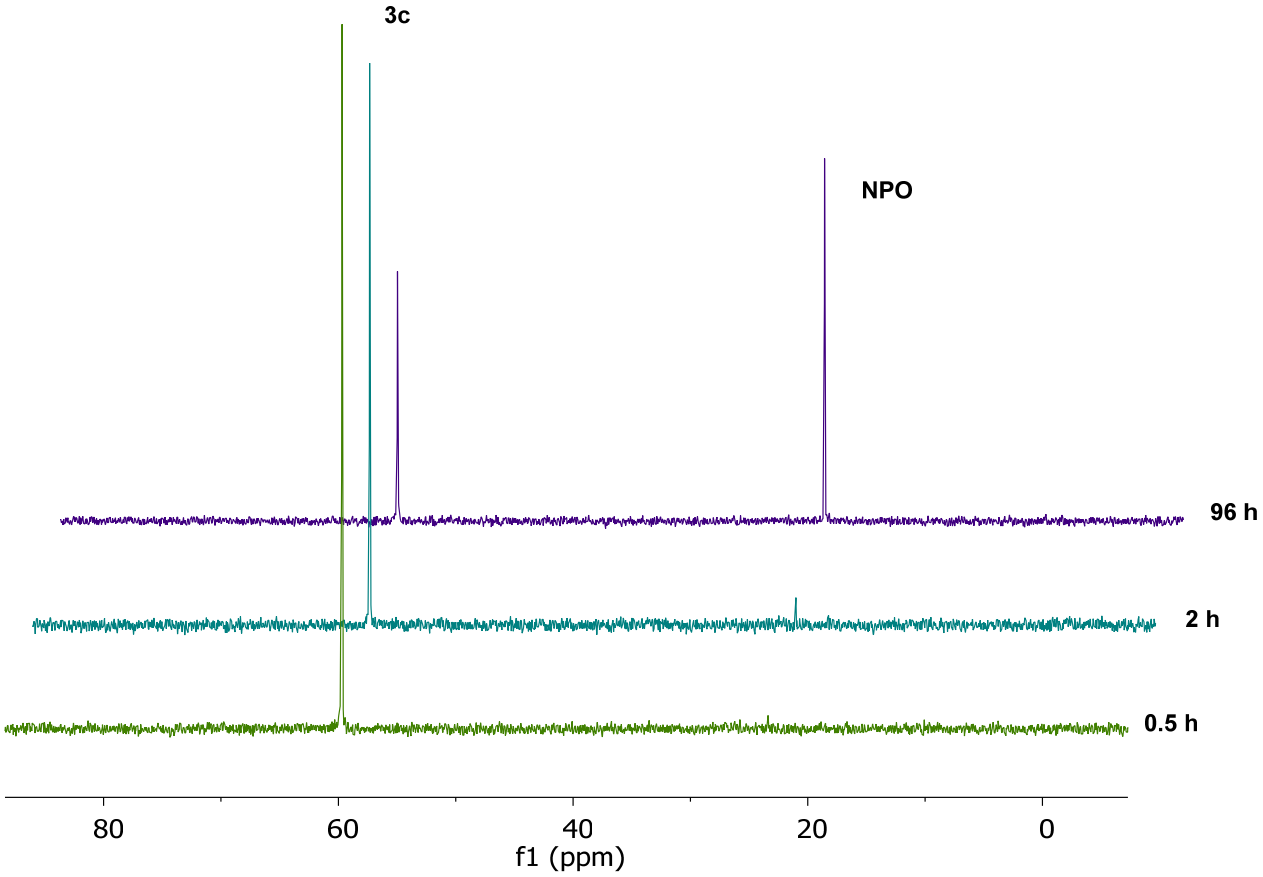

Figure S18. Study of the stability of **3c** in C_6D_6 (0.50 ml) in the presence of 6 equiv. isopropanol (10 µl).

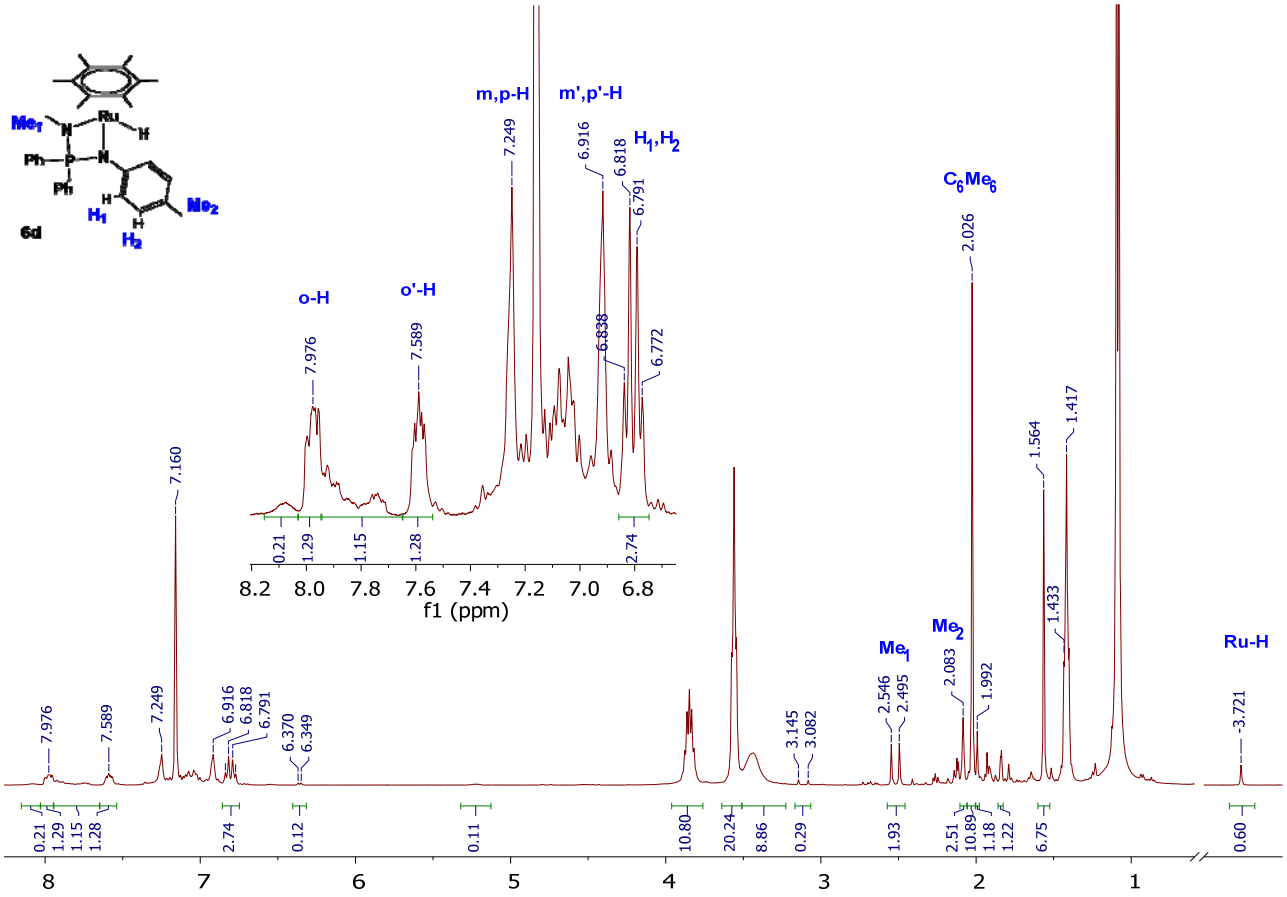

Figure S19. ^{1}H NMR spectrum of **3d** in C_6D_6/^{i}PrOH (500/20 µL) recorded 1 hour after adding NaHMDS (1.5 equiv.).

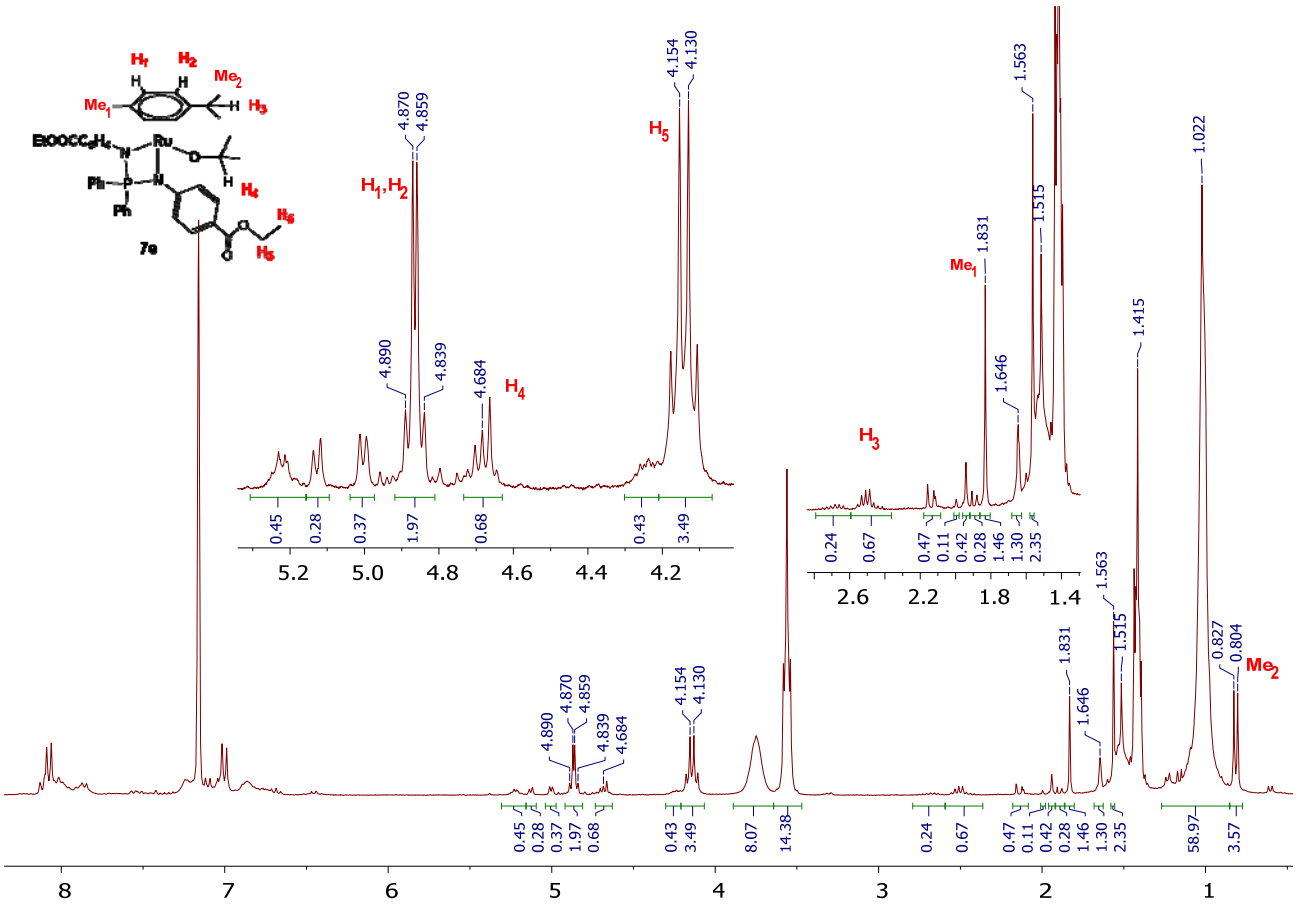

Figure S20. ^{1}H NMR spectrum of **3e** in C_6D_6/^{i}PrOH (500/10 µL) recorded 15 minutes after adding NaHMDS (1.5 equiv.). The characteristic signals for compound **7e** are marked.

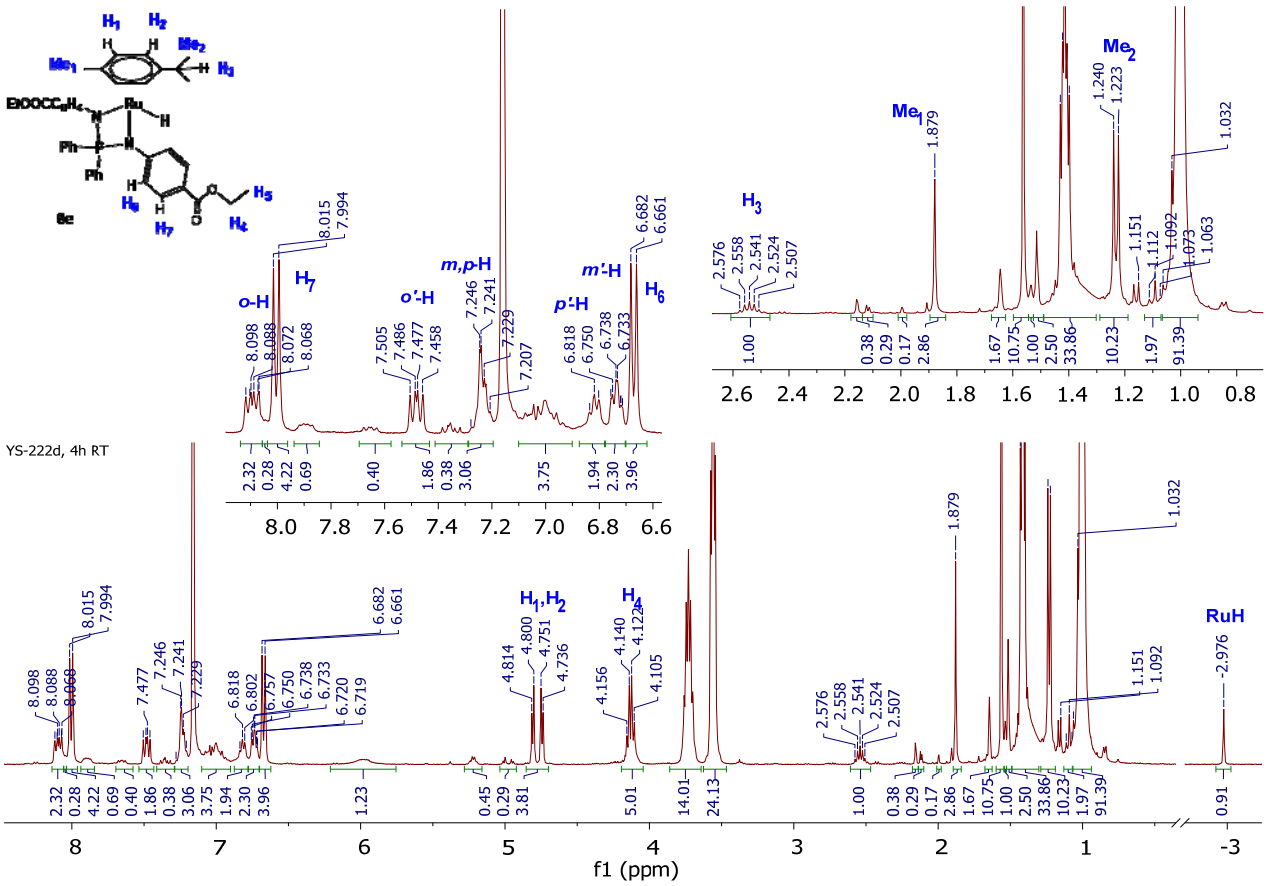

Figure S21. ^{1}H NMR spectrum of **3t** in C_6D_6/^{i}PrOH (500/10 µL) recorded 4 hours after adding NaHMDS (1.0 equiv.). The characteristic signals for compound **6e** are marked.

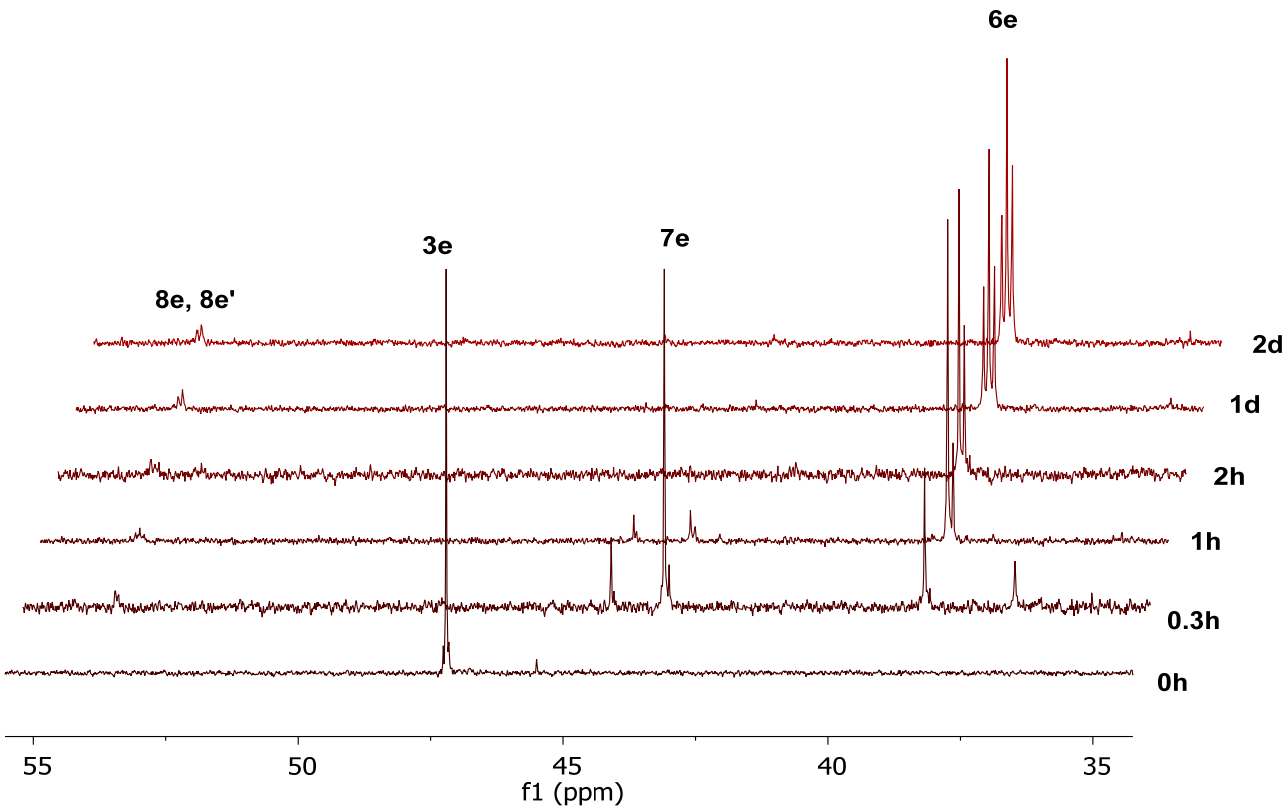

Figure S22. $^{31}P\{^{1}H\}$ NMR monitoring of the reaction of **3e** in $C_6D_6/^{i}PrOH$ with NaHMDS (1.5 equiv.).

Résumé en français

1. Synthèse, structure et réactivité de complexes iminophosphonamides (NPN) arènes de ruthénium.

1.1. Synthèse de complexes iminophosphonamides (NPN) arènes de ruthénium.

Les nouveaux complexes NPN arène chlorure de ruthénium à 18 électrons [(η^6-arène)RuCl{$R_2P(N\text{-}R')_2$}] (**3**) ont été synthétisés à partir des complexes arènes dichlorures [(η^6-arène)$RuCl_2$]$_2$ par échange avec les anions iminophosphonamide, qui ont été engendrés *in situ* par déprotonation d'aminoiminophosphoranes (**1**). A leur tour, les composés **1** ont été obtenus par monodéprotonation de sels diaminophosphonium (**2**) synthétisés par condensation de Kirsanov à partir de sels de bromophosphonium engendrés *in situ* avec des amines primaires. Un schéma général de la synthèse est résumé dans le Schéma 1.

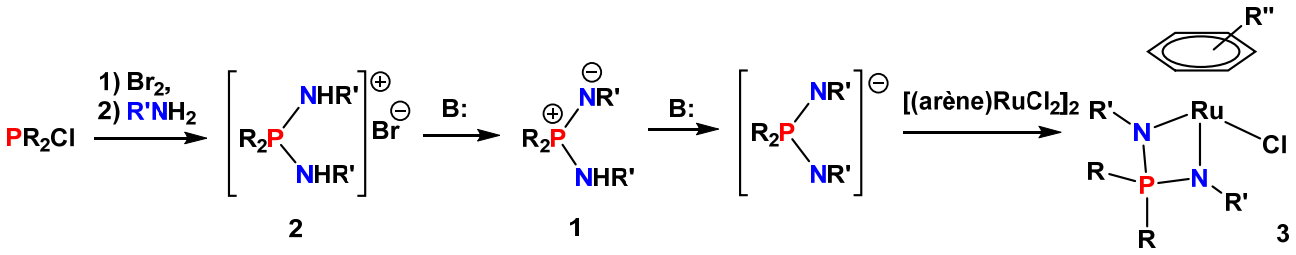

Schéma 1. Synthèse des complexes NPN arènes ruthénium **3**.

Les aminoiminophosphoranes **1a-e** avec différents substituants sur les atomes d'azote et de phosphore ont été utilisés en tant que précurseurs des ligands NPN (Figure 1).

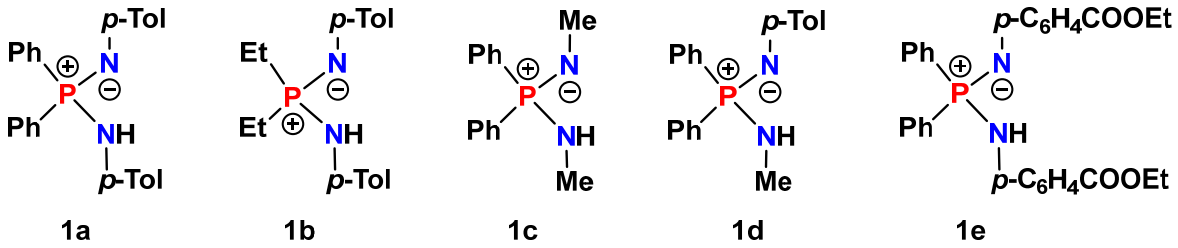

Figure 1. Aminoiminophosphoranes 1a-e.

La synthèse de **1a-c,e** a été réalisée à partir des sels de diaminophosphonium **2a-c,e.** Il faut noter que l'aminoiminophosphorane **1d,** asymétrique par rapport à la substitution des atomes d'azote (R'= Me/*p*-Tol), a été synthétisé en une seule étape contournant la formation du sel de diaminophosphonium (Schéma 2).

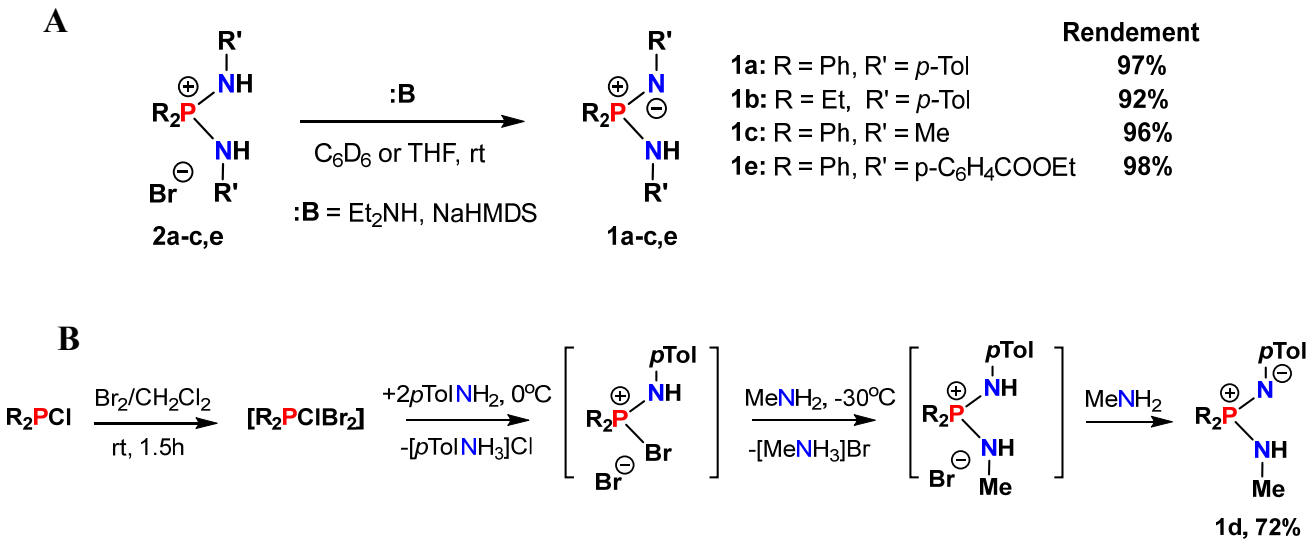

Scheme 2. (**A**) Synthèse des aminoiminophosphoranes **1a-c,e** et (**B**) aminoiminophosphorane **1d.**

Les anions iminophosphonamides $[R_2P(NR')(NR'')]^-N$, engendrés *in situ* par la réaction de **1a-e** avec base (NaHMDS, Et_2NH), réagissent avec les complexes dimères de ruthénium $[(\eta^6\text{-}C_6Me_6)Ru(\mu\text{-}Cl)Cl]_2$ et $[(\eta^6\text{-}p\text{-Cymene})Ru(\mu\text{-}Cl)Cl]_2$ pour fournir les complexes à 18 électrons (18e) ruthénium hexaméthylbenzène (**3a-d**) et *p*-cymène (**3e,f**) correspondants avec le ligand chélatant bidentate **NPN** (Schéma 3).

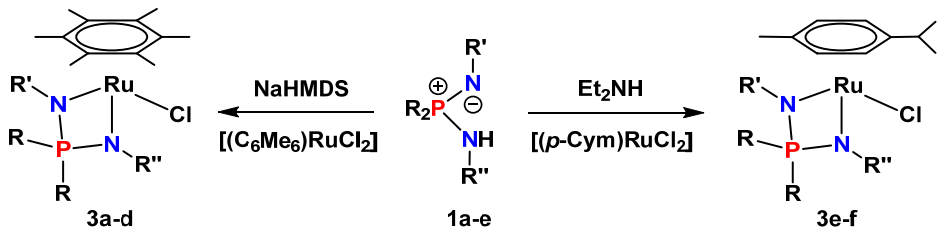

		Rendement
3a:	R = Ph, R' = R'' = *p*-Tol, Rx = C_6Me_6	**86%**
3b:	R = Et, R' = R'' = *p*-Tol, Rx = C_6Me_6	**73%**
3c:	R = Ph, R' = R'' = Me, Rx = C_6Me_6	**62%**
3d:	R = Ph, R' = Me, R'' = *p*-Tol, Rx = C_6Me_6	**77%**
3e:	R = Ph, R' = R'' = *p*-$C_6H_4CO_2Et$, Rx = *p*-Cym	**93%**
3f:	R = Ph, R' = R'' = *p*-Tol, Rx = *p*-Cym	**88%**

Schéma 3. Synthèse des complexes NPN chlorures de ruthénium à 18e **3a-f.**

Le ligand chlorure dans **3a-c** a été facilement échangé avec des anions non-coordinants (PF_6^-, BF_4^-) par traitement avec les sels de sodium correspondants dans le dichlorométhane pour fournir les nouveaux complexes cationiques à 16 électrons (16e) **4a-c** avec un rendement presque quantitatif. De toute évidence, le replacement de C_6Me_6 dans **3a** par le *p*-cymène conduit au renforcement de la liaison Ru-Cl, car l'abstraction de l'anion chlorure dans le complexe **3f** a lieu seulement par l'action d'un sel soluble d'argent avec formation du complexe cationique **4f** (Schéma 4). Tous les complexes de ruthénium à 18 et 16 électrons ont été caractérisés par spectroscopie RMN et analyse élémentaire. Leurs structures moléculaires ont été confirmées par études cristallographiques au rayons-X sur monocristal.

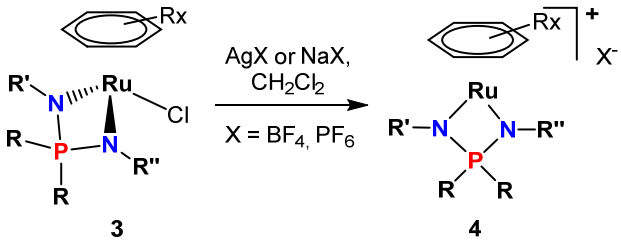

				Yield
4a:	R = Ph, R' = R'' = *p*-Tol,	Rx = C_6Me_6,	X = PF_6	**96%**
4b:	R = Et, R' = R'' = *p*-Tol,	Rx = C_6Me_6,	X = BF_4	**93%**
4c:	R = Ph, R' = R'' = Me,	Rx = C_6Me_6,	X = PF_6	**96%**
4f:	R = Ph, R' = R'' = *p*-Tol,	Rx = *p*-Cymene,	X = PF_6	**91%**

Schéma 4. Synthèse de complexes NPN cationiques de ruthénium à 16e **4a-c,f.**

1.2. Structures des complexes NPN arènes ruthénium.

Structure moléculaire. Les complexes **NPN** à 18e **3a-f** montrent une géométrie de type « tabouret de piano » à trois pattes avec une configuration pseudo-octaédrique des ligands autour de l'atome de ruthénium : trois sites de coordination occupés par le η^6-arène, deux par le ligand chélate κ^2-NPN et un par le ligand chlorure (Figure 2). Les complexes cationiques à 16e **4a-c,f** montrent comme attendu une une géométrie « tabouret de piano » à deux pattes avec le ligand chélatant **NPN** positionné de manière presque perpendiculaire au cycle arène (Figure 3).

La distance Ru-arène (centroïde) dans les deux types de complexes se trouve dans la plage 1.652 – 1.675 Å, ce qui est inhabituel pour des complexes « half-sandwich » arènes de ruthénium neutres à 18e et cationiques à 16e avec ligands κ^2-N,N. Les distances Ru-N moyennes (2.14 – 2.16 Å) pour les complexes à 18e **3** sont significativement plus longues que dans les complexes cationiques à 16e **4** (2.02 – 2.04 Å), alors que pour les complexes similaires arènes amidinates de ruthénium, cette différence est moindre. La nature du

ligand arène influence la longueur de la liaison Ru-Cl (2.428 – 2.445 Å dans **3a-d** et 2.411 – 2.415 Å dans les complexes de *p*-cymène **3e,f**). Le raccourcissement de la liaison Ru-Cl indique le probable renforcement de la liaison, comme également mis en évidence par la réactivité moindre vis-à-vis de la dissociation de l'ion chlorure dans la synthèse de **4f**.

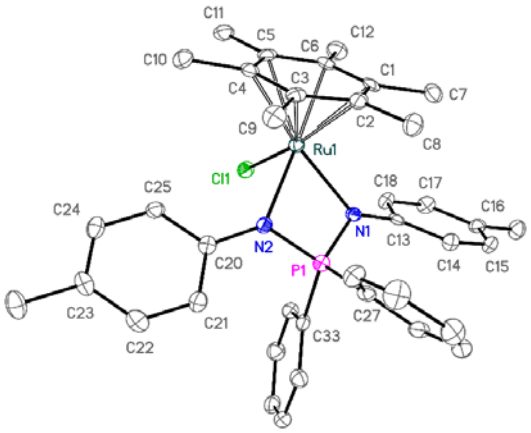

Figure 2. Structure du complexe **3a**.

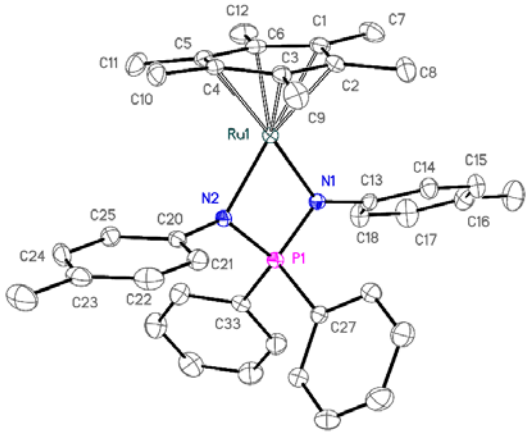

Figure 3. Structure du complexe **4a**.

La géométrie du métallacycle à quatre chaînons RuNPN est une caractéristique structurale importante de ces complexes iminophosphonamides. Pour les complexes **3a-f** et **4a-c,f**, ce cycle dévie légèrement de la planéité avec un angle de pliement α = 0.5 – 13.8°, ce qui est très différent du pliement important jusqu'à α = 40° observé pour les complexes amidinate à 16 électrons.

Structure électronique. La planéité du métallacycle et la liaison Ru-N raccourcie dans le complexes iminophosphonamide arène ruthénium à 16e **4a-c,f**, ainsi que leur plus forte stabilité, indiquent une stabilisation de l'atome de ruthénium électroniquement insaturé grâce à la π-donation additionnelle par les atomes d'azote du ligand. L'orbitale haute occupée (HOMO) du ligand **NPN** zwitterionique peut avoir une symétrie C_{2v} ou C_s. Dans le dernier cas elle peut transférer sa densité électronique π à l'orbitale d_{xz} du métal localisée dans le plan du ligand (Figure 4A) de manière efficace. En revanche, la symétrie C_{2v} de la HOMO du ligand amidinate permet la donation π uniquement par coordination latérale du ligand amidinate, résultant en un repliement important du métallacycle à quatre chaînons (Figure 4B). En effet, les complexes **NCN** ruthénium électroniquement insaturés peuvent être stabilisés par coordination π intramoléculaire du ligand amidinate, conduisant

au pliement important du metallacycle Ru–N–C–N. La coordination latérale du ligand amidinate stabilise ces complexes à 16e de manière inefficace car elle affaiblit les liaisons M–N σ; ces complexes sont très réactifs.

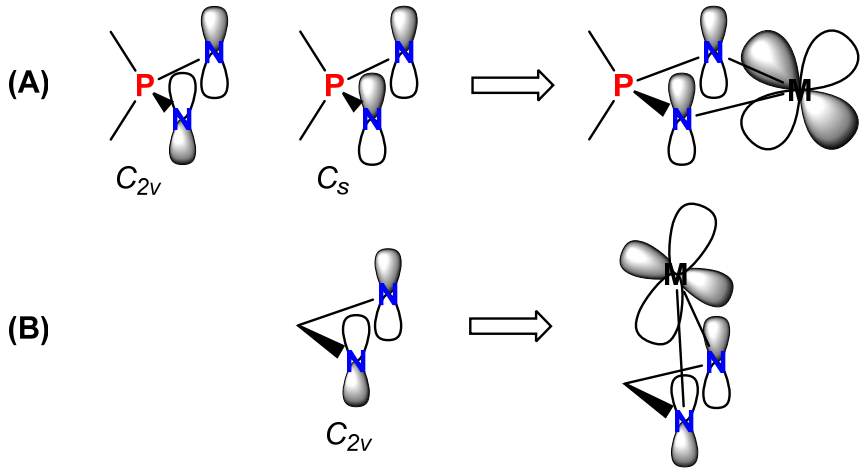

Figure 4. Dessin schématique des HOMO des ligands (**A**) **NPN** et (**B**) **NCN** (à gauche); interactions possibles π avec les orbitales d du métal (à droite).

Dans les spectres UV-vis, les complexes **4a-c,f** à 16e montrent une bande large d'intensité moyenne avec λ_{max} = 540 – 590 nm, qui est déplacée vers les énergies plus faibles par rapport aux complexes à 18ē correspondants **3a-c,f** (bande avec λ_{max} = 430 – 450 nm). Un tel déplacement vers des longueurs d'onde plus grandes est caractéristique des transitions de 18- à 16-électrons pour les complexes. Dans les complexes à 18ē **3a-b,f** les substituants du ligand arène et de l'atome de phosphore n'affectent pas la position de la bande d'absorption des spectres UV-vis (450 nm). Seuls les groupements Me fortement donneurs sur les atomes d'azote de **3c** déplacent légèrement λ_{max} vers des plus grandes énergies (430 nm). En même temps, seule la nature du ligand arène est primordiale pour la position de cette bande dans les complexes NPN à 16e **4a-c,f**. Le remplacement du fragment C_6Me_6 par le *p*-cymène entraîne un déplacement notable de la bande d'absorption vers les énergies plus faibles ($\Delta\lambda_{max}$ = 40-50 nm).

D'après des résultats de modélisations réalisées par la théorie de la fonctionnelle de densité (DFT)[4] pour **3a**, **3f**, **4a** et **4f** en phase gaz avec la fonctionnelle PBE et des fonctions de base def2-TZVP, la bande d'absorption à longueur d'onde plus grande pour les

[4] The calculation was carried out by Dr. Oleg A. Filippov (INEOS RAS, Moscow).

complexes NPN arène de ruthénium à 16e est attribuée à une transition *d-d**. La HOMO est située à des énergies proches (-7.4 eV en phase gaz et -5.1 eV dans le CH_2Cl_2) pour les complexes **4a** et **4f**. Pour ces deux complexes, l'orbitale basse vacante (LUMO) est une combinaison de l'orbitale vide d_{yz} de l'atome de ruthénium et de l'orbitale occupée π B_2 du ligand arène, dont l'énergie dépend du pouvoir donneur de l'arène. Il en résulte que l'énergie de la LUMO et, par conséquent, la $\Delta E = E_{LUMO} - E_{HOMO}$, est plus faible de 0.4 eV pour **4f** que pour **4a**.

1.3. Echange de ligands pour les complexes iminophosphonamide arène ruthénium.

*Dissociation du ligand chlorure pour les complexes **3** à 18e.*

La dissociation pour les complexes **3** en solution, avec formation des complexes cationiques $[\mathbf{4}]^+Cl^-$ (Schéma 5), a été étudiée par spectroscopies RMN et UV-vis.

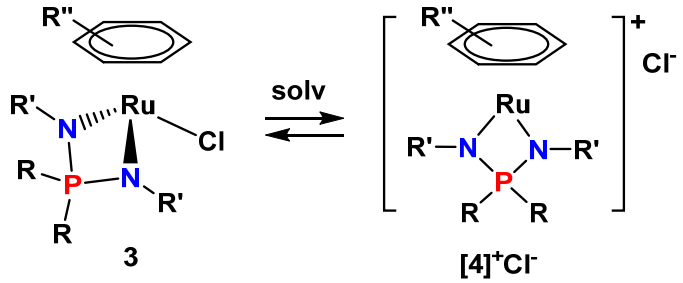

Schéma 5. Dissociation du chlorure dans les complexes **3**.

La position de l'équilibre dépend de la polarité du solvant et de la température. Elle peut être déterminée à partir du déplacement chimique de la résonance de l'atome de phosphore dans le spectre RMN $^{31}P\{^1H\}$ des complexes **3** vers les plus faibles fréquences par rapport au déplacement du même signal dans le solvant apolaire C_6D_6. Les substituants donneurs sur les atomes d'azote facilitent la dissociation. La dissociation est observée même dans le solvant moyennement polaire CD_2Cl_2 pour le complexe **3c** contenant le ligand NPN fortement donneur substitué à l'azote par les groupements méthyles, alors qu'elle est évidente seulement dans des solvants fortement polaires tels le méthanol et le nitrométhane pour les complexes **3a,b**. Les spectres RMN ^1H et $^{13}C\{^1H\}$ dans le $CDCl_3$ et le CD_2Cl_2 des composés **3a-d,f** montrent seulement un jeu de signaux pour les deux substituants chimiquement inéquivalents R_a et R_b sur l'atome de phosphore (Figure 5).

Apparemment, un échange rapide entre les deux substituants au phosphore a lieu dans les solvants polaires. Dans le cas du complexe **3e** uniquement, contenant les plus forts substituants accepteurs sur les atomes d'azote, deux jeux de signaux ont été observés pour les phényles dans le $CDCl_3$. Par ailleurs, ces signaux sont élargis pas le phénomène dynamique d'échange.

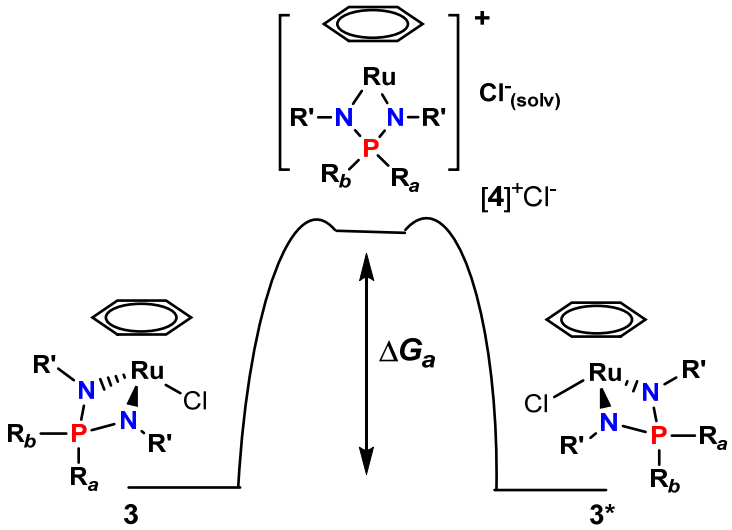

Figure 5. L'échange entre les positions R_a et R_b résultant de la dissociation de la liaison Ru-Cl.

L'échange des positions des substituants R_a et R_b dans les complexes **3** a été étudié par la méthode de spectroscopie RMN 2D ^{1}H EXSY. La constante de vitesse et l'enthalpie libre d'activation $\Delta G_{ex}^{\neq}$ de l'échange ont été calculées à partir des intensités intégrées des pics croisés et diagonaux. Les paramètres d'activation du processus d'échange ($\Delta H_{ex}^{\neq}$, $\Delta S_{ex}^{\neq}$) ont été obtenus à partir de la dépendance de la constante de vitesse k_{ex} en fonction de la température (Figure 6).

Pour **3b-d**, cet échange est observable même dans des solvants apolaires (benzène, toluène). Pour **3b**, les paramètres d'activation du processus d'échange ont été obtenus à partir de la dépendance de la constante de vitesse de l'échange en fonction de la température (k_{ex}) dans le toluène-d_8 dans la plage 230 – 315 K grâce à l'équation de Eyring : $\Delta H^{\neq}_{ex}$ = 8.4±0.2 kcal/mol et $\Delta S^{\neq}_{ex}$ = -29±1 cal/(mol•K) (Figure 27B). La valeur négative et grande de l'entropie d'activation met en évidence un état de transition du processus d'échange hautement ordonné, qui résulte de la nécessité de réorganiser les dipôles des molécules de solvant pour la solvatation non-spécifique de l'ion chlorure chargé. La

constante de vitesse k_{ex} observée pour **3b** (1.6 s^{-1} pour des solutions dans le toluène-d_8 à 295 K) est indépendante de la concentration du complexe dans la plage 8–40 mM, ce qui est en accord avec un processus dissociatif.

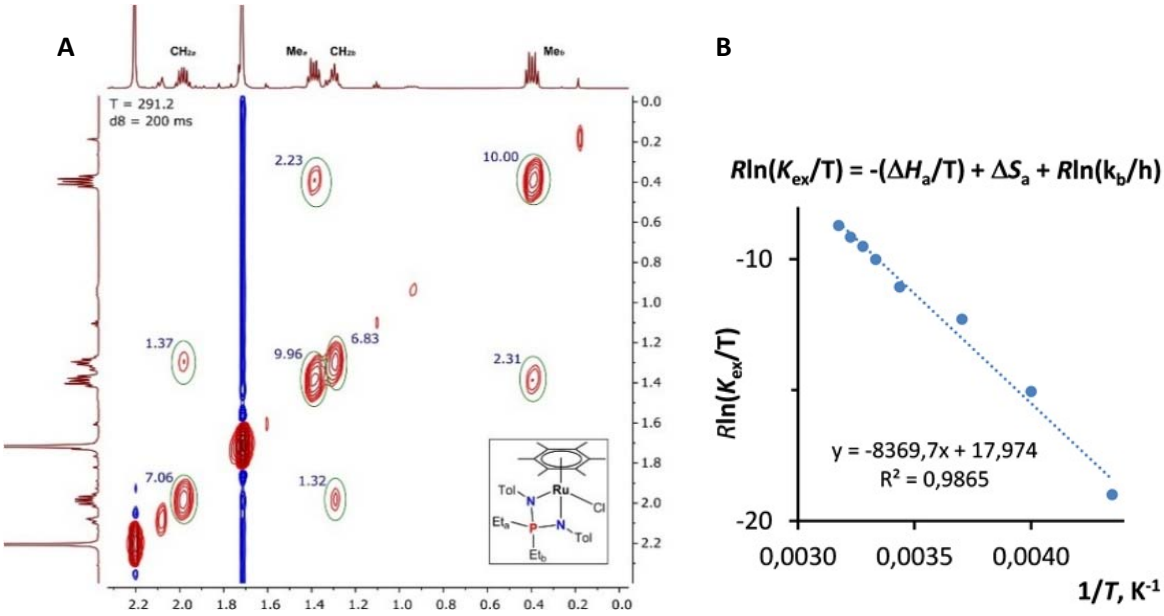

Figure 6. (**A**) RMN 2D EXSY ^{1}H de [(η^6-C_6Me_6)RuCl{Et_2P(N-p-Tol)$_2$}] (**3b)** dans le toluène-d_8 à 293 K avec un temps de mélange de t_{mix} = 200 ms; (**B**) représentation graphique des données $RlnK_{ex}$ vs 1/T.

Le complexe **3c** donne lieu à une dissociation trop favorable dans le benzène (k_{ex} > 100 s^{-1}) pour l'application de la même approche. La constante k_{ex} pour ce complexe a donc été obtenue à partir de la température de coalescence (T_c) des signaux *o*-H des substituants phényles sur l'atome P (T_c = 328 ± 5K). Les complexes **3a**, **3e**, et **3f** sont caractérisés par des vitesses de dissociation plus faibles (k_{ex} <0.1 s^{-1}) que la limite de la technique RMN. Les enthalpies d'activation du processus d'échange, $\Delta H_{ex}^{\neq}$, ont été calculées dans l'hypothèse que l'entropie d'activation, $\Delta S_{ex}^{\neq}$, soit similaire pour tous les complexes **3**, ce qui semble justifié car la contribution principale est la solvatation de l'ion chlorure. Avec un degré de confiance raisonnable, il est possible de faire l'hypothèse que l'enthalpie d'activation $\Delta H_{ex}^{\neq}$ est proche de l'enthalpie de dissociation thermodynamique de la liaison Ru–Cl, ΔH_d. En conséquence, il est possible d'établir la série d'enthalpies de dissociation pour tous les complexes chlorures: **3e** > **3a**, **3f** (>10 kcal/mol) > **3b** (8.4 kcal/mol) > **3d** (7.9 kcal/mol) > **3c** (5.7 kcal/mol). En conclusion, l'étude RMN a montré que la tendance

des complexes NPN de ruthénium à dissocier le ligand chlorure augmente avec l'introduction de substituants donneurs sur les atomes de phosphore et azote.

L'équilibre de dissociation des complexes **3b-c** (Scheme 5) a été étudié dans des solvants de polarité différente par l'utilisation de la spectroscopie UV-visible. Les complexes **3** et **4** diffèrent par la position d'une bande d'absorption : $\Delta\lambda$ = 70-140 nm. La diminution de la température déplace l'équilibre (Scheme 5) vers la forme dissociée. A partir de la dépendance de la constante de dissociation de la température (190-298K) pour le composé **3c**, l'enthalpie et l'entropie standards du processus de dissociation ont été calculées avec l'équation de van't Hoff (ΔH_d = -5.0±0.2 kcal/mol, ΔS_d = -27±1 cal/(mol•K)) (Figure 7). La valeur étrangement négative et large de la variation de l'entropie pour ce processus de dissociation est attribuée à la nécessité de réorganiser les dipôles des molécules de solvant autour des espèces chargées qui se forment suite à la dissociation. Pour le composé **3b**, la dissociation a été observée seulement dans le solvant nitrométhane, très polaire : ΔH_d = 3.5±0.2 kcal/mol, ΔS_d = 0.3±0.6 cal/(mol•K).

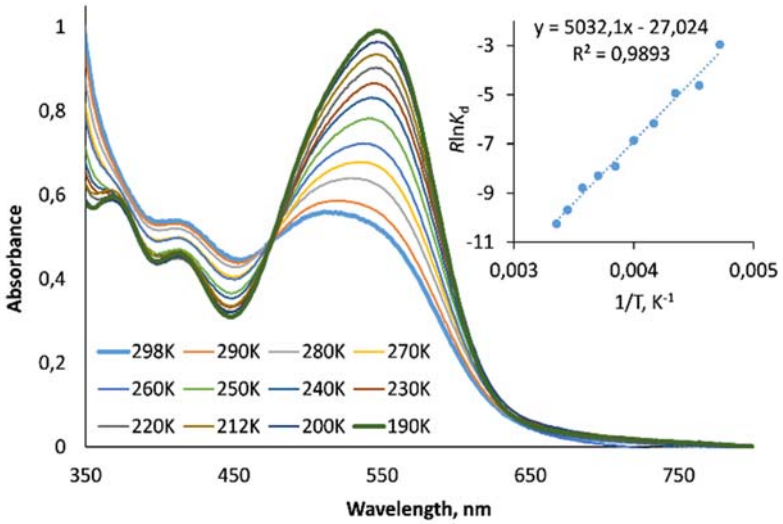

Figure 7. Spectres UV-vis de **3c** dans le CH_2Cl_2 à 298-190K.

Enfin, les données spectroscopiques UV-vis confirment les conclusions faites sur la base des données des études RMN, c'est-à-dire que la dissociation de la liaison Ru-Cl pour les complexes iminophosphonamides arènes **3a-f** est favorisée par les substituants donneurs sur les atomes d'azote et par les solvants à plus forte polarité. Le complexe **3c** avec le ligand NPN le plus donneur est capable de dissocier complètement dans le dichlorométhane à basse température.

*Coordination de ligands extérieurs aux complexes cationiques **4** à 16e.*

Les complexes NPN cationiques **4** sont formellement électroniquement insaturés (16e). En revanche, comme le ligand NPN peut agir en tant que donneur de 4 ou de 6 électrons, une compensation de la lacune de densité électronique du métal est possible grâce à une donation π additionnelle. Dans la section précédente, nous avons montré que même l'anion chlorure des complexes **3** peut se dissocier assez facilement. Dans cette section, les études du pouvoir coordinant de différents ligands neutres (L = MeCN, Py, et CO) vis-à-vis des complexes de ruthénium à 16e **4** pour former des complexes cationiques à 18e [(arène)Ru(NPN)(L)]$^+$, [**4**(L)], (un exemple est donné pour le complexe **4a** dans le schéma 29) sont détaillés. Les trois ligands L sélectionnés sont des donneurs σ à 2e avec des pouvoirs π-acides significativement différents : MeCN < Py < CO. L'interaction avec des ligands fortement σ-donneurs et faiblement π-accepteurs, c'est à dire acétonitrile et pyridine, a été étudiée par spectroscopies UV-vis et RMN.

A température ambiante, les complexes avec acétonitrile et pyridine sont stables uniquement en présence d'un fort excès (10-100 equiv.) du ligand et les constantes d'addition sont $K_c \sim 2$ (**4a·MeCN**) and $K_c \sim 37$ (**4a·Py**). A températures faibles, dans le cas de la pyridine, l'équilibre est déplacé complètement vers l'adduit **4a·Py** à 18e, même en l'absence d'un excès notable de pyridine (Figure 8). L'enthalpie ΔH_c (-12.4±0.5 kcal/mol) et l'entropie ΔS_c (-36±2 cal/(mol•K)) de la réaction de complexation ont été obtenues à partir de la variation de K_c avec la température.

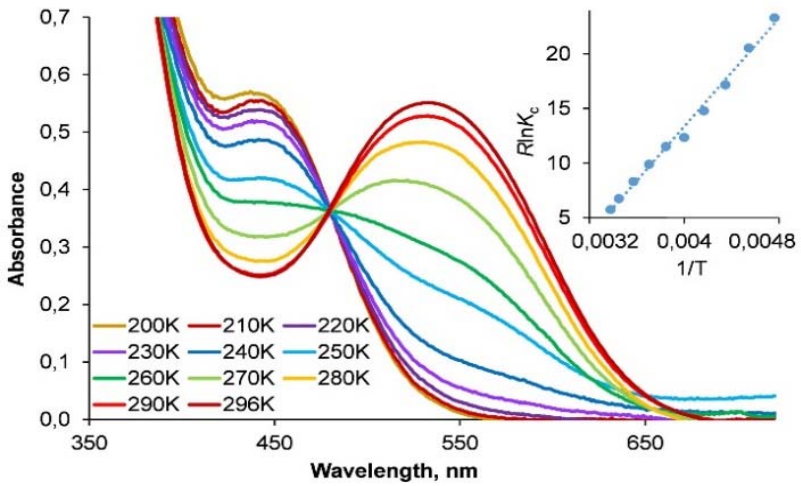

Figure 8. Spectres UV-vis de **4a** en présence de Py (1:2) dans le CH_2Cl_2 à 200-296 K. Le graphe dans le cadre montre la variation de $RlnK_c$ avec 1/T.

En comparaison avec l'acétonitrile et la pyridine, le monoxyde de carbone est un accepteur π plus fort. Il réagit facilement avec **4a,f** pour donner les adduits à 18e **5a,f** stables. La réaction est quand même réversible et une décoordination de CO aisée a lieu par évaporation du solvant pour redonner **4a,f**. Néanmoins, les produits **5a,f** ont pu être isolés par précipitation à partir des solutions dans le CH_2Cl_2 par addition d'un excès de diéthyl éther. Même si **5a** et **5f** dégagent du CO lentement à l'état solide sous vide, des analyses élémentaires satisfaisantes ont pu être obtenues pour les deux produits et leurs structures ont été établies par diffraction des rayons-X (Figure 9).

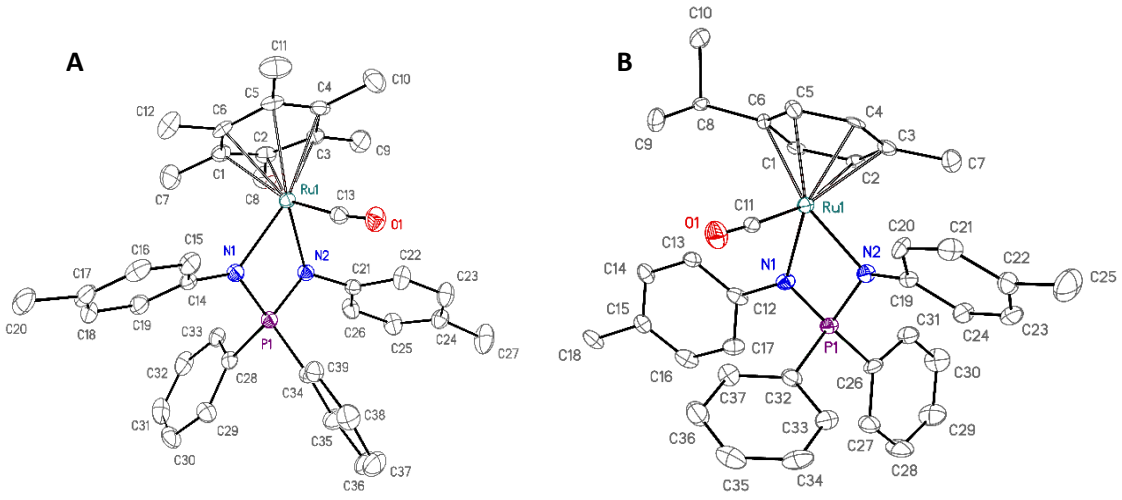

Figure 9. Structures des complexes cationiques carbonyles **5a** (**A**) et **5f** (**B**). Distances (Å) et angles (°) de liaisons sélectionnés :
$[(\eta^6\text{-}C_6Me_6)Ru(CO)\{Ph_2P(N\text{-}p\text{-}Tol)_2\}]^+PF_6^-$ (**5a**): Ru-C_6Me_6(centroïde) 1.769(1), Ru-C(O) 1.871(3), Ru-N_1 2.112(2), Ru-N_2 2.116(2), C-O 1.145(3), N_1-Ru-N_2 69.20(9), Ru-N_1-P-N_2 164.60(15), $\Sigma(N_1)$ 348.3(5), $\Sigma(N_2)$ 359.3(5), Ru-C_{13}-O_1 174;
$[(\eta^6\text{-}p\text{-cymène})Ru(CO)\{Ph_2P(N\text{-}p\text{-}Tol)_2\}]^+PF_6^-$ (**5f**): Ru-*p*-cymène(centroïde) 1.768(3), Ru-C(O) 1.879(9), Ru-N_1 2.095(7), Ru-N_2 2.120(6), C-O_1.145(10), N_1-Ru-N_2 68.9(3), Ru-N_1-P-N_2 165.8(4), $\Sigma(N_1)$ 353.7(13), $\Sigma(N_2)$ 355.3(14), Ru-C_{11}-O_1 176.

Les complexes **5a** et **5f** sont les premiers dérivés arènes carbonyles de ruthénium avec n'importe quel type de ligand κ^2-N,N-anionique chélatant caractérisés par diffraction des rayons-X. Les deux complexes montrent une géométrie « tabouret de piano » à trois pattes avec une configuration pseudo-octaédrique des ligands et une géométrie linéaire

pour la fonction Ru-C-O (angle de liaison de 174 – 176°), typique des ligands carbonyles liés par le mode terminal. Les deux produits donnent lieu à des bandes intenses de vibrations d'élongation CO dans le spectre IR à 1984 cm^{-1} (**5a**) et 2012 cm^{-1} (**5f**). La fréquence ν_{CO} plus élevée pour **5f** met en évidence une rétrodonation π Ru→CO plus faible par rapport à **5a** à cause du pouvoir donneur différent des deux ligands arènes. Ces fréquences sont substantiellement inférieures par rapport à celles des complexes arènes carbonyles de ruthénium avec des ligands amidinates électroniquement plus pauvres, [(η^6-C_6H_6)Ru(CO){$PhC(N^tBu)_2$}](BAr^F_4) (2050 cm^{-1}), mais proches de celles des complexes arènes carbonyles de ruthénium avec des ligands dianioniques dithiolates, [(η^6-C_6Me_6)Ru(CO)($S_2C_6H_4$)] (ν_{CO} = 1951 cm^{-1}), [(η^6-C_6Me_6)Ru(CO)$(SXyl)_2$] (ν_{CO} = 1965 cm^{-1}) et de celle du complexe cyclopentadiényle avec le ligand κ^2-N,N neutre TMEDA, [(η^5-C_5H_5)Ru(CO)(TMEDA)](BAr_4) (ν_{CO} = 1968 cm^{-1}). Ceci indique les propriétés intermédiaires des ligands NPN en tant que donneurs d'électrons entre les ligands monoanioniques et dianioniques, ce qui est en bon accord avec leur structure zwitterionique.

De manière surprenante, un barbotage de CO dans la solution de **4c** engendre un produit stable, **5c'**, résultant de l'addition de deux molécules de CO, dont une s'est insérée dans l'une des deux liaisons Ru–N pour donner lieu à un métallacycle carbamoyle. Le produit **5c'** a été complètement caractérisé, y compris par diffractométrie aux rayons-X sur monocristal (Figure 10).

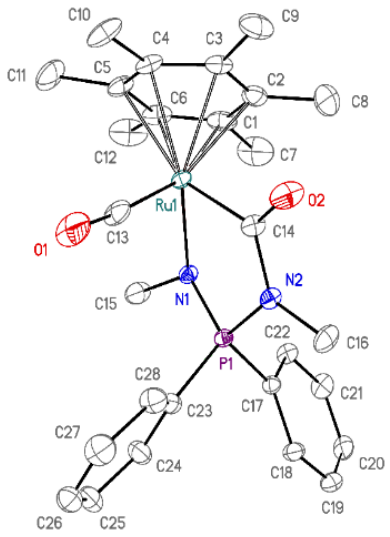

Figure 10. Structure du cation [(η^6-C_6Me_6)Ru(CO){$(CONMe)Ph_2P(NMe)$}]$^+PF_6^-$(**5c'**). Longueurs (Å) et angles (°) de liaison sélectionnés : Ru-C_6Me_6 (centroïde) 1.828(1), Ru-N_1 2.107(2), Ru-C(O)N 2.042(3), C=O 1.211(4), N-C(O) 1.414(3), Ru-C(O) 1.859(3), C-O 1.143(4), N_1-Ru-C(O) 83.15(10), Σ(N_1) 349.7(5), Σ(N_2) 359.3(6), Ru-C_{13}–O_1 176 .

Le spectre RMN $^{13}C\{^1H\}$ de **5c'** révèle deux signaux correspondant à des noyaux C de type carbonyle : un singulet à δ 198.2 et un doublet à δ 192.8 ($^2J_{CP}$ = 19.6 Hz). Tous les substituants sur les atomes de N et P dans **5c'** sont inéquivalents et donnent lieu à deux jeux de signaux pour les groupements méthyles et phényles dans les spectres ^1H et $^{13}C\{^1H\}$. Le spectre IR de **5c'** montre deux bandes carbonyles fortes à 1984 cm^{-1} (CO lié au métal) et à 1644 cm^{-1} (C=O carbamoyle), dont la deuxième est typique des amides organiques.

D'après l'étude IR (233–298 K), la carbonylation de **4c** est une réaction en deux étapes comportant un premier stade réversible (Schéma 6). Le monoadduit **5c** formé initialement n'est stable qu'à basse température et se dismute en complexe carbonyle-carbamoyle **5c'** et complexe **4c** initial quand il est chauffé à température ambiante.

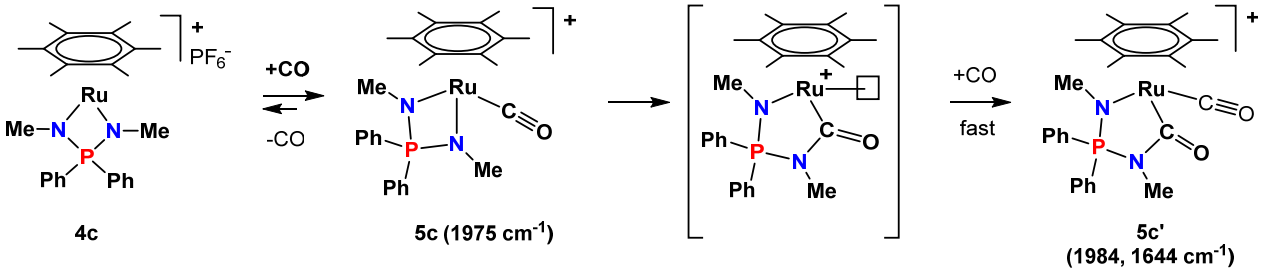

Scheme 6. Réaction de **4c** avec le monoxide de carbone dans CH_2Cl_2.

En conclusion, dans cette première partie du travail, deux séries de nouveaux complexes iminophosphonamides arènes de ruthénium à 18e et 16e ont été synthétisés, pour dix d'entre eux la structure a été confirmée et analysée par diffraction des rayons-X, le processus d'échange de ligand entre complexes à 18 et 16 électrons a été étudié, et la structure de trois complexes arènes carbonyles cationiques de ruthénium a été confirmée. Ces derniers sont les premier exemples de complexes arènes carbonyles cationiques avec un ligand κ^2-N,N. Les caractéristiques structurales des complexes NPN de ruthénium à 18 et 16 électrons, la stabilité accrue des complexes à 16e, ainsi que les fréquences de vibration du groupement terminal CO sont en accord avec la structure zwitterionique du ligand NPN. Ce ligand semble être un donneur σ et π très fort, capable de donner soit 4e ou 6e et rentre en compétition de manière efficace avec des ligands extérieurs pour fournir de la densité électronique supplémentaire à l'ion métallique insaturé, afin de stabiliser les complexes pauvre en électrons.

2. Etude de l'activité catalytique des complexes 3 et 4 en hydrogénation de l'acétophénone par l'isopropanol.

Les complexes iminophosphonamides arènes de ruthénium neutres (chlorures, **3**) et cationiques (**4**) ont été testés en tant que catalyseurs en hydrogénation par transfert d'une cétone modèle (l'acétophénone à 1-phényléthanol) par l'isopropanol (Schéma 7).

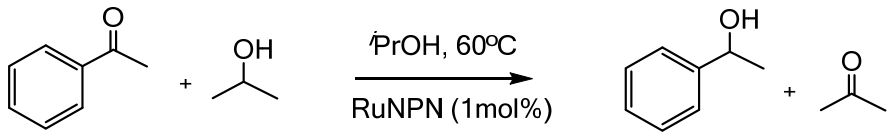

Schéma 7. Hydrogénation par transfert de l'acétophénone par l'isopropanol avec des complexes NPN arènes de ruthénium.

D'abord, ce processus a été étudié en détail pour le complexe **3f**, car les spectres RMN permettent l'identification aisée des signaux CH α et β (substituants méthyle et isopropyle) du fragment *p*-cymène, ce qui est pratique pour l'identification des intermédiaires impliqués dans le cycle catalytique. Le complexe **3f** montre une faible activité dans cette réaction à 60°C (TOF = 7 h^{-1}), mais celle-ci augmente suite à l'addition d'une base forte, le NaHMDS (TOF = 78 h^{-1}). Le mécanisme de cette réaction a été étudié en détails par l'utilisation de réactions modèles avec suivi RMN et par des études cinétiques.

2.1. Etudes du mécanisme de la réduction de l'acétophénone catalysée par 3f.

Expériences modèles. Le complexe **3f** ne réagit par avec l'isopropanol à température ambiante, mais il est converti en complexe hydrure [(*p*-Cymene)RuH{Ph_2P(N-*p*-Tol)$_2$}] (**6f**) lentement à 60°C, réaction qui est accompagnée par une décomposition partielle en oxyde de phosphine, Ph_2P(O)NHTol (PO) et en aminoiminophosphorane (NPNH, **1a**). Le complexe **6f** (δ 33.1 en RMN $^{31}P\{^1H\}$ et δ -3.1 en RMN ^1H) est engendré sélectivement par traitement de **3f** avec un équivalent d'une base forte (NaHMDS) dans l'isopropanol (Schéma 8). Un suivi de cette réaction par RMN $^{31}P\{^1H\}$ montre la présence d'un intermédiaire caractérisé par une résonance à δ 38.5. Dans le spectre RMN ^1H, ce composé montre des signaux proches de ceux de **3f**. Il est provisoirement attribué au complexe

isopropopanolate [(η^6-*p*-cymene)Ru(O^{i}Pr){Ph_2P(N-*p*-Tol)$_2$}] (**7f**). Cet intermédiaire s'accumule dans les premières minutes, puis se convertit complètement en complexe hydrure **6f** par élimination β-H de l'acétone en 30 min (Figure 11).

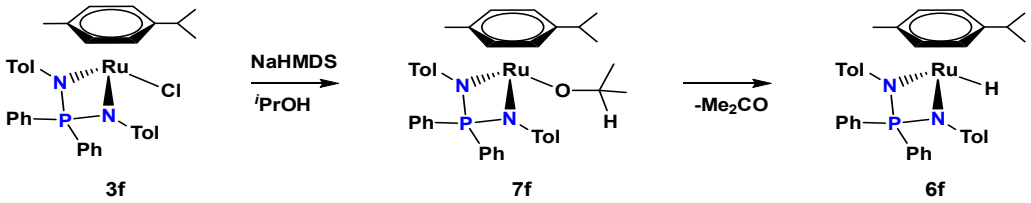

Scheme 8. Génération du complexe arène hydrure **6f.**

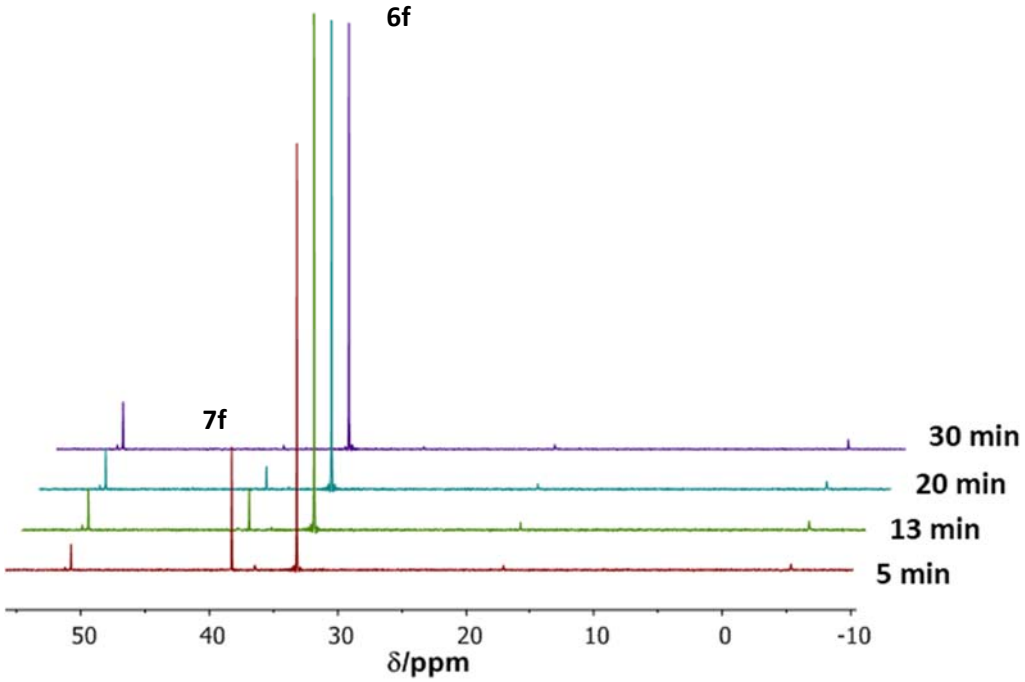

Figure 11. Suivi RMN $^{31}P\{^1H\}$ de la génération de **6f** dans le mélange C_6D_6/^{i}PrOH à température ambiante.

Une tentative préparatoire visant à isoler **6f** par évaporation de la solution d'isopropanol, suivie par dissolution dans le C_6D_6, conduit à son isomérisation pour donner un mélange de complexes cyclohexadiényles isomériques **8f** et **8f'**, caractérisés par des signaux RMN $^{31}P\{^1H\}$ à δ 50.6 et 51.1 (Schéma 9). Ces nouveaux complexes sont toujours présents en mélange avec le complexe **6f** initial. Ils ont été caractérisés par spectroscopie RMN ^1H, $^{31}P\{^1H\}$ et $^{13}C\{^1H\}$ NMR. La structure du complexe cyclohexadiényle a été confirmée par diffraction des rayons-X sur monocristal (Figure 12).

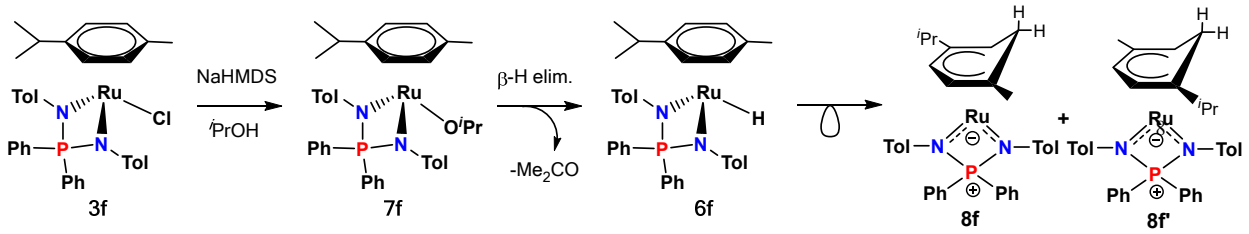

Scheme 9. Réarrangement du complexe hydrure **6f** en complexes cyclohexadiényles **8f** et **8f'** pendant les tentatives d'isolation de **6f**.

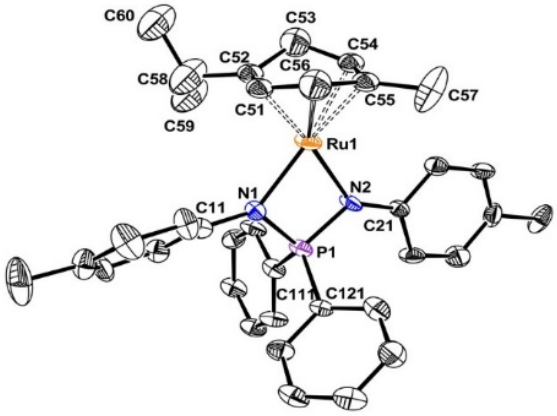

Figure 12. Structure moléculaire des complexes cyclohexadiényles. La structure moyenne illustrée résulte du désordre de composition entre les isomères **8f** et **8f'** (1:1).

La génération du complexe hydrure **6f** par une méthode alternative (**3f** et $NaBHEt_3$ dans le C_6D_6 pur, sans aucun ^{i}PrOH), conduit encore une fois au mélange du complexe hydrure **6f** (65%) et des complexes cyclohexadiényles **8f**/**8f'** (35%) et, au fil du temps, la fraction des complexes cyclohexadiényles augmente à 60%. Probablement, dans un solvant apolaire, **6f** est moins stable qu'en présence d'isopropanol et se convertit rapidement en **8f** et **8f'**.

L'isomérisation de **6f** en **8f**, **8f'** dans un solvant apolaire (benzène, toluène) est soit irréversible, ou alors le processus réversible est très lent à l'échelle de temps de la RMN. Ceci est suggéré par les études RMN 2D ^{1}H EXSY réalisées dans le C_6D_6 et dans le toluène-d_8 dans la plage de températures 25 – 80°C, qui ne révèlent aucun pic hors diagonale entre la résonance de l'hydrure de **6f** (δ ^{1}H à -3.04) et la résonance du groupement méthylène de l'isomère cyclohexadienyle **8f** (δ ^{1}H à 2.67). D'après le spectre RMN ^{31}P{^{1}H}, lorsque le mélange **6f**/(**8f**+**8f'**) (35/65) est chauffé de 25°C à 80°C, les complexes cyclohexadiényles,

thermodynamiquement plus favorables, s'accumulent jusqu'à environ 84%. Ensuite, lorsque ce mélange est refroidi à température ambiante, le rapport molaire obtenu à haute température ne change pas (Figure 13). Par conséquent, les complexes cyclohexadiényles sont thermodynamiquement plus favorables et leur transformation inverse en **6f** doit transiter par un état de transition à énergie élevée.

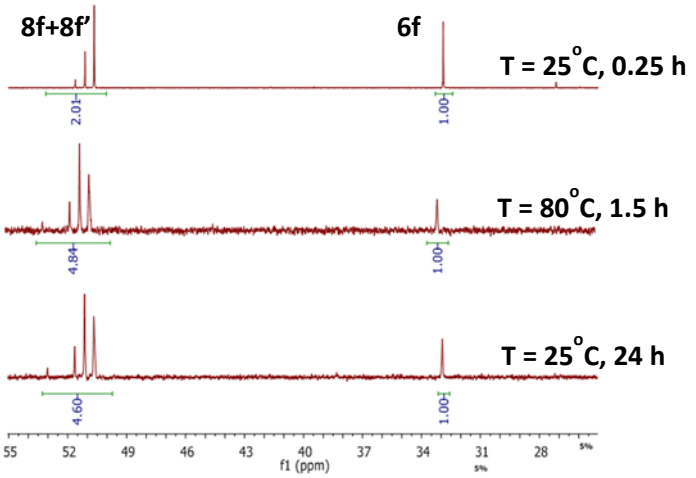

Figure 13. Spectres RMN $^{31}P\{^{1}H\}$ du mélange **6f**/**8f**/**8f'** dans le toluène-d_8, après avoir été préparé à partir de **3f**/NaHMDS (1/1) dans ^{i}PrOH pur.

En outre, le traitement thermique prolongé a résulté en l'apparition de deux nouvelles résonances à δ 51.6 et à δ 53.0 dans le spectre RMN $^{31}P\{^{1}H\}$, qui pourraient correspondre aux deux isomères **8f^{Me}**, **8f^{iPr}** moins favorables (Schéma 10).

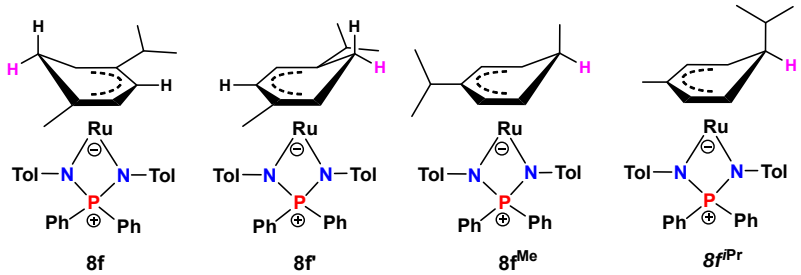

Scheme 10. Isomères possibles du complexe cyclohexadiényle **8f**.

La modélisation DFT (fonctionnelle B97D) a été utilisée pour calculer les énergies relatives des isomères **8f**, **8f'**, **8f^{Me}** and **8f^{iPr}**, en simplifiant le système par le complexe modèle [(η^5-C_6H_5(Me)^{i}Pr)Ru(HNP$_2$NH)] (**8f(H)**), où tous les substituants sur les atomes de N et P du ligand NPN ont été remplacés par des atomes de H. Comme espéré, les calculs

montrent que les isomères **8f(H)** et **8f'(H)** sont les plus stables. Leurs énergies relatives sont proches et plus faibles que celles de **8f^{iPr}(H)** et **8f^{Me}(H)**.[5] La formation préférentielle de l'isomère **8f** à température ambiante indique un contrôle cinétique du processus de transfert de l'atome d'hydrogène de l'atome de Ru à l'atome de C du cycle arène.

La modélisation DFT a également confirmé la forte barrière d'activation pour le réarrangement de **6f** en complexes cyclohexadiényles **8f**. En utilisant les modèles simplifiés [(η^6-C_6H_6)Ru(PhNPPh$_2$NPh)H] (**6F**) et [(η^5-C_6H_7)Ru(PhNPPh$_2$NPh)] (**8F**), les calculs montrent une faible préférence énergétique pour la structure cyclohexadiényle de **8F**. L'énergie de l'état de transition **TSB** pour le réarrangement **6F**/**8F** est élevée (36 kcal/mol par rapport à **6F**). Elle est associée à la forte distorsion nécessaire pour la géométrie du complexe. Ceci est cohérent avec l'observation expérimentale de l'interconversion lente entre **6f** et **8f**, ainsi qu'entre les isomères **8f** entre eux, ce qui requiert le transit par le complexe **6f**.

La stabilisation de **6f** augmente en présence d'alcool grâce à la formation d'une "liaison dihydrogène " [(η^6-*p*-Cym)Ru(NPN)H···HA]. Le signal hydrure dans le spectre RMN ^{1}H du complexe **6f** dans le benzène-d_6 (δ -2.96) est déplacé vers les champs plus forts (de 0.02–0.20 ppm) en fonction de la quantité d'alcool ajouté et de son pouvoir donneur de proton : ^{i}PrOH (δ -2.98 – -3.01), TFE (δ -3.16). Dans le spectre IR, la bande d'élongation de la liaison Ru-H à 1850 cm^{-1} est accompagnée par l'apparition d'une nouvelle bande à plus basse fréquence à 1830 cm^{-1} et 1822 cm^{-1} en présence, respectivement, de TFE et HFIP. Ces variations observées dans les spectres IR et RMN sont symptomatiques de la formation de complexes avec liaisons dihydrogène.

L'addition de 10 équiv. d'un donneur de proton plus fort – le hexafluoroisopropanol (HFIP) - conduit à l'évolution de H_2 (signal en RMN ^{1}H à δ_{H2} = 4.51) et à la formation du complexe arène à 16e **[4f]$^+$((CF$_3$)$_2$CHO$^-$)**, caractérisé par un signal RMN ^{31}P{^{1}H} à δ 72.3 (Schéma 11). Il faut noter que **6f** réagit lentement avec TFE pour donner un nouveau signal ^{31}P{^{1}H} élargi à δ 43.2, correspondant au complexe alkoxide à 18e [(η^6-*p*-Cym)Ru(NPN)(OCH$_2$CF$_3$)] (**9f**) (Schéma 12).

L'étude de la réaction inverse – l'interaction de **6f** avec l'acétone – a montré que la présence de faibles quantités de ce composé n'a aucun effet sur le signal RMN ^{1}H de la fonction RuH. Dans l'acétone-d_6 pure, en revanche, un fort blindage (de 0.57 ppm) du

[5] Les calculs ont été effectués par les Prof. E. Deydier and Prof. R. Poli (LCC CNRS, Toulouse).

signal ^{1}H de l'hydrure est observé. Ce phénomène peut être rationalisé par l'établissement d'un équilibre de transfert d'hydrure, probablement impliquant un complexe σ à 18e, [(η^6-*p*-cymene)Ru^{+}(NPN)···HCMe$_2$O^{-}] (**9f**). Un tel processus devrait a priori conduire au blindage du signal hydrure, semblable à celui observé pour la liaison dihydrogène. Le complexe **9f** est un intermédiaire présumé dans la formation du complexe isopropylate **7f**.

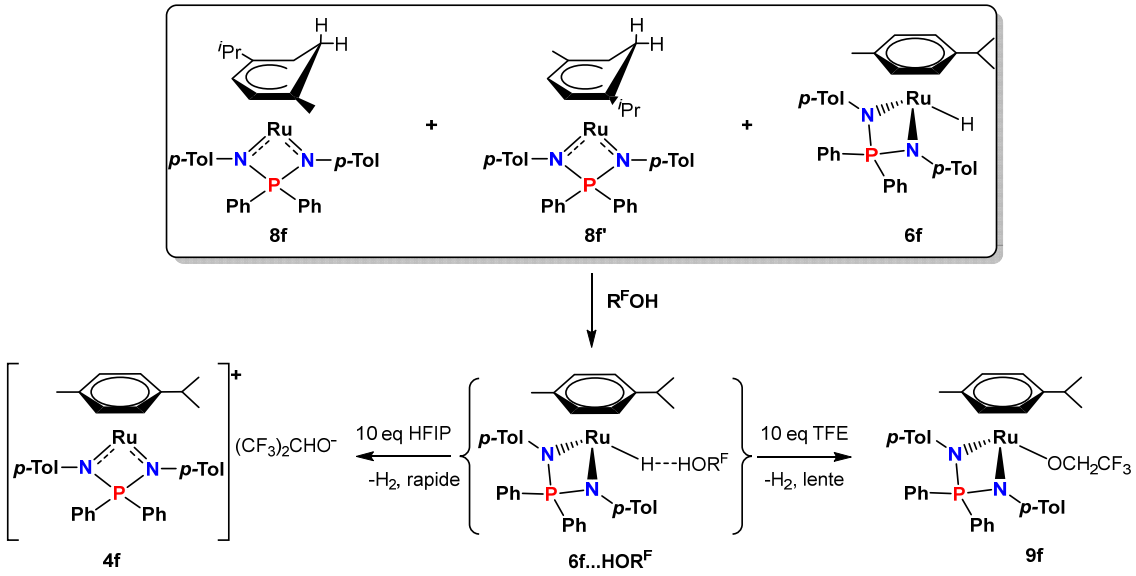

Scheme 11. Réactions de **6f**/**8f**/**8f'** avec des alcools fluorés.

*Dégradation du complexe **6f**.*

Un suivi de la réaction du complexe **3f** avec NaHMDS/^{i}PrOH dans le C_6D_6 par spectroscopie RMN ^{1}H montre la formation, outre les composés déjà décrits précédemment (**6f**, **8f**/**8f'**, **7f**), de faibles quantités de $Ph_2P(O)NH$-*p*-Tol (NPO, δ 16.9) et aminoiminophosphorane **1a** (NPNH, δ -5.5), voir Figure 14. En général, les oxydes d'aminophosphines $Ph_2P(O)NHAr$ se forment par décomposition hydrolytique des aminoiminophosphoranes, $Ph_2P(NAr)(NHAr)$, ou des haloiminophosphoranes, $Ph_2PBr(NHAr)$. Après sa formation, **6f** se dégrade lentement à température ambiante conduisant à une augmentation des quantités de NPO, NPNH, et des isomères cyclohexadiényles **8f** and **8f'**, ainsi qu'à l'apparition de deux composés additionnels caractérisés par des signaux ^{31}P{^{1}H} à δ 27.4 et 26.2 (**10** and **10'**), dont l'accumulation est très lente pendant plusieurs jours (Figure 14). Ces nouveaux composés se forment également pendant les tentatives d'isolation de **6f**.

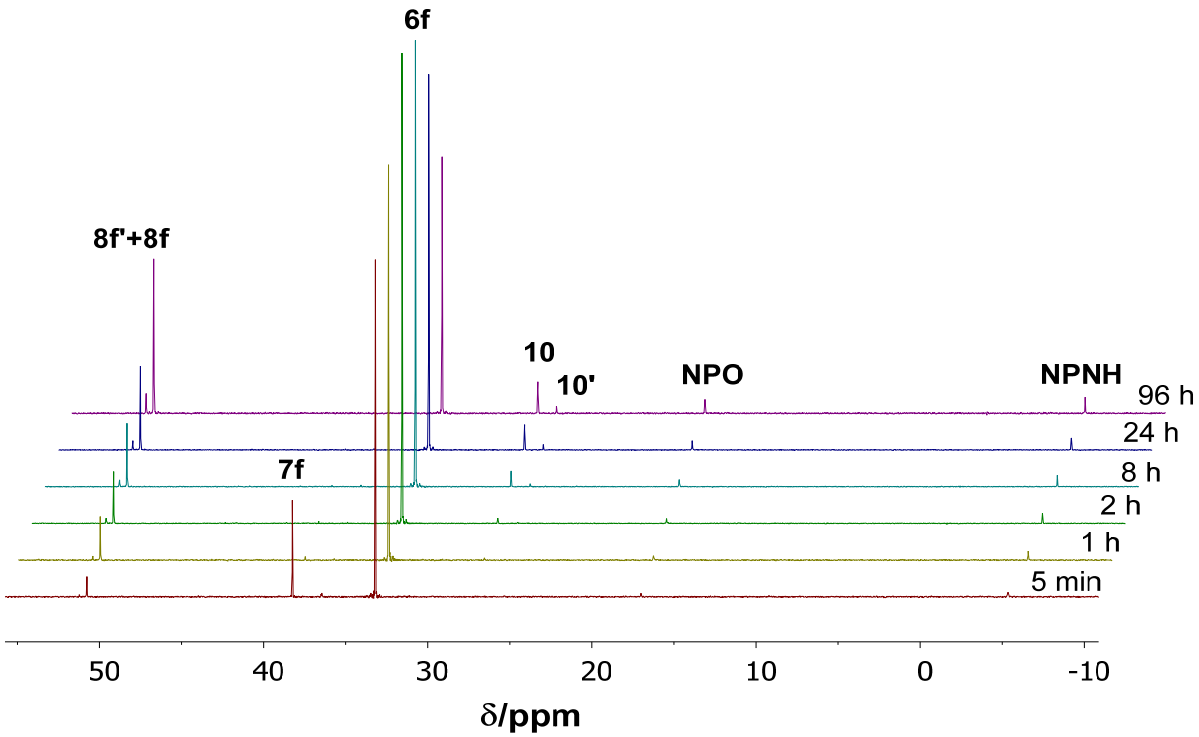

Figure 14. Suivi prolongé par RMN $^{31}P\{^{1}H\}$ de la réaction de **3f** avec NaHMDS/^{i}PrOH dans C_6D_6 à température ambiante.

Les signaux $^{31}P\{^{1}H\}$ de **10**/**10'** sont proches aux signaux du sel de diaminophosphonium correspondant, $Ph_2(NH\text{-}p\text{-}Tol)_2^+Br^-$ (δ 28.0 dans le $CDCl_3$) et du complexe de palladium avec le ligand κ^1-NPNH, *trans*-$[PdCl_2\{(p\text{-}C_6H_4{}^{i}PrN)PPh_2(NH\text{-}p\text{-}C_6H_4{}^{i}Pr)\}_2]$ (δ 26.4 dans le $CDCl_3$). Le spectre RMN ^{1}H du mélange des composés **10** et **10'** contient les signaux RuH déplacés vers les hauts champs par rapport à **6f** et des signaux caractéristiques de ligands *p*-cymène asymétriques avec quatre doublets CH aromatiques et deux groupements méthyles non équivalents pour les substituants ^{i}Pr.

Vraisemblablement, les deux composés peuvent correspondre à des complexes « half-sandwich » de ruthénium avec trois ligands monodentates différents, dont un doit être un hydrure. Ces observations nous permettent de faire l'hypothèse que ces complexes correspondent à [(η^6-*p*-cymene)Ru(H)(κ^1-NPNH)(O^{i}Pr)] avec un ligand NPNH κ^1-coordiné. Les deux composés **10**/**10'** sont probablement des isomères avec différentes configurations des liaisons hydrogène : le ligand κ^1-NPNH donne lieu à une liaison hydrogène soit avec le ligand hydrure, soit avec l'atome d'oxygène du ligand isopropanolate (Schéma 12).

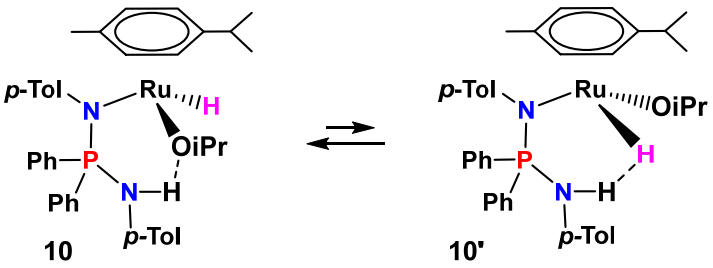

Scheme 12. Structures possibles des complexes **10**/**10'**.

La quantité accrue de **10**,**10'** dans l'échantillon du complexe **6f** après séparation de sa solution mère résulte probablement du fait que la majorité de l'isopropanol et des bases, qui sont capables de protéger l'hydrure vis-à-vis du processus de décomposition, sont enlevés. Le chauffage prolongé de **6f** en présence d'isopropanol conduit à la décoordination totale du ligand NPN avec formation de l'aminoiminophosphorane **1a**, avec décomposition partielle en NPO.

Tous les processus ayant lieu pour **3f** et **6f** dans l'isopropanol sont résumés comme suit (Schéma 13). En l'absence de base à températures élevées, le complexe chlorure **3f** a tendance à la dissociation de l'ion chlorure pour former le complexe cationique à 16e **[4f]$^+$Cl$^-$**. L'isopropanol peut remplacer réversiblement l'anion chlorure pour produire l'adduit **11f** à 18e; ces deux complexes (**11f** et **[4f]$^+$Cl$^-$**) sont présents en faible concentration et ne sont donc pas observables. La déprotonation du complexe **11f** conduit à un intermédiaire isopropoxide **7f** qui, suite à une élimination β, forme un complexe hydrure **6f** relativement stable. Probablement, le complexe **6f** se décompose lentement à cause de la protonolyse d'une liaison Ru-N, donnant lieu aux intermédiaires hydrures asymétriques **10** et **10'** observés. La décoordination successive de NPNH dans ces complexes par l'excès d'isopropanol conduit à la formation d'un complexe isopropanolate solvaté (**12**). Ce produit n'a pas été détecté directement, mais on peut noter que la formation de complexes [(arène)Ru(μ-OR)$_3$Ru(Arene)]$^+$ similaires a été reportée dans des conditions proches de celles employées ici. Il est important de noter que la génération de **6f** requiert le piégeage du HCl libéré. En l'absence d'une base extérieure, le proton peut se lier à l'atome d'azote basique du ligand NPN. Suite à cela, la destruction du complexe a lieu avec relargage de NPNH, qui peut ensuite servir à son tour de base. En conséquence, en

absence de base, la génération de l'hydrure **6f** est accompagnée par la décomposition partielle du complexe NPN.

En présence d'une base, le complexe isopropanolate **7f** se forme quantitativement et rapidement à partir de complexe chlorure initial **3f** sous l'action de l'anion isopropanolate à température ambiante, suivie par l'élimination β-H avec formation de **6f**. Comme le complexe **7f** ne contient aucun site de coordination vacant, ce qui est nécessaire pour une transformation à **6f** concertée intramoléculaire, et comme la décoordination partielle du ligand NPN bidentate ou du ligand cymène est improbable, cette transformation procède alors vraisemblablement via une dissociation ionique suivie par un transfert de l'hydrure à partir de l'intermédiaire complexe-σ **9f**.

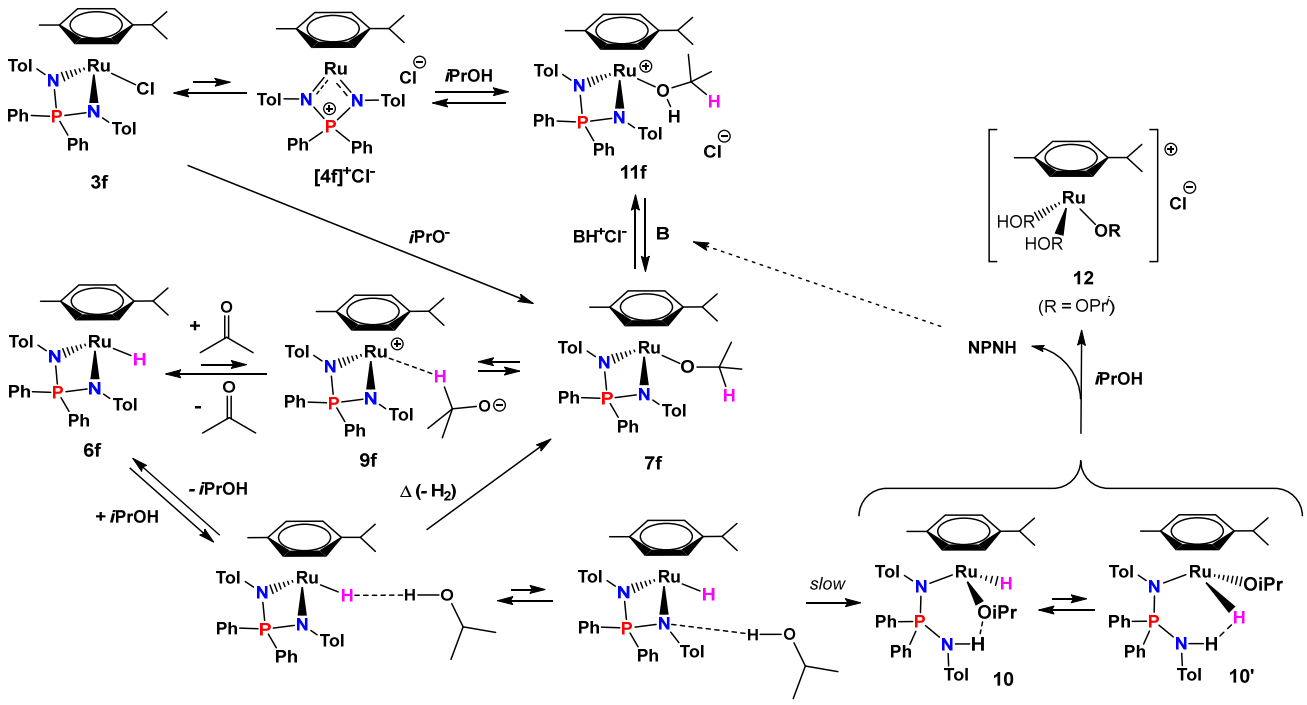

Scheme 13. Mécanisme proposé pour la génération de l'hydrure **6f** à partir de **3f** et transformations associées.

*Cinétique de la réduction de l'acétophénone catalysée par **3f**.*

Dans toutes les études cinétiques, la réduction de l'acétophénone a été accomplie par l'utilisation du complexe **3f**, à partir duquel le complexe hydrure **6f** correspondant a été engendré *in situ* par l'utilisation d'un équivalent de NaHMDS. Une série d'expériences à température constante (40°C) et à différentes concentrations du catalyseur ont permis de déterminer la loi de vitesse comme ayant un ordre 1 par rapport au substrat (Acp) et par

rapport au catalyseur : v = k[Ru][Acp]. Ces expériences ont ainsi fourni la constante de vitesse du second ordre k = 0.033 ± 0.003 $M^{-1}{\cdot}s^{-1}$ (Figure 15).

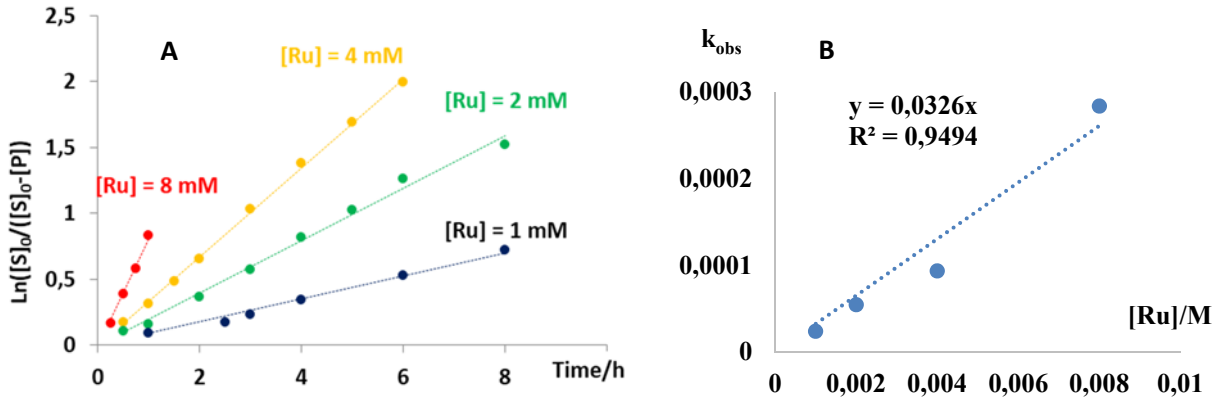

Figure 15. (**A**) Courbes cinétiques de la formation du 1-phényléthanol à différentes concentrations de catalyseur **3f** à 40°C. (**B**) Graphe de la constante observée de pseudo-premier ordre (k_{obs}) en fonction de la concentration de **3f**.

La Figure 16 montre la cinétique de pseudo-premier ordre à quatre différentes températures. L'analyse des valeurs de k en fonction de la température par la relation de Eyring a rendu possible la détermination de l'enthalpie et de l'entropie d'activation pour l'hydrogénation catalytique de l'acétophénone : $\Delta H^{\ddagger}$ = 9.7±1.3 kcal/mol et $\Delta S^{\ddagger}$ = -31±4 cal/(mol*K). L'entropie d'activation fortement négative signale un état de transition hautement ordonné pour l'étape déterminante, par rapport à l'état de repos.

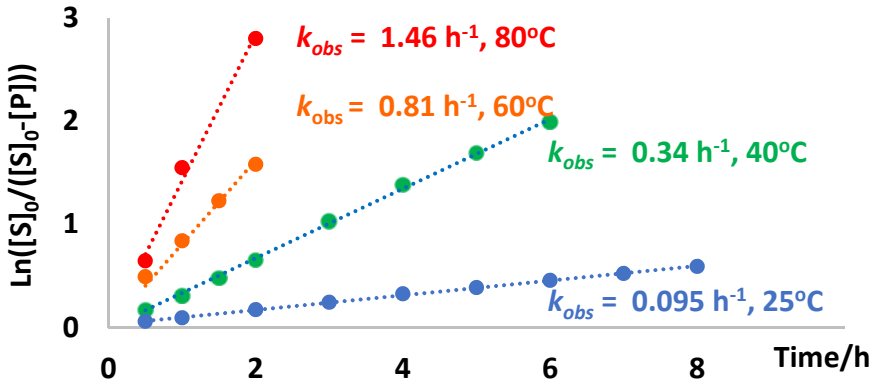

Figure 16. Cinétique pour la formation du 1-phényléthanol à différentes températures.

La combinaison des études stœchiométriques, spectroscopiques et catalytiques et des calculs théoriques par DFT converge pour proposer l'implication du complexe hydrure **6f** en tant qu'espèce catalytiquement active. En revanche, il est impossible d'envisager soit un chemin de type Noyori (transfert bifonctionnel et concerté à sphère externe proton/hydrure du catalyseur au substrat), soit un chemin de coordination/insertion pour cette même espèce, car le complexe ne contient ni de ligand déprotonable, ni des sites de coordination pouvant être libérés facilement car il est saturé avec des ligands fortement coordonnés.

Les études spectroscopiques décrites plus haut suggèrent l'accessibilité aisée à une espèce isopropopanolate à partir de **6f** et d'acétone, soit comme complexe neutre **7f** avec liaison Ru-O, soit comme un isomère zwitterionique, le complexe σ **9f**. Il est alors possible d'envisager un transfert d'hydrure à sphère externe de **6f** à l'acétophénone en passant par l'intermédiaire **9f'**, similaire à **9f**, possiblement en équilibre avec l'isomère 1-phényléthanolate lié par l'oxygène, **7f'**. Le produit 1-phényléthanol peut alors être généré par échange de proton avec le solvant, ce qui peut avoir lieu soit directement soit via la paire d'ions dissociée (complexe $\mathbf{[4f]}^+$ et alcoolate libre). Cette dernière possibilité est suggérée par l'observation de $\mathbf{[4f]}^+$ libre en présence de l'hexafluoroisopropanolate moins coordinant. Le complexe **9f** peut alors compléter le cycle par le processus de transfert d'hydrure inverse. Ce cycle catalytique est résumé dans le Schéma 14. Il est pertinent de remarquer que des catalyseurs sans ligands déprotonables ont déjà été montrés compétents pour un mécanisme ionique à sphère externe avec un transfert d'hydrure comme première étape, suivi par la protonation de l'alcoolate intermédiaire, pour l'hydrogénation ionique (le proton provenant dans ce cas d'un ligand H_2 activé). Même pour le catalyseur de Noyori, qui contient bien un ligand potentiellement déprotonable, il a été suggéré que le mécanisme le plus favorable n'est pas concerté et comporte un transfert de proton du ligand H_2 activé.

L'activation du complexe **3f** a lieu sous l'action d'un ion isopropanolate avec formation d'un intermédiaire isopropanolate **7f** qui, suite à l'élimination β d'hydrure, donne le complexe **6f** relativement stable. Nous émettons l'hypothèse que le complexe **6f** attaque la molécule d'acétophénone directement avec transfert de l'hydrure à l'atome de carbone du carbonyle pour former l'intermédiaire zwitterionique [(*p*-Cym)Ru^+(NPN){HCR_2O^-}] (**9f'**). D'après les résultats de calculs théoriques, **9f'** est

stabilisé par des molécules d'alcool et est en équilibre avec le complexe isomère alcoolate **7f'**, qui est l'état de repos du catalyseur. L'échange entre **7f** et **7f'** a lieu via le complexe cationique **[4f]**$^{+}$ ou par échange de proton avec le solvant. L'entropie d'activation fortement négative du processus catalytique résulte de l'état de transition hautement organisé avec coordination de la molécule de cétone et des molécules de solvant pour la stabilisation de l'intermédiaire **9f'**.

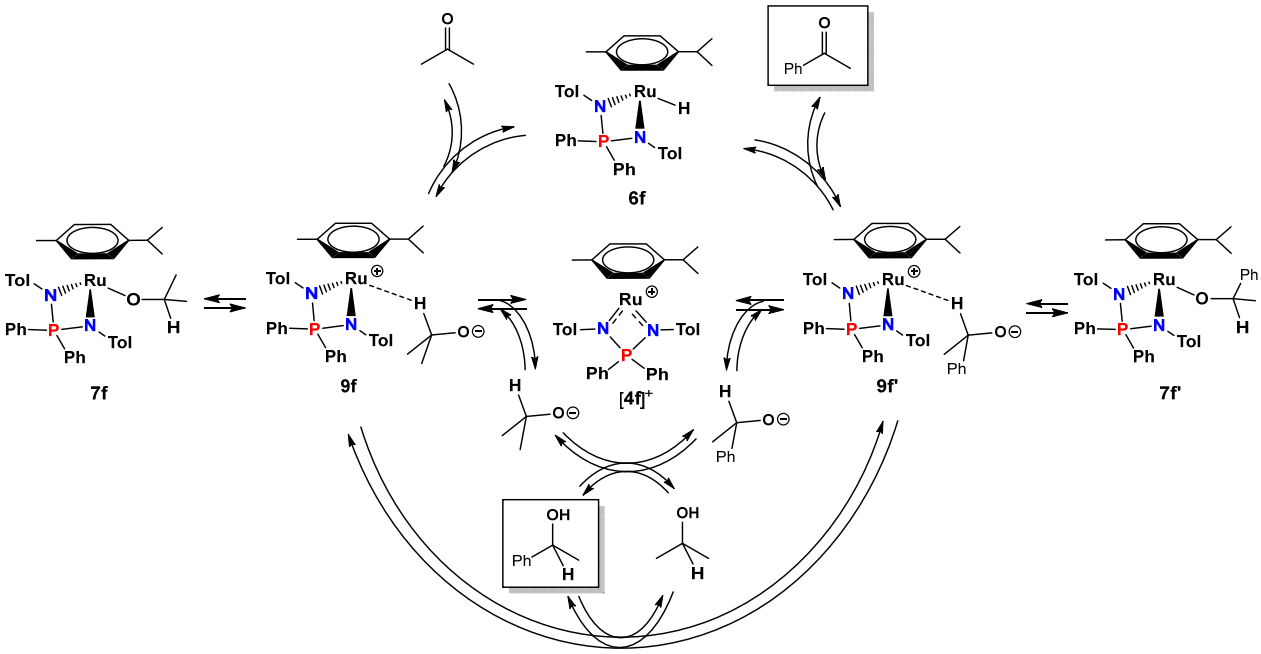

Scheme 14. Mécanisme proposé pour l'hydrogénation par transfert catalysée de l'acétophénone par l'isopropanol.

Selon ce mécanisme, le complexe chlorure de ruthénium [(η^6-*p*-cymene)RuCl(NPN)] (**3f**) est un précatalyseur pour la réaction d'hydrogénation par transfert de cétones avec isopropanol. L'espèce catalytique active est le complexe hydrure [(η^6-*p*-cymene)RuH(NPN)] (**6f**). Bien que ce complexe hydrure ait tendance à s'isomériser en complexe cyclohexadiényle, il est stabilisé dans l'isopropanol grâce à la formation d'une liaison dihydrogène. L'étape limitante du processus est la formation du complexe σ zwitterionique **9f**, où l'anion alcoolate est lié par l'atome de carbone méthine (CH) à l'atome de ruthénium. Cette étude de mécanisme semble être la première comportant l'hydrogénation par transfert avec un transfert d'hydrure à sphère externe en présence d'un catalyseur sans ligands déprotonables.

2.2. Effet des substituants des atomes de N et P et de l'arène sur l'activité catalytique des complexes iminophosphonamides arènes de ruthénium.

Cette section présente les résultats de l'étude de l'activité catalytique des complexes **3a-e**. Pour tous ces complexes, les conditions pour la formation des complexes hydrures correspondants, [(arene)RuH(NPN)] (**6a-e**), ont été établies par l'utilisation de la réaction modèle de **3a-e** avec isopropanol en présence d'un équivalent de NaHMDS dans un mélange C_6D_6/^{i}PrOH = 500/40 µL à température ambiante avec un suivi par spectroscopie RMN ^{1}H et ^{31}P{^{1}H}. La vitesse de formation des complexes hydrures augmente avec l'introduction de substituants donneurs sur le ligand arène et sur les atomes de N et P du ligand NPN. Le temps nécessaire pour la transformation totale du complexe isopropanolate initialement formé aux complexes **6a-e** est comprise entre <5 min (**6c**) et 2h (**6a**). La stabilité des complexes hydrures varie inversement avec la vitesse de leur formation : les dérivés N-aryles sont stables plus d'un jour, alors que **6c** se décompose en une demi-heure après sa formation. Les complexes **6a**, **6b**, **6d**, **6e** ont été caractérisés par spectroscopie RMN ^{1}H et ^{31}P NMR *in situ*.

Concernant l'activité catalytique en réduction de l'acétophénone avec isopropanol en présence de NaHMDS, l'activité augmente en présence d'une sphère de coordination plus riche en densité électronique. A 40°C, la constante de vitesse du second ordre k (s^{-1}•M^{-1}) diminue dans l'ordre : **3c** (0.049) > **3f** (0.023) > **3d** (0.0092) > **3e** (0.0070) > **3a** (0.0057) > **3b** (0.0033). Pour tous les complexes, une étude de la variation de la constante de vitesse avec la température a été effectuée. Les paramètres d'activation du processus établis ($\Delta H^{\neq}$ et $\Delta S^{\neq}$) sont reportés dans la Figure 17. Malheureusement, le composé **3c** se décompose rapidement dans les conditions de la réaction au-dessus de 40°C.

Les paramètres d'activation de la réaction catalytique suggèrent que la réaction procède par le même mécanisme, via la formation d'un complexe hydrure actif **6**, pour tous les complexes NPN contenant uniquement des substituants aryles à l'azote (**3a**, **3b**, **3e**, **3f**). Pour ces complexes, les valeurs de $\Delta H^{\neq}$ et $\Delta S^{\neq}$ se placent dans des plages étroites, entre 9.7 et 11.7 kcal/mol pour $\Delta H^{\neq}$ et entre 31 et 37 kcal/(mol*K) pour $\Delta S^{\neq}$. Dans cette série, on observe un accord entre l'enthalpie d'activation et l'activité du catalyseur : les complexes *p*-cymène avec des substituants plus donneurs à l'azote sont plus actifs.

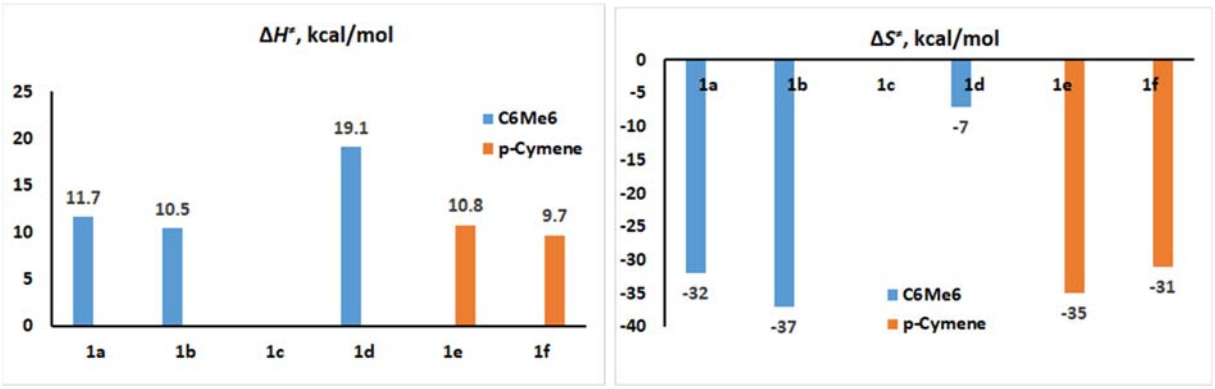

Figure 17. Paramètres d'activation $\Delta H^{\neq}$ et $\Delta S^{\neq}$ pour la réduction catalytique de l'acétophénone dans l'isopropanol, catalysée par **3a-f** en présence de NaHMDS.

Les paramètres d'activation pour le complexe **3d** contenant un substituant N-méthyle sont très différents des autres : la valeur de $\Delta H^{\neq}$ est presque double (19.1 kcal/mol) alors que l'entropie d'activation est beaucoup plus faible, indiquant clairement que l'état de transition déterminant n'est pas très ordonné pour ce système. Apparemment, les complexes avec substitution N-méthyle **3c** et **3d** suivent un cycle catalytique différent. En effet, ces précatalyseurs montrent une forte activité également en absence de base ; à 40°C, les constantes de vitesse du second ordre k ($s^{-1} \cdot M^{-1}$) sont 0.015 (**3c**) et 0.0092 (**3d**). Les valeurs déterminées de $\Delta H^{\neq}$ and $\Delta S^{\neq}$ sont respectivement 24±2 (**3c**), 22.4±0.8 (**3d**) kcal/mol et 9±6 (**3c**), 4±3 (**3d**) kcal/(mol*K). Les paramètres d'activation obtenus sont proches pour les deux complexes et proches de ceux du complexe **3d** en présence de base. Cela suggère qu'une base n'est pas nécessaire pour l'activation de ces complexes. Les espèces principales détectées par RMN $^{31}P\{^{1}H\}$ dans le mélange catalytique sont les complexes cationiques $[\mathbf{4c}]^+$ et $[\mathbf{4d}]^+$, formés par dissociation des complexes chlorures correspondants dans le solvant polaire (isopropanol). Ces complexes constituent l'état de repos du catalyseur. Il faut remarquer que, en absence de base, ces complexes sont beaucoup plus stables et capables de catalyser la réaction à températures élevées sans décomposition notable.

Sur la base des données obtenues, il est possible de faire l'hypothèse que la réaction procède par un chemin classique à sphère externe de type Noyori-Ikaria : l'état de transition déterminant pour l'étape de déshydrogénation de l'isopropanol a une structure péricyclique dans laquelle l'atome d'hydrogène méthine de l'isopropanol est transféré à l'atome de ruthénium et le proton de l'hydroxyle est simultanément transféré à l'atome d'azote

basique (Schéma 15). Les résultats expérimentaux, notamment a) enthalpie d'activation élevée et entropie d'activation légèrement positive et b) complexe cationique à 16e en tant qu'état de repos du catalyseur, sont en bon accord avec ce mécanisme.

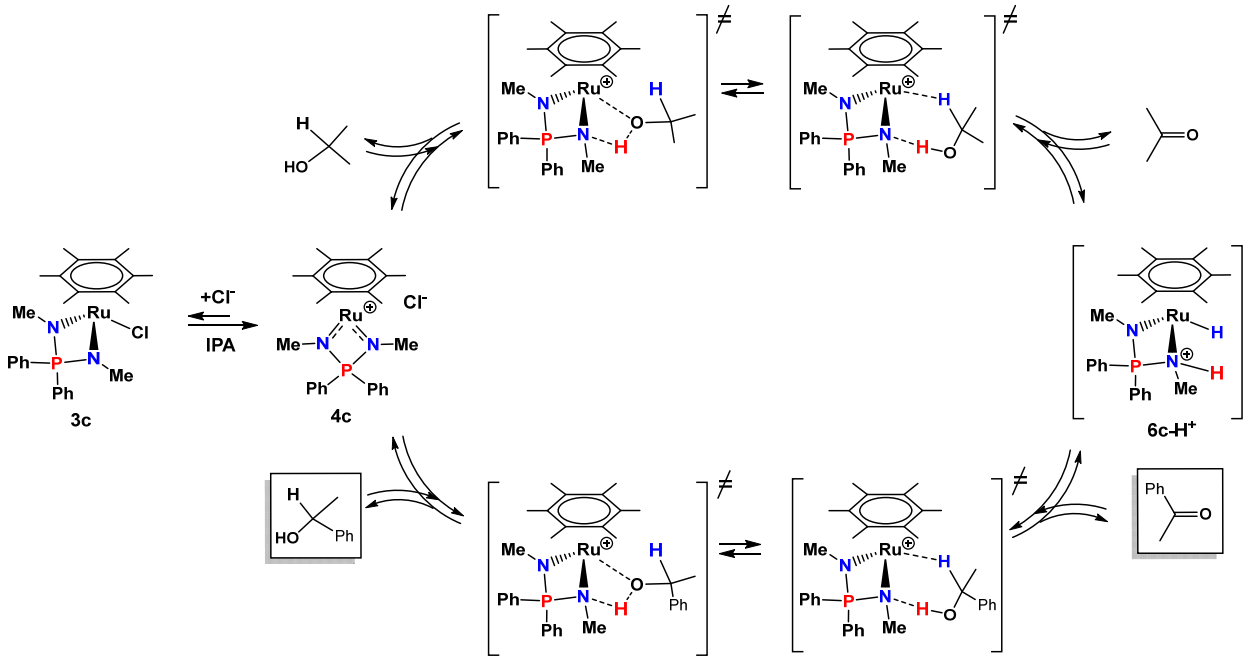

Scheme 15. Mécanisme proposé pour la réaction d'hydrogénation par transfert catalysée par les complexes NPN arènes de ruthénium **3c,d** en absence de base.

Nous émettons l'hypothèse que l'espèce catalytique est le complexe hydrure **6c-H**$^+$, protoné à l'atome d'azote, dont la concentration à l'état stationnaire en conditions catalytiques est faible. Il se formerait grâce à la forte basicité de l'atome d'azote dans les complexes NPN de ruthénium avec substituants N-méthyles à 18e. L'état de repos du catalyseur est le complexe cationique à 16e **4c**, dans lequel les doublets libres des atomes d'azote sont impliqués en donation π à l'atome de ruthénium. Ainsi, leur basicité est estompée. En revanche, la coordination d'un ligand extérieur au centre de ruthénium rend le complexe à nouveau à 18e et les atomes d'azote redeviennent fortement basiques, comme il a été démontré par exemple par la carbonylation du composé **3c**. Possiblement, l'activation des doublets libres de l'azote dans le complexe **4c** est promue par la coordination réversible de la molécule d'isopropanol pendant la réduction catalytique de l'acétophénone. Dans ce cas, un changement du mode de coordination de la molécule d'alcool de κ-O à κ-H sur l'atome de ruthénium peut constituer l'étape limitante du cycle catalytique, ce qui impliquerait un état de transition avec faible variation de l'entropie. Il

faut noter qu'en présence d'une base, le complexe **6c-H**$^+$ peut également agir en tant qu'espèce catalytique active. En revanche, l'état de repos du catalyseur serait dans ce cas le complexe hydrure **6c**, qui se décompose beaucoup plus rapidement que le complexe stabilisé **4c**. Le mécanisme proposé du cycle catalytique par les complexes **3c** et **3d** est en bon accord avec les données expérimentales obtenues à ce jour.

Résultats principaux et conclusions.

8. Une série de nouveaux complexes NPN arènes de ruthénium à 18 et 16 électrons **3a-f**, **4a-c**, **f**, avec différents substituants sur les atomes d'azote et de phosphore, ont été obtenus. Tous ces complexes ont été complètement caractérisés par des méthodes spectroscopiques, leur composition a été confirmée par analyses élémentaires et leurs structures ont été établies par diffraction des rayons-X sur monocristal.
9. Il a été établi que les complexes NPN chlorures de ruthénium neutres à 18e peuvent dissocier le ligand chlorure avec formation de complexes cationiques formellement à 16e. Ce processus procède plus aisément dans des solvants plus polaires et en présence de substituants plus fortement donneurs d'électrons sur le ligand NPN. Les enthalpies de dissociation de la liaison Ru-Cl pour les composés **3a-f** ont été déterminées.
10. L'interaction des complexes NPN à 16e **4a** avec les ligands labiles acétonitrile et pyridine a été étudiée par les spectroscopies RMN et UV-vis. Les adduits carbonyles plus stables des complexes cationiques **4a**,**c**,**f** ont été isolés, caractérisés par des méthodes spectroscopiques, et leurs structures ont été établies par diffraction des rayons-X sur monocristal. Les complexes **4a**,**f** donnent des adduits monocarbonyles **5a**,**f**, et le complexe **4c** avec les substituants N-méthyles plus fortement donneurs forme un adduit carbonyle-carbamoyle **5c'**. Les propriétés physico-chimiques des complexes NPN de ruthénium confirment donc la structure zwitterionique du ligand NPN et son fort caractère donneur ($4\sigma/2\pi$).
11. Il a été montré pour la première fois que des complexes iminophosphonamide de ruthénium sont des catalyseurs actifs pour l'hydrogénation de cétones par transfert

en présence d'une base forte. L'activité catalytique augmente avec l'introduction de substituants donneurs sur l'arène et sur le ligand NPN.

12. En travaillant avec le complexe *p*-cymène de ruthénium **3f**, une série de réactions modèles a permis d'établir les intermédiaires clés de la catalyse d'hydrogénation de cétones. En présence d'une base, la formation d'un complexe hydrure de ruthénium précédemment inconnu **6f** a été observée dans l'isopropanol. Ce complexe hydrure est capable de former des adduits avec liaison dihydrogène avec des alcools de différente nature (isopropanol, TFE, HFIP), qui peuvent alors être déshydrogénés pour produire du dihydrogène et former des complexes cationiques à 16e de type **4**. Le complexe **6f** se réarrange avec formation d'un mélange de complexes η^5-cyclohexadiényles isomères **8f** et **8f'**, catalytiquement inactifs, dont la structure a été établie par diffraction des rayons-X.

13. La cinétique de réduction de l'acétophénone par les complexes **3a-f** en présence d'une base a été étudiée en détail. La loi de vitesse a été montrée de premier ordre en substrat et en catalyseur pour **3f**. Les paramètres d'activation $\Delta H^{\neq}$ et $\Delta S^{\neq}$ mesurés indiquent un état de transition de l'étape limitante du cycle catalytique hautement organisé lorsque les complexes **3a**, **3b**, **3e**, **3f** avec des substituants N-aryles sont utilisés en tant que précatalyseurs. En revanche, les paramètres $\Delta H^{\neq}$ and $\Delta S^{\neq}$ pour la réaction catalysée par les complexes **3c**, **3d** avec des substituants N-méthyles, outre l'activité même en absence de base, indiquent que ces systèmes suivent un mécanisme alternatif.

14. Sur la base du travail expérimental accompli, ainsi que des calculs DFT pour le système avec substituants N-aryles, un mécanisme a pu être proposé pour l'hydrogénation par transfert de l'acétophénone avec l'isopropanol catalysée par les complexes NPN **3** en présence de base. Dans ce mécanisme, le complexe hydrure **6** est l'espèce active et l'étape déterminante du cycle catalytique est le transfert de l'hydrure de l'atome de ruthénium à l'atome de carbone du carbonyle de la cétone avec formation d'un intermédiaire zwitterionique **9**.